

**INVESTIGATION ON LASER BEAM AND MICRO
ELECTRO DISCHARGE MACHINING BASED HYBRID
MICROMACHINING**

BY

MIR AKMAM NOOR RASHID

A dissertation submitted in fulfillment of the requirement for
the degree of Doctor of Philosophy (Engineering).

**Kulliyyah of Engineering
International Islamic University Malaysia**

MARCH 2024

ABSTRACT

This research aims to develop a sequential hybrid micromachining technique that combines the advantages of laser beam micromachining (LBMM) and micro electro-discharge machining (μ EDM). LBMM has the disadvantage of low machining quality, although laser machining offers a very fast processing time. While micro μ EDM takes a longer time and has a slower material removal rate (MRR), the final product is of higher quality than laser-machined parts. This research shows that the sequential machining process (LBMM followed by μ EDM) improves quality of the machined product with a faster processing time. In the process the LBMM is used to machine a pilot feature, and μ EDM is then used to complete the feature. In the first-stage of this research, we conducted experiments on stainless steel (type SS304) to determine how different input parameters of LBMM (laser power, scanning speed, and pulse frequency) affected the performance of the finishing technique, that is, the μ EDM in this case. In this 1-D machining or micro-hole drilling, it was observed that the output performance of μ EDM was significantly influenced by the laser input parameters, particularly scanning speed and power. The results of our research indicate that the μ EDM finishing time can be significantly increased by using a higher laser scanning speed at a lower laser power during the pilot machining. However, the processing time for the EDM operation is shortened if the pilot hole drilling is done at a slower scanning speed and with a higher laser power. Our findings verify that the LBMM-based sequential machining technique leads to a significant reduction in machining time, tool wear, and instability (in terms of short circuit/arc) when compared to a purely μ EDM process. The results of the experiment show that the input and output parameters of the sequential process have strong relationships. Because of this, a dual-stage modeling approach based on ANNs was developed to forecast the results of the sequential process. To evaluate the output performance of LBMM- μ EDM based sequential process, in first step the laser parameters were varied and the μ EDM input parameters was constant. In the second step, both the laser input parameter and the μ EDM input parameters were altered in the subsequent phase of the research. The dual-stage modeling method was used, and this time the μ EDM input parameters (voltage, capacitance, and EDM speed) were not kept the same. Root Mean Square Errors (RMSEs) were calculated for each data set and each output parameter (i.e., μ EDM time, machining instability/short circuit count, and tool wear) to figure out the model accuracy. Average RMSE was calculated to be 0.050 (95% accuracy), 0.040 (96% accuracy), and 0.110 (89% accuracy) for the previously mentioned parameters. In this study's final phase, 3-D hybrid micromachining (milling) was tested using Response Surface Methodology (RSM) to identify the significant factors influencing this sequential hybrid micromachining. It was observed that laser milling input parameters (scanning speed, power, frequency, and loops) affecting significantly on the output responses of μ EDM milling time, tool wear and machining instability (short circuit/arc count).

ABSTRACT IN ARABIC

يهدف هذا البحث إلى تطوير تقنية ميكانيكية هجينة متسلسلة تجمع بين مزايا التصنيع الدقيق لشعاع من عيب في جودة LBMM يعاني (μ EDM) وآلة التفريغ الكهربائي الدقيقة (LBMM) الليزر micro التصنيع الرديئة ، على الرغم من أن وقت معالجة المعالجة بالليزر سريع جداً. بينما يستغرق فإن المنتج النهائي يتميز بجودة ، (MRR) وقتاً أطول ويكون معدل إزالة المواد فيه أبطأ μ EDM متبوعة (LBMM) أعلى من الأجزاء المشكلة بالليزر. يوضح هذا البحث أن عملية المعالجة المتسلسلة LBMM تعمل على تحسين جودة وقت المعالجة أسرع. في هذه العملية ، يتم استخدام (μ EDM) بـ ، لإكمال الميزة. في المرحلة الأولى من هذا البحث μ EDM لتشغيل ميزة تجريبية ، ثم يتم استخدام لتحديد كيفية تأثير معلمات الإدخال المختلفة (SS304 النوع) أجرينا تجارب على الفولاذ المقاوم للصدأ (μ EDM) طاقة الليزر ، وسرعة المسح ، وتردد النبض (على أداء تقنية التشطيب ، أي LBMM) في μ EDM في هذه الحالة. في هذه المعالجة الآلية أحادية الأبعاد أو الثقب الصغير ، لوحظ أن أداء خرج قد تأثر بشكل كبير بمعلمات إدخال الليزر ، وخاصة سرعة المسح وقوته. تشير نتائج بحثنا إلى أن وقت يمكن زيادته بشكل كبير باستخدام سرعة مسح ليزر أعلى بطاقة ليزر أقل أثناء μ EDM الانتهاء من المعالجة التجريبية. ومع ذلك ، إذا تم استخدام سرعة المسح المنخفضة وطاقة الليزر الأعلى لحفر يؤكد بحثنا أنه بالمقارنة مع عملية μ EDM. الفتحة التجريبية ، فسيتم تقليل وقت المعالجة لعملية تقلل بشكل كبير من وقت المعالجة LBMM بحتة ، فإن تقنية المعالجة المتسلسلة القائمة على μ EDM وتآكل الأداة ، وعدم الاستقرار) من حيث عدد الدوائر القصيرة. (تشير النتائج التجريبية إلى علاقات ، قوية بين معلمات الإدخال والإخراج للعملية المتسلسلة. لهذا السبب ، تم تطوير نهج نمذجة ثنائي المرحلة يعتمد على الشبكات العصبية الاصطناعية للتنبؤ بنتائج العملية المتسلسلة. كان من الممكن استخدام بالنظر إلى LBMM الجزء الأول من نموذج المرحلة مزدوجة لعمل تنبؤات حول نتائج عملية مثل منطقة دخول) LBMM مجموعة من القيم لليزر. في المرحلة الثانية ، تم استخدام النتائج المتوقعة في المرحلة اللاحقة μ EDM الفتحة التجريبية ، تم تعديل كل من معلمة إدخال الليزر ومعلمات إدخال من البحث. تم استخدام تقنية النمذجة ثنائية المرحلة مرة أخرى ، ولكن هذه المرة لم يتم الاحتفاظ تم حساب أخطاء جذر متوسط التربيع (μ EDM) الجهد والسعة وسرعة) ثابتة EDM بمعلمات إدخال / وعدد الدارة القصيرة ، μ EDM لكل مجموعة بيانات لكل معلمة إخراج) أي وقت (RMSEs)

ليكون 0.050)دقة 95% (و RMSE الانحناء ، وتآكل الأداة (لتقييم دقة النموذج .تم حساب متوسط (دقة 96% (و 0.110)دقة 89% (للمعاملات المذكورة سابقاً .في المرحلة النهائية من هذه 0.040 الدراسة ، تم اختبار المعالجة الدقيقة الهجينة ثلاثية الأبعاد)الطحن (باستخدام منهجية سطح الاستجابة لتحديد العوامل المهمة التي تؤثر على هذا التصنيع الدقيق الهجين المتسلسل .لقد وجد أن (RSM) معاملات إدخال الطحن بالليزر)سرعة المسح ، والطاقة ، والتردد ، والحلقات (تؤثر بشكل كبير على وارتداء الأداة والدائرة القصيرة ، μ EDM استجابات المخرجات لوقت طحن



APPROVAL PAGE

The thesis of Noor Rashid Mir Akmam has been approved by the following:



Tanveer Saleh
Supervisor

Azhar Bin Mohd Ibrahim
Co-supervisor

Muhammad Mahbubur Rashid
Co-Supervisor

Syamsul Bahrin Bin Abdul Hamid
Co-Supervisor

Ahsan Ali Khan
Internal Examiner

Yusri Bin Yusof
External Examiner

Akram M Z M Khedher
Chairman

DECLARATION

I hereby declare that this thesis is the result of my own investigations, except where otherwise stated. It has not been previously or concurrently submitted as a whole for any other degrees at IIUM or other institutions.

Noor Rashid Mir Akmam

Signature.....		Date.....
		08/03/2024



INTERNATIONAL ISLAMIC UNIVERSITY MALAYSIA

**DECLARATION OF COPYRIGHT AND AFFIRMATION OF
FAIR USE OF UNPUBLISHED RESEARCH**

**DESIGN AND IMPLEMENTATION OF AN ADAPTIVE
CONTROL IN THE BATTERY MANAGEMENT SYSTEM OF
AN ELECTRIC VEHICLE**

I declare that the copyright holder of this thesis are jointly owned by the student and IIUM.

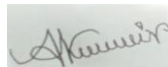
Copyright © 2024 Noor Rashid Mir Akmam and International Islamic University Malaysia. All rights reserved.

No part of this unpublished research may be reproduced, stored in a retrieval system, or transmitted, in any form or by any means, electronic, mechanical, photocopying, recording or otherwise without prior written permission of the copyright holder except as provided below

1. Any material contained in or derived from this unpublished research may only be used by others in their writing with due acknowledgement.
2. IIUM or its library will have the right to make and transmit copies (print or electronic) for institutional and academic purpose.
3. The IIUM library will have the right to make, store in a retrieval system and supply copies of this unpublished research if requested by other universities and research libraries.

By signing this form, I acknowledged that I have read and understand the IIUM Intellectual Property Right and Commercialization policy.

Affirmed by Noor Rashid Mir Akmam



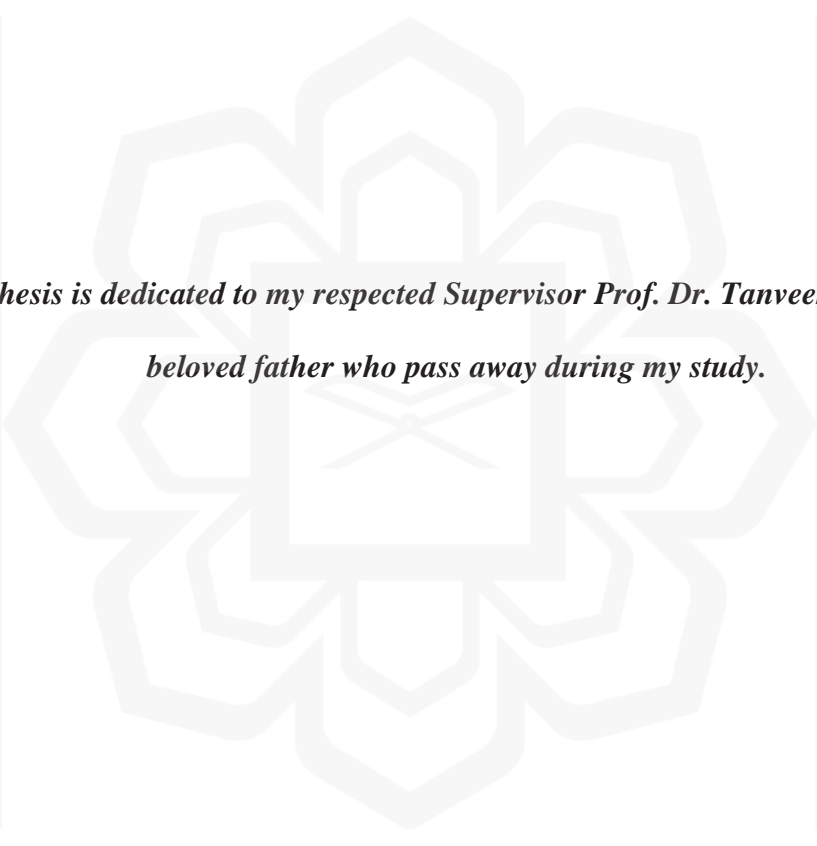
08/03/2024

.....

.....

Signature

Date



This thesis is dedicated to my respected Supervisor Prof. Dr. Tanveer Saleh & my beloved father who pass away during my study.

ACKNOWLEDGEMENTS

Almighty Allah is one who bestowed upon me his compassion and strength to overcome all kinds of difficulties. I am humbly showing my gratitude to Almighty Allah swa for letting me through this successful journey.

Prof. Dr. Tanveer Saleh, my supervisor, is also very deserving of my gratitude for his indispensable help in making this project a success. To this day, I still refer back to the advice and direction he gave me throughout the entire process of drafting and conducting experiments for my project. I also extend my gratitude to my co-supervisors for their unwavering belief in me and for permission to present my defense. I would like to mention here that in my research work which is reported in this thesis is conducted with complete integrity. All the data collected are true. To the best of my knowledge, there is no wrongdoing involved in the data collection, characterization, analysis, modelling and reporting of the research. Parts of the study have been published in two journal articles: (article1:<https://doi.org/10.1007/s00170-021-06908-8>)and(article2:<https://doi.org/10.1007/s00170-021-07910-w>). For the, (article1) I was the first author, hence, I included all the results from this article. However, as for (article2), I am one of the co-authors but not the first author; hence, I did not include the results of (article2) extensively in my thesis. Although, some results from article 2 have been included for the sake of completeness of this thesis.

I also would like to articulate my gratitude to the lab staff of the Tool and Die lab, especially Br. Mohammad Noor, Br. Ibrahim Razali (Metrology lab), Br. Zahir who helped me to cut my workpiece (Workshop lab) and my very close brother Wazed Ibne Noor, Wan Ahmad, Safiuddin, Mahmood, and Shohag Mollik all of them did great sacrifices in our SMART lab. In this long journey, all the staff of UIA (specially Dr. Zakaria Mohd Zain, Dr. Rafiq, Dr. Sher Afghan Khan, Dr. Ahmad Jazlan) were excellent in manner and behavior. I also remember my Master Supervisor Dr. Nor Khairusshima mam who taught me mechanical machining, DOE, and so many things. I am showing my highest gratefulness for your kind support (Jazak Allahu Fid Darain).

Lastly, I'd like to submit my heart felt gratitude to my entire family members for their untiring support and patience as I worked on this project. Special duaa from my two sons (Abdullah & Abdur Rahman) played an important role to come up into this extent.

Alhamdulillah, once more we admire Allah for His boundless compassion concerning us, one of which has allowed me to effectively carry out the script of this thesis.

TABLE OF CONTENTS

Abstract	iii
Abstract in Arabic	iv
Approval Page.....	vi
Declaration	vii
Copyright Page.....	viii
Acknowledgements.....	x
Table of Contents	xi
List of Tables	xiv
List of Figures	xv
List of Abbreviations	xxiii
List of Symbols	xxvi
CHAPTER ONE: INTRODUCTION	1
1.1 Background of Study.....	1
1.2 Problem Statement	5
1.3 Research Philosophy	6
1.4 Research Objectives	7
1.5 Significance of The Study	8
1.6 Scope of the Study.....	8
1.7 Research Methodology.....	9
1.8 Thesis Arrangement	12
CHAPTER TWO: LITERATURE REVIEW	14
2.1 Introduction	14
2.2 Laser Beam Micromachining (LBMM)	14
2.2.1 Basic Principle of Laser Beam Micromachining (LBMM).....	15
2.2.2 Recent Research on Laser Beam Micromachining (LBMM).....	16
2.3 Micro Electro Discharge Machining (μ EDM)	23
2.3.1 Basic Principle of Micro–Electro Discharge Machining (μ EDM).....	24
2.3.2 Recent Research on Micro Electro Discharge Machining (μ EDM).....	27
2.4 Comparison Between LBMM and Micro EDM.....	30
2.5 Hybrid Micromachining.....	31
2.6 Various Hybrid Machining Techniques Used for LBMM and μ EDM.....	33
2.7 Modelling Techniques Used for Micromachining Processes.....	36
2.7.1 Empirical Modelling.....	37
2.7.3.1 Statistical Modeling	37

2.7.3.2 Modeling Based on Artificial Intelligence.....	42
2.8 Summary	47
CHAPTER THREE: MATERIALS AND METHODOLOGY	48
3.1 Introduction	48
3.2 Laser Beam Micromachining (LBMM) Process.....	48
3.2.1 LBMM Experimental Parameter	48
3.2.2 Workpiece: Stainless Steel	49
3.3 Micro Electro Discharge Machining (μ EDM) Process.....	51
3.3.1 Micro EDM Parameters	51
3.4 Characterization	53
3.4.1 Scanning Electron Microscopy of Laser Machined Holes	53
3.4.2 Scanning Electron Microscopy of μ EDM-Finished Holes.....	54
3.4.4 Alicona Optical Profiling System.....	55
3.5 Experimental Setup Hybrid Micromachining (LBMM- μ EDM).....	56
3.6 Cleaning of the Sample Before Characterization	60
3.7 Methodology for the Modeling	60
3.7.1 Modelling of the LBMM- μ EDM Drilling with Constant EDM Parameter.....	60
3.7.2 Modeling of the LBMM- μ EDM Drilling with Variable EDM Parameter	63
3.7.3 Modelling of the LBMM- μ EDM Milling with Constant EDM Parameter	66
3.8 Summary	67
CHAPTER FOUR: RESULTS AND DISCUSSION	68
4.1 Introduction	68
4.2 Effect of the LBMM Parameter on the Hybrid LBMM- μ EDM Process	68
4.2.1 Morphological Comparison of the Hole Quality (LBMM- μ EDM).....	69
4.2.2 Study of μ EDM Machining Time for Laser- μ EDM Process	71
4.2.3 Study of μ EDM Machining Stability and Tool Wear for laser- μ EDM process	82
4.2.4 Study of Residual spatter Zone for Laser- μ EDM Process	86
4.3 Modelling of the LBMM- μ EDM Drilling Process without Changing the μ EDM Parameters	88
4.3.1 Modelling Performance and Accuracy	89
4.3.2 Modelling Performance Parameters	89
4.3.3 Study of the Model Performance	90
4.3.4 Study of Parametric Effects	94
4.4 Modelling of the LBMM- μ EDM Drilling Process Changing the μ EDM Parameters.	105
4.4.1 Modelling Performance	105
4.4.2 Study of the first-stage Model Performance	105
4.4.3 Study of the second-stage Model Performance	108
4.4.4 Study of the Overall Performance of the Dual-Stage ANN Model	111
4.4.5 Parametric Study.....	113
4.4.5.1 Machining Time for μ EDM.....	113

4.4.5.2 Short circuit/arcing count.....	118
4.4.5.3 Study on tool wear for μ EDM	123
4.5 Modelling of LBMM- μ EDM-Based Hybrid Micro-milling.....	127
4.5.1 Model Development for Responses.....	127
4.5.2 Response Performance of Output Models	130
4.5.2.1 Model for μ EDM Milling time.	130
4.5.2.2 Model for Tool wear	140
4.5.2.3 Model for Short circuit.....	148
4.5.3 Summary.....	156
CHAPTER FIVE: CONCLUSION AND RECOMMENDATION	159
5.1 Conclusion	159
5.2 Recommendations.....	161
References	163
Publications	173
Appendix A: Dataset first-stage Experiment Used in Section 4.2 and 4.3	174
Appendix B: Dataset second-stage Experiment Used in Section 4.4	181
Appendix C: Dataset 3rd Stage Experiment Used in Section 4.5	189

LIST OF TABLES

Table 2.1	Overview of the micro-EDM capabilities	28
Table 2.2	Various hybrid machining techniques that was used previously for LBMM and μ EDM machining process	35
Table 2.3	Summary table of various modeling techniques previously used for micromachining processes	45
Table 3.1	LBMM process	49
Table 3.2	Definition of LBMM process variables	49
Table 3.3	Mechanical properties of stainless steel 304	50
Table 3.4	Micro EDM process	52
Table 3.5	Definition of micro EDM process variables	52
Table 3.6	Correlation coefficient between various LBMM inputs and outputs	61
Table 3.7	Correlation coefficient between various LBMM inputs and outputs	64
Table 3.8	The level and parameter settings chosen for the experiments	66
Table 3.9	Values of machining variable and levels	66
Table 3.10	Box Behnken design of input and output responses	67
Table 4.1	LBMM input parameters in Box Behnken design	128
Table 4.2	Box Behnken design responses for the LBMM- μ EDM milling	129
Table 4.3	Fit summary for μ EDM milling time	130
Table 4.4	Table Analysis of variance for μ EDM milling time	131
Table 4.5	Summary Statistic for μ EDM milling time	133
Table 4.6	Fit summary for μ EDM tool wear	141
Table 4.7	Analysis of variance for μ EDM milling tool wear	141
Table 4.8	Summary Statistic for μ EDM milling tool wear	142
Table 4.9	Fit summary for μ EDM milling short circuit	149
Table 4.10	Analysis of variance for μ EDM milling short circuit	150
Table 4.11	Summary of model statistics for μ EDM milling short circuit	151
Table 4.12	Summary of the main results based on my research objectives	157

LIST OF FIGURES

Figure 1.1	Perception of Laser- μ EDM hybrid micromachining	7
Figure 1.2	Figure of LBMM- μ EDM Process Explaining its Operational based Sequential Process	10
Figure 1.3	Flowchart of the whole research work	12
Figure 2.1	Figure Schematic diagram of laser beam micromachining	16
Figure 2.2	a) Long pulse b) Short pulse	21
Figure 2.3	Advanced laser micromachining	22
Figure 2.4	a) Nanosecond laser holes b) Femto second laser holes	23
Figure 2.5	EDM process mechanism	26
Figure 2.6	Basic principle of micro EDM Figure	27
Figure 2.7	Wire Electro Discharge grinding (WEDG) method	28
Figure 2.8	Classification of hybrid micro-machining processes	32
Figure 2.9	CCD for 3 levels and 5 factors	40
Figure 2.10	The cube for BBD	41
Figure 3.1	Workpiece and fixture used for hybrid micromachining process	51
Figure 3.2	LBMMed hole measurement from the SEM images (a) entry area, (b) exit area, (c) HAZ, and (d) recast layer	54
Figure 3.3	Alicona Optical Profiling System	56
Figure 3.4	Shows how the laser scanning is carried out during the LBMM process	57
Figure 3.5	Photograph of the Fibre Laser Setup (a) and Photograph of the μ EDM procese Setup	58
Figure 3.6	The μ EDM tool's pre-machined LBMMed hole centering method's. Scale bar = 200 μ m	59
Figure 3.7	Ultrasonic bath cleaning machine	60
Figure 3.8	Correlation between various LBMM output and μ EDM output	62
Figure 3.9	LBMM- μ EDM process dual-stage ANN model flow and architecture	63
Figure 3.10	LBMM- μ EDM process dual-stage ANN model flow and architecture (drilling with Variable EDM Parameter)	65

- Figure 4.1 The structural representation of various micro holes produced by pure a) LBMM, b) pure μ EDM, and c) LBMM- μ EDM based hybrid processes. The processing parameters of the LBMM was 15.5W, 50mm/s, and 20kHz. Scale bar = 100 μ m 70
- Figure 4.2 The figure shows the comparison between LBMM- μ EDM and pure μ EDM: compared parameters are machining time, number of short circuits, and tool wear 71
- Figure 4.3 Comparative study of the structure of the micro holes produced by (a) the LBMM machining (b) LBMM- μ EDM machining and (c) purely μ EDM machining. Scale bar = 100 μ m 71
- Figure 4.4 The impact of the laser parameters used in the first-stage of machining on the processing time of the second-stage EDM for the final pilot hole finishing? The machining uncertainty is displayed by the error bar 72
- Figure 4.5 The correlation between laser incident power, scanning speed, and the zone of faster and slower μ EDM machining time (used for pilot hole drilling using the LBMM process) 74
- Figure 4.6 Demonstrates how the laser power and scanning speed used for the pilot hole machining affect the discharge current and frequency during the EDM process: (a) the discharge current variation, and (b) the discharge frequency variation 75
- Figure 4.7 The impact of laser power and pulse frequency on LBMM pilot hole entry area. (a) Scanning was 50 mm/s. (b) 500 mm/s scanning speed. (c) Scanning speed was 950 mm/s. (d) 1400 mm/s scanning speed. All examples had 75 loops. The error bar represents overall uncertainty 77
- Figure 4.8 The SEM pictures of the LBMMed holes' entry region created with various incident laser powers. There are four different laser power levels: (a) 6.4W, (b) 9.4W, (c) 12.5W, and (d) 15.5W. There were 75 loops, the scanning speed was 50 mm/s, and the laser pulse frequency was 5 kHz for every hole. Bar scale: 100 μ m. The entry area is marked with a black edge marker 78

Figure 4.9	The average impact of the laser scanning speed on the pilot hole entry area that the LBMM process machined. To plot this graph, all the data for each scanning speed have been averaged up	79
Figure 4.10	The effect of the incident laser power and pulse frequency on the exit area of the pilot holes made by the LBMM process. (a) scanning speed 50 mm/s. (b) scanning speed 500 mm/s. (c) scanning speed 950 mm/s. (d) scanning speed 1400mm/s. In every case, there were 75 loops. The error bar shows the overall uncertainty	80
Figure 4.11	The impact of the incident laser scanning speed on the exit area of the pilot holes made by the LBMM process. (a) scanning speed of 50 mm/s, (b) scanning speed 500 mm/s, (c) scanning speed 950 mm/s, and (d) scanning speed 1400 mm/s. All of the holes had a laser pulse frequency of 15 kHz, 75 loops, and 6.4W of incident laser power. Scale bar = 100 μ m	81
Figure 4.12	The relationship between average laser power and scanning speed and the amount of material removed by the LBMM process	82
Figure 4.13	The amount of laser power used to drill the pilot holes determines the average amount of tool wear and the number of short circuits that occur during the μ EDM process. (a) 50 mm/s scanning speed. b) 500 mm/s scanning speed. (c) 950 mm/s scanning speed. d) 1400 mm/s scanning speed. Each time, there were 75 loops total	84
Figure 4.14	Tool wear and short circuits in relation to μ EDM time. Tool wear versus μ EDM time (a). (b) EDM time versus short circuits. The experimental variation is displayed by the error bar	85
Figure 4.15	The relationship, as a function of laser incident power and laser scanning speed (used for pilot hole drilling using the LBMM process), between the average tool wear rate and the frequency of short circuits Tool wear rate (A) and short circuit occurrence rate (b)	86
Figure 4.16	LBMM- μ EDMed holes and pure μ EDMed holes are compared. Both holes show that there is no spatter zone left on the area around the holes. Scale bar = 100 μ m	88

Figure 4.17	The dual-stage ANN model's holistic performance for μ EDM machining time, machining instability (short circuit), and tool wear	91
Figure 4.18	Performance evaluations for the first-stage model, second-stage model, and overall performance are compared	92
Figure 4.19	Experimental and dual-stage ANN model comparison for a) μ EDM machining time, b) machining instability (short circuit/arc) count, and c) tool wear	93
Figure 4.20	Variation in the amount of time needed for μ EDM machining at different scanning speeds for LBMMed pre-machined holes at various laser powers. The data on the graph are experimental values, predicted values based on the parameters of the actual LBMMed holes, and estimates based on the parameters of the predicted LBMMed holes. The pre-machined holes were produced using 6.4 W, 9.4 W, 12.5 W, and 15.5 Watt laser-powers, respectively	96
Figure 4.21	μ EDM machining time with loop count Variation for LBMMed pre-machined holes machining at 11.9Watt laser-power, 400 mm/s Scanning Speed, and 10 kHz Pulse repetition rate. The data on the graph are experimental values, predicted values based on the parameters of the true LBMMed holes, and estimates based on the parameters of the predicted LBMMed holes	97
Figure 4.22	Effect of laser power and machining instability/arc frequency for pre-machined LBMMed holes at various scanning rates with a fixed loop count of 75. The graph shows experimental values, predicted values, and estimates based on the parameters of the true LBMMed holes: (a) 50 mm/s, (b) 500 mm/s, (c) 950 mm/s, and (d) 1400 mm/s	101
Figure 4.23	How Watt laser-power affects the rate of tool wear for pre machined holes produced by LBMM. The data on the graph are experimental values, predicted values based on the parameters of the true LBMMed holes, and estimates based on the parameters of the predicted LBMMed holes. The pre-machined holes were produced at different scanning speeds,	

	constant loop count of 75 including (a) 50 mm/s, (b) 500 mm/s, (c) 950 mm/s, and (d) 1400 mm/s	103
Figure 4.24	How loop count affect machining instability (short circuit/arcing) rate and rate of tool wear for LBMMed pilot holes. The data on the graph comes from experiments, predictions based on the parameters of real LBMMed holes, and estimates based on predictions of the parameters of LBMMed holes. The graphs show how the (a) rate of machining instability (short circuits/arcing) and (b) rate of tool wear change for pre-machined holes scanned at 400mm/s with a 10.66Watt laser-power & 10 KHz pulse repetition rate	104
Figure 4.25	Experimental and dual-stage ANN model comparison for the first-stage model, (a) volume removed, (b) HAZ, and (c) recast layer	107
Figure 4.26	Prediction accuracy of the first-stage model's four variables, including the volume removed, the HAZ, and the Recast layer	108
Figure 4.27	μ EDM machining time, machining instability (short circuit/arc) count, and tool wear prediction accuracy from the second-stage model	109
Figure 4.28	Experimental and dual-stage ANN model comparison for second-stage a) μ EDM machining time, b) short circuit/arcing count, and c) tool wear	110
Figure 4.29	The dual-stage ANN model's holistic performance for μ EDM machining time, short circuit/arcing count, and tool wear	112
Figure 4.30	Evaluation of the first-stage model, the second-stage model, and the overall efficiency	112
Figure 4.31	μ EDM machining time with LBBMed pre-machined holes at laser power 6.4 W and scanning speed 50 mm per second. The graph shows experimental, predicted, and estimated values from μ EDMed holes' parameters. The holes were machined at (a) 3 μ m EDM speed (b) 10 μ m EDM speed	114
Figure 4.32	Energy used for LBBMed pre-machined holes at scanning speed 1400 mm per second and EDM speed 3 μ m/sec affects μ EDM machining time. The graph shows experimental, predicted, and estimated values	

- from μ EDMed holes' parameters. Pre-machined LBMM holes at (a) 6.4 Watt laser-power and (b) 15.5 Watt laser-power 116
- Figure 4.33 μ EDM machining time for LBBMed pre-machined holes at laser power 6.4 W and EDM speed 3 μ m/sec. The graph shows experimental, predicted, and estimated values from μ EDMed holes' parameters. Pre-machined LBMM holes at (a) 50 mm per second scanning speed (b) 1400 mm per second scanning speed 117
- Figure 4.34 μ EDM Short circuit count with LBBMed pre-machined holes at laser power 6.4 W and scanning speed 50 mm per second. The graph shows experimental, predicted, and estimated values from μ EDMed holes' parameters. The holes were machined at (a) 3 μ m EDM speed (b) 10 μ m EDM speed 120
- Figure 4.35 Variation of μ EDM short circuit with energy used for LBBMed pre-machined holes at scanning speed 1400 mm per second and machining EDM speed 3 μ m/sec. The graph shows experimental, predicted, and estimated values from μ EDMed holes' parameters. Pre-machined LBMM holes (a) 6.4 Watt laser-power (b) 15.5 Watt laser-power 121
- Figure 4.36 μ EDM Short circuit for LBBMed pre-machined holes at laser power 6.4 W and EDM speed 3 μ m/sec. The graph shows experimental, predicted, and estimated values from μ EDMed holes' parameters. Pre-machined LBMM holes at (a) 50 mm per second scanning speed (b) 1400 mm per second scanning speed 122
- Figure 4.37 Variation of μ EDM Tool wear with Energy for pre-machined LBMMed holes machined with 6.4 Watt laser-power and 50 mm/s scanning speed. Experimental values predicted values from the actual μ EDMed holes' parameters and estimates from predicted EDMed holes' parameters comprise the graph's data. The holes were machined at EDM speeds of (a) 3 μ m and (b) 10 μ m 124
- Figure 4.38 Variation of μ EDM short circuit with energy used for LBBMed pre-machined holes at scanning speed 1400 mm per second and machining EDM speed 3 μ m/sec. The graph shows experimental, predicted, and

	estimated values from μ EDMed holes' parameters. Pre-machined LBMM holes at (a) 6.4 Watt laser-power (b) 15.5 Watt laser-power	125
Figure 4.39	μ EDM tool wear for LBBMed pre-machined holes at laser power 6.4 W and EDM speed 3 μ m/sec. The graph shows experimental, predicted, and estimated values from μ EDMed holes' parameters.	
	Pre-machined LBMM holes at (a) 50 mm per second scanning speed (b) 1400 mm per second scanning speed	126
Figure 4.40	Normal probability of residuals for μ EDM milling time	134
Figure 4.41	Plot of residuals versus predicted values for μ EDM milling time	136
Figure 4.42	Plot of residuals against run order for μ EDM milling time	137
Figure 4.43	3-D response surface plot for the μ EDM milling time (Power and Scanning speed effect)	138
Figure 4.44	3-D response surface plot for the μ EDM milling time (Loop and frequency effect)	139
Figure 4.45	Model competency (Actual Vs Predicted) for the μ EDM milling time	140
Figure 4.46	Normal probability of residuals for μ EDM milling tool wear	143
Figure 4.47	Plot of residuals against predicted values for μ EDM milling tool wear	144
Figure 4.48	Plot of residuals against run order for μ EDM milling tool wear	145
Figure 4.49	3-D response surface plot for the μ EDM milling tool wear (Power and scanning speed effect)	146
Figure 4.50	3-D response surface plot for the μ EDM milling tool wear (loop and frequency effect)	147
Figure 4.51	Actual Versus predicted data plot for μ EDM milling tool wear	148
Figure 4.52	Normal probability of residuals for μ EDM milling short circuit	151
Figure 4.53	Plot of residuals against predicted values for μ EDM milling short circuit	152
Figure 4.54	Plot of residuals against run order for μ EDM milling short circuit	153
Figure 4.55	3-D response surface plot for the μ EDM milling short circuit (Power and Scanning speed effect)	154
Figure 4.56	3-D response surface plot for the μ EDM milling short circuit (frequency and loop effect)	155

Figure 4.57 Scattered plots of predicted against the actual values for μ EDM milling short circuit



LIST OF ABBREVIATIONS

ANFIS	Adaptive neuro fuzzy inference system
ANN	Artificial Neural Network
ANOVA	Analysis of variance
BPNN	Backpropagation Neural Network
CNC	Computer Numerical Control
DoE	Design of Experiment
DW	Direct Write
ECDM	Electro-chemical discharge machining
ECM	Electrochemical machining
ECSM	Electrochemical spark machining
ED	Electro discharge
EDAG	Electrical discharge abrasive grinding
EDM	Electrical discharge machining
EMM	Electrochemical micromachining
f	Frequency
FEM	Finite element method
GA	Genetic Algorithm
GFRP	Glass fiber reinforced polymer
GUI	Graphical user interface
JECM	Jet electrochemical machining
LAJECM	Laser-assisted jet electrochemical machining

1-D	One-dimensional
2D	Two-dimensional
3D	Three-dimensional
LM-ECM	A hybrid micromachining method combining LBMM and EMM
MEMS	Micro-electromechanical systems
MIMO	Multi-input multi-output
MRR	Material Removal Rate
MSE	Mean Squared Error
Nd:YAG	Neodymium-doped Yttrium Aluminium garnet
OC	Overcut
OMM	On-machine measurement
P	Power
PMMA	Poly(methyl methacrylate)
PSO	Particle Swarm Optimization
R	Correlation coefficient
Ra	Average surface roughness
RBNN	Radial Basis Neural Network
RC	Resistor–capacitor
ReLu	Rectified linear activation unit
RMSE	Root Mean Squared Error
RSM	Response surface methodology
Ry	Maximum peak-to-valley roughness height
SEM	Scanning Electron Microscope

SS304	Stainless Steel
TWR	Tool wear rate
VRR	Volume removal rate
μ -EDM	Micro-electro discharge machining



LIST OF SYMBOLS

fs	Femtosecond
Hz	Hertz
J/cm ²	Jule per centimeter square
kg/cm ²	Kilogram per centimeter square
kHz	Kilohertz
mm	Milimeter
mm/s	Millimeter per second
mm ²	Millimeter square
ms	Millisecond
mins	Minutes
nF	Nanofarad
nm	Nanometer
ns	Nanosecond
nos	Numbers
s	Seconds
Ti ₆ Al ₄ V	Titanium alloy
TiAlN	Titanium aluminium nitride
V	Volts
W	Watt
W/cm ²	Watt per centimeter square

μg	Microgram
μm	Micrometer
μm	Micro-meter
$\mu\text{m/s}$	Micrometer per second
CO_2	Carbon dioxide



CHAPTER ONE

INTRODUCTION

1.1 BACKGROUND OF STUDY

In many areas, including the medical, automotive, biotechnology, and electronics industries, the application of micro-parts and parts with micro-features has become essential. Microsystem-based products have been emphasized as key value-added components for many industrial sectors and as significant suppliers to a sustainable economy (Kibria Bhattacharyya J Paulo Davim Editors, 2017). The capabilities of micro-manufacturing processes must constantly be improved in order to create the necessary micro-products affordably and consistently. This is necessary to keep up with the growing sophistication of micro-component design. Thus, micromachining research targets to improve current methods and develop new ones to meet future micromanufacturing needs such as components for lab-on-chips, fluidic graphite channels for fuel cell applications, long microchannels, shape memory alloy "stents," high-precision equipment, advanced communication technology components, and more (Debnath et al., 2017).

The MEMS technologies, such as photolithography on a silicon substrate, use the earliest micro-machining techniques. The methods employed, however, are only suitable for a small number of working materials and can only be used to fabricate quasi-three-dimensional shapes with low aspect ratios (Ahmad Athif Mohd Faudzi, Yaser Sabzehmeidani, 2020). The use of conventional material removal techniques like drilling, milling, grinding, and turning for micro-machining has developed as a response to the limitations of MEMS-based machining processes (Koç & Özel, 2011). In addition to

creating holes using micro drilling and cylindrical shapes using micro turning, complex three-dimensional structures, and profiles are also created using micro milling and micro grinding techniques. Although the adoption of conventional machining techniques increased machining versatility compared to MEMS-based techniques, conventional machining techniques also have drawbacks. The fabrication of micro parts with more complex structures and lower rigidity is typical, and problems with machining progressive materials with extreme hardness, chemical mismatch of the workpiece and cutting tool materials, and issues with rigidity are common (N. Kumar et al., 2020). Using unconventional machining methods for micro-machining is one way to overcome these constraints.

Ultrasonic machining (USM), focused ion beam machining (FIBM), focused laser beam machining (LBM) (Gujrathi et al., 2021), and electrical discharge machining (EDM) (Y. Li et al., 2016) are a few of these methods. Each of these methods has distinct process qualities that help them excel at particular micro-machining operations. For instance, USM is a mechanical machining technique that works best with brittle and hard materials because the material is removed through mechanical abrasion. Micromachining is to be categorized into two groups broadly as tool-based and Beam-based micromachining. Laser, ion, photolithography, and electron beam micromachining are examples of beam-based techniques. On the other hand, tool-based micromachining uses processes like micro-milling, micro-electrochemical machining, and micro-electro-discharge machining (Chavoshi & Luo, 2015). The gap between the macro and microdomains has already been shown to be closed by micromachining, which has successfully produced intricate 2D and 3D microstructures on a span of engineering materials with great accuracy and precision.

In recent years, laser micromachining has drawn significant attention for various engineering products. Modern biomedical technology uses LBMM (Laser Beam Micro-Machining) to create microfluidic passageways, MEMS, and a variety of other devices like catheters and stents (Miller et al., 2009). It is a part of the beam-based micromachining subfield. By melting and vaporizing the material with a laser beam that is focused, LBD (Laser Beam Drilling) removes the material. The LBD process has advantages for its applicability of wider range of materials as well as its faster processing time. On the other hand, low circularity, recast layer, heat-affected zone (HAZ), and taper are potential flaws in one-dimensional laser beam drilling (LBD) holes. The μ EDM method is rid of chatter effect, vibration-related, and mechanical stress problems because of its built-in noncontact material elimination mechanism. Micro EDM is primarily an electrothermal process that makes use of repeated numerous electric sparks to remove materials from conductive workpiece of any hardness (Nadda & Nirala, 2020). Additionally, μ EDMed surfaces have virtually no HAZ compared to LBMMed surfaces. However, μ EDM has a number of shortcomings. The significant flaw is that it has a low material removal rate (MRR). In addition to poor MRR, certain spark gaps and tool wear also restrain the quality of attributes produced by μ EDM.

In a hybrid micromachining technique, the advantages and drawbacks of both LBMM and μ EDM techniques can be balanced out by applying them in turn. Prior research has focused on sequential micromachining using laser- μ EDM (Al-Ahmari et al., 2016). In the past, researchers looked into a combined nanosecond pulsed laser and EDM micromachining method for holes and microstructures (Kim et al., 2010). Other researchers have also reported on a micromachining technique for making a fuel nozzle that is based on laser-

μ EDM. According to L. Li et al. (2006) the projected method reduced drilling time and cost by 70% and 42%, respectively. In comparison to pure μ EDM drilling, the production rate was also developed by 90% while preserving the hole feature as good as pure μ EDM. A little research has been conducted on how the LBMM input parameters affect the overall presentation of the sequential method but the overall performance of LBMM and μ EDM input parameters effect not described in the form of ANN based modeling.

The output parameters of both LBMM and μ EDM are directly impacted by the input parameters and machining circumstances. The ability to develop a model among the input and output of the machining procedure is obviously of great interest to the researchers. Researchers have created and used a wide range of strategies to mathematically model various response parameters of LBMM and μ EDM Modelling approaches have been initiated through the application of various analytical and numerical methods. In current years, models based on artificial neural networks (ANN) have been successfully used to predict the output factors of both the LBMM and the μ EDM separately. ANNs have formerly demonstrated their capacity to be effective estimators of stochastic and deterministic processes. To achieve the desired performance, however, it is imperative to investigate the correlation between the input and output for the LBMM- μ EDM based hybrid micro-drilling and micro-milling process. In this study, during the micro drilling process, the impact of LBMM input parameters on the output execution of micro EDM was measured while the EDM input parameters were constant. Secondly, LBMM input parameters were altered while the EDM input parameters remained unchanged. Laser Power, Scanning Speed, and Loop Count have been selected as the LBMM input parameters. The modelling of the LBMM- μ EDM process was carried out in two phases. In

the first phase LBMM input parameters were varied to predict the LBMMed pits characteristic parameters such as (entry and exit areas, HAZ and recast layer areas). Then these characteristic parameters were used to model the μ EDMs output parameters such as machining time, stability, and tool wear. In this phase of the model the μ EDM input control parameters were kept constant. In the second phase of the modelling of the LBMM- μ EDM based micro-drilling μ EDM input control parameters were also varied.

Lastly in this research work, 3-D hybrid micromachining (milling) was tested using RSM to detect the effect of input parameters of laser beam micro milling (scanning speed, power, frequency, and loops) on the output responses of micro EDM milling. Stainless steel (0.2 mm for micro-drilling and 0.5 mm for micro-milling) was the material chosen for the experiment.

1.2 PROBLEM STATEMENT

Micromachining is widely used now a days due to the high demand of product miniaturization. In hybrid machining technology, the integration of diverse machining methods is employed to capitalize on the distinct advantages offered by each technique. LBMM and Micro Electro discharge Machining (μ EDM) can be effectively combined to enhance machining performance. While LBMM is known for its swift machining process, it often falls short in delivering high-quality output due to issues such as the Heat Affected Zone (HAZ) and recast layer. On the other hand, μ EDM excels in producing features with superior quality but suffers from a considerably slow machining rate. To address this challenge, a sequential hybridization of LBMM and μ EDM is employed to leverage the strengths of both processes. In the LBMM- μ EDM based hybrid micromachining process,

an initial microfeature is generated by the LBMM process, followed by the fine finishing of the LBMMed feature through μ EDM.

Previous studies have explored LBMM- μ EDM based sequential hybrid drilling, recognizing its apparent advantages (L. Li et al., 2016). However, limited research has been conducted on understanding how the input parameters of LBMM impact the output performance of the sequential process. This aspect is crucial for extracting optimal results from the LBMM- μ EDM sequential process. Furthermore, our literature survey, as discussed in the following chapter, indicates a lack of significant research on mathematical modeling that correlates the process input parameters with various performance indicators. This gap in knowledge underscores the need for further exploration and analysis in order to enhance the understanding and optimization of the LBMM- μ EDM hybrid machining process. This research aims to address this research problem of the LBMM- μ EDM based sequential hybrid micromachining.

1.3 RESEARCH PHILOSOPHY

Laser micromachining is predominantly a thermal machining process, which causes a tapered hole, increases the recast layer, and dominant heat-affected zone, and reduces the circularity, but the machining process is very fast and higher material removal rate. However, micro EDM is the machining process, which is an electro thermal process and creates a momentary spark between the electrode and workpiece that remove material from the surface. The machining performance of micro EDM is very slow and a fine finishing product is produced but HAZ, Taperness angle, Circularity, and Overcut are negligible. The assimilation of the above two processes could be the way of obtaining superior quality products with high production rates. A mathematical model could be developed to optimize

and validate the objective function. Figure 1.1 shows the concept of hybrid micromachining. In this method harsh machining could be conducted out by laser and finish machining could be done using μ EDM. Both machining should be performed in a single machine or sequential machining to eliminate workpiece setup error.

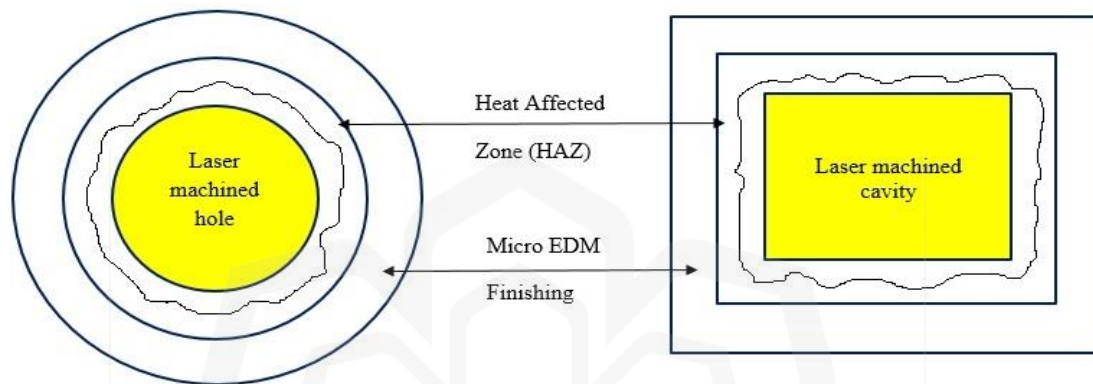


Figure 1.1 Perception of Laser- μ EDM hybrid micromachining

1.4 RESEARCH OBJECTIVES

The aim of this study is to make a mutual hybrid micromachining model for LBMM- μ EDM based that can be used as a framework for hybrid micromachining. To reach the main goals, the following objectives need to be determined.

1. To experimentally examine the Laser- μ -EDM based hybrid micromachining (micro drilling and micro milling) process on stainless steel (SUS 304) in terms of various performance indicators such as Machining time, Tool wear, Machining instability/short circuit count.

2. To develop a mathematical model for hybrid micro drilling describing the relationship between the primary processes' (LBMM) input parameters and secondary process's (μ EDM) output parameters.

3. To develop a mathematical model for hybrid micro milling describing the affiliation between the primary processes (LBMM) input parameters and the secondary processes (μ EDM) output parameters.

1.5 SIGNIFICANCE OF THE STUDY

Previous researchers have investigated sequential hybrid micromachining using LBM and micro EDM machining. However, it is still unclear how various laser parameters and μ EDM parameters affect overall process performance. The significance of this study is that it investigates how various laser and μ EDM parameters contribute to the overall performance of the hybrid process. Also, an experimental model has been established to mathematically formulate the process performance as a function of several parameters from laser and μ EDM.

1.6 SCOPE OF THE STUDY

The scope of the research is limited to the workpiece material austenitic stainless steel (SUS 304) as this is one of the most widely used engineering materials. However, the result can be still qualitatively extended for other metallic materials. The rectangular dimension of the workpiece is 22.5×22.5 mm which is suitable for the fixture available for the machines. The thickness of the material was not varied and was kept fixed at 0.2mm. The laser that was used for this study was a nanosecond pulsed fiber laser with a rated average power of 20W. The EDM power supply was an RC type where the open circuit voltage and capacitor can be varied for different discharge energy. The modeling approach was based on experimental modeling because of the stochastic nature of the μ EDM process where empirical modeling is the most suitable approach.

1.7 RESEARCH METHODOLOGY

The experimental analysis and modeling of the sequential laser- μ EDM micro-drilling and micro-milling of stainless steel are the main topics of this study. Furthermore, a unique dual-stage model was employed which is ANN based model has been used for creating the extrapolative model. It divides the representation of the sequential process' input and output factors into two stages. The approach taken to achieve each goal of the suggested project is described in the section that follows.

LBMM micro-drilling comes first in the order of events. A fiber laser setup was used to prepare the stainless-steel workpiece and create the micro holes on the workpiece. The component that scans through the workpiece surface to imitate the circular microhole structure is the X/Y galvanometer. First, the scanning path is tracked horizontally, then it is traced vertically, and finally, it is traced horizontally in the opposite direction. For even more precise machining, the μ EDM finishing operation was performed after the LBMM machining (Figure 1.2). A coordinate tracking technique based on a microscope and camera was developed in order to accurately middle the tool of the μ EDM instrument on the middle of the LBMMed hole.

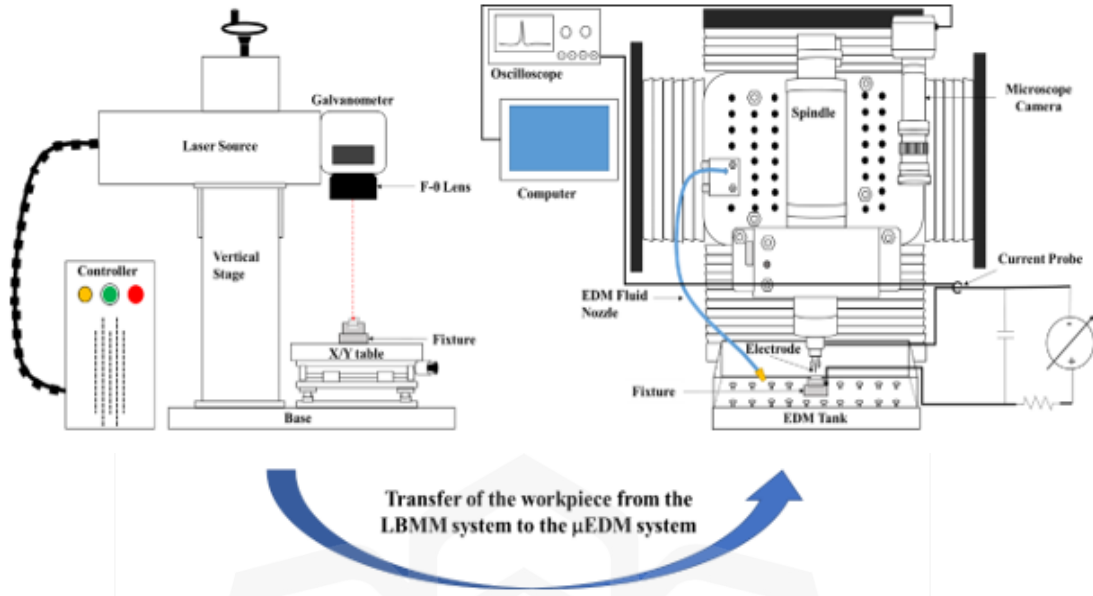


Figure 1.2 Figure of LBMM- μ EDM Process Explaining its Operational based Sequential Process (Rashid et al., 2021)

LBMM machining time, its variable like loop count, scanning speed, pulse repetition rate and laser power can be changed. To determine how they affected the sequential process' output parameters, all of these variables were modified. Four outcomes of the LBMM method were examined for this research (Entry Area, Exit Area, Haz Area, and Recast Area). The amount of tool wear, the machining instability (short circuits/arc) count, and the μ EDM machining time were selected as the performance parameters. The μ EDM input strictures were held persistent so that the effect of the LBMM input constraints on the μ EDM performance parameters could be studied. Output parameters were determined using SEM and ImageJ tool. The dataset for the drilling process, which contained all the input and performance parameters, was created after the characterization was complete. A correlation analysis was done on this dataset to determine the relevant process parameters for the experiment and modeling. The study found a significant correlation among the LBMM output parameters and the μ EDM performance parameters. An ANN modelling

approach was adopted to model the LBMM- μ EDM based microdrilling operation. Scatterplots of the numerous input and output factors were used to support the correlation study in further detail. The nonlinear relationship between the various LBMM inputs and μ EDM outputs was also made clear by the scatterplots.

Finally, a sequential LBMM- μ EDM hybrid micro-milling was carried out based on RSM (response surface methodology) to identify the most significant factors influencing this sequential hybrid micro-milling. It was found that laser milling input parameters (scanning speed, power, frequency, and loops) affecting significantly on the output responses of μ EDM machining time and tool wear. The study's overall methodology (flowchart) and the necessary steps to meet the goals are displayed in Figure 1.3.

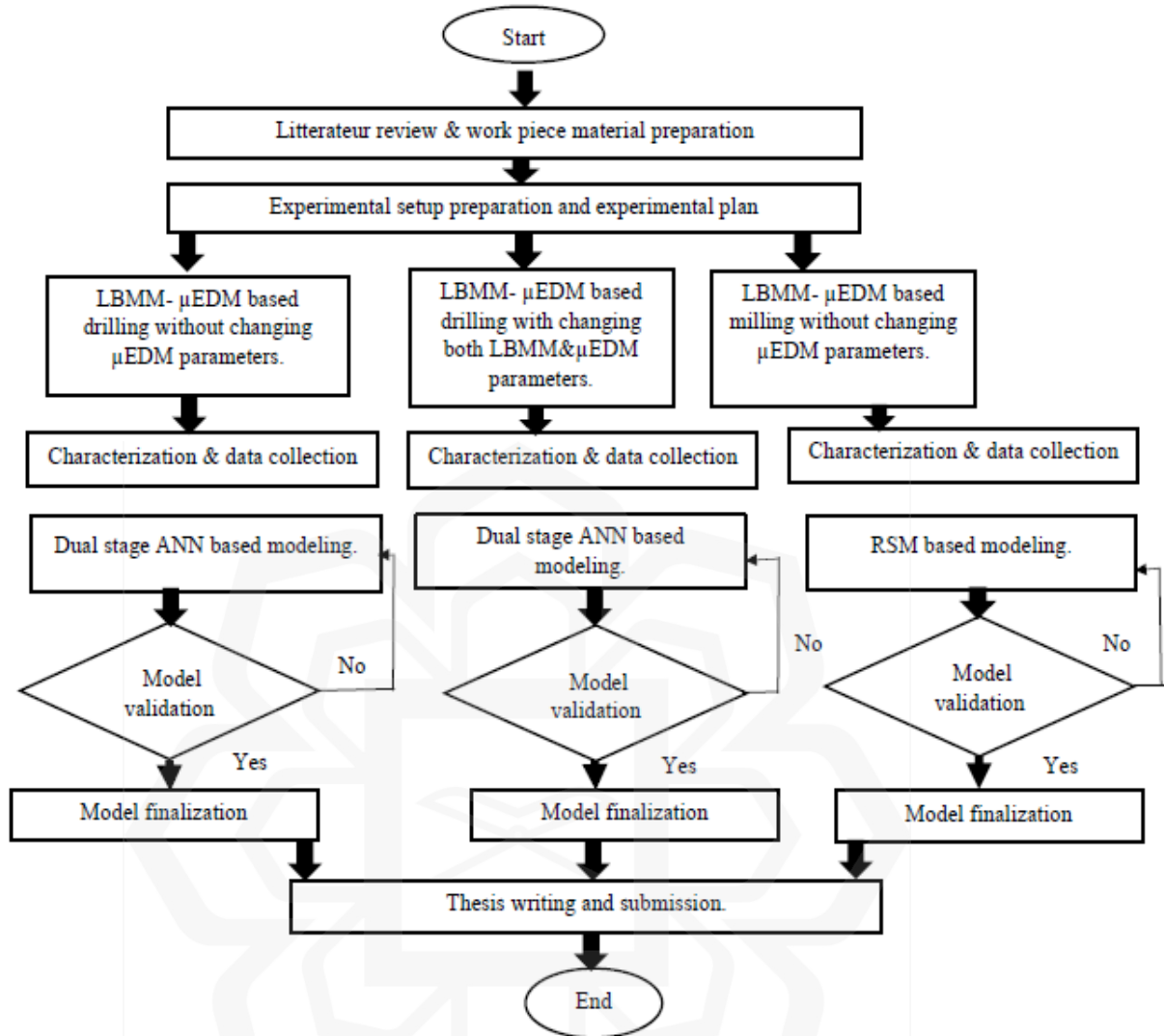


Figure 1.3 Flowchart of the whole research work

1.8 THESIS ARRANGEMENT

This research thesis is split into five chapters. The core points of each chapter are summarized below.

In the first chapter, there is an introduction that explains the general point of view of the thesis. It talks about the history of the research, the problem statement, research objectives, philosophy, methods, and scope.

Chapter Two comprises a thorough literature study on various aspects of Laser Beam Micromachining (LBMM), Micro Electro Discharge Machining (μ EDM), Hybrid Micromachining, LBMM & μ EDM based Hybrid Micromachining, and Experimental modeling techniques used for micromachining have been surveyed in this chapter.

Chapter three describes the overall methodology of this research. The chapter includes various machining parameters and an experimental plan for the study of the LBMM-micro EDM process. Also, the methodology of various characterization of the samples has been discussed in this chapter. The experimental plan with modeling of the LBMM-micro EDM drilling and milling has been discussed too.

Chapter four talks about the results and gives a summary. It also talks about how the parameters of the laser affect sequential laser beam micromachining and micro electro-discharge machining. The chapter also has discussed various results related to the empirical modelling of the proposed LBMM- μ EDM combined sequential hybrid process. Finally, the chapter has been concluded with a treatise and gist of the findings.

Chapter five lists the endings regarding the investigational results. This chapter details the suggestions for future work and the foremost impacts of this research.

CHAPTER TWO

LITERATURE REVIEW

2.1 INTRODUCTION

This chapter presents a literature review of LBMM and μ EDM as a method of hybrid micromachining. This chapter will cover a few sections: 1. Basics principles of LBMM and μ EDM, 2. Comparison between LBMM and μ EDM, 3. Hybrid micromachining based on LBMM- μ EDM, and 4. Review of experimental modeling techniques used for micromachining. Finally, the conclusion of the literature review will draw the research gap.

2.2 LASER BEAM MICROMACHINING (LBMM)

Laser beam micromachining has become very popular in modern times due to its numerous excellent features, such as non-interaction and wear-less machining, improved tractability, and the potential for a elevated degree of mechanization, etc. It is acting as a versatile fabrication process. As a result, laser beam micromachining is frequently used to create tiny components of different metals, ceramics, and polymers for use in the automotive and medical industries, among other fields. Semiconductors and solar cells are also made using an LBMM process (Zhu et al., 2013). Lasers beam micromachining have a wide range of pulse durations, from femtoseconds to microseconds, a range of wavelengths, and discrete pulse repetition rates, from one pulse per second to millions of pulses per second. This makes it possible to make micromachined parts that are complex and have a high aspect ratio. In micromanufacturing, the laser beam micromachining method is used to eliminate material by quickly heating, melting, and evaporating it. This is done in areas like cutting, drilling, milling, welding, and surface texturing. Also, using lasers with very short pulse

durations can reduce some of the bad effects of LBMM such as heat affected zone (HAZ), such as recast burr formation, and so on, during micromachining.

2.2.1 Basic Principle of Laser Beam Micromachining (LBMM)

The LBMM is applied to eliminate material from the workpiece through the process of thermal ablation (Mishra & Yadava, 2015). A typical setup for laser micromachining includes a number of components (Figure 2.1), similar to those found on CNC machine tools. It is equipped with a central computer that can control and move the stages, as well as position the workpiece at the precise focal point. During the machining process, the controller also has the ability to adjust the pulse and pause the laser pulses as needed.

The power from the laser beam is absorbed and converted to heat when it is focused on the work surface. While the absorptivity of any substance depends on its optical property, the effectivity of the laser-based machining increases with an increase in absorptivity. Light couples with the workpiece's free electrons when it comes into contact with metal; this process rests on the conversion of photonic energy to electron vibrational energy (Dubey & Yadava, 2008b; Faisal et al., 2019). The atoms are knocked out when the excited electrons begin to collide with nearby atoms. The knocked-off atoms go through the same process again, which causes an extreme temperature increase that conducts and creates a temperature distribution. Strong absorbers will melt and vaporize at high temperatures, which will result in thermal excision. If the material has a low absorptivity, the combining will also be very low, and the temperature won't rise enough to remove the material. The vaporization rate is significantly influenced by the power density during machining (Richa Agrawal, 2016). A shockwave is produced if the vaporization rate is high enough. After the laser pulse, the pressure of the shockwave accelerates the ejection of the molten metal.

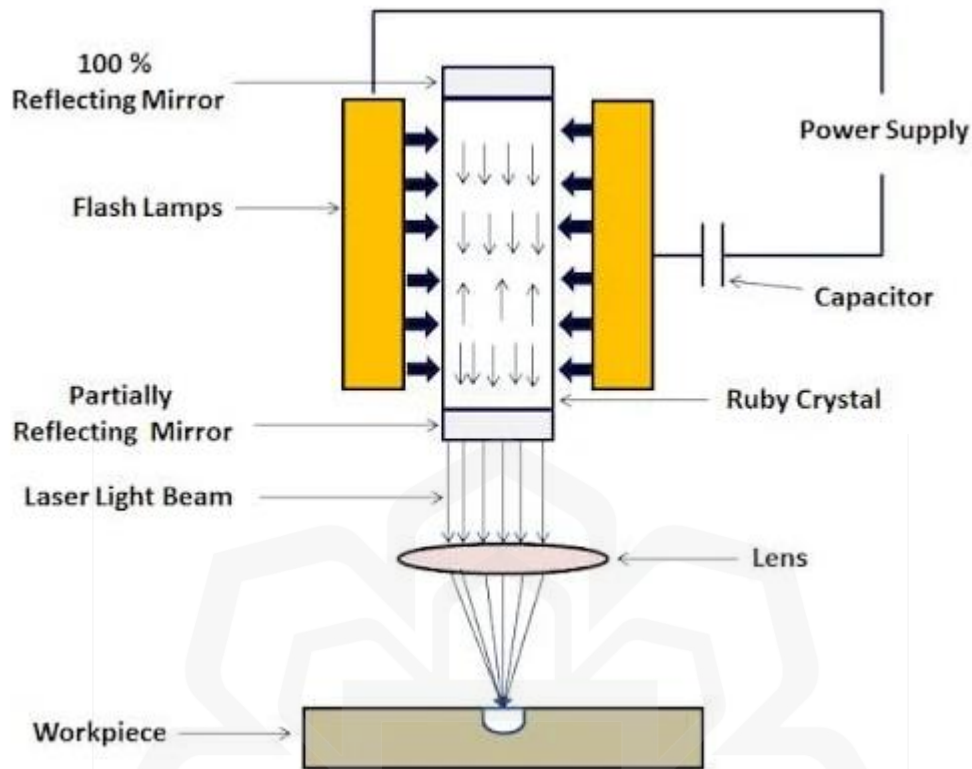


Figure 2.1: Figure Schematic diagram of laser beam micromachining (E. A. Kumar, 2022)

2.2.2 Recent Research on Laser Beam Micromachining (LBMM)

Nowadays, heavy equipment, aerospace, marine, chemical, and automotive industries use laser beam micro drilling because of its high operating rate, flexibility, machining speed, precision, repeatability, and duplicability. Tissue engineering for biochips utilizing laser-based micro/nano machining (Gautam & Pandey, 2018).

Laser beam micromachining is performed in three definite ways. In the first step of direct writing, the workpiece is moved comparative to a fixed laser beam, or it is scanned while the workpiece remains fixed, to create the desired microfeatures. In the case of the mask projection technique, a different approach is taken to create features on the workpiece. To

achieve the desired workpiece shape, a mask is patterned and then illuminated by a laser that has been shaped and homogenized to ensure that the laser's intensity is distributed uniformly across the mask's exposed area. The pattern is then estimated using a projection lens onto the work surface. In the interference technique, a beam splitter splits a laser beam and super-positions it to create interference patterns. Because of the distinctive intensity variation in these interference patterns, the work surface can be periodically micro-machined. Thermal ablation is a very helpful technique for removing material from metal and ceramics when better ablation efficiency requires maintaining tinier thermal diffusivity and greater values of the incorporation coefficient (Hocheng et al., 2014).

Paul et al. (2020) examined laser micromachining efficiency. It emphasizes industrial short-pulse laser system adaptability. They excel at drilling and cutting ceramics and metals. Ablation is irradiating evaporation and melt expulsion, according to Dubey & Yadava (2008b). Molding these conditions allows high-quality micro-level drilling and cutting (Faisal et al., 2019). Short pulse lasers intensify surface targets and raise material properties to significant limits. Raj et al. (2019) used laser micromachining to metalize microfluidic polymer stacks. Laser micromachining creates polymeric layers that stick metal foils together. Laser machining with polymers without chemical additives was shown in their study. R.P. Patel, (2014) investigated laser micromachining for cutting aluminum-based alloys. Faisal et al. (2019) reported finite element modelling (FEM) to build elemental models of laser micromachining of the micro electromechanical system (MEMS). Their research could help the laser micromachining process to replace conventional machining. (Prakash & Kumar, 2015) also studied laser processing for micro-component development.

Their work on short pulsed lasers, micro, nanosecond, and ultrafast lasers expanded the use of laser in micromachining more efficiently.

Sen et al. (2014) investigated various parametric effects on groove geometry, including depth, surface roughness, and width, for fiber laser machining where the workpiece material was Ti-6Al-4V of 0.11 cm depth. Ti-6Al-4V is often used for hip and dental fittings because it is not harmful to bodies, protects against corrosion, is biocompatible, doesn't wear out easily, and doesn't cause inflammation. Different process parameters, like the amount of passes (1–8), scanning speed (40–1000 mm/s), and pulse frequency, are used to examine the effect of miniaturized scale grooves on their parameters (50–100 kHz), and normal power utilization (2.5–30 W). Faisal et al. (2019) reported a low-cost, high-quality laser micromachining method for waveguide structures with a pulse repetition rate up to 10 KHz. This process can machine waveguide components of different heights and widths to 1 μm accuracy as the researchers demonstrated. Fiber lasers are being used by numerous industrial zones to cut, drill, and solder a variety of materials (Williams, 2014). Additionally, they are employed for micromachining, engraving, and even the processing of light films like indium tin oxide (Norman, 2010). For example, Borse & Kadam, (2018) used a fiber laser to carry out micro-milling operations in Inconel 718. LBMM micro milling was conducted to find out how scanning speed, power, and frequency affected the output responses of surface roughness, depth of cut, and material removal rate-based RSM. When optimized, the lowest surface roughness of 0.372 μm was achieved whenever the power percentage was 30%, pulse frequency 38 KHz, and scanning speed 990 mm per second. Fibre lasers can also machine non-metals. Hendow & Shakir (2010) machined silicon with a 10 ns fibre laser. Cutting, drilling, and scribing were examined.

Mishra & Yadava (2015) reviewed laser beam micromachining (LBMM). An synopsis is provided to understand LBMM's current capabilities and constraints. Nano, Pico, and femtosecond-based laser machining studies have been carried out. LBMM process parameters have been explained. Shalahim et al. (2010) used a FEM simulation to model laser micromachining of acrylic material to create edges without flaws in a short amount of time. The right material model, temperature characteristics of the material being processed, and mesh design in FEM modeling were discovered from the simulation results. The boundary condition and material model significantly affected the simulated results.

Förster et al. (2021) discuss short-pulse laser system functions. It's easy setting up, reasonable cost, and high productivity make it widely applicable. Drilling, cutting, and material removal are some of the examples where a short pulse laser system can be used. Gower (2000) discussed industrial laser machining. Several industries use pulsed lasers for micro via, pipe hole drilling, and ink jet printer nozzles. Laser machining accuracy and effectiveness are studied in various fields. Laser—polymer interaction can cause photothermal or photochemical ablation or laser micromachining. Both photothermal and photochemical removal systems are capable of producing the laser micromachining or excision phenomenon during laser—polymer relationship. Thus, the exclusion system is a combination of photochemical and photothermal actions, as polymers show strong absorption in ultraviolet infrared wavelengths but weak captivation at visible and nearly-infrared spectra In photothermal removal, the polymer is rapidly liquefied and vaporized, while the photon energy of the laser light breaks down the polymer's covalent bonds. For photochemical removal to occur, the intermolecular binding energies of the polymer must be greater than the power of the photons at that wavelength (Brown & Arnold, 2010).

The excimer laser can produce 308 and 248 nm of wavelength while utilizing the mixture of XeCl and KrF discretely. The frequency is modified over Nd: YAG lasers with a main wavelength of 1064 nm have third and fourth harmonic wavelengths of 355 and 266 nm, respectively (Dubey & Yadava, 2008a). Sharma & Yadava (2018) used a pulsed Nd: YAG laser beam to test the heat-affected zone (HAZ) on a 2.5 mm carbon fiber composite plate. Their study suggests that the HAZ increases with pulse width, energy, and frequency, and decreases with feed rate. They also observed that pressurized air-assisted laser machining results higher heat-affected zone, while argon has a smoother cut surface and a lower HAZ. Pulsed laser micromachining can be done in two different period ranges. The first is a long pulse, and the second is an ultra-fast or ultra-short pulse (Figure 2.2). In a long-pulse laser, the laser beam is focused inside a vacuum chamber onto a solid target that is to be deposited. This makes it easy for heat to spread to the surrounding area, which lowers the overall efficiency of machining. The machining zone's boiling of the work material scatters molten metal droplets. Heat dispersion creates a heat-affected zone near the machining zone's periphery, where heating and cooling waves propagate and cause thermal stress and micro cracks.

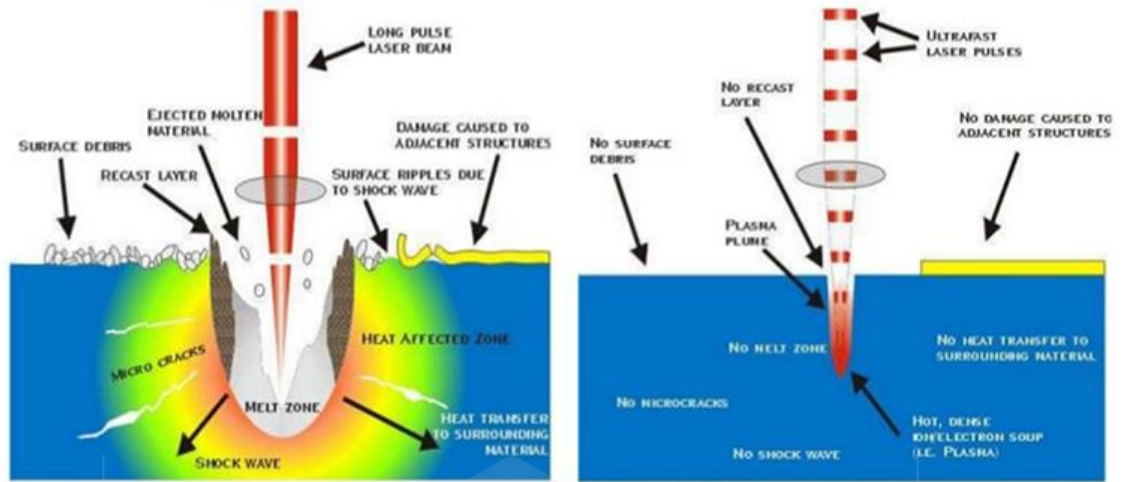


Figure 2.2: a) Long pulse b) Short pulse (Faisal et al., 2019)

However, nanosecond, picosecond, and femtosecond lasers have higher machining efficiency and better removal because the time between pulses is very short, entrapping the laser energy. nanosecond lasers and femtosecond lasers are two of the most recent and well-liked short-pulsed lasers. The mechanism of femtosecond and nanosecond laser ablation has been described by (L. Li et al., 2006). Figure 2.3 depicts how nanosecond laser ablation removes evaporated substance from the contact region inside 3-5 ns of each laser pulse hitting the surface, resulting in fast machining. Although holes can be quickly machined with nanosecond lasers, the resulting extreme heat-affected zone (HAZ), and recast layer are not favorable (X. Li & Guan, 2020). This is due to the fact that the material is almost entirely removed during the nanosecond machining following the thermal process. HAZ and recast layer are two unfavorable surface characteristics that must be eliminated to improve quality. Picosecond pulsed lasers are preferred because they produce less heat and do not create heat-affected zones.

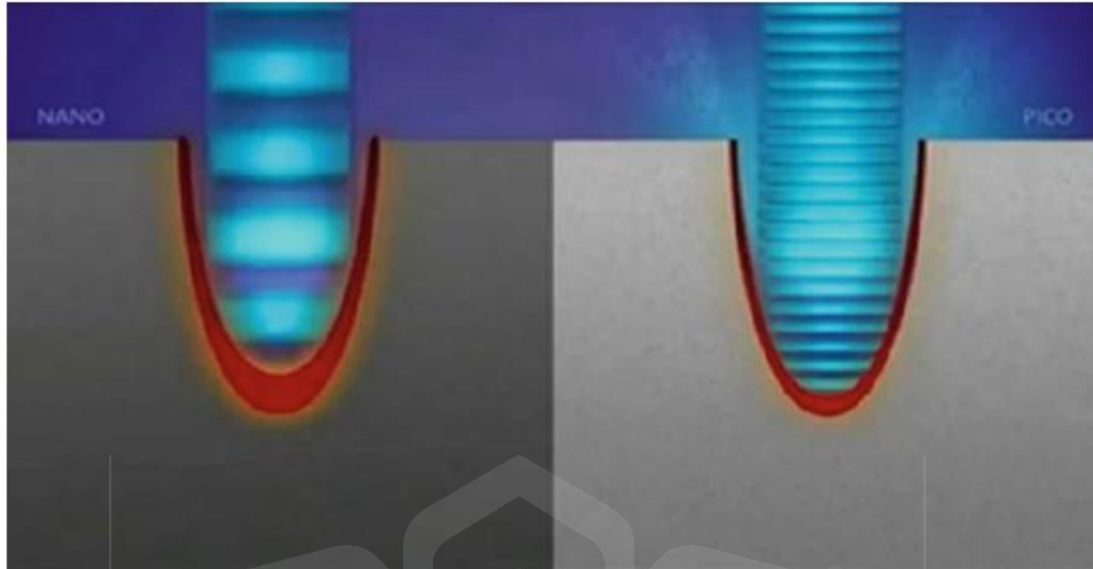


Figure 2.3: Advanced laser micromachining (Faisal et al., 2019)

Miniaturization in microelectronics means smaller features and holes, which require higher tolerances. Advance laser micromachining (Figure 2.3) is ideal for precision, consistency, faster throughput, higher yields, and lower manufacturing costs.

Femtosecond or ultrashort laser pulses improve hole quality and machining speed. Compared to nanosecond lasers, it has a shorter pulse breadth (10^{-15} s) and higher peak power (10^{13} – 10^{14} W/cm²). Femtosecond laser ablation produces high-quality work and precise components (Casalino et al., 2017). Laser micromachining allows precise and flexible material processing, according to Gujrathi et al. (2021), to automate etching and ablation, they researched on three process which is the step of artificial intelligence. Femtosecond is one of the super laser machining process of polyuria aerogels was described by Bian et al. (2011). Polyurea aerogel has excellent mechanical and thermal properties. Femtosecond lasers cut polyurea aerogel without contacting and minimizing collateral damage.

In comparison to nanosecond pulsed lasers, it has a much smaller pulse thickness (10–15 s) and a much higher peak power (10^{13} – 10^{14} W/cm²). Figure 2.4 demonstrates the acceptable accuracy and structural integrity that can be attained when using ultrashort laser technology to create micro-holes. However, the extremely high initial cost of ultrashort laser technology is one of its limitations (Russbueltd et al., 2016).

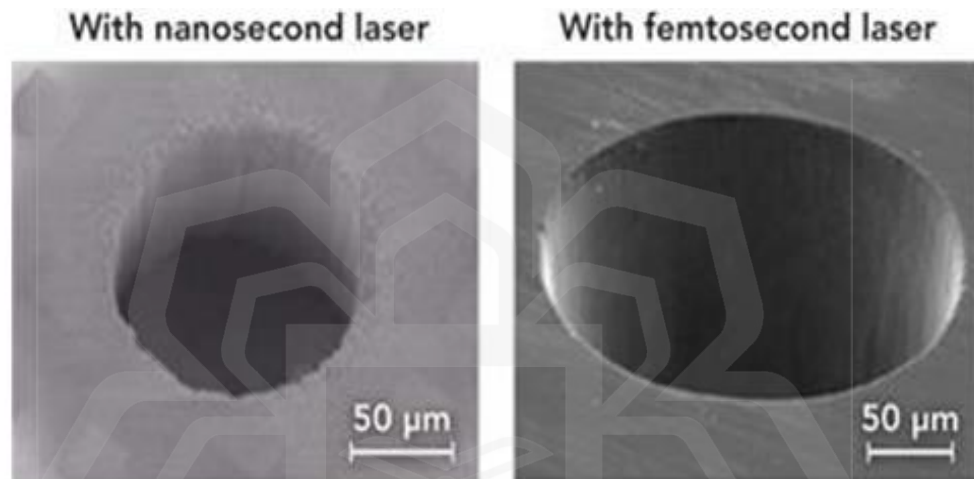


Figure 2.4: a) Nanosecond laser holes b) Femto second laser holes (Hamad, 2016)

2.3 MICRO ELECTRO DISCHARGE MACHINING (μ EDM)

Micro EDM is a variation of EDM where the produced features and used tools are in the size of sub-millimeter range. It is widely known as a nontraditional machining technique that plays a substantial role when the size of the feature is tiny, and the workpiece is difficult to machine (by conventional method) yet electrically conductive. Currently, micro EDM is widely utilized to manufacture complex components for the aircraft, automotive, MEMS, biomedical, and molds & dies sectors. It is an process which is operated electro-thermally that utilizes frequent and controlled sparks to erode conductive objects such as metals, metallic alloys, semiconductor wafers etc. with whatsoever mechanical hardness. As

compared to standard laser machined products, micro EDM can manufacture components with high quality (Al-Ahmari et al., 2016). In comparison to ultra-short pulse laser machining systems, it is also less expensive. However, micro EDM method has a much slower machining rate. There are typically two methods to complete the micro EDM procedure. Die sinking EDM is the name of the first method, which uses a 1-Dimensional motion of the EDM tool or die to leave the die's impression on the specimen. Die-sinking μ EDM is used, for instance, to make tiny holes for nozzles. The second method creates 3D micropatterns on the workpiece by scanning it in 3D motion with a cylindrical tool, similar to how traditional milling is done.

2.3.1 Basic Principle of micro–Electro Discharge Machining (μ EDM)

The μ EDM is a nontraditional way to the machine. It uses a sequence of electric sparks between two electrodes that are immersed in a dielectric fluid to remove electrically conductive material. Sparks from an electrical discharge are thought to be the main way that μ EDM removes material from the workpiece by melting and evaporating it (Rajurkar et al., 2006). Micro EDM has the following major advantages over traditional machining processes because of the way it removes material. Its schematic figure is shown in Figure 2.6

1. Able to cut materials that are challenging to work with as long as they are electrically conductive.
2. Deformation-free because the machining process uses no mechanical cutting force.
3. Capable of producing complicated 3D profiles with superior accuracy and high aspect ratios.

4. High surface quality and no burrs are present in the machined parts

Micro EDM is a necessary procedure in various industries, including die-making, automotive, aerospace, and medical devices, due to its significant advantages. The schematic for the widely used μ EDM process mechanism is shown in Figure 2.5. The gap amid the tool electrode and the workpiece electrode gets smaller as the energized tool electrode is fed toward the workpiece, and the electric field strength in the gap gets stronger. When the gap is less significant than a critical value, the high electric field strength breaks down the dielectric material. This is when a spark starts. After the spark starts, a channel of plasma starts to grow. During discharge, the material on both electrodes melts and evaporates in the plasma channel, which is hot and has a lot of pressure. The time of the discharge is controlled by the plus generator. After the discharge, the dielectric fluid washes away some of the melted and evaporated material, leaving craters on both electrodes and restoring the dielectric force. Because the objects properties and polarities are different, the workpiece wears away faster than the tool electrode. By repeating the discharge cycle, the workpiece is left with a surface profile that is a mirror image of the tool electrode.

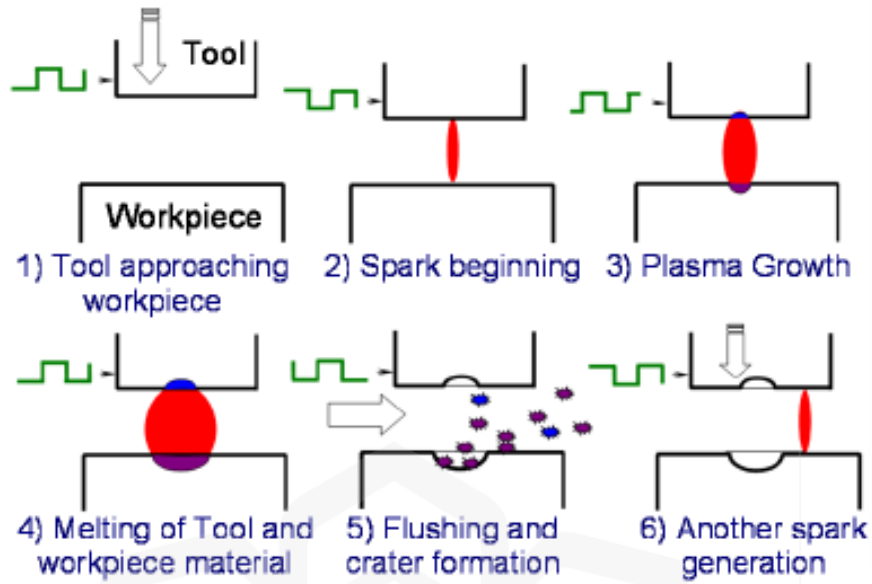


Figure 2.5: EDM process mechanism (M. K. Pradhan, 2010)

Die-sinking EDM, wire-EDM, EDM drilling, and EDM milling are examples of micro-EDMs, which are scaled-down versions of the corresponding EDM processes. Contrasted to macro EDM, the discharge energy of micro-EDM is very low, falling between 10^{-7} and 10^{-5} joules. Micro-EDM is able to form micro features because each pulse's unit material removal is decreased by minimized discharge energy. Micro-EDM has been used as a supplemental process in micro-hole drilling, intricate 3D machining, microtool machining, etc.

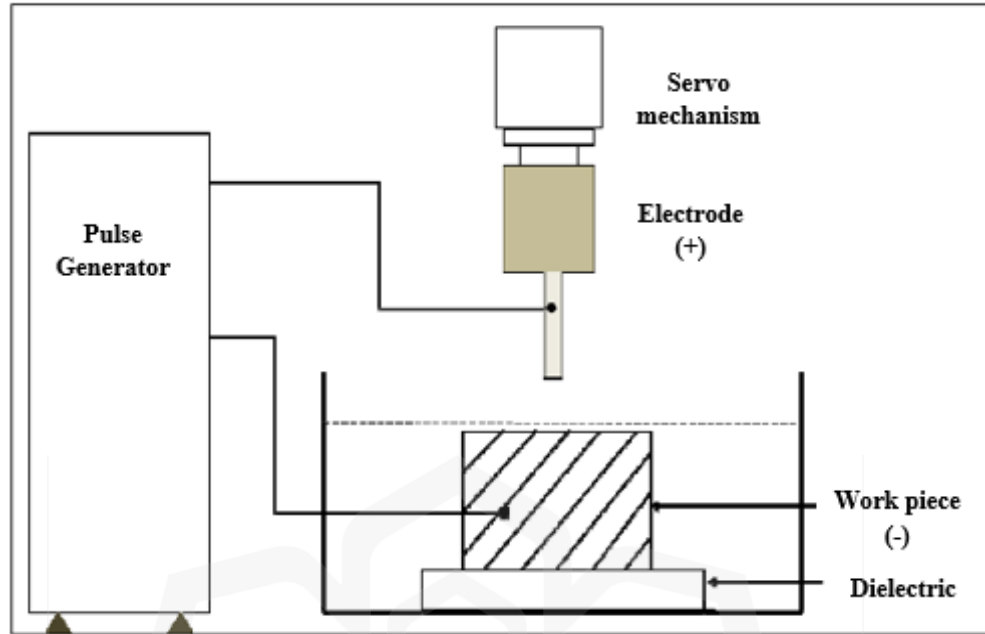


Figure 2.6: Basic principle of micro EDM Figure (Rajurkar et al., 2013)

2.3.2 Recent Research on Micro Electro Discharge Machining (μ EDM)

Micro-EDM study has gotten a lot of attention because of the trend toward making things smaller and because it can be used to make accurate micro-parts no matter how hard the workpiece is. Injection nozzles, spinneret holes for synthetic fibers, electrical and optical devices, micro-mechanical components, medical components, surgical instruments, and micro-tools are just some of the many examples of where micro-EDM has been put to use (Mahendran et al., 2010). Table 2.1 gives an overview of what can be done with micro-EDM.

Table 2.1 Overview of the micro-EDM capabilities (Liu et al., 2010)

Micro-EDM variant	Geometric complexity	Min.feature size (μm)	Min.aspect ratio	Surface qualityRa (μm)
WEDM	3D	3	~ 100	0.1-0.2
Die-Sinking	3D	~ 20	~ 15	0.005-0.3
Milling	3D	~ 20	10	0.2-1
Drilling	3D	5	~ 25	0.05-0.3
WEDG	3D	3	30	0.5

The most important step in the progression of the μEDM procedure was the introduction of Wire Electro-Discharge Grinding (WEDG) (Masuzawa et al., 1985). In WEDG, a metal wire serves as the electrode. This wire slides along a groove in a wire guide as the micro rods are machined in a manner analogous to grinding. The WEDG principle is depicted here in Figure 2.7. Because the problem of electrode wear is avoided to

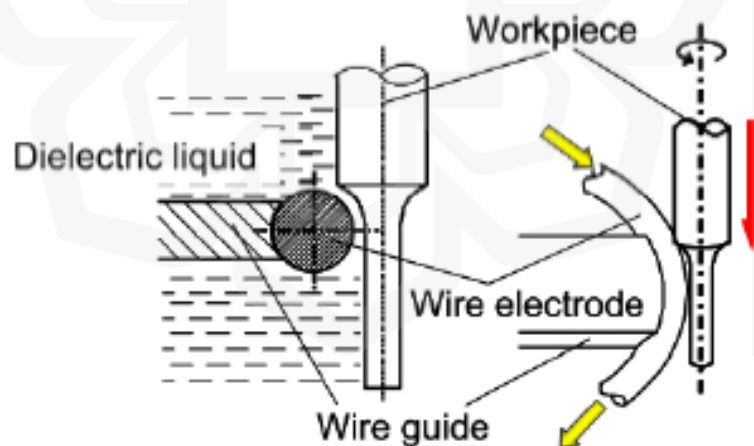


Figure 2.7: Wire Electro Discharge grinding (WEDG) method (Masuzawa et al., 1985)

the moving wire, the rod be able to be machined to a identical high degree of accuracy. In addition, it has been stated that the discharge energy can be decreased to produce a rod with

a diameter of only 1 micrometer (D'Urso et al., 2016). When it comes to organizing micro-pins and micro-spindles for micro-EDM, WEDG is the solution to the problem.

The tool position and machine coordinate will misalign if the tool is pre-machined and mounted. Thus, coordinate misalignment introduces a serious geometric error, especially in micromachining. WEDG is compact and machine integrable. WEDG allows on-machine tool making, minimizing coordinate misalignment-related machining errors. WEDG's machine's precise micro electrode allows high-precision micro-EDM (L. Zhang et al., 2015). The WEDG unit machines the rod, then reversing the polarity, it becomes a tool.

WEDG is enhanced by a sophisticated CNC controller, allowing for greater efficiency and effectiveness. Electrodes of many different shapes can be fabricated using this method. Further, WEDG is a great method for producing micro tools because it can machine any electrically conductive material, regardless of its stiffness, such as tungsten carbide. The results from using WEDG-machined tools for micro-drilling (Hasan et al., 2017), micro-milling (Wang et al., 2021), and micro-punching (Chern et al., 2006) have been extremely encouraging.

EDM milling uses a simple shape electrode and a CNC machine to create complex 3D geometry. In die-sinking EDM, it solves the issue of designing and fabricating complex electrodes. Sometimes it is difficult to machine the electrode for a micro die sinking EDM, especially at the micro level. As a result, micro-EDM milling is becoming increasingly popular in micromachining (Bissacco et al., 2010).

Micro-EDM milling is affected by high electrode wear due to geometric error and accuracy loss (Richard & Giandomenico, 2018). The Uniform Wear Method (UWM), which

accumulates longitudinal tool wear costs and a tool path-generating algorithm, improves micro-EDM milling precision (Bissacco et al., 2010). UWM contours layers with very small electrode feed. Only the electrode bottom is machined. After machining each layer, the electrode end is always flat. The to-and-fro scanning path also flattens the workpiece. UWM and CAD/CAM systems simplify tool path initiation. Micro-EDM milling is powerful for 3D micro-complex geometry (Zeng et al., 2012).

Other EDM techniques, including WEDM and EDM drilling, have also been effectively applied to the micro-scale. With the help of WEDG, very small electrodes can be machined for micro EDM drilling. It has been possible to machine holes with a 5 μm diameter. By lowering the wire diameter in WEDM from 200 μm to 250 μm to 10 μm to $\mu\text{50 m}$ (Masuzawa et al., 1997), micro-WEDM can be achieved.

2.4 COMPARISON BETWEEN LBMM AND MICRO EDM

The major drawback of μEDM is that it is a very time-consuming process compared to traditional methods, but Laser micromachining is a very rapid material removal process (Miller et al., 2009). It is also a microfabrication process, but the machining quality is significantly inferior to micro EDM. It generates a heat affected zone (HAZ) on the work piece material during hole formation (Jabbareh & Asadi, 2013). However, micro-electro-discharge machining (micro EDM) can fabricate higher-quality micro features without forming dominant HAZ zone. A hybrid technique that combines the benefits of micro EDM and LASER micromachining is necessary to address the issues raised by these two types of machining. In this hybrid machining process, the micro EDM operation will come after the rough machining is completed by the laser.

2.5 HYBRID MICROMACHINING

Hybrid micromachining procedures, which involve the amalgamation of two or more machining techniques, are gaining popularity among both manufacturers and academic researchers.

Hybrid machining processes do not have a clear definition (Zhu et al., 2013). A logical digit of definitions for hybrid machining processes have occasionally been put forth by researchers like (Shao & Rajurkar, 2015; Lauwers et al., 2014), etc. According to Aspinwall et al. (2001), the combination of machining operations can be conceptualized as either an assisted machining attempt, where two or more processes are used concurrently or as a hybrid machining approach, where two or more processes are applied independently on a single machine. Hybrid machines can carry out a variety of tasks, including mechanical milling and turning, all in one location. According to a strict definition provided by Curtis et al. (2009), a technique can only be referred to as a "hybrid" refers to the simultaneous use of two or more material removal processes. Hybrid machining procedures use the concurrent and measured interaction of machining mechanisms and energy sources to maximize performance, according to the 2014 definition by the CIRP collaborative working group on hybrid processes. Assisted and combined are two types of hybrid micro-machining methods (as shown in Figure 2.8)

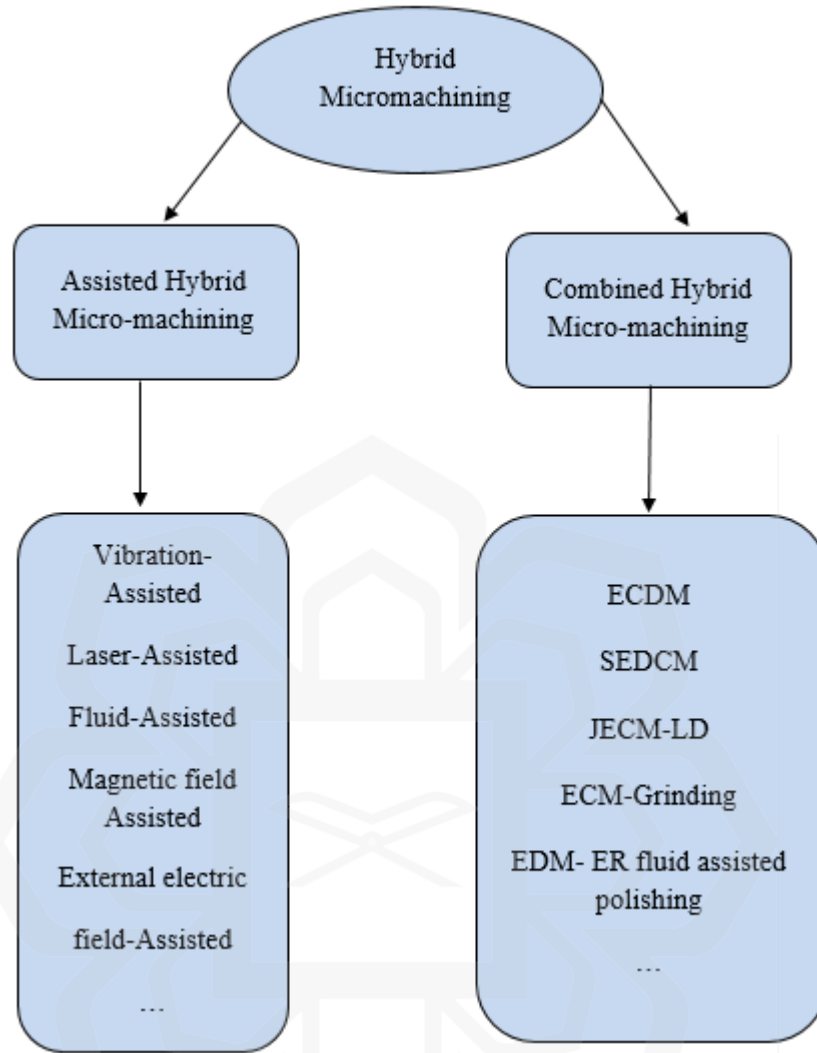


Figure 2.8: Classification of hybrid micro-machining processes (Chavoshi & Luo, 2015)

The advancement of hybrid micromachining methods enhances the benefits of fundamental processes while minimizing their drawbacks (Lauwers et al., 2014). Due to their superior accuracy compared to other methods, hybrid micromachining processes hold great potential to develop more complex parts with better dimensional features, faster machining accuracy, shorter machining times, etc., There is a vast amount of possibilities in studying

these procedures to better understand and optimize machining characteristics, expand application areas, refine process characteristics, etc.

2.6 VARIOUS HYBRID MACHINING TECHNIQUES USED FOR LBMM AND μ EDM.

In hybrid machining technology, various types of machining is combined in where EDM and laser machining have been utilized. One of the hybrid machining concepts is electrochemical discharge machining (ECDM), which is the combination of electro discharge machining and electrochemical machining (Kumar et al., 2020). In an ECDM setup, it is common practice to make use of a smaller tool electrode in addition to a larger counter-electrode. They are both connected to a voltage source, and the workpiece, along with them, is only very slightly submerged in the electrolytic solution.

The DC battery produces a potential difference across the electrodes after the circuit is complete, which causes the electrolyte to deteriorate chemically and build up gas bubbles around the tool. Voltage affects bubble coating. Increasing voltage sparks across the tool-workpiece gap, and machining. Unlike μ EDM, ECDM can micromachine nonconductive materials. EDM-based other hybrid machining includes electrical discharge abrasive grinding (EDAG) which is better than ECM, EDM because it combines the EDM and grinding for machining electrically conductive materials. The most important benefits of EADG is self-dressing where the electro discharge simultaneously erode workpiece and tool (wheel) (Shrivastava & Dubey, 2014).

Numerous studies have investigated the hybrid micromachining method of vibration assisted EDM (Maity & Choubey, 2019). Although these hybrid approaches have shown some promise, they have yet to be implemented at a scale where they can significantly

boost efficiency. Studies of laser-assisted machining methods have been testified by a number of researchers in recent years. In the past, researchers have proposed using electrochemical micromachining (EMM) as part of a sequential hybrid micromachining process that also includes laser-based micro-machining (LBMM) (Sun et al., 2018). The recast layer which was generated from LBMM process that was removed by the EMM finishing operation. LBMM-EMM was measured against other forms of individual machining. The surface of LBMM-EMM was smoother and cleaner than that of LBMM alone. LBMM-EMM outperformed EMM in terms of productivity (51.35%) and accuracy (30.43%). laser-assisted milling (Ding et al., 2012), turning (Arrizubieta et al., 2015), and laser-assisted waterjet machining are a few of the other reported laser-assisted machining technologies (Feng et al., 2019).

The LBMM and μ EDM methods each have their own set of advantages and disadvantages that are integral to the way of their operation. The hybrid micromachining method, which sequentially applies LBMM and μ EDM, was experimentally evaluated to maximize the advantages of both procedures (Afiq Rashid et al., 2016). The machining was executed using a Mikrotol DT-110 machine equipped with both LBM (Laser Beam Machining) and EDM units. SP100C SPI 100 W Fibre Laser was used for laser machining. Overall, the hybrid process improved surface characteristics, smoothness, oxide layer removal, and machining efficiency. A study reported that their projected hybrid LBMM-EDM micro-drilling process caused in a 50–65% reduction in machining time and a 40%–65% increase in material removal rate (MRR) for the machined holes (Al-Ahmari et al., 2016). Research was conducted on LBMM-EDM based micro-drilling for Ni-Ti-based shape memory alloys (SMA) in order to bring the quality of the holes produced by LBMM-based micro-drilling

closer to that of pure LBMMed holes. The holes were also free of any surface imperfections caused by the LBMM's predecessor. To significantly increase the machining rate while preserving the quality of the machined feature, other researchers also tested the synergistic fusion of LBMM and μ EDM (Yeo et al., 2009). The machining setup of the EDM tool on the LBMMed pilot hole, which is not sufficiently explained in the prior research, is a challenge for LBMM- μ EDM sequential machining (Al-Ahmari et al., 2016; Kim et al., 2010). To address the alignment issue, a new optical measurement-based system was created. Additionally, a study on the impacts of the different LBMM parameters on the LBMM- μ EDM process' overall performance was conducted (Rashid et al., 2021b). In comparison to pure μ EDM, the LBMM- μ EDM process could reduce the time required to fabricate micro-holes by a factor of 2.65 while maintaining the same level of circularity and free of recast layer quality. With the μ EDM process, it was observed that high laser power and low scanning speed cut machining time by a lot more than low laser-power and fast scanning speed. Table 2.2 shows the summary of various hybrid machining techniques those were used previously for LBMM and μ EDM machining process.

Table 2.2 Various hybrid machining techniques that was used previously for LBMM and μ EDM machining process.

Authors and year of publication	Machining process used	Major Findings
Ding et al (2012).	Laser-assisted milling	LAMM, as per finite element model simulations, can mitigate or eliminate the generation of Built-Up Edge (BUE) during micromachining of challenging materials when the workpiece material is appropriately preheated before employing the cutting tool.
Arrizubieta et al. (2015)	Laser-assisted turning	The model proved valuable in forecasting the thermal profile of a Laser Assisted Turning (LAT) component under various operational conditions, aiding in the identification of optimal process parameters.

Al-Ahmari et al. (2016)	LBMM- μ EDM sequential machining	Compared to the conventional micro-EDM method, there is a 50–65% reduction in machining time without compromising the quality of the micro-holes.
Afiq Rashid et al. (2016)	Sequential LBM-EDM hybrid micromachining (slot milling)	The LBM-EDM hybrid slot milling process enhanced machining efficiency, oxide layer removal, smoothness, and surface properties.
Sun et al. (2018)	Laser & Electrochemical machining	When LM-ECM machining is utilised instead of single laser machining, the material surface is enhanced. Accuracy and efficiency both increased by 30.43% and 51.35%, respectively.
Maity & Choubey, (2019)	Vibration-assisted EDM	The MRR increased (35%) with the increase of vibration amplitude
Feng et al (2019).	Laser-assisted hybrid waterjet machining	Both laser machining and hybrid laser-waterjet micromachining exhibit oxidation behaviour. On the other hand, compared to laser machining, which produces silicon dioxide with an oxygen percentage of more than 30%, the silicon dioxide produced by the hybrid laser-waterjet micromachining method has an oxygen content of roughly 5%.
Rashid et al. (2021). The significant portion of this thesis has been published in this paper.	LBMM- μ EDM based sequential hybrid micromachining	Lowered machining duration, tool wear, and instability (measured by short circuit count) by factors of 2.5, 9, and 40, respectively.

2.7 MODELLING TECHNIQUES USED FOR MICROMACHINING PROCESSES

From a system engineering perspective, modeling is crucial to advancing physical process quality. As a result, micro machining process and modeling micro-scale is a crucial issue for effective manufacturing, according to numerous reports from around the world. Good models also lessen the possibility of unexpected tool breakage, which could result in damage to the workpiece or even to the machine tool. This reduces the need for expert operators and lowers costs. Due to the small tool diameters used in micro machining and

the high surface roughness quality required in these procedures; process supervising is also of utmost importance.

2.7.1 Empirical modelling

An empirical model is a representation created from the affiliation in between input factors and output factor based on experimental data. Empirical modeling can also be carried out using any kind of computer modeling technique that is based on empirical observations and can be modeled using the empirical modeling approach. This method was created at Warwick University in England as a fresh approach to computer-based modeling (Harfield, 2012). Previous research into laser-assisted jet electrochemical machining (LAJECM) led to the formation of an empirical model for estimating LAJECM's volume removal rate (VRR) and taper angle (Wilson, P., & Mantooth, 2013). In conclusion, statistical and artificial intelligence modeling can be categorized as empirical modeling.

2.7.3.1 Statistical modeling

A statistical model assumes the observed data as apart from a larger population. Models often idealize the data-generating process. Model assumptions define a set of possibility distributions, some of which are considered to approximate a data set (Beruvides et al., 2014).

2.7.3.1.1 Regression Analysis

Regression study is a statistical method for estimating the correlations between variables namely independent and dependent variables. There are a variety of regression modeling methods described in the literature, including non-parametric regression, Bayesian linear regression, and linear and non-linear regression. Generally, the regression model can be express as

$$y = \beta_0 + \beta_1 X_1 + \beta_2 X_2 + \beta_3 X_3 \dots\dots\dots(1)$$

Where X_1 , X_2 , and X_3 are predictor variables and y is the criterion variable & coefficients of regression are β_0 , β_1 , β_2 , and β_3 .

Regression models are frequently used in micromachining methods to create a parametric relationship between productivity, surface quality, and material removal rate, as well as force, motion, and acoustic emission, among other factors (N et al., 2014).

2.7.3.1.2 Design of Experiment (DOE)

DOE use statistical analysis to forecast product property performance in all conditions within the constraints of the experimental design. Moreover, correlations between process and product parameters are found. The design of experiments generates needed data with minimal experimentation. It is a powerful tool for collecting and analyzing data that can be used in a wide range of experiments. It enables the variation of multiple inputs to observe their effect on a desired output (response). For the purpose of determining whether or not a mathematical model that was derived from regression analysis adequately describes the depth of the machined area and the surface roughness, a statistical ANOVA is utilized. During the pulsed Nd:YAG laser experiment, DOE was cast-off to perform multi-objective hole characteristics optimization. Micro-drilling with a YAG laser performed on a sheet of gamma-titanium aluminide alloy (Rajesh et al., 2017). In order to predict the dimensional accuracy of the biased surface during the end-milling process, (Arnaiz-González et al., 2016) combined DOE and ANN.

2.7.3.1.3 Response Surface Methodology (RSM)

RSM practices mathematical and statistical methods to develop, analyze, improve, and optimize experimental processes. It helps design, develop, and improve new products and

processes. RSM becomes expensive when multiple input variables may affect the process or product performance and quality. Performance measurement and quality characteristics are response variables and input variables are independent variables. Biswas et al. (2010) did the experimental design based on RSM to run Nd: YAG laser micro drilling on titanium nitride-alumina composite. Using ANOVA analysis, Feng et al. (2019) showed how to determine the most important method parameters for hybrid micromachining of silicon carbide wafers using a laser and waterjet. Models based on RSM were used to explain the depth, width, and MRR of the microgrooves.

2.7.3.1.4 Central Composite Design

The CCD process, created by Box and Wilson, is a very effective way to decline the number of experiments in research with numerous factors and levels. Compared to other experimental design approaches, CCD has more benefits. For example, it offers accurate predictions when researching the linear and quadratic collaboration effects of system-influencing variables. Contrarily, interactions that go unnoticed by Plackett and Burman's experimental techniques and Box-Behnken have less analysis than in the case of CCD (Calfee & Piontkowski, 2016). As a result, CCD has been extensively utilized in the fields of science and engineering (Moradi & KaramiMoghadam, 2019).

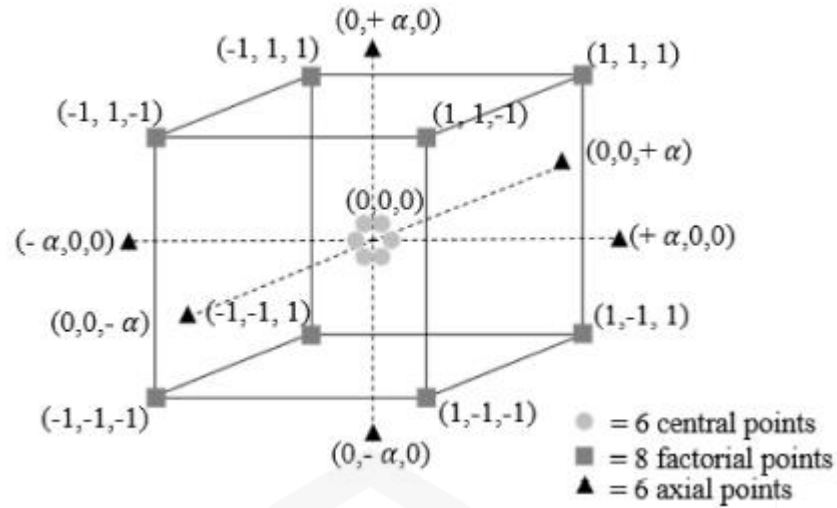


Figure 2.9: CCD for 3 levels and 5 factors (El-Khoury et al., 2020)

As shown in Figure 2.9, The CCD has 3 main parts, which are 2^k+2k+m . The two-level factorial part of CCD has $2k$ factorial points at the junctions of a cube to show its shape in space (Figure 2.9). The number 2 in the last cube design expression comes from the levels. $k = 3$ for factors. The other part of CCD is fixed in the middle of the design space and involves of m center points, the middle levels of all investigated factors. Replicating these points estimates experimental error, detects fitted data curvature, and validates model sufficiency. Therefore, it is unnecessary to replicate the entire experimental design. The final component of CCD defines the axial points. A CCD consists of $2k$ axial points, which verify new high levels (the lowest and highest level) for each factor. As a result, the entire experimental design does not need to be replicated (Calfee & Piontkowski, 2016). On the basis of five factors, (Dhupal et al., 2008) used CCD to optimize the micro-grooving of Al_2TiO_5 ceramics by an Nd: YAG laser. The advantage of CCD over FFD is that each factor has five levels, allowing for the development of a more accurate statistical model while requiring a smaller number of test experiments. It was discovered that the CCD, like the FFD, enables the optimization of various laser micromachining problems; it is also

incredibly effective if the precise location of the optimal point is known. For experimenting the appearances of the interactions between the design factors on the model, the CCD method can explore a broad process space and capture a strong curvature.

2.7.3.1.5 Box Behnken Design

Box-Behnken designs (BBD) (S. Pradhan et al., 2021) are a class of 2nd order designs that are rotatable or closely rotatable and are based on incomplete factorial designs with three levels (Figure 2.10). Its graphical illustration can be seen in one of two ways for three factors:

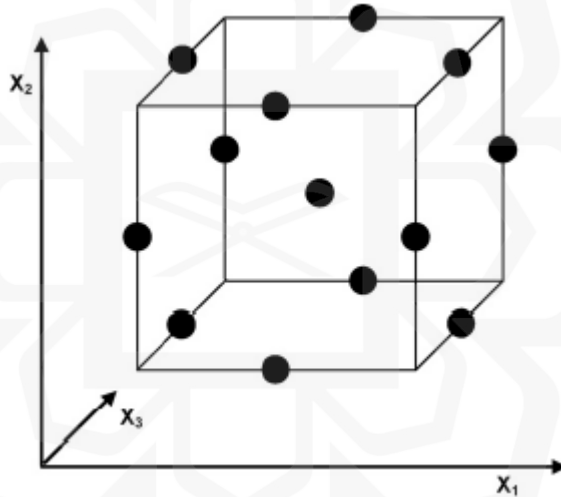


Figure 2.10: The cube for BBD (Ferreira et al., 2007)

The formula $N=2k(k-1) + C_0$, where k is the number of factors and C_0 is the number of middle points, is used to calculate the numerical number of experiments (N) necessary for the advance of BBD. For comparison, $N=2^k + 2k + C_0$ represents the number of experiments for a central composite design. The BBD differs from combinations in that it does not contain factors that are concurrently at their highest or lowest levels for all combinations. These designs are therefore helpful in preventing experiments carried out under ultimate

circumstances, for which unacceptable results may occur. On the other hand, they are not recommended for circumstances in which we would like to know the responses at the extremes, or the cube's vertices.

2.7.3.2 Modeling Based on Artificial Intelligence

Artificial intelligence (AI) techniques are a group of modeling techniques widely used by researchers in the field of manufacturing. Artificial Neural Networks, fuzzy and neuro-fuzzy systems, and probabilistic approaches are the most frequently used methods for simulating physical processes that draw inspiration from artificial intelligence.

2.7.3.2.1 Artificial Neural Network (ANN)

The utmost well-known and established AI-based modeling technique is artificial neural networks. This method, which was developed to approximate functions, was heavily influenced by the network structure of biological brains. The artificial neuron, a crude mathematical simulation of the biological neuron, serves as the foundation for the entire concept of the artificial neural network. Artificial Neural Network (ANN) is a commonly employed supervised learning algorithm with forward and reverse passes. It is composed of three layers known as the input layer, the hidden layer, and the output layer. Backpropagation is one of the most popularly employed artificial neural network techniques (K. Zhang et al., 2020; Dhara et al., 2008). In order to prevent the model from being overfitting, regularization is a technique that modifies a number of model parameters. The advantage of Bayesian-regularized ANN over other training algorithms is that it can do away with the need for a drawn-out cross-validation process while still maintaining robustness by removing the possibility of being overfitted (Burden & Winkler, 2008). To effectively approximate a variety of random processes, some specialized neural network

classes recognised as stochastic neural networks can be used (Aggarwal, 2018). In a recent study, it was discovered that Bayesian neural networks are among the stochastic neural networks that are good at approaching stochastic methods (Bennamoun, 2022). In addition, the artificial neural network-based modeling approach is being contemplated as a possible soft computing tool that can be used for anticipating processes such as EDM, which is one of the machining techniques that was utilized in this investigation (M Azadi Moghaddam, 2020; P. M & D, 2020; Suganthi et al., 2013).

It is not uncommon for numerical and analytical models to have difficulties in their approximation of the results of various processes when subjected to actual experimental conditions. Detailed, highly nonlinear relationships between inputs and outputs were discovered through experimental analysis of the aforementioned sequential micromachining (LBMM- μ EDM). The overall quality of the combined method has been found to be affected by the quality of the first micromachining process applied in the sequence. To the best of the authors' knowledge, neither an analytical nor an empirical model of the laser- μ EDM process has been developed as of yet. Analytical models may be incapable of capturing the governing relationship between input and output data for a diverse range of experimental values and conditions. But to evaluate using numerical models which is computationally exclusive and inadequate to come up exact value (Parandoush & Hossain, 2014).

2.7.3.2.2 Fuzzy Expert System (FES)

Since the vast majority of knowledge in the world is uncertain and imprecise, every description of a real system will inevitably include some information that is inaccurate or incomplete. A fuzzy strategy based on fuzzy sets seems to be the best approach to handle

such circumstances (Mohd Adnan et al., 2015). Over the past two decades, FL has been successfully utilized to solve a variation of real-world issues, particularly when modeling complex and imprecise systems in science and engineering. By using an intelligent Fuzzy Expert System (FES), Pandey & Dubey (2013) examined the kerf quality of Ti alloy during pulsed laser cutting. An analytical prediction model of kerf width in relation to the erosion front was explained by Hossain et al. (2016). In order to determine the minimum kerf width and variations on the top and base sides of a duralumin sheet, Pandey & Dubey (2012) developed the FES model.

2.7.3.2.3 Adaptive Network-based Fuzzy Inference System (ANFIS)

The ANFIS Model, which employs neural network-like neuro-adaptive learning techniques (Karaboga & Kaya, 2019). ANFIS builds a fuzzy inference system (FIS) from an input/output data set, and the membership function parameters are tuned using the backpropagation algorithm or other similar optimization methods. While Ho et al. (2009) used ANFIS for the prediction of surface roughness in end milling. A Graphical User Interface (GUI) has been created and integrated to model the laser machining method using ANFIS, and it has been demonstrated that this has the greatest ability to predict the complex and nonlinear behavior of laser processing responses ((Rao et al., 2009). Shivakoti et al. (2019) used an ANFIS system to predict the output parameters of the lathe machine, such as surface finish and tool life criteria. ANFIS and ANN have been used to forecast the SR of the workpiece during hard turning (Alajmi & Almeshal, 2020). Table 2.3 shows the summary table of modeling techniques used for micromachining processes.

Table 2.3 Summary table of various modeling techniques previously used for micromachining processes.

Authors and year publication	Micromachining Process	Modeling techniques used	Major Findings
Pajak et al. (2004)	Laser-assisted jet electrochemical machining (LAJECM)	Multivariate regression model	Compared to a single Jet-ECM, material removal using LAJECM has reached up to 20.3%.
Dhupal et al. (2008)	Micro grooving	Central Composite Design (CCD)	Lower cutting speed (10 mm per second) is advised to achieve lesser deviations in the micro-groove depth and taper angle.
Suganthi et al. (2013)	Combining micro-wire electrical discharge grinding and micro-electrical discharge machining (EDM) in a single process.	ANFIS-ANN	The ANFIS-based model demonstrates superior performance compared to the pure neural network model in terms of accuracy in prediction.
Pandey& Dubey (2013)	Laser cutting (slot channel)	Fuzzy Expert System (FES)	By lowering the kerf deviations to 50% and 71% at the top and bottom sides, respectively, the geometrical precision of laser-cut Duralumin sheet has been significantly increased.
Arnaiz-González et al. (2016)	Ball end-milling process	DOE and ANN	The precision achieved is 1.83 μm in root mean squared error (RMSE) with a correlation coefficient of 0.897 through a 10 \times 10 cross-validation approach. These findings indicate that RBFs consistently outperform MLPs in various scenarios.

Hossain et al. (2016)	Laser beam machining	Fuzzy Logic-Based Prediction Model	It was discovered that the prediction ability's accuracy and the values of 3.852% and 0.994, respectively, for the kerf width in CO ₂ laser cutting are satisfactory.
Rajesh et al. (2017)	Nd:YAG Laser micro drilling	DOE was cast-off	The response surface methodology (RSM) predicted models were discovered to be quite similar to the experimental values.
Feng et al. (2017)	laser-waterjet-based hybrid micromachining	CCD	Microgroove depth, width, and MRR all had mean discrepancies of 8.07%, 2.60%, and 9.60%, respectively. On the other hand, MRR (17.62%) and depth (15.71%) had very high maximum errors.
Feng et al. (2019)	Hybrid micromachining (laser & waterjet)	RSM based model	On the cut side of the hybrid laser-waterjet micromachining, there is no HAZ or recast layer. Scaly recast layers on the cut's sides and a 50–100 µm-wide HAZ are seen in the laser-cut machined image.
Moghaddam & Kolahan, (2020)	EDM process	ANN	With less than 1% error, the modelling technique (BPNN) can accurately imitate the real EDM process. Additionally, the PSO algorithm's outcomes with less than 4% error are highly efficient in the optimization process.

Alajmi & Almeshal, (2020)	Turning	ANFIS based data driven modelling	According to simulations, ANFIS accurately predicts surface roughness for the dry turning process, with RMSE = 4.86%, MAPE = 4.95%, and R2 = 0.984.
P.M & D (2020)	Wire-EDM	ANN	The model exhibited a 95% accuracy in predicting outcomes during the confirmation tests.

2.8 SUMMARY

This chapter discusses recent research trends on various micromachining techniques especially those involving μ EDM and LBMM. The chapter also highlighted the various pros and cons of the above processes. Process hybridization has also been discussed. In the second part of the chapter various modeling techniques have been discussed which are typically used in describing micromachining. Finally, based on the literature review it can be fairly determined that a little research has been carried out in the field of LBMM- μ EDM based hybrid machining which describes the consequence of different laser parameters on the total performance of the hybrid process. This thesis aims to contribute to minimizing this research gap.

CHAPTER THREE

MATERIALS AND METHODOLOGY

3.1 INTRODUCTION

This research aims to study and experimentally model LBMM- μ EDM based sequential hybrid micromachining process. As such, this chapter describes various details of the experimental and characterization procedure. Also, this chapter details out the modeling approach used for this research.

3.2 LASER BEAM MICROMACHINING (LBMM) PROCESS

This section presents the experimental parameter of LBMM, the definition of LBMM process variables, and other related experimental procedures.

3.2.1 LBMM Experimental Parameter

Sequential Laser- μ EDM micro drilling and micro milling have been carried out during the machining process to create tiny holes and channels on the stainless-steel workpiece. Four parameters—Scanning Speed, Loop count, Laser Average Power, and Pulse Repetition Rate were changed in the LBMM process. Entry Area, Exit Area, HAZ, and Recast Layer were studied as the four output parameters for LBMMed holes. Table 3.1 shows various parameters of the LBMM process with the respective range.

Table 3.1 LBMM process

Parameter name	Value
Laser spot size (μm)	40
Laser pulse duration (ns)	100
Laser scanning speed (mm/s)	50-1400
Laser average power (W)	6.4-15.5
Laser pulse repetition rate (kHz)	5-20

The definition of all the LBMM process variables is tabulated in Table 3.2

Table 3.2 Definition of LBMM process variables

Parameters Name	Symbol	Unit	Definition
Laser Loop Count	-	nos	The number of passes the laser beam makes across the surface of the material for each hole.
Laser Scanning Speed	-	mm/s	The speed at which the laser beam moves across the surface during each pass.
Laser Average Power	P	W	An expression of the average power emission over time.
Laser pulse repetition rate	f	kHz	The number of emitted laser pulses per second.
Entry Hole Area	-	mm^2	The area of the hole at the entrance where the laser beam first hits the surface.
Exit Hole Area	-	mm^2	The area of the hole at the exit after the LBMM process is finished.
Heat Affected Zone	HAZ	mm^2	The non-melted area of metal has undergone changes in material properties because of exposure to high temperatures.
Recast Layer	-	mm^2	The resolidified layer of molten material was not ejected from the hole due to laser micro-drilling.

3.2.2 Workpiece and Tool

This research used commercially available stainless steel (SS304) as the sample workpiece. SS 304 is the most familiar form of stainless steel used around the world due to its excellent corrosion resistance, availability, and value. It can survive corrosion from most oxidizing acids. The durability and good machining performance make it ideal for multipurpose

applications comparing to other hard materials. The impressive post machining formability and diverse field of applications has drawn the great attraction to choose SS304 as the sample workpiece. The thickness of the workpiece was 0.2 mm for hybrid drilling and 0.5 mm for hybrid milling. For convenience, the bought steel sheets were divided into smaller pieces with an approximate dimension of 25mm by 25mm. The mechanical properties of the SS304 workpiece are tabulated (Table 3.3). Figure 3.1 shows the stainless-steel workpiece with the fixture used in the LBMM experiment.

Table 3.3 Mechanical properties of stainless steel 304 (R. Kumar et al., 2020)

Property	Value
Yield strength	30ksi
Tensile strength	75ksi
Specific Heat Capacity	0.500 J/g-°C
Melting Point	1450 °C
Thermal Expansion	17.2 x 10 ⁻⁶ /K
Modulus of Elasticity	193 GPa
Thermal Conductivity	16.2W/m.K
Electrical Resistivity	0.072 x 10 ⁻⁶ Ω .m

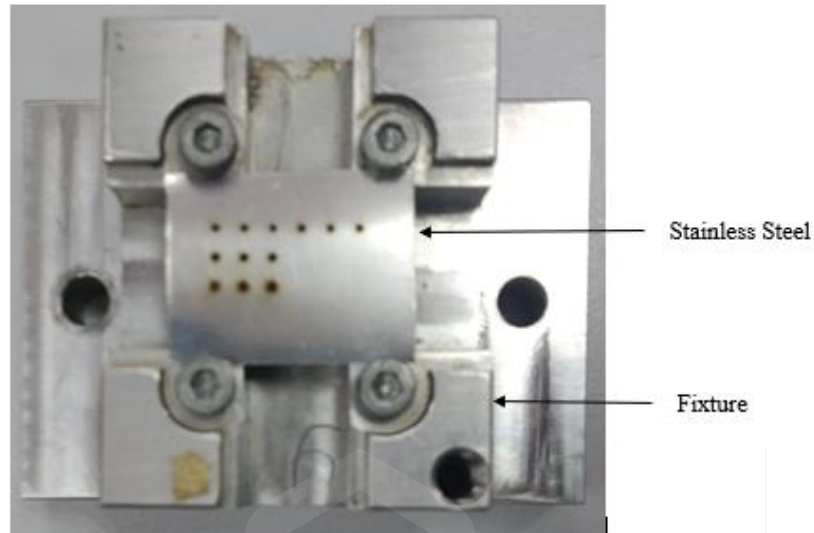


Figure 3.1 Workpiece and fixture used for hybrid micromachining process.

μ EDM Electrode (tool) has a function to transfer electrical charges and erode the workpiece into the desired form. Electrodes can be made from any electrically conductive material, in theory. However, some materials are more appropriate than others depending on the workpiece and type of EDM generator. The tungsten electrode of 500 microns diameter was used in the μ EDM machining process.

3.3 MICRO ELECTRO DISCHARGE MACHINING (μ EDM) PROCESS

This section presents the experimental parameters used and investigated during micro EDM, the definition of μ EDM process variables, and other related experimental procedures.

3.3.1 Micro EDM Parameters

Micro-EDM operation has been conducted in multiple phases for this research. In the first phase of the research (LBMM- μ EDM hybrid drilling) all μ EDM parameters (voltage, capacitor, feed speed, and spindle speed) were kept constant at 80V, 1nF, 5 μ m/s, and 500 RPM for the finish operation. During this stage, LBMM parameters were varied as detailed

in the initial section. In the second-stage of the research (LBMM- μ EDM hybrid drilling) both the LBMM and μ EDM parameters were varied. Finally, at the third stage (LBMM- μ EDM hybrid milling) μ EDM parameters were kept constant and LBMM parameters were speckled. Table 3.4 shows various μ EDM input parameters with a range of variations. Table 3.5 defined the μ EDM process variables.

Table 3.4 Micro EDM process

Parameter name	Value
μ EDM applied voltage (V)	80-110
μ EDM discharge capacitor (nF)	0.01-100
μ EDM feed speed ($\mu\text{m/s}$)	3-10
μ EDM electrode diameter (mm)	0.5
μ EDM electrode material	Tungsten (W)

Table 3.5 Definition of micro EDM process variables

Parameters Name	Symbol	Unit	Definition
μ EDM Machining Time	-	mins	The time is taken for μ EDM machining to be finished for each LBMMed hole.
Short Circuit/Arcing Count	-	nos	The number of short circuits/arcing occurring during the μ EDM machining of each LBMMed hole.
Tool wear	-	μm	The gradual shortening of the machining tool during the μ EDM finishing operation for each LBMMed hole.

3.4 CHARACTERIZATION

This section concentrates on the characterization methods that were used to gather the data. Scanning Electron Microscopy (SEM) was used to examine the micro-holes created by the sequential micromachining process. Alicona machine was utilized to determine the surface roughness of the laser beam micro-milled workpiece. A third-party image analysis program (ImageJ) (Schmid et al., 2010) was utilized to determine the entry and exit areas of the holes (both for the LBMMed and the micro EDMed holes) after all of the SEM images were taken.

3.4.1 Scanning Electron Microscopy of Laser Machined Holes

After the LBMM procedure, the holes will be characterized by scanning electron microscopy (SEM: JSM-IT100 InTouch Scope™). Using a third-party picture exploration program (ImageJ) (Schneider et al., 2012) was employed to measure the entry area, exit area, HAZ, and recast layer of individual hole were identified following proper calibration (ImageJ). ImageJ tool has a function for measuring the highlighted area of an image if the calibration is performed properly. As illustrated in Figure 3.2 (a) and (b) a yellow boundary is sketched to determine the entrance and exit zones, correspondingly. Also, the methodology for determining the HAZ and recast layer for LBMMed holes is shown in Figure 3.2 (c) and (d). It is clear that the hole area and the recast layer at the edge of the hole are both part of the outlined HAZ area in Figure 3.2 (c). The recast area is indicated by a yellow outline in Figure 3.2 (d). The area of the combined entry and recast layers is subtracted from the entire area of the heat-affected region that extends from the hole's center to determine the HAZ. The SEM measurements and characterizations of the holes will also be performed afterward the μ EDM method.

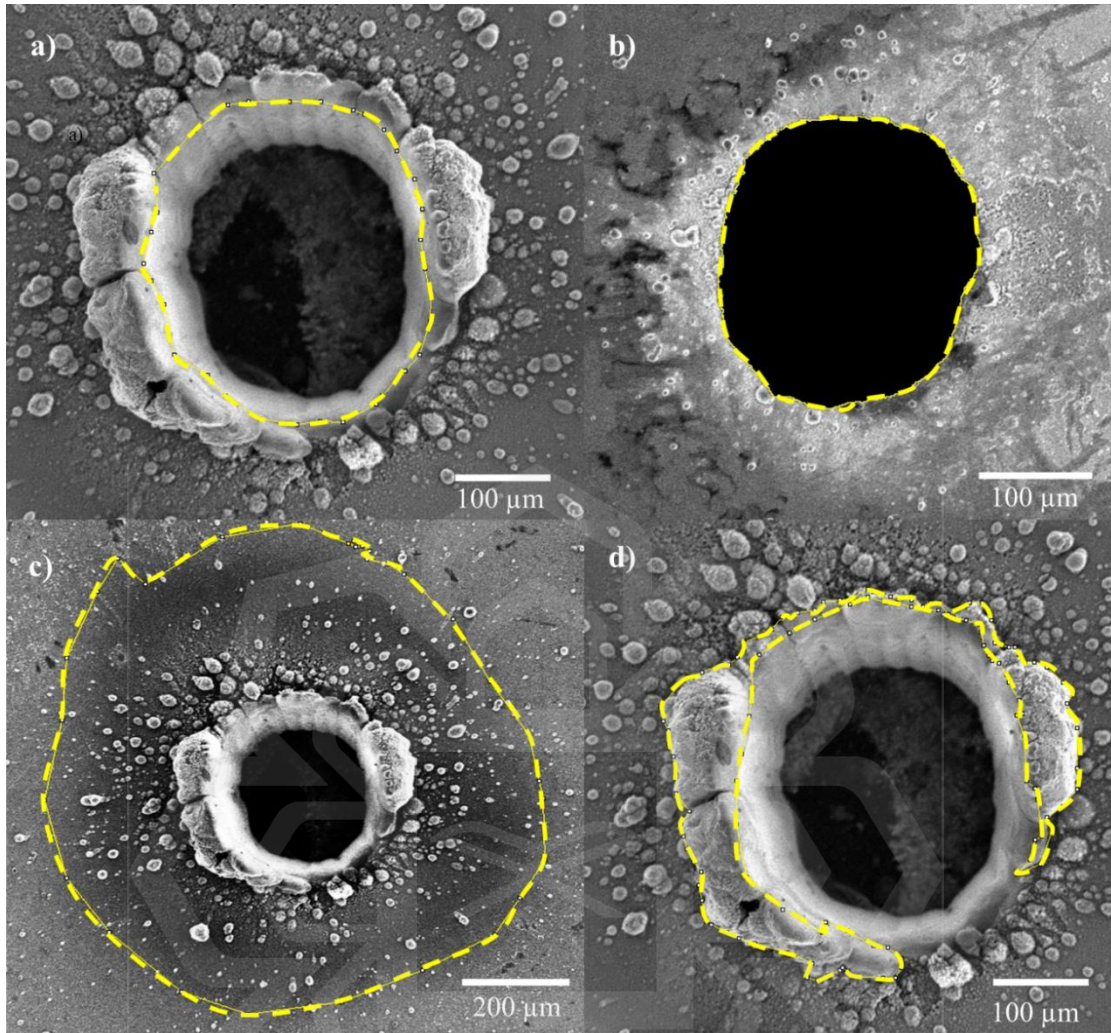


Figure 3.2 LBM Med hole measurement from the SEM images (a) entry area, (b) exit area, (c) HAZ, and (d) recast layer (Noor et al., 2021a)

3.4.2 Scanning Electron Microscopy of μ EDM-Finished Holes

Each hole's drilling time (by micro EDM) is directly recorded from the machine. Arcing (repeated discharges without allowing the gap voltage to reach open circuit voltage) and short circuits (electrodes touching the workpiece without any discharge) have both been reported to be harmful to EDM (Yeo et al., 2009). The DT110 controller can identify short circuits/arcing by continuously observing the electrical characteristics of the μ EDM process. Every time a short circuit/arcing incident occurs, the machine emits a loud beeping

tone. This aids the user in keeping track of how many short circuit/arc incidents occurred throughout the entire μ EDM method. The length of a single beeping signal is examined to be fixed and unaffected by the machining instability (short circuit/arc) condition; rather, the repetition rate of the beep noise shifts as the arcing increases or decreases. So, counting the number of beeps when there is a short circuit or arcing is a good way to explain the μ EDM's performance. As each LBMMed hole's μ EDM is finished, the machine keeps track of the overall machining time. This information is then employed for the analysis. By touching the electrode to the conductive workpiece and then to the conductive surface, the DT110 machine controller can automatically find the conductive surface. Before individual μ EDM procedure begins, the electrode was relocated down until it touches the workpiece, at which point the Z coordinate is written down. After the machining process, the same step is done again, and the difference between the two Z coordinates was recorded as the vertical tool wear. Before every operation of μ EDM, the bottom side of the tool was leveled using reversal μ EDM (Singh et al., 2017) to get rid of any preference during the investigational analysis.

3.4.4 Alicona Optical Profiling System

Alicona Optical Profiling System Measuring: model NT 1100 is operated to assess the surface roughness of the LBMMed stainless steel workpiece, as shown in Figure 3.3. By scanning the machined surface, the microscope gathers surface data. The field of view (FOV) and objective lens options were chosen to show the magnification. The length, infrared back scan, and threshold percentage modulation are all user configurable.



Figure 3.3 Alicona Optical Profiling System

3.5 EXPERIMENTAL SETUP HYBRID MICROMACHINING (LBMM- μ EDM)

Initially, LBMM was used to create holes smaller than a millimeter in diameter, with a target size of 200 μm , and then, μEDM will be used for precise finishing. Stainless steel SS304 was used for the 0.2 mm thick workpieces in this study. In order to carry out the LBMM micro-drilling, a desktop fiber laser machine with Ytterbium Doped that had a power rating of 20 W was utilized. This machine employed a pulsed laser with a wavelength of 1060 nm and a focal length of 200 mm. The laser has a spot size of 40 μm . As such, the laser beam will be scanned across the workpiece using an X/Y galvanometer (with a maximum scan angle of $\pm 15^\circ$ and a resolution of 12 μrad). After initially scanning the workpiece horizontally, the laser spot shifts vertically by 10 μm before scanning horizontally in the reverse direction. This procedure was repeated until the complete target area has been

mapped out. Scanning is performed multiple times, with the number of loops determined experimentally. The laser spot and its scanning path are shown together in Figure 3.4. The built-in graphical user interface (GUI) of the LBMM system makes it easy to configure the machine for precise machining. Variables in the graphical user interface for a pre-programmed feature. Once the LBMM procedure for micro-drilling was completed, the workpiece and mending were moved to the μ EDM machine (DT110). CNC (computer numerical control) programs direct the μ EDM machine's translational movement. The μ EDM function of the machine is powered primarily by an RC pulse generator.

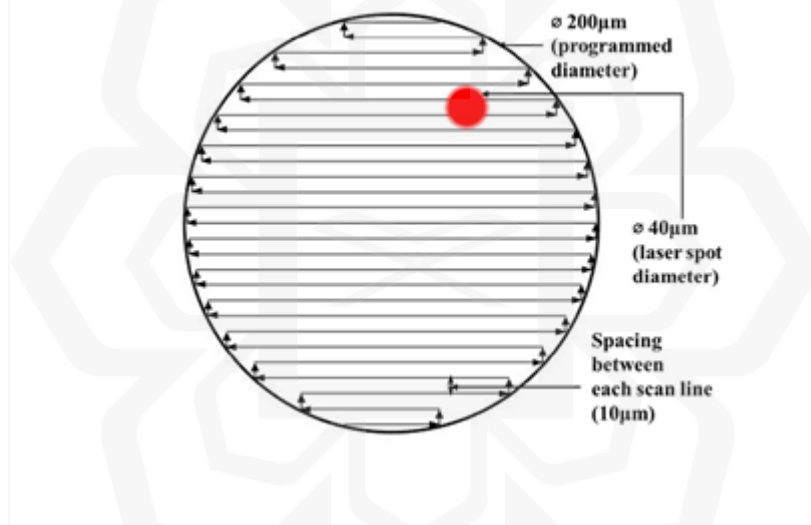
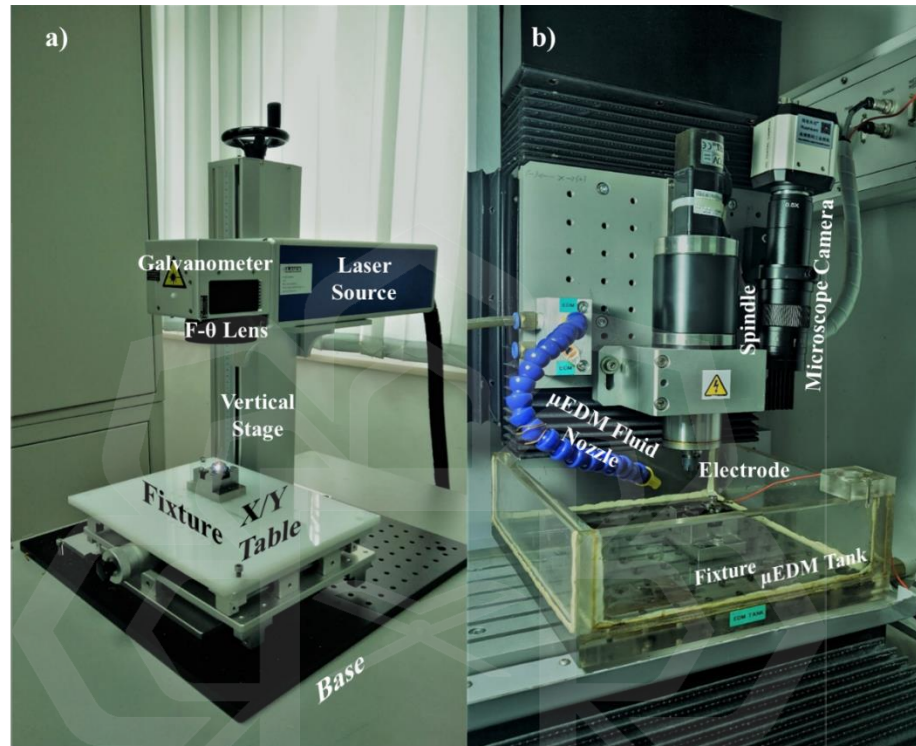


Figure 3.4 Shows how the laser scanning is carried out during the LBMM process (Rashid et al., 2021)

The finishing operation by μ EDM was carried out using a Tungsten Electrode with a diameter of 0.5 mm.

Micro holes were drilled in a square lattice pattern on the workpiece using the LBMM technique at the initial phase. A stopwatch (0.01 sec resolution) was used to record the elapsed time during hole machining in real-time. Then, the EDM (DT110) machine will be used for the final polishing. The LBMM and the μ EDM setup are shown in Figure 3.5 (a-b). On-machine measurement (OMM) consists of a high-magnification optical lens and a

high-resolution digital camera was used to precisely position the Tungsten tool above the LBMMed holes. The OMM was placed in close proximity to the EDM spindle, as shown in Figure 3.5 (b).



Workpiece moved from LBMM setup to μ EDM setup after drilling of pilot holes

Figure 3.5 Photograph of the Fibre Laser Setup (a) and Photograph of the μ EDM process Setup (Rashid et al., 2021b).

To begin μ EDM machining, the electrode was centered in the LBMMed holes, which was done with the assist of the installed OMM and the location feedback from the DT110 machine. To start, a reference hole was machined in close proximity to the LBMMed hole arrays. Using the DT110 EDM machine's linear scale feedback, the reference hole

coordinates (x_1, y_1) were determined. The camera is then aligned with the virtual crosshair at the top of the reference hole, and its coordinates are saved (DX, DY) . After that, the camera was repositioned over the exact center of the LBMMed hole. Point (DX_n, DY_n) was recorded, where n is the hole's corresponding index in the LBMMed array. Following this, we determine the distance (dx_n, dy_n) between the position hole (DX, DY) and each of the LBMMed holes (DX_n, DY_n) on the array.

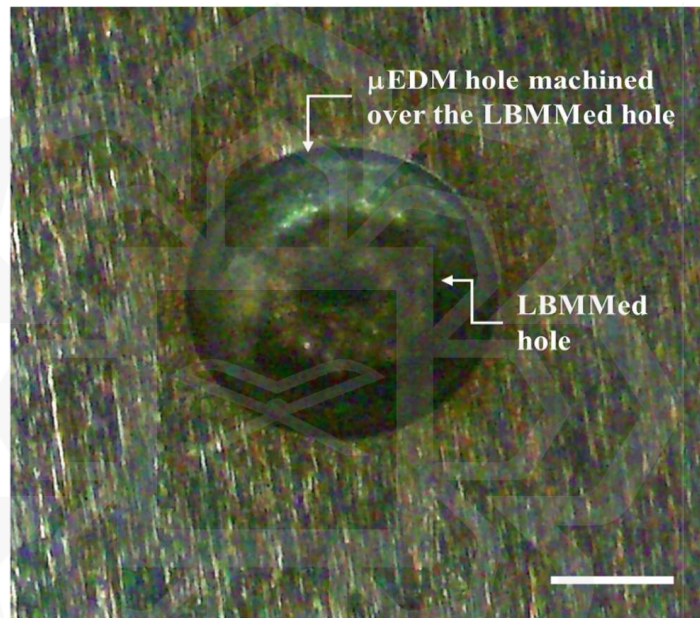


Figure 3.6 The μ EDM tool's pre-machined LBMMed hole centering method's. Scale bar = $200\mu\text{m}$ (Rashid et al., 2021b).

Finally, the tungsten tool was positioned on the LBMMed hole by adding the variation (dx_n, dy_n) to the reference hole's coordinate (x_1, y_1) . This positioning system has a theoretical accuracy of within $2\mu\text{m}$. Figure 3.6 demonstrates that the OMM system allows for the precise placement of the μ EDM tool above the pilot holes.

3.6 CLEANING OF THE SAMPLE BEFORE CHARACTERIZATION

The samples were cleaned using a Branson 3510 ultrasonic cleaner (Figure 3.7) to make them clean and free of any foreign contamination.



Figure 3.7 Ultrasonic bath cleaning machine (Branson 3510)

3.7 METHODOLOGY FOR THE MODELING

The modeling section will cover three steps, which is 1. Modeling of the LBMM- μ EDM drilling with constant EDM parameter, 2. Modeling of the LBMM- μ EDM drilling with variable EDM parameters, and 3. Modeling of the LBMM- μ EDM milling with constant EDM parameter.

3.7.1 Modelling of the LBMM- μ EDM Drilling with Constant EDM Parameter

This research study used the process parameters listed in Appendix A to carry out the sequential LBMM-EDM micro-drilling process. Following the experimentation, various data were recorded which were divided into training and testing sets. ANN modeling

technique was used for the first two sets of models focusing on the LBMM- μ EDM based drilling. During the modelling process a suitable topology with proper algorithm and hyperparameters were selected. The ANN modeling was carried out in two stages. The ANN based modeling (first stage) was adopted to find out the effect of LBMM input parameters to the output parameters such as Entry area, Exit areas of the holes. In the second stage of modeling the output parameters of LBMM was used as a input parameter to predict the output performance of micro EDM. The selection of model input and output parameters were chosen based on the correlation study as summarized in Table 3.6. The pulse repetition rate was found to have an insignificant correlation for any output of the LBMM process and hence discarded from the model input. As for the second-stage it can be seen from Figure 3.8 that Entry Area, Exit Area, HAZ, and recast layer (LBMM outputs) all have substantial correlations with μ EDM performance outputs hence considered during the modeling. Figure 3.9 shows the architecture of the dual-stage ANN model where the EDM input parameters were kept constant. Figure 3.10 shows the model flow where the μ EDM process parameters were varied such as voltage, capacitor, and EDM feed rate.

Table 3.6 Correlation coefficient between various LBMM inputs and outputs

Correlation Table				
	Output Variables→			
Input Variables ↓	Entry Area	Exit Area	HAZ	Recast layer
Laser Power	0.83	0.92	0.82	0.71
Scanning Speed	-0.66	-0.86	-0.34	-0.57
Loop Count	-0.09	0.98	0.93	0.09
Pulse repetition rate	-0.13	0.13	-0.14	0.12

Loop count correlates positively with Exit Area and HAZ with correlation values of 0.98 and 0.93, respectively. In this experiment the entry area and RL are totally not fully dominant by the loop count because after few passes of loop count the shape of entry and recast layer creation become free size and this is also primarily dependent on the thermal energy absorption quality of workpiece. It was also found that pulse repetition rate has no significant effect on LBMM output parameters. The laser input parameters are considered as important variables to develop the LBMM process modeling even though pulse repetition rate has no discernible impact on the output performances. In this experimental run some of the input parameters has no correlation with output parameters.

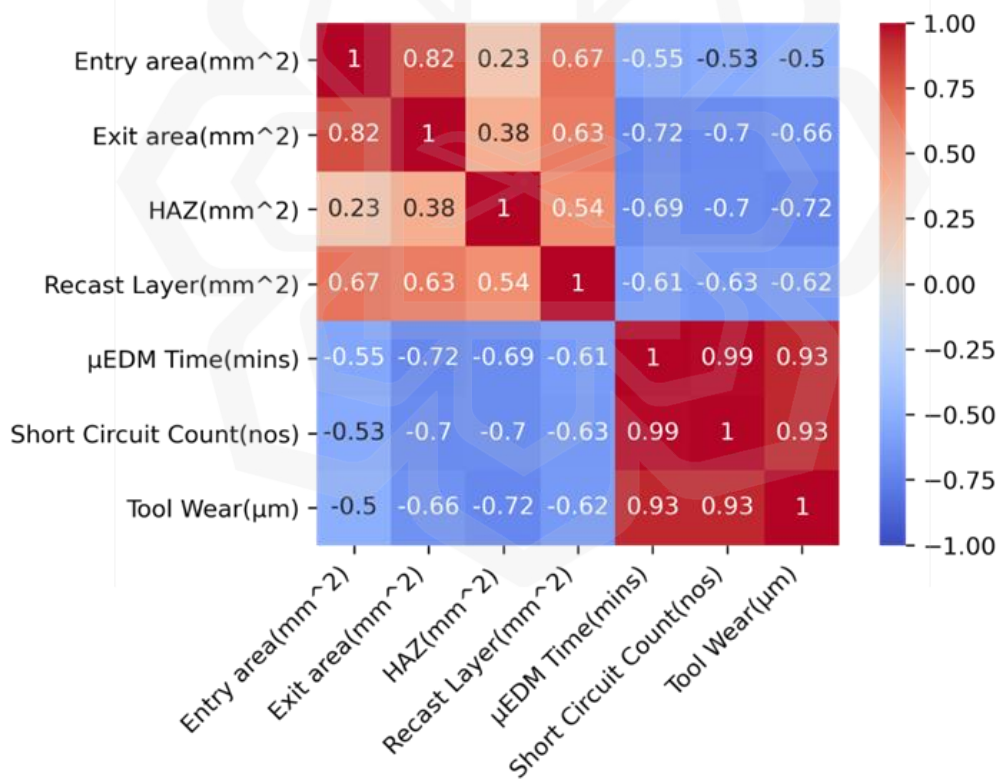


Figure 3.8 Correlation between various LBMM output and μEDM output (Noor et al., 2021a).

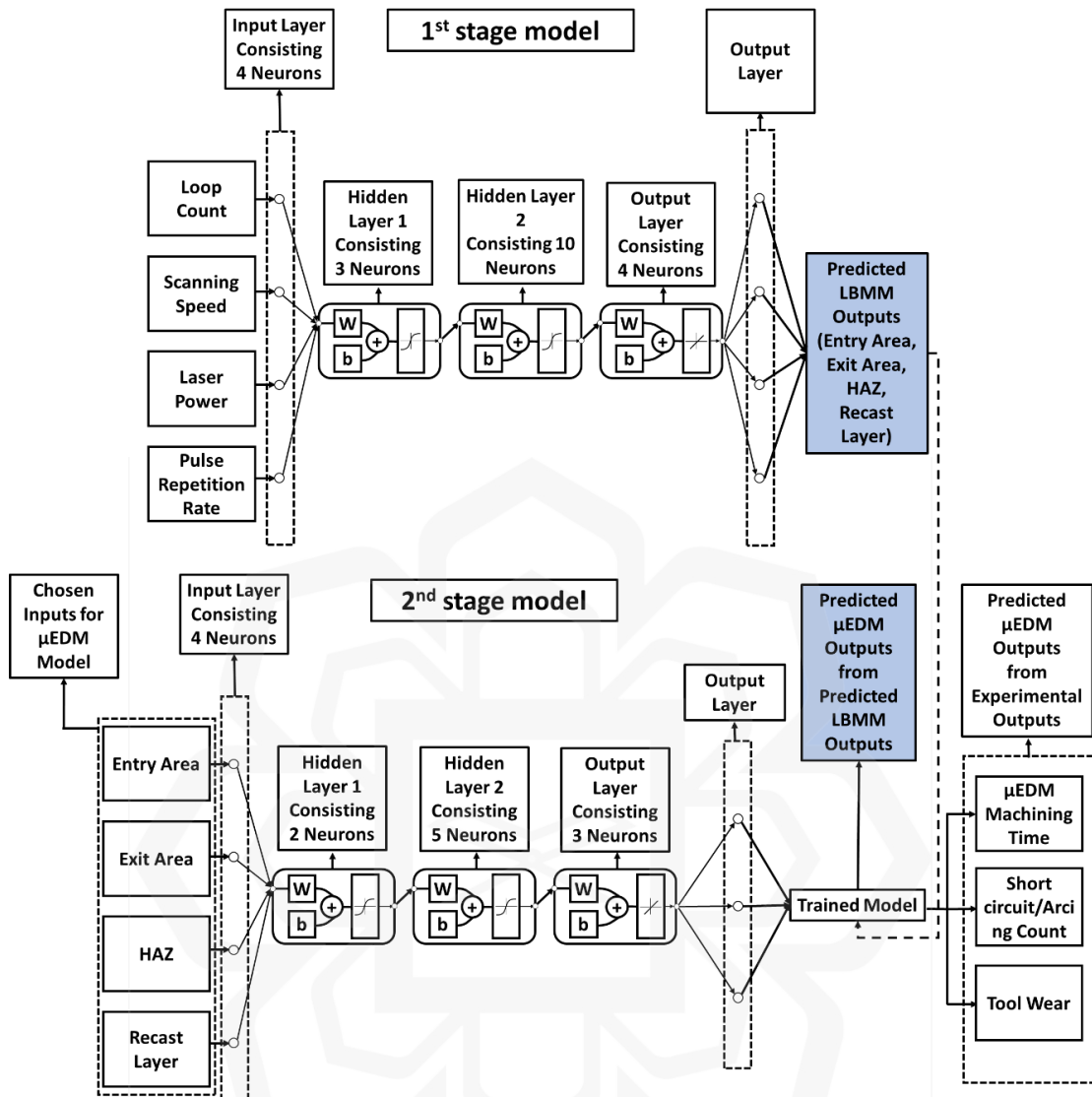


Figure 3.9 LBMM-μEDM process dual-stage ANN model flow and architecture (Noor et al., 2021)

3.7.2 Modeling of the LBMM- μEDM Drilling with Variable EDM Parameter

The second phase of this modeling will be conducted as like the Modeling of the LBMM-μEDM Drilling with constant EDM Parameters but here EDM parameters will be changed at the second-stage of modeling. Additionally, this model is developed following MIMO techniques that forecasts the various objective variables using a linked model, referred to

in this report as a "dual-stage ANN model." In the proposed model, initial LBMM inputs are used to predict different LBMM outputs. In the second-stage, various LBMM outputs and various μ EDM inputs are served into the model as inputs to assess the amount of time required for μ EDM machining, the likelihood of short circuits and arcing, and tool wear. The model will be put into practice in accordance with Figure 3.10.

The correlation study aids in the selection of appropriate predictors for the LBMM- μ EDM process template. All potential key in (LBMM) that were altered in accordance with Table 3.7 are regarded as input throughout the modeling method for the first-stage model (first-stage). All of the LBMM outputs are fairly well affected by laser power and scanning speed.

Table 3.7 Correlation coefficient between various LBMM inputs and outputs

Correlation Table			
	Output Variables→		
Input Variables ↓	Volume removed	HAZ	Recast layer
Laser Power	0.5067	0.4343	0.5139
Scanning Speed	-0.6948	-0.3143	-0.4951
Pulse repetition rate	0.0487	-0.0059	-0.0759

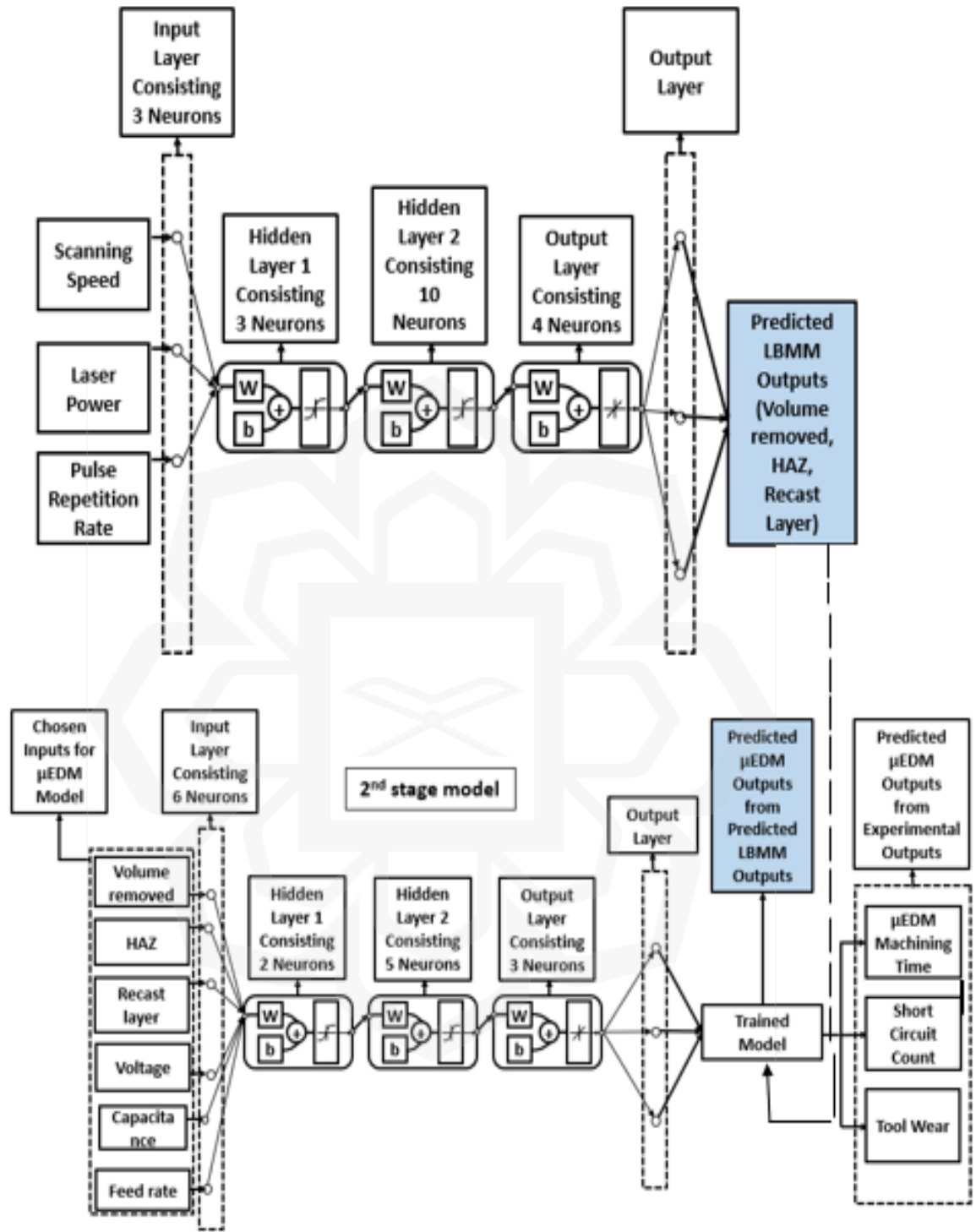


Figure 3.10 LBMM-μEDM process dual-stage ANN model flow and architecture (drilling with Variable EDM Parameter)

3.7.3 Modelling of the LBMM- μ EDM Milling with Constant EDM Parameter

The final phase of hybrid micro milling (LBMM- μ EDM) RSM-based modeling was used with the EDM input parameters kept constant. The various laser parameters are described in Table 3.8 and 3.9. Table 3.10 shows the complete experimental runs.

Table 3.8 The level and parameter settings chosen for the experiments.

Parameter/Factors	Low value	High value
Scanning speed (mm per second)	1500	2500
Power (%)	20	90
Pulse repetition rate (KHz)	5	15
Loops (nos)	5	15

Table 3.9 Values of machining variable and levels

Variables	-1	0	1
Scanning speed (mm per second)	1500	2000	2500
Power (W)	20	55	90
Pulse repetition rate (KHz)	5	10	15
Loops (nos)	5	10	15

Table 3.10 Box Behnken design of input and output responses

Std	Run	Factor 1 A:SS mm/s	Factor 2 B:Power %	Factor 3 C:Freq KHz	Factor 4 D:Loop nos	Response 1 Time s	Response 2 TW um	Response 3 Shortcircuit nos
16	1	2000	90	15	10	30.96	29	47
25	2	2000	55	10	10	41.6	31	57
24	3	2000	90	10	15	34.56	26	77
11	4	1500	55	10	15	38.03	19	61
5	5	2000	55	5	5	38.93	26	77
6	6	2000	55	15	5	44.86	28	70
9	7	1500	55	10	5	41.38	29	78
4	8	2500	90	10	10	38.85	26	90
2	9	2500	20	10	10	47.02	27	68
15	10	2000	20	15	10	48.23	33	109
1	11	1500	20	10	10	45.28	31	87
10	12	2500	55	10	5	46.83	31	106
3	13	1500	90	10	10	38.36	31	74
22	14	2000	90	10	5	36.36	29	104
7	15	2000	55	5	15	38.61	23	59
14	16	2000	90	5	10	34.03	23	44
19	17	1500	55	15	10	42.9	33	79
23	18	2000	20	10	15	43.36	24	52
13	19	2000	20	5	10	52.5	41	107
18	20	2500	55	5	10	44.15	31	96
20	21	2500	55	15	10	48.71	36	85
17	22	1500	55	5	10	44.93	28	77
8	23	2000	55	15	15	36.85	26	54
12	24	2500	55	10	15	37.08	24	61
21	25	2000	20	10	5	48.68	39	97

3.8 SUMMARY

This chapter details out experimental setup, procedure for experimentations as well as characterization and finally describes various steps involved in the modelling process.

CHAPTER FOUR

RESULTS AND DISCUSSION

4.1 INTRODUCTION

This chapter presents the experimental findings of the LBMM- μ EDM based hybrid micromachining. It discusses the parametric effect of the LBMM parameters as well as the μ EDM parameters on the overall performance of the process. The chapter also presents various aspects of the modelling of the LBMM- μ EDM process using the artificial neural network. Finally, this chapter detailed out the study on LBMM- μ EDM-based micro-milling using Response Surface Methodology (RSM).

4.2 EFFECT OF THE LBMM PARAMETER ON THE HYBRID LBMM- μ EDM PROCESS

In this study, the outcomes of laser input parameters (scanning speed, laser power and pulse repetition rate) on the performance of the finishing technique, in this case EDM, are experimentally investigated on stainless steel (type SS304). One-dimensional machining (such as micro hole drilling) is the scope of the work. This work has been published in “The International Journal of Advanced Manufacturing Technology” [Rashid, M. A. N., Saleh, T., Noor, W. I., & Ali, M. S. M. (2021). Effect of laser parameters on sequential laser beam micromachining and micro electro-discharge machining. *The International Journal of Advanced Manufacturing Technology*, 114, 709-723. <https://doi.org/10.1007/s00170-021-06908-8>].

4.2.1 Morphological Comparison of the Hole Quality (LBMM- μ EDM)

Figure 4.1 provides a morphological comparison of the hole quality among the three processes used, namely LBMM, μ EDM, and LBMM- μ EDM. LBMM method performs the best in terms of machining time as it can drill the hole in less than one minute, yet in regards to the quality of the hole LBMM performed the worst as it resulted in a thick recast layer and low circularity. Alternatively, the quality of the holes machined by μ EDM and LBMM- μ EDM sequential process was almost identical. However, the time taken for LBMM- μ EDM sequential process to drill the hole was approximately ~ 2.6 x times lower as compared to the pure μ EDM method as shown in Figure 4.2. The above findings are also in line with the results reported by previous researchers (Al-Ahmari et al., 2016). Figure 4.2 also shows that the occurrence of the short circuit during the LBMM- μ EDM process was much smaller as compared to the standard μ EDM process (~ 40 x) which indicates that LBMM- μ EDM is more stable in contrast to pure EDM.

Additionally, vertical tool wear was also found to be almost ~ 9 x lower for the case of sequential micromachining. The reason for the improved machining stability and lower tool wear is because in the LBMM- μ EDM method, the total material to be eliminated from the workpiece is lesser in comparison to the pure μ EDM. Moreover, Figure 4.3 shows the tilted scanning electron microscopic views of the holes. It can be seen from Figure 4.3 (a) that the pilot hole machined by the LBMM process contains a significant recast layer (similar to Figure 4.1) with a non-uniform inner surface. The recast layer can be entirely removed, and a hole with a uniform inner-surface can be created by the subsequent μ EDM-based finishing operation Figure 4.3 (b). Further note that the quality of the LBMM- μ EDM hole Figure 4.3 (b) is as good as the pure μ EDM hole Figure 4.3 (c) in terms of the inner-

surface uniformity and minimized recast layer. In the next sections, we will discuss how various LBMM parameters influence different performance indicators of the LBMM- μ EDM-based sequential micromachining. Among the three Laser parameters that we varied in this study (pulse frequency, scanning speed and power) pulse frequency did not show any dominant influence on the performance of the said sequential micromachining process.

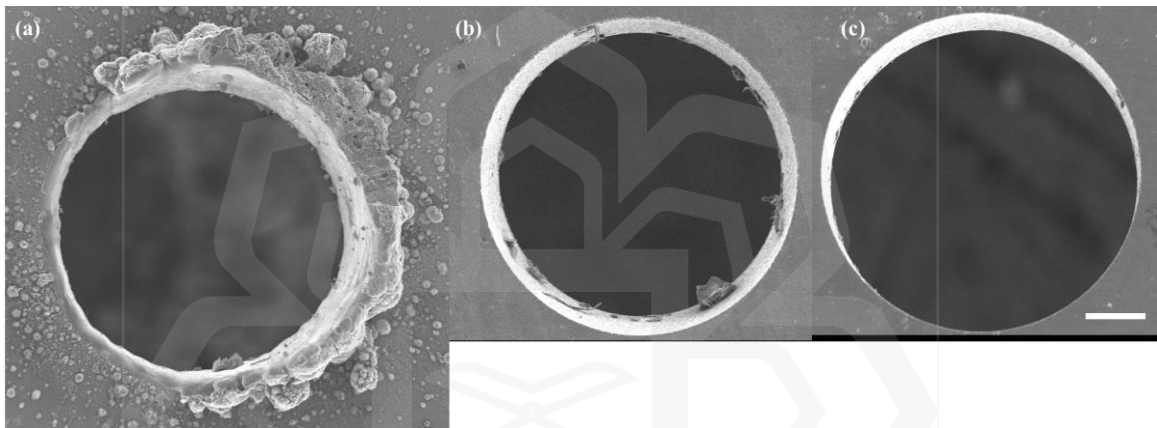


Figure 4.1: The structural representation of various micro holes produced by pure a) LBMM, b) pure μ EDM, and c) LBMM- μ EDM based hybrid processes. The processing parameters of the LBMM was 15.5W, 50mm/s, and 20kHz. Scale bar = 100 μ m (Rashid et al., 2021b).

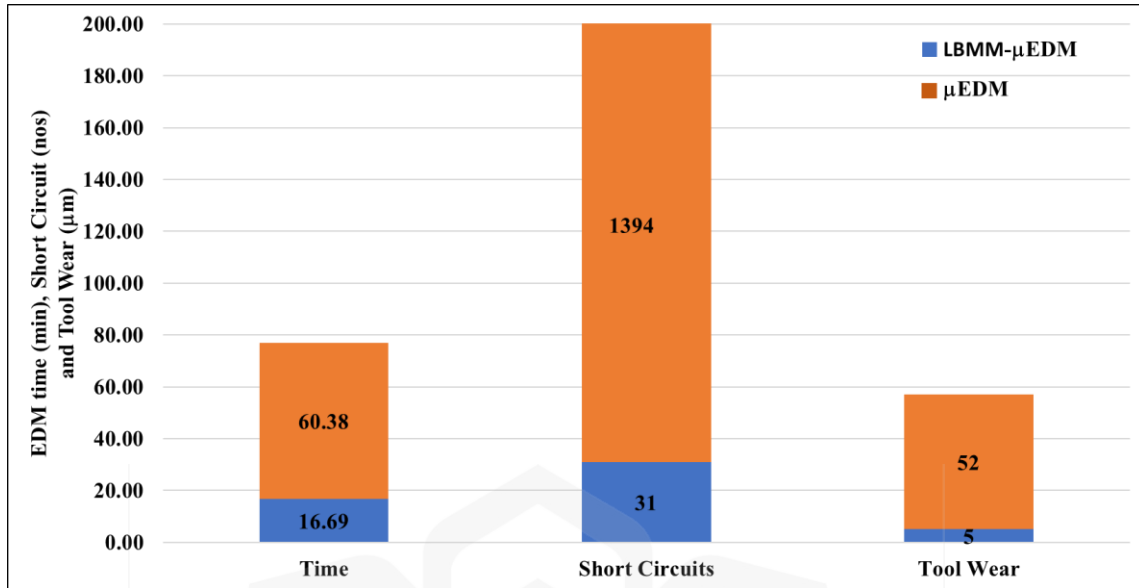


Figure 4.2: The figure shows the comparison between LBMM-μEDM and pure μEDM: compared parameters are machining time, number of short circuits, and tool wear (Rashid et al., 2021b).

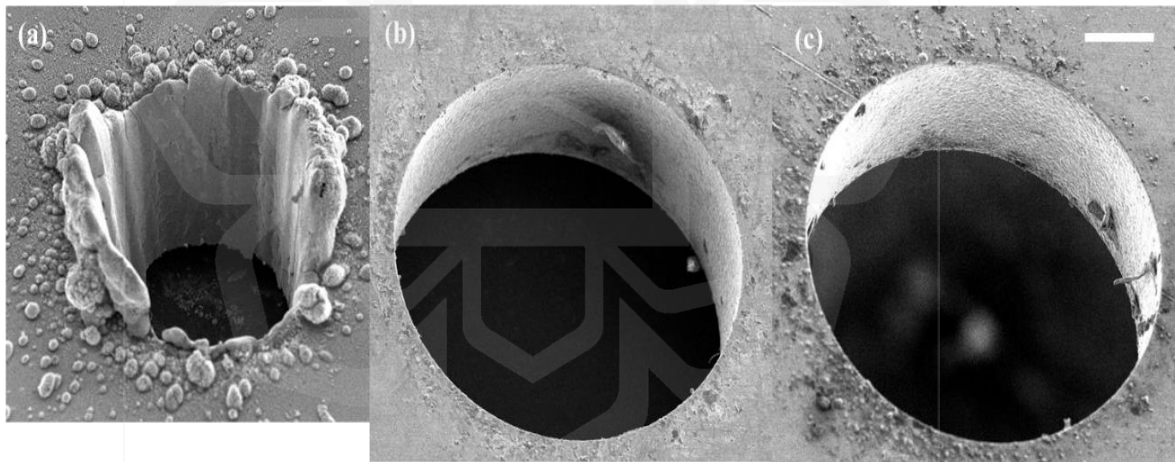


Figure 4.3: Comparative study of the structure of the micro holes produced by (a) the LBMM machining (b) LBMM-μEDM machining and (c) purely μEDM machining. Scale bar = 100 μm (Rashid et al., 2021b).

4.2.2 Study of μEDM machining time for laser-μEDM process

As previously indicated, the LBMM-μEDM-based sequential micromachining process used in this study was designed to fine-finish the LBMMed holes. First, the LBMM was

utilised, and then the μ EDM machining was applied. The finishing time by μ EDM was significantly longer than the time required for the machining of the LBMM. The variation of the μ EDM machining time for the pilot holes drilled with different laser power, scanning time, and pulse frequencies is shown in Figure 4.4. Our research validates that there is no discernible impact of pulse frequency on μ EDM machining time. We found that it takes less time for μ EDM to fine-finish pilot holes that are machined with a higher laser power and a slower scanning speed. The result is different for the LBMMed holes that are machined at a high scanning speed.

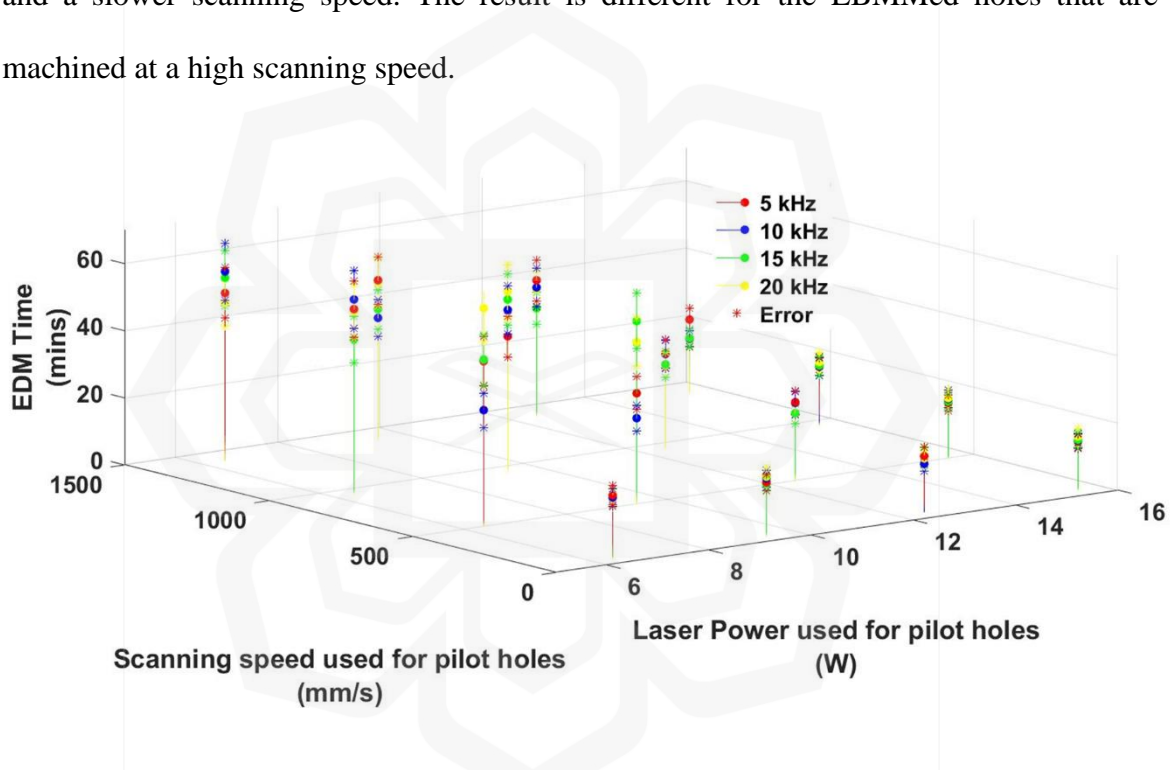


Figure 4.4: The impact of the laser parameters used in the first-stage of machining on the processing time of the second-stage EDM for the final pilot hole finishing? The machining uncertainty is displayed by the error bar (Rashid et al., 2021b).

As the laser pulse frequency was found to have a random effect on the final machining time by μ EDM, it was averaged up. Figure 4.5 shows the effect of laser power and scanning speed (with the frequency effect being averaged) on the final μ EDM time to get more quantitative insight into the whole process. It can be inferred from Figure 4.5 that if a

scanning speed of less than or equal to 200 mm/s is used with any range of laser power (6.4W to 15.5W) for the LBMM operation, then the final μ EDM operation can be completed within 30 mins. Further, for high laser power (≥ 13 W) even the highest scanning speed can be used for the LBMM machining yet the final finishing procedure by μ EDM can be done in less than or equal to 30 mins. Figure 4.6 shows the average discharge frequency and discharge current measured during the μ EDM ing operation of the LBMMed holes. This Figure (Figure 4.6 (a) and Figure 4.6 (b)) also reinforces the finding that the machinability improves for the LBMMed holes processed with higher laser power and lower scanning speed as both discharge frequency and discharge value increases due to the improvement in the ease of machining (Mahardika et al., 2008). The phenomena observed in Figure 4.4 and Figure 4.5 can be described from the study of the LBMMed holes entry, exit area, and removed volume during the LBMM process.

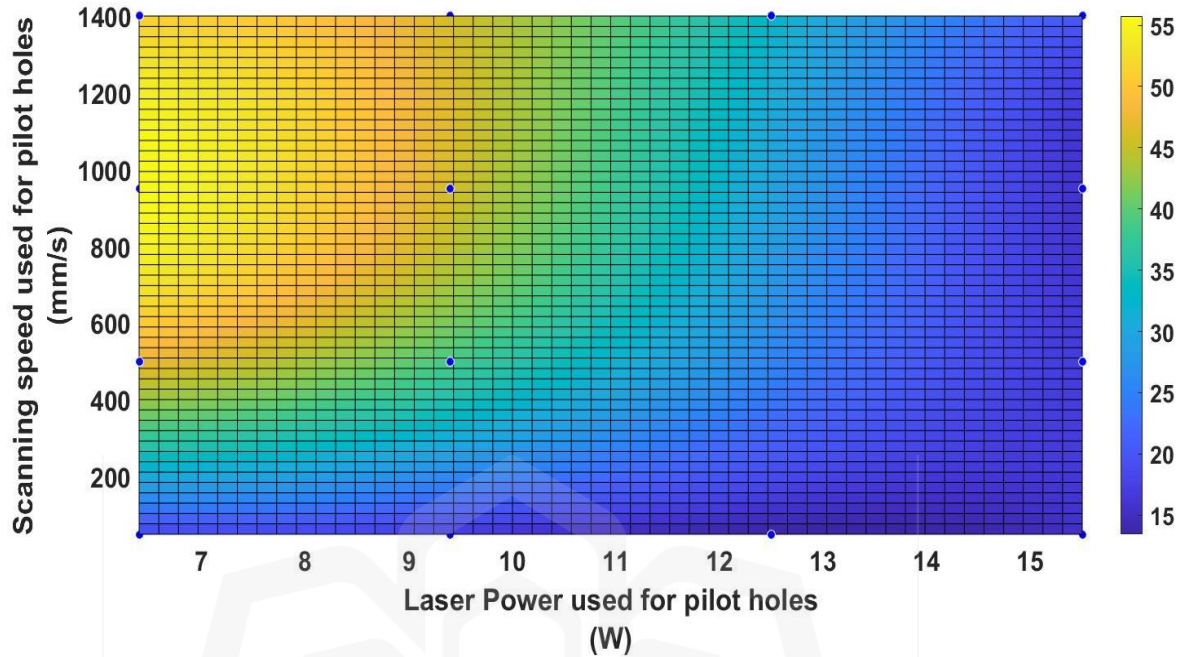
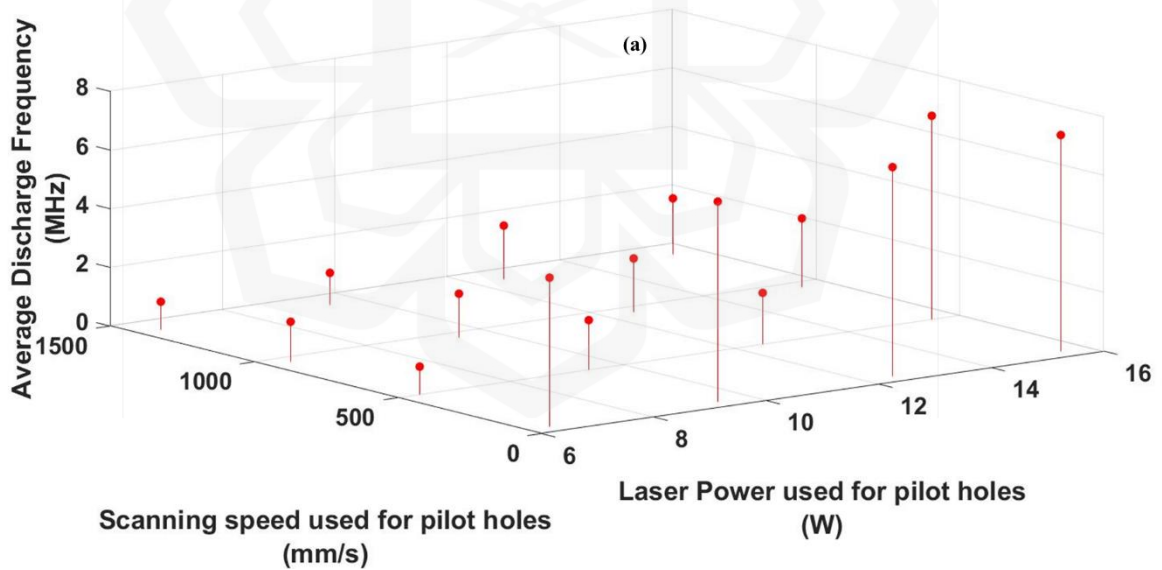


Figure 4.5: The correlation between laser incident power, scanning speed, and the zone of faster and slower μ EDM machining time (used for pilot hole drilling using the LBMM process) (Rashid et al., 2021b).



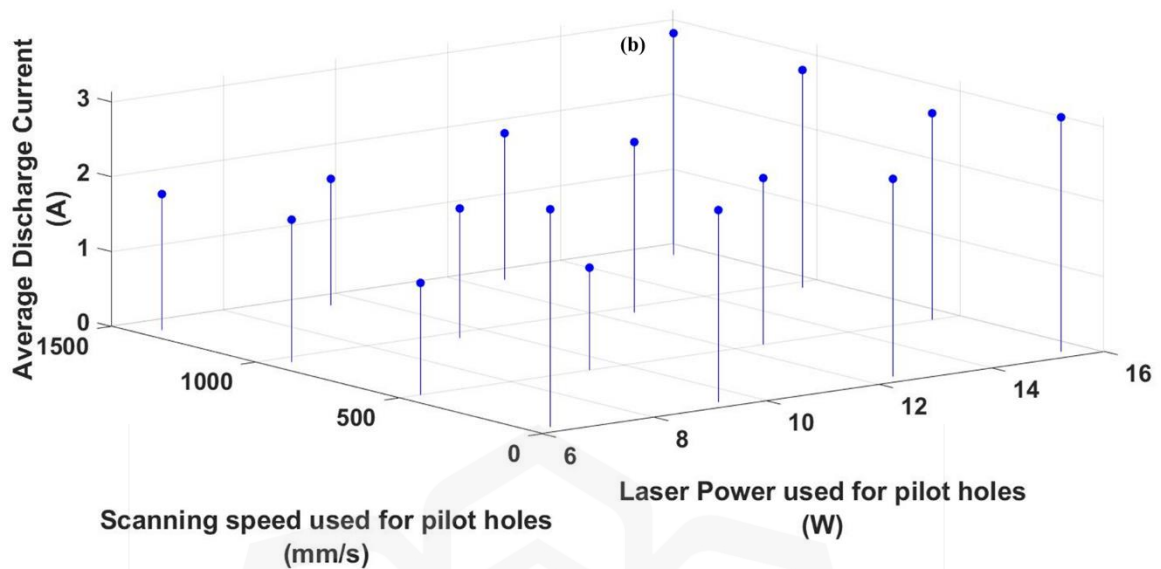


Figure 4.6: Demonstrates how the laser power and scanning speed used for the pilot hole machining affect the discharge current and frequency during the EDM process: (a) the discharge current variation, and (b) the discharge frequency variation. (Rashid et al., 2021b).

Figure 4.7 describes the effect of laser power and pulse frequency on the entry area of the initial holes for different laser scanning speeds. It can be realized from Figure 4.7 (a-d) that, the holes' entry area has an increasing trend with the laser power. However, we could not find any significant relation between the entry area and the pulse frequency of the laser. Further, Figure 4.8 shows the SEM images of the holes machined at different laser power which also confirms the increasing trend in the entry area (Figure 4.8a-d) with the incident laser power. On the other hand, Figure 4.9 describes that higher laser scanning speed averagely causes the entry area of the LBMMed holes to be reduced. Negarestani & Li, (2012) stated that in the LBMM process, the incident energy density is proportional to the laser power and inversely proportional to the scanning speed. In our study, as the incident

energy became higher with the increase in the laser power, the entry area of the hole was also expanded.

Similarly, lower energy density due to the faster scanning speed decreased the holes' entry area. Regarding the exit area of the LBMMed holes, phenomena similar to the entry area were observed, as shown in Figure 4.10 (a-d). However, it can be said that the effect of scanning speed was found to be more dominant on the variation of the exit area as compared to the entry area, which is also visible from the SEM images, as shown in Figure 4.11 (a-d). At a slow-scanning speed like 50 mm/s, we had holes significantly penetrated for the whole range of power. As the scanning speed was equal or more than 500 mm/s laser power less than or equal to 9.4W could not melt and vaporize the material enough to result in LBMMed holes with substantial exit area. Also, Figure 4.12 demonstrates that the volume of material removed during the LBMM process increases with increasing average laser power and decreases with higher scanning speed. The trend of the μ EDM machining time observed in Figure 4.4 and Figure 4.5 is the effect of LBMMed holes' volume resulting from laser power and scanning speed variation. As mentioned, the higher incident laser power and lower scanning speed caused significant removal of material during the pilot hole machining by the LBMM process. Therefore, during the μ EDM operation, the machine was required to remove lesser material which caused in faster processing time (Figure 4.4 and Figure 4.5).

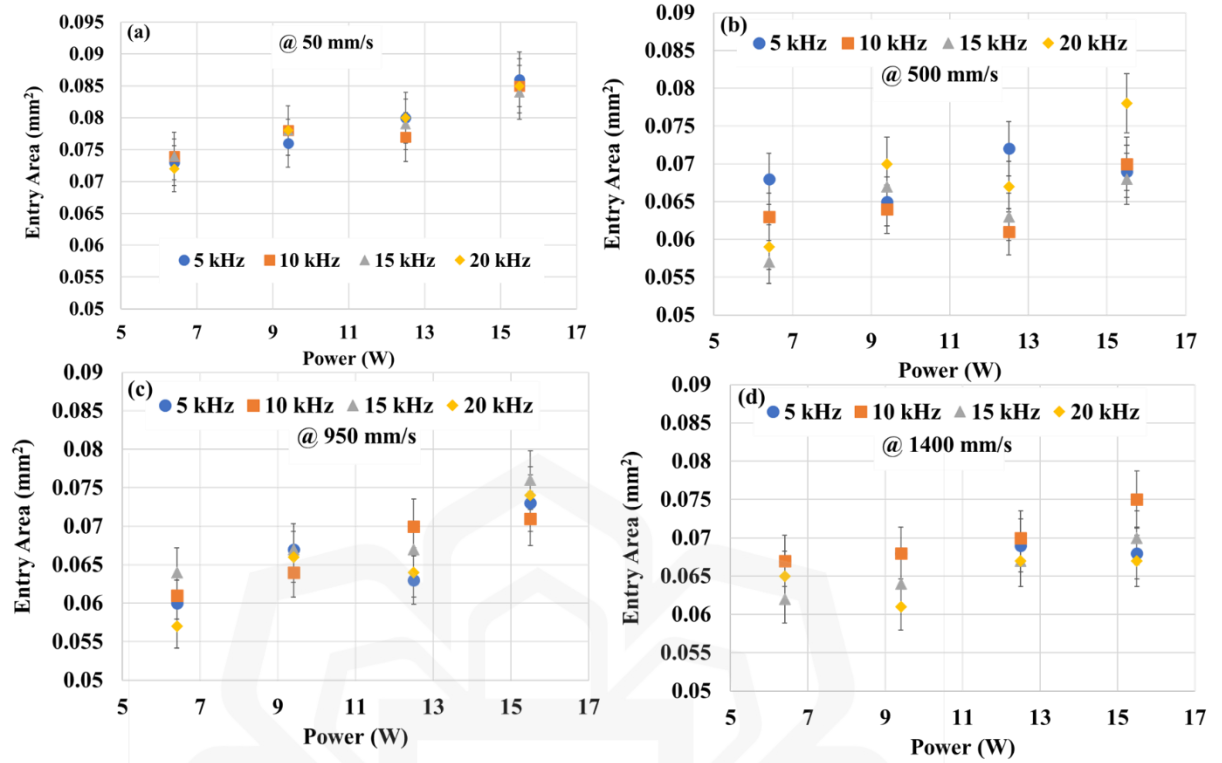


Figure 4.7: The impact of laser power and pulse frequency on LBMM pilot hole entry area. (a) Scanning was 50 mm/s. (b) 500 mm/s scanning speed. (c) Scanning speed was 950 mm/s. (d) 1400 mm/s scanning speed. All examples had 75 loops. The error bar represents overall uncertainty (Rashid et al., 2021b).

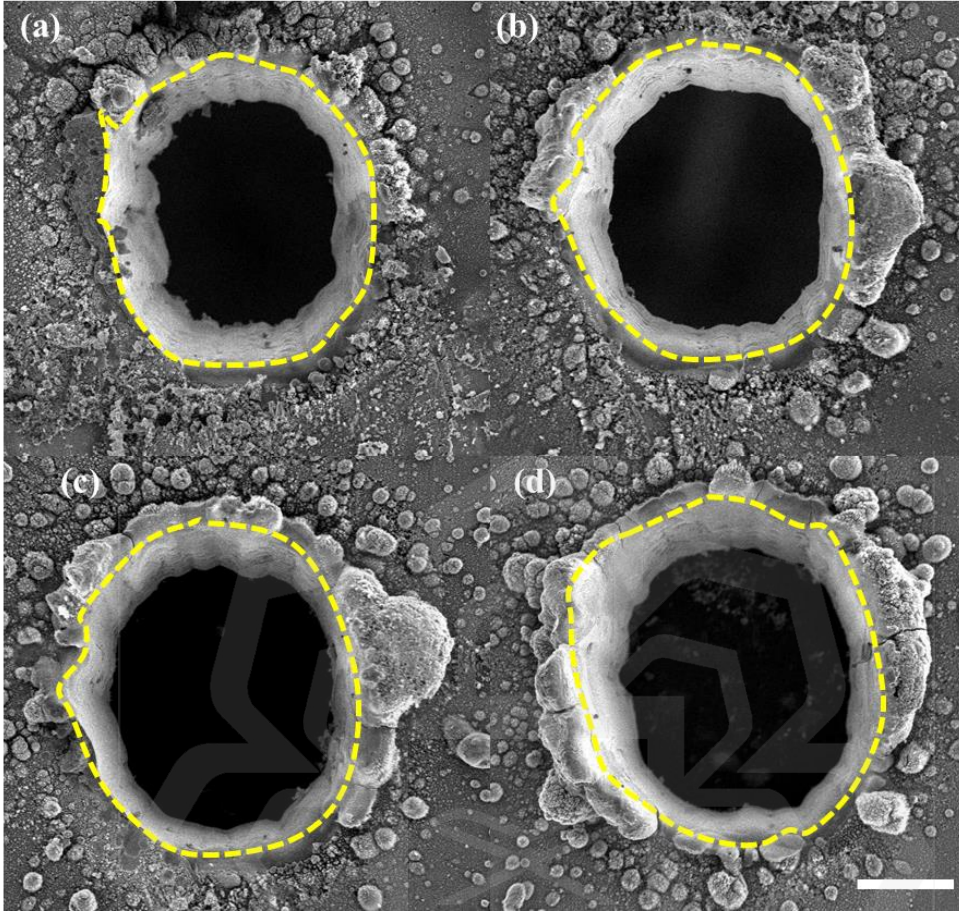


Figure 4.8: The SEM pictures of the LBMMed holes' entry region created with various incident laser powers. There are four different laser power levels: (a) 6.4W, (b) 9.4W, (c) 12.5W, and (d) 15.5W. There were 75 loops, the scanning speed was 50 mm/s, and the laser pulse frequency was 5 kHz for every hole. Bar scale: 100 μ m. The entry area is marked with a black edge marker (Rashid et al., 2021).

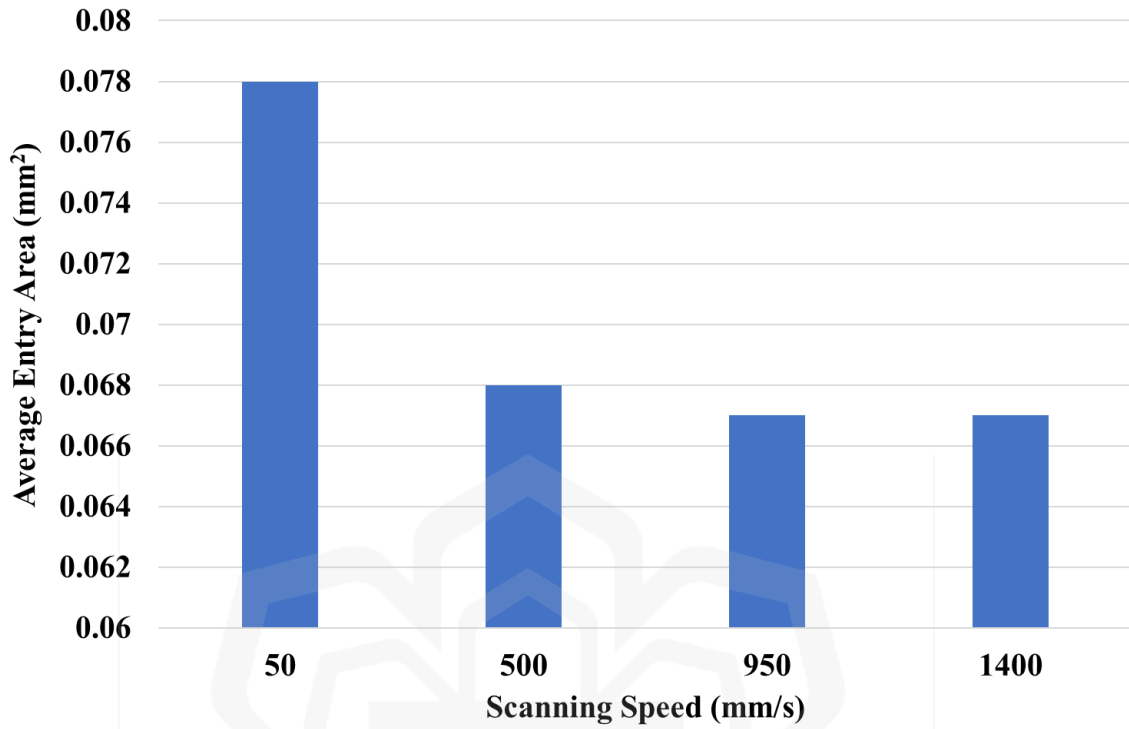


Figure 4.9: The average impact of the laser scanning speed on the pilot hole entry area that the LBMM process machined. To plot this graph, all the data for each scanning speed have been averaged up. (Rashid et al., 2021)

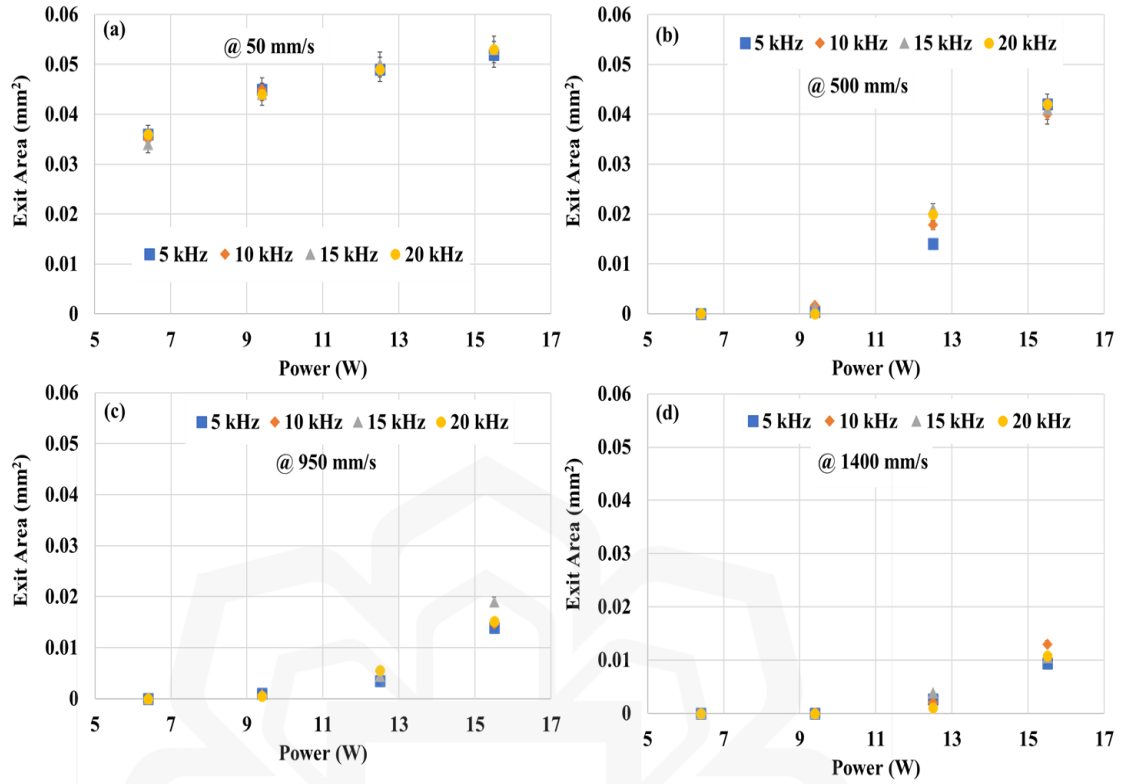


Figure 4.10: The effect of the incident laser power and pulse frequency on the exit area of the pilot holes made by the LBMM process. (a) scanning speed 50 mm/s. (b) scanning speed 500 mm/s. (c) scanning speed 950 mm/s. (d) scanning speed 1400mm/s. In every case, there were 75 loops. The error bar shows the overall uncertainty (Rashid et al., 2021b).

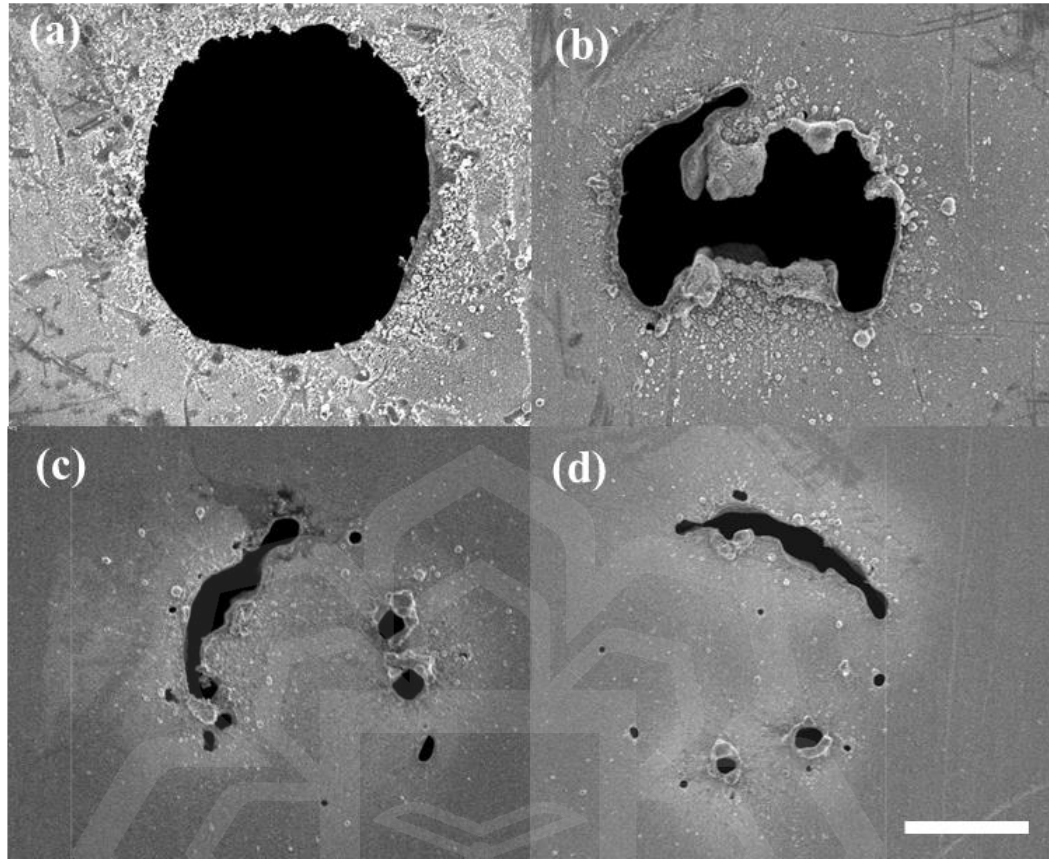


Figure 4.11: The impact of the incident laser scanning speed on the exit area of the pilot holes made by the LBMM process. (a) scanning speed of 50 mm/s, (b) scanning speed 500 mm/s, (c) scanning speed 950 mm/s, and (d) scanning speed 1400 mm/s. All of the holes had a laser pulse frequency of 15 kHz, 75 loops, and 6.4W of incident laser power. Scale bar = 100 μm (Rashid et al., 2021b).

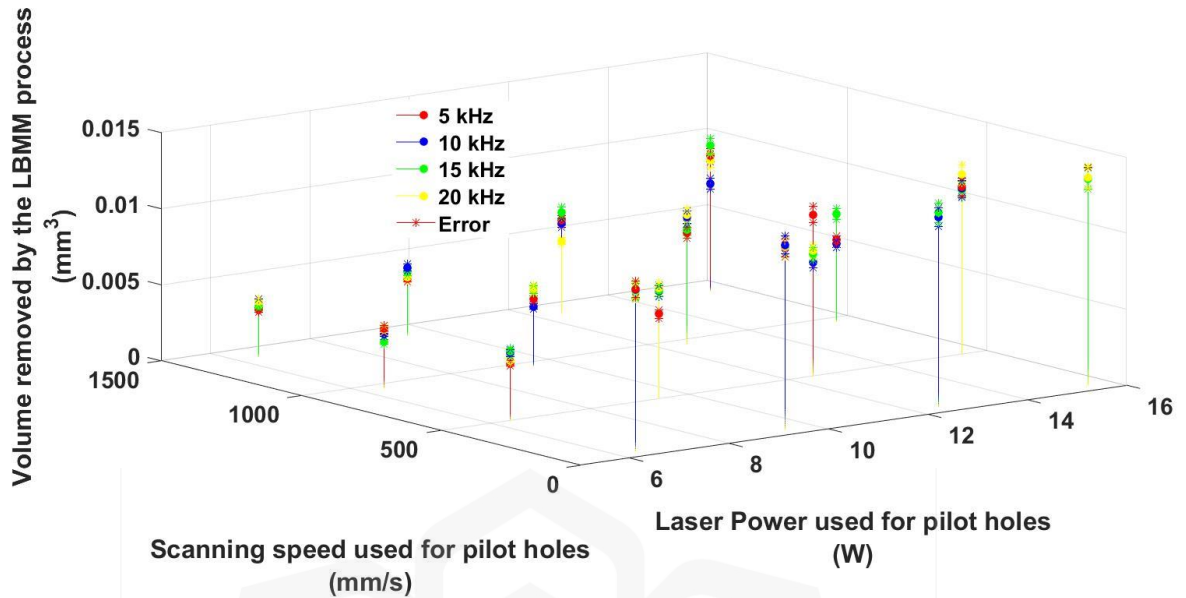


Figure 4.12: The relationship between average laser power and scanning speed and the amount of material removed by the LBMM process (Rashid et al., 2021b).

4.2.3 Study of μ EDM Machining Stability and Tool Wear for laser- μ EDM process

Machining stability for the μ EDM process (secondary operation of LBMM- μ EDM machining) is denoted by the short circuits' occurrence during the operation. The DT110 μ EDM machine is designed in such a way that if there is a detection of the short circuit during the μ EDM process, the tool path of the electrode will be reversed to overcome the temporary short circuit condition. The μ EDM operation is said to be unstable if too many short circuits are detected in a single machining process. As μ EDM is an electrothermal method, it causes the electrode to be worn out also due to repeated sparks. In this study, we have measured both the short circuit, and the vertical tool wear by the method explained in section two. As described in Figure 4.13 (a-d), it is clear that both tool wear and short circuit during μ EDM finishing decrease if higher laser power and slower laser scanning speed are used during the LBMM-based rough drilling. This phenomenon can be explained by Figure 4.14 which shows that both tool wear and the number of short circuits during μ EDM is

highly correlated (positively) with the μ EDM time with the correlation factors 0.92 Figure 4.14 (a) and 0.99 Figure 4.14 (b) respectively. This means higher μ EDM time will cause more increased tool wear and short circuit occurrence due to the more extended tool and workpiece interaction. Figure 4.5 confirms that if higher laser power and slower scanning speed are used for LBMM drilling, then μ EDM ing time required for fine finishing of the LBMMed holes will be reduced hence lower tool wear and short circuit occurrence during the operation. If the LBMM process uses the power of 6.4W with a scanning speed as high as 1500 mm/s, then the tool wear and short circuit can go up to ~58 mm and ~1045 respectively which is almost similar to that of pure μ EDM. However, if a high power of 15.5W or above is employed with any range of scanning speed, then the tool wear and the number of the short circuit will be around ~10 mm and ~100 respectively which is substantially reduced than the pure μ EDM (Figure 4.2). Figure 4.15 (a-b) provides additional evidence that the laser input parameters used for the pilot hole machining have a significant impact on not only the total tool wear and short circuits but also the average rate of tool wear and average rate of short circuit. If a high laser scanning speed is used at a low laser incident power during the LBMM process, the rate of tool wear and short circuit during the μ EDM process can increase to as high as 1mm/min and 20nos/min, respectively. The volumetric size of the LBMMed pilot holes decreases with increasing scanning speed and loWatt laser-power during the LBMM process (Figure 4.12). Because of this, the tool had to remove more material from the workpiece during μ EDM, which led to the formation of more debris. Tool wear and short circuit rates both rise as a result. On the other hand, because the LBMMed holes with larger volume of material removed require less material to be removed by the EDM operation, we saw higher discharge current and more frequent

sparking during the process (we monitored the discharge current). As a result, there were fewer short circuits and less tool wear.

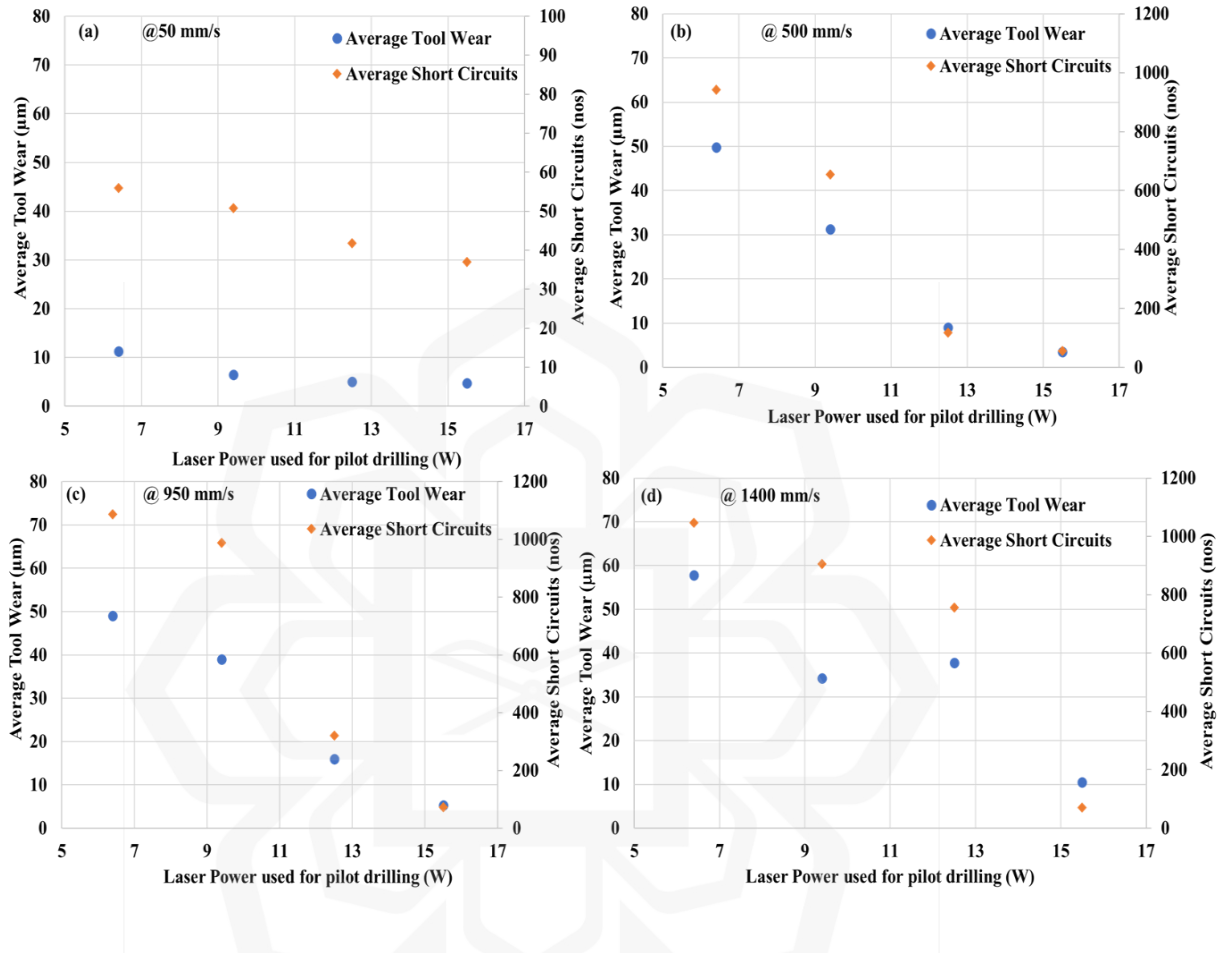


Figure 4.13: The amount of laser power used to drill the pilot holes determines the average amount of tool wear and the number of short circuits that occur during the μ EDM process. (a) 50 mm/s scanning speed. (b) 500 mm/s scanning speed. (c) 950 mm/s scanning speed. (d) 1400 mm/s scanning speed. Each time, there were 75 loops total (Rashid et al., 2021b).

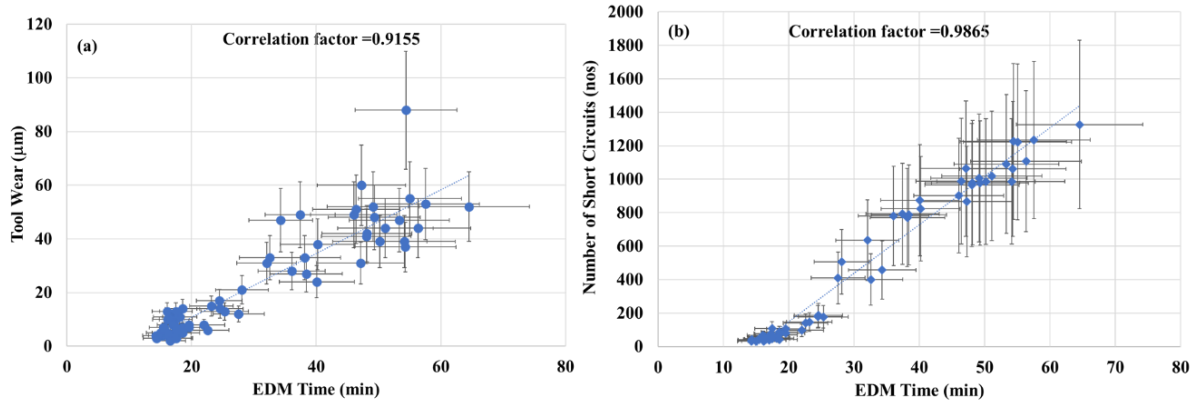
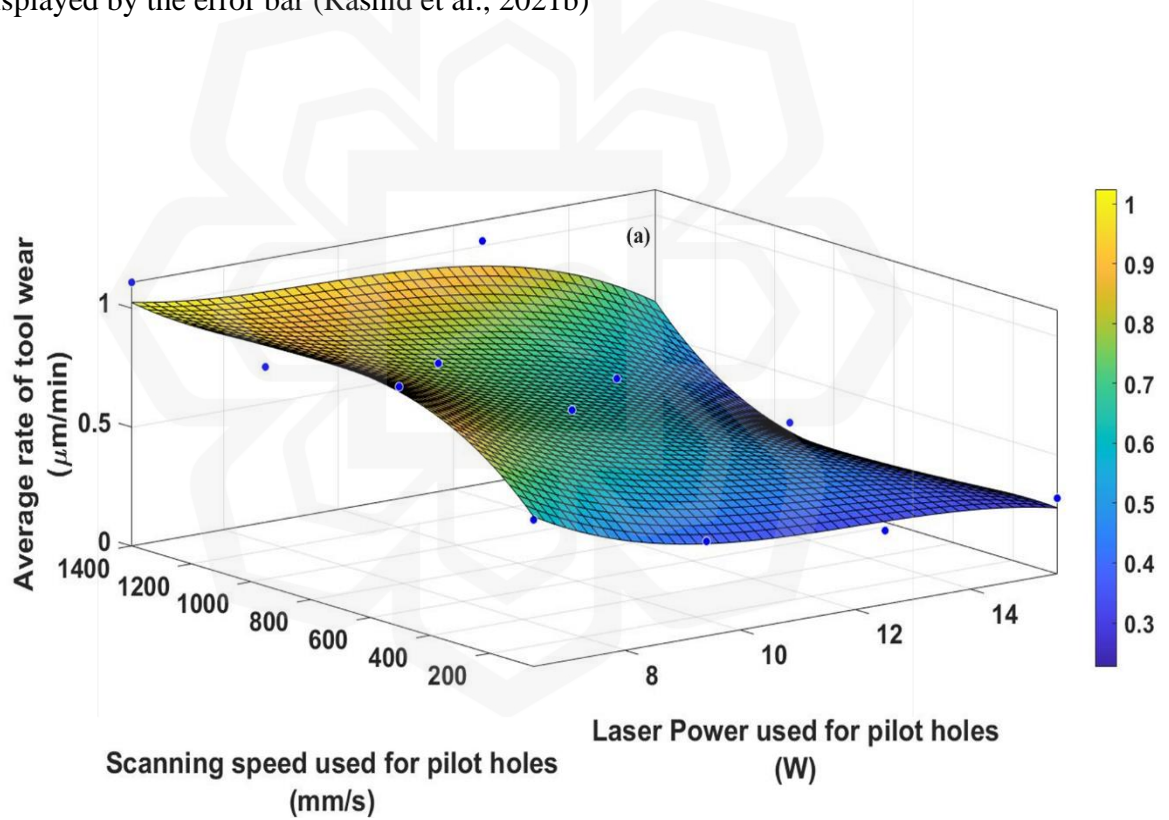


Figure 4.14: Tool wear and short circuits in relation to μEDM time. Tool wear versus μEDM time (a). (b) EDM time versus short circuits. The experimental variation is displayed by the error bar (Rashid et al., 2021b)



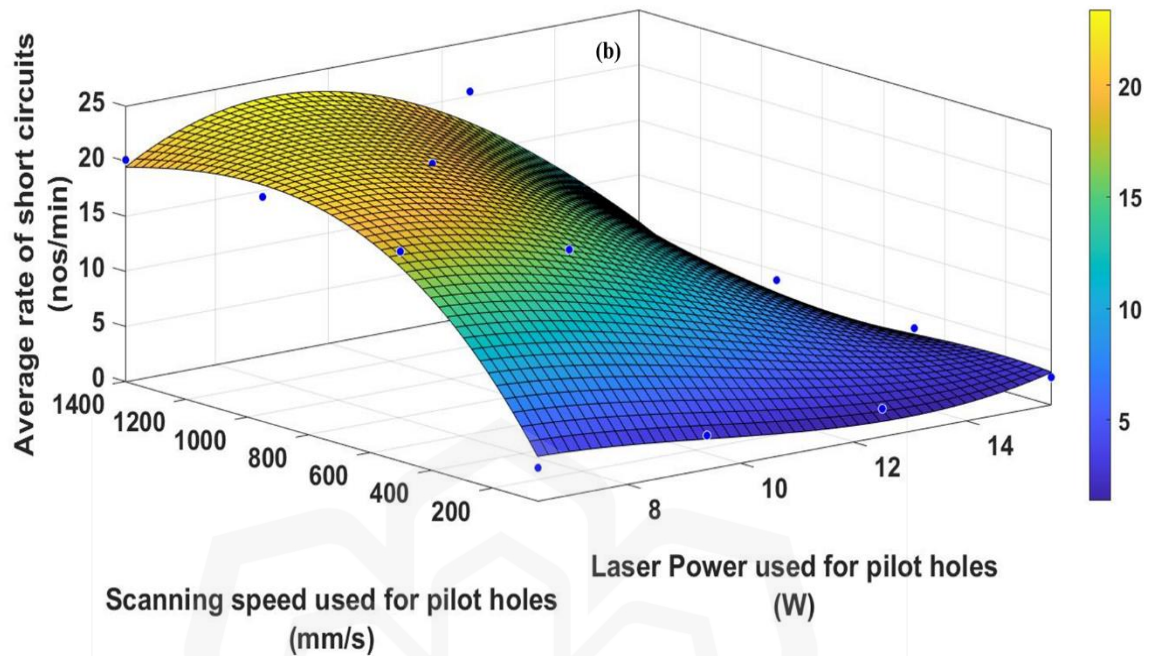


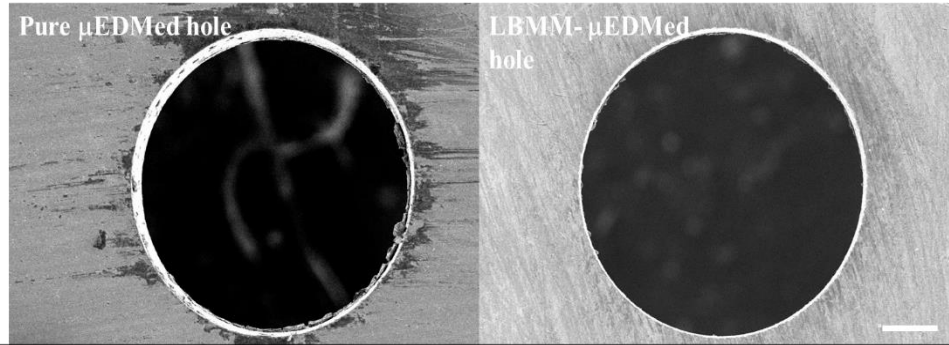
Figure 4.15: The relationship, as a function of laser incident power and laser scanning speed (used for pilot hole drilling using the LBMM process), between the average tool wear rate and the frequency of short circuits Tool wear rate (A) and short circuit occurrence rate (b) (Rashid et al., 2021b).

4.2.4 Study of Residual spatter zone for laser- μ EDM process

The area with residual spatter from the LBMM procedure should be completely eradicated during the sequential LBMM- μ EDM micromachining (Demir et al., 2010). However, our research has shown that the μ EDM process may not be able to completely remove the spatter zone if a high laser power (15.5W) and slow scanning speed are employed for the pilot hole drilling (using LBMM) with the currently programmed diameter of 200 mm. This problem can be solved in two ways, in the first method the sample plate can be cleaned with an Isopropyl alcohol (IPA) wipe followed by cleaning in an ultrasonic bath as suggested by (Schaeffer & Kardos, 2008). In the second method, the programmed diameter of the LBMM process could be optimized in such a way that the finishing operation by

μ EDM could altogether remove the residual spatter zone from the surface as generated by the LBMM. We experimentally tried several diameters and found out that if 100 μ m is used for the LBMM (laser power 6.4W, scanning speed 200 mm/s, pulse frequency 20 kHz) then μ EDM could completely remove the residual spatter zone. Figure 4.16 shows the comparison between the two holes machined with μ EDM and LBMM- μ EDM process. It is quite clear from the two pictures (Figure 4.16) that both the holes are completely clean from any spatter in the surroundings of the holes. It is obvious that by reducing the LBMMed diameter to half, the performance parameter of the μ EDM process is compromised. However, it is still significantly better than pure μ EDM as described in Figure 4.16 which shows that machining time, tool wear, and short circuit occurrence were improved by 95%, 4 x, and 2.5 x respectively.

The choice between the two processes (IPA wipe and ultrasonic bath or reducing the LBMMed hole size) for complete removal of the residual spatter depends on the user's preference. If the users go for IPA wipe and ultrasonic bath-based cleaning technique, then they can go for aggressive parameters during the LBMM process, i.e., higher programmed diameter and high laser power. However, if the users do not have the facilities mentioned above, then they need to choose a lower diameter for the LBMM process with lower power and elevated scanning speed.



μEDM time	61.26	31.35 (improved by more than 95%)
Tool wear (μm)	73	14 (improved by more than 400%)
Short Circuits Count (nos)	1327	367 (improved by more than 250%)

Figure 4.16: LBMM-μEDMed holes and pure μEDMed holes are compared. Both holes show that there is no spatter zone left on the area around the holes. Scale bar = 100 μm (Rashid et al., 2021b)

4.3 MODELLING OF THE LBMM-μEDM DRILLING PROCESS WITHOUT CHANGING THE μEDM PARAMETERS

Experiments were run using these process parameters to examine the effects of LBMM inputs on different output parameters. The performance of the sequential LBMM-μEDM process was predicted utilizing a dual-stage Artificial Neural Network-based model as a function of the different LBMM inputs. Not much study has been carried out that to describe the LBMM-μEDM based hybrid model accurately. Loop count, scanning speed, and average laser power are the LBMM input parameters that influence the μEDM machining time, tool wear, and machining uncertainty (short circuit/arc) count of the hybrid process. The pulse repetition rate was found have negligible accomplish on the performing of the overall hybrid process hence it was not considered for the modelling study. The study's main objectives are to create a robust model for predicting the various hybrid micro-drilling performance parameters utilizing LBMM input parameters and to determine whether the novel modelling approach can accurately represent the different parametric

effects. The main subjects of this section are the modelling performance and the analysis of the outcomes. The validity of the model has been investigated and verified. To demonstrate the physics underlying the results, the overall trend of the predicted outputs has been discussed and interpreted. This work has been published in “The International Journal of Advanced Manufacturing Technology” (Noor et al., 2021b). [Noor, W. I., Saleh, T., Rashid, M. A. N., Mohd Ibrahim, A., & Ali, M. S. M. (2021). Dual-stage artificial neural network (ANN) model for sequential LBMM- μ EDM-based micro-drilling. The International Journal of Advanced Manufacturing Technology, 117(11-12), 3343-3365. <https://doi.org/10.1007/s00170-021-07910-w>]

4.3.1 Modelling Performance and accuracy

The overall architecture of the model is described in Figure 3.9. Both stages of the dual-stage ANN model's modeling performance have been measured. This section examines the performance of the individual stages of the model as well as the overall performance of the model because the model's overall accuracy is influenced by the first-stage's prediction accuracy.

4.3.2 Modelling Performance Parameters

The following equations define the root mean square error, which is the performance criterion for the model used in this study:

$$y_{iRMSE} = \sqrt{\frac{\sum_{j=1}^N (y_{i_{j_{\text{actual}}}} - y_{i_{j_{\text{predicted}}}})^2}{N}} \quad (4.1)$$

$$N_{RMSE} = \frac{\sum_{i=1}^n y_{iRMSE}}{n} \quad (4.2)$$

Here, the root mean square error for each modelled variable is $y_{i_{RMSE}}$ in this case. $y_{i_{j_{actual}}}$ is the experimental result for the j_{th} observation's i_{th} variable. The i_{th} variable of the j_{th} observation's predicted output, on the other hand, $y_{i_{j_{predicted}}}$ is according to the developed ANN model. N_{RMSE} is the total network RMSE, which is determined by arithmetically averaging the RMSE of all the relevant variables, and n is the total number of variables. Equations (5) and (6), in which $P_{accuracy_i}$ is the prediction accuracy for the i_{th} variable and $P_{accuracy_N}$ is the overall network accuracy, define the accuracy.

$$P_{accuracy_i} = (1 - y_{i_{RMSE}}) \times 100\% \quad (4.3)$$

$$P_{accuracy_N} = (1 - N_{RMSE}) \times 100\% \quad (4.4)$$

For both phases of the model, the aforementioned four equations have been employed. The first-stage model, the proposed dual-stage ANN model's final output variables—entry area, exit area, recast layer, HAZ, μ EDM time, tool wear, and a number of short circuit/arcing—were used as the input variables for the second-stage model. The detail of the input and outputs of the model can be found in Figure 3.10

4.3.3 Study of The Model Performance

The overall performance of the model was identified based on first-stage and second-stage modelling in where the first-stage LBMM inputs (scanning speed, power, pulse repetition rate, and loop count) were employed to predict the output of first-stage (entry area, exit area, HAZ, and recast layer). In order to observe the inclusive performance parameters of the LBMM- μ EDM process, namely machining time, tool wear, and short circuit/arching count, these outputs were then fed into the second-stage model. The RMSE value of each

variable was calculated by comparing it against the actual experimental data. Micro EDM machining time, machining instability (short circuit/arc) count, and tool wear RMSE value was 0.1272, 0.1085, and 0.097 respectively. Figure 4.17 shows the holistic accuracy of μ EDM machining time, short circuit/arching count, and tool wear which is in a range of ~87 to ~90%. Figure 4.18 compares the first-stage, second-stage, and holistic performance of the model. It can be seen that the first-stage model significantly affects the holistic performance of the model. Figure 4.19 described the actual and predicted value of μ EDM machining time, short circuit/arching count, and tool wear by following dual-stage ANN modeling.

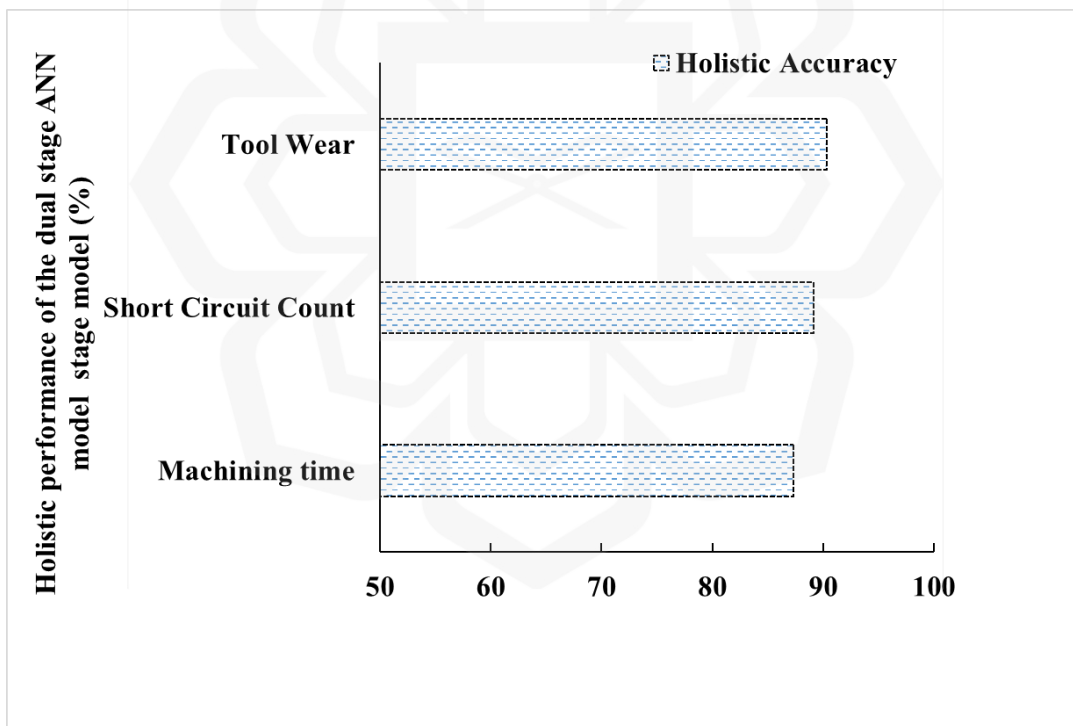


Figure 4.17: The dual-stage ANN model's holistic performance for μ EDM machining time, machining instability (short circuit), and tool wear (Noor et al., 2021a).

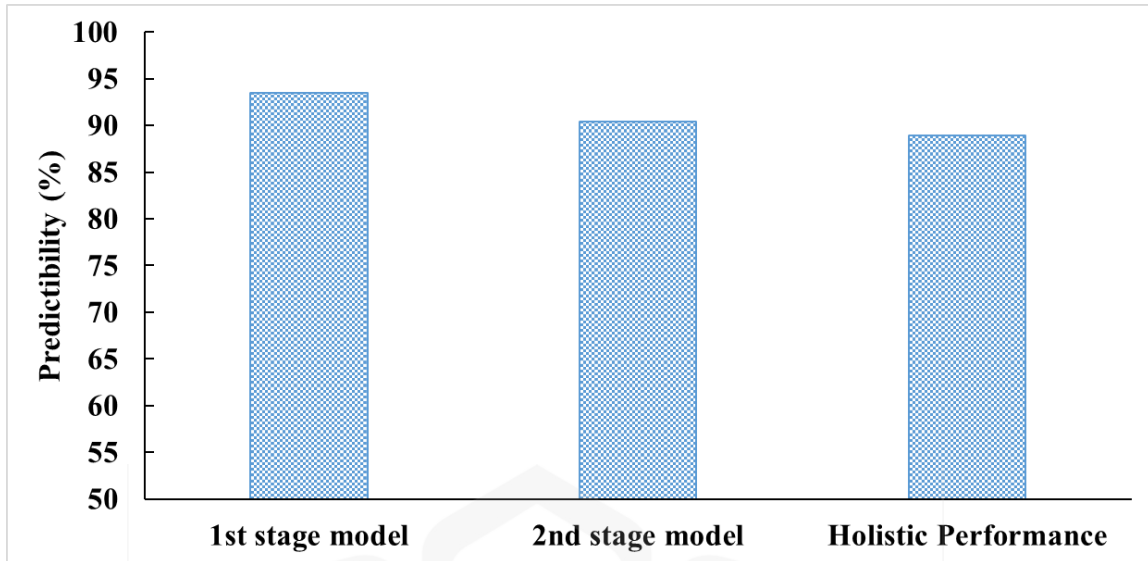
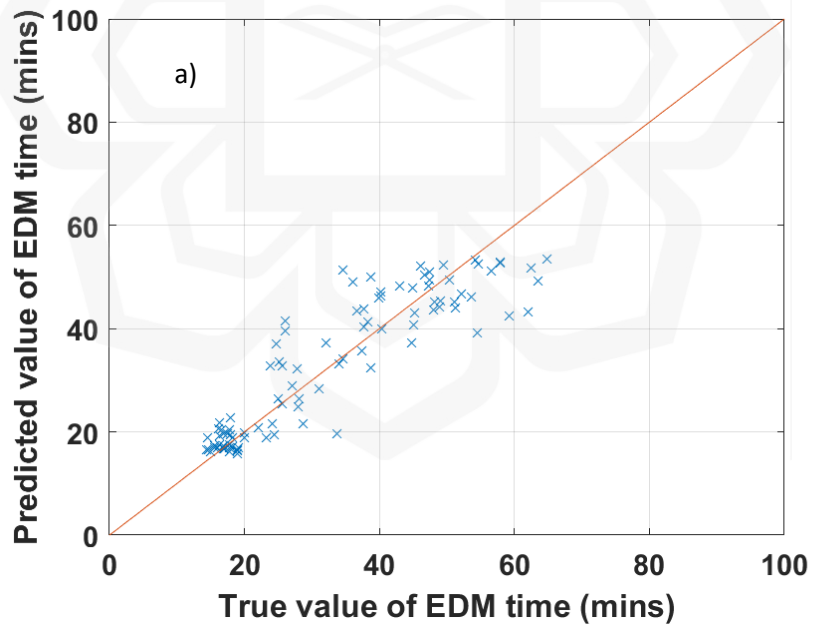


Figure 4.18: Performance evaluations for the first-stage model, second-stage model, and overall performance are compared (Noor et al., 2021a)



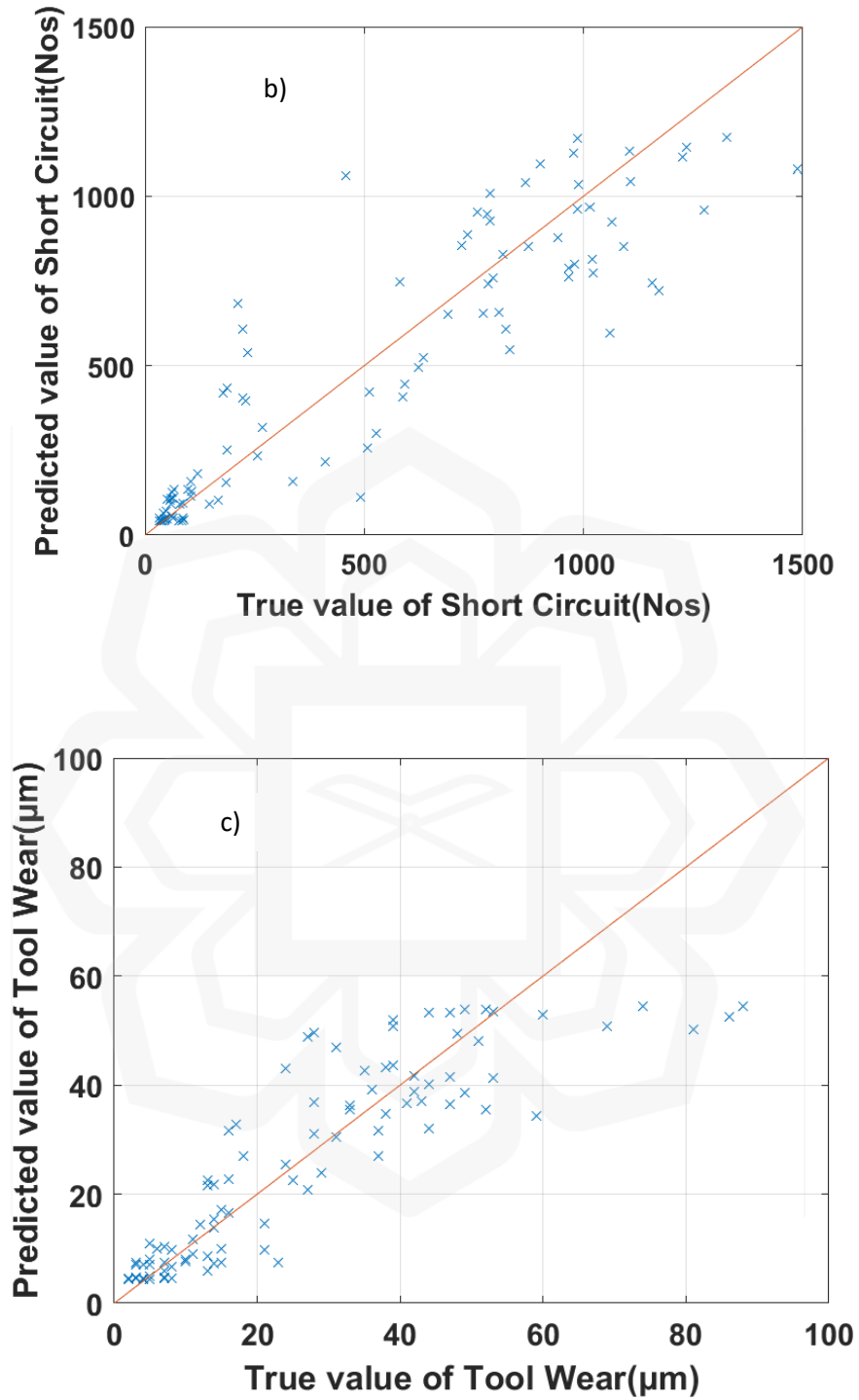
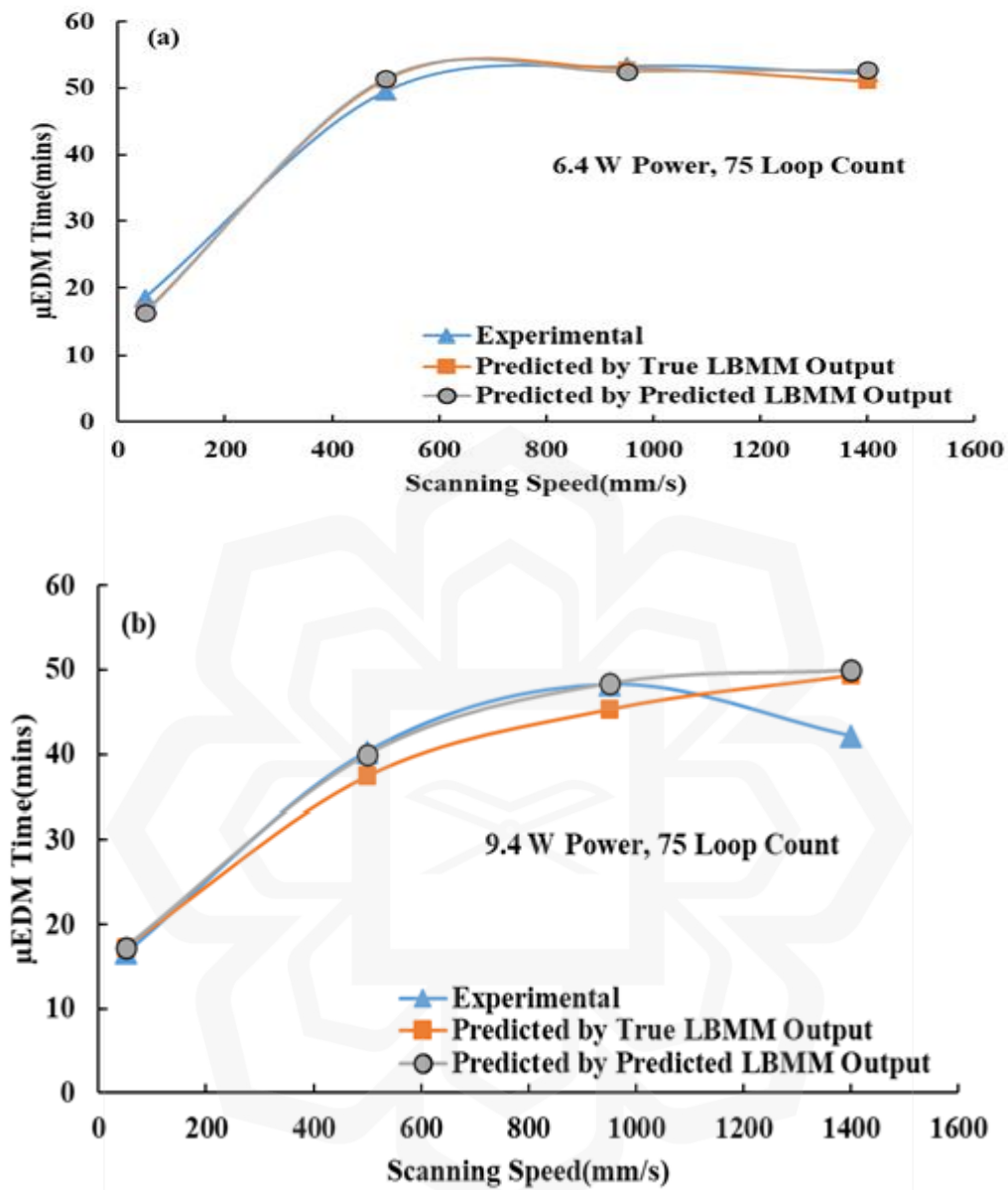


Figure 4.19: Experimental and dual-stage ANN model comparison for a) μ EDM machining time, b) machining instability (short circuit/arc) count, and c) tool wear (Noor et al., 2021a).

4.3.4 Study of parametric Effects

The machining time of the LBMM- μ EDM process is a major factor in determining its throughput. Figure 4.20 (a-d) depicts the cumulative impact of laser scanning speed and incident power applied to pre-machine the pilot holes on the μ EDM finishing time. When the laser scanning speed is elevated during the pilot machining of the LBMM- μ EDM combined process, it results in the removal of a reduced amount of material. Consequently, the subsequent μ EDM time increases. This phenomenon is particularly noticeable during the transition when the laser scanning speed is below 500mm per second (Figure 4.20 (a)). In cases where the speed exceeds 500mm per second and is coupled with low Watt laser-power, the LBMM process struggles to effectively remove substantial material, leading to a consistent and relatively high μ EDM finishing time. As mentioned above, it can be seen from Figure 4.20 (a-d) that higher scanning speeds used for pilot hole machining by the LBMM process require more time to complete the final finishing operation by μ EDM. It could happen because a higher laser scanning speed gets less time contact with the workpiece which causes a lower volume removal rate by the LBMM process. As shown in Figure 4.20 (d) that the scanning speed effect was less prominent in high-power zones such as 15.5W. Figure 4.20 (a-d) also indicates that if the laser scanning speed is as low as 50 mm/s (loop count is constant at 75), μ EDM finishing operation takes the same amount of time (15 to 20 minutes) no matter how much power is used to machine the LBMMed holes. Figure 4.20 suggest that if the applied laser power is more than 12.5 W then finishing time μ EDM operation can be achieved in less than 20 minutes provided the scanning speed during the LBMM process is less than 400 mm per second (loop count should be constant of 75).



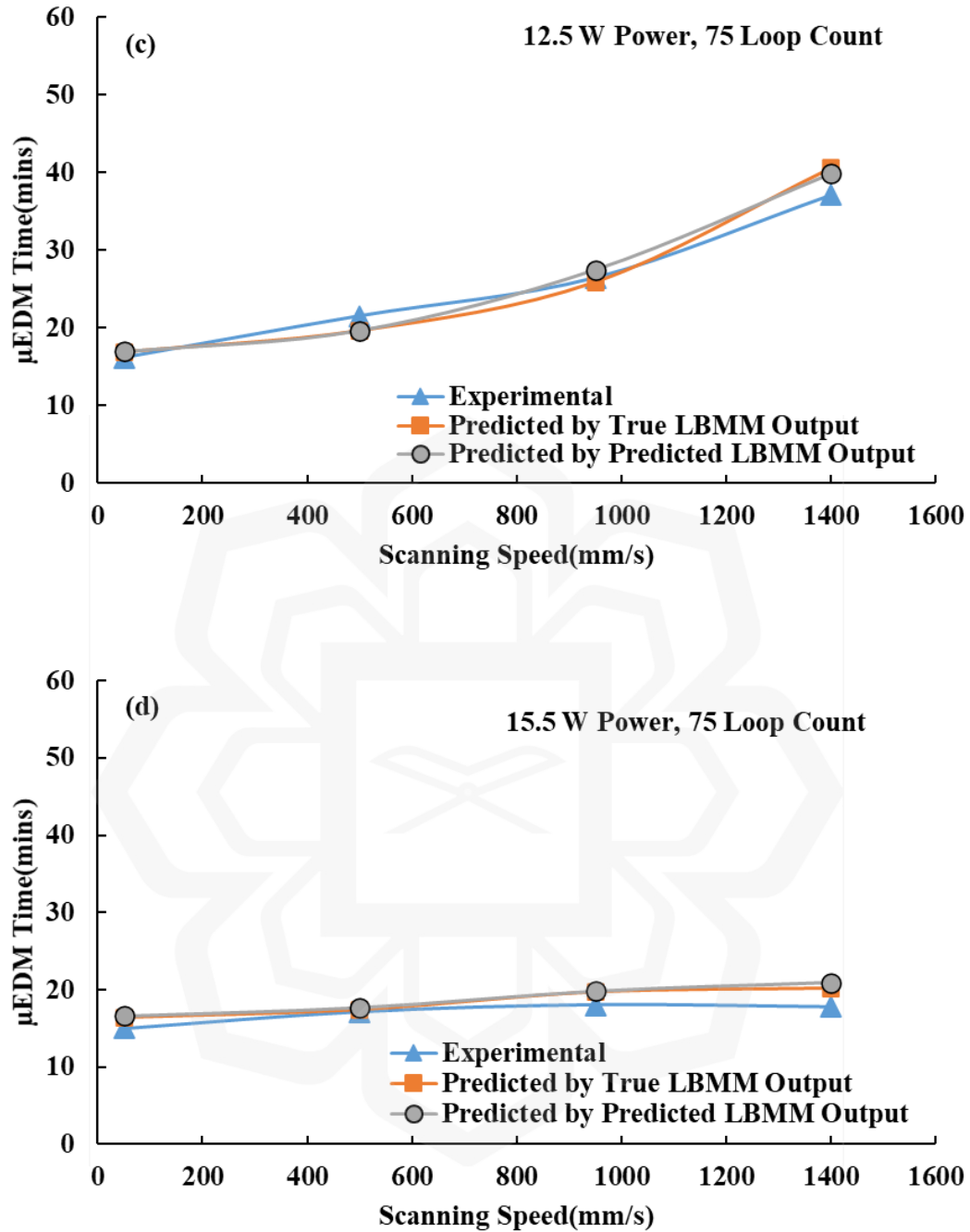


Figure 4.20: Variation in the amount of time needed for μ EDM machining at different scanning speeds for LBMMed pre-machined holes at various laser powers. The data on the graph are experimental values, predicted values based on the parameters of the actual LBMMed holes, and estimates based on the parameters of the predicted LBMMed holes. The pre-machined holes were produced using 6.4 W, 9.4 W, 12.5 W, and 15.5 Watt laser-powers, respectively (Noor et al., 2021a).

Figure 4.21 illustrated that the μ EDM finishing operation time become shorter while the laser loop count number was higher.

As previously observed in the analysis of the correlation coefficient, the influence of loop count on LBMM outputs, such as entry area and recast layer, was found to be negligible (refer to Table 3.6). However, with an increasing number of loops, the thermal dealings concerning the material and the laser intensified. Consequently, the exit area and the Heat-Affected Zone (HAZ) correlated with LBMMed holes expanded. As the thermal contact deepened with each pass, the laser-ablated holes exhibited increased depth with a higher loop count. Ultimately, this led to a reduced amount of material that needed to be removed in the final μ EDM operation.

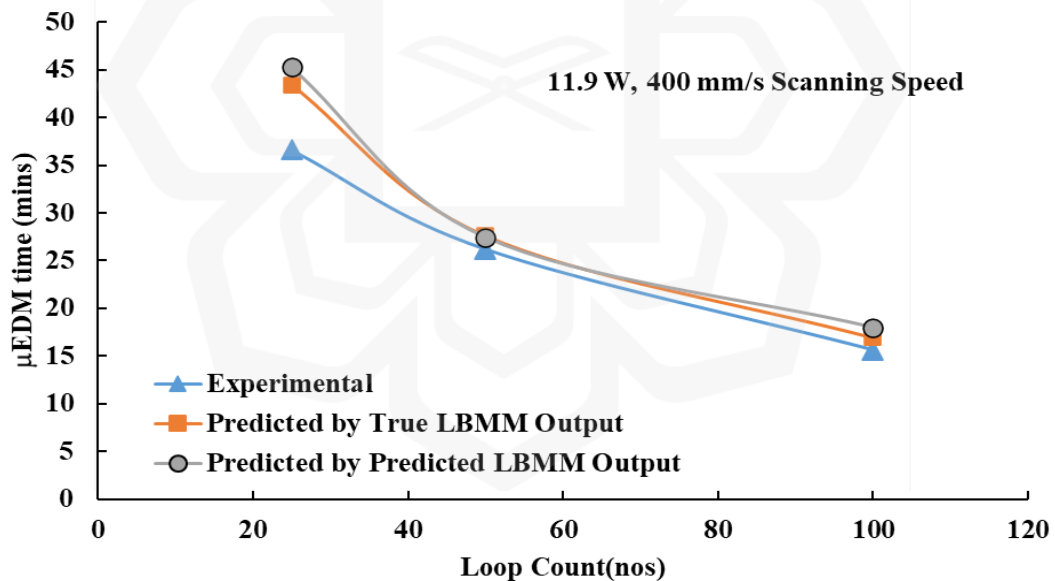


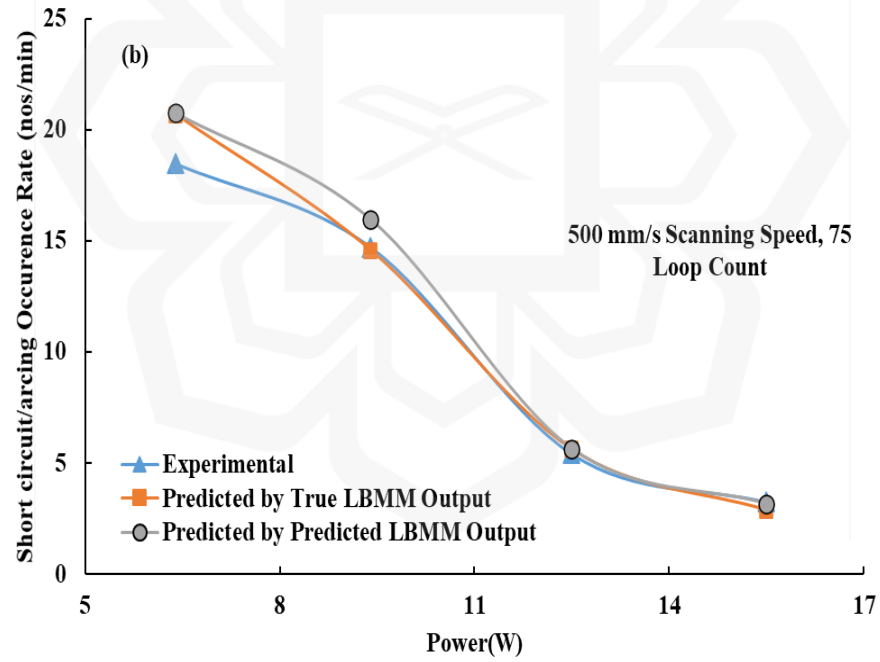
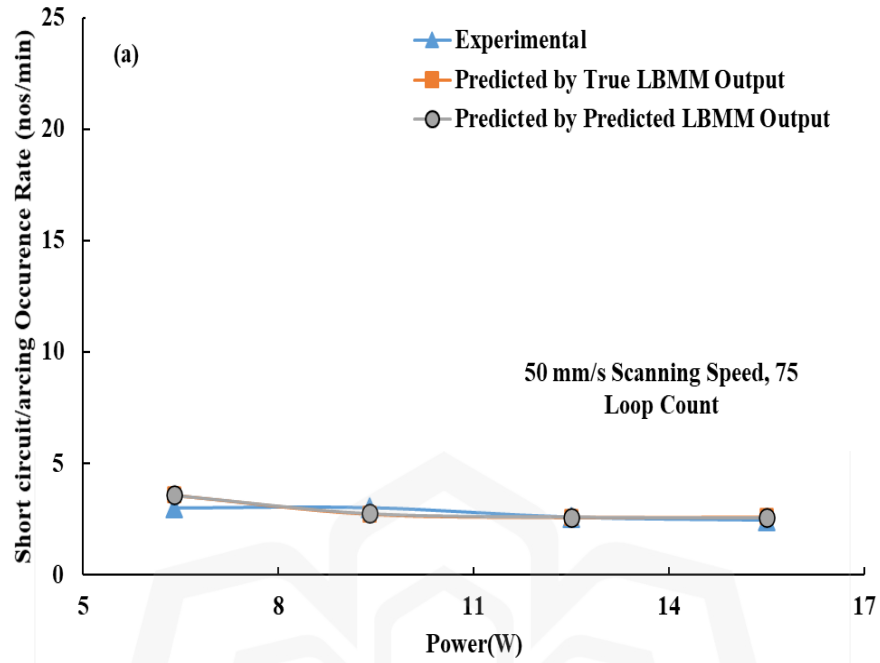
Figure 4.21: μ EDM machining time with loop count Variation for LBMMed pre-machined holes machining at 11.9Watt laser-power, 400 mm/s Scanning Speed, and 10 kHz Pulse repetition rate. The data on the graph are experimental values, predicted values based on the parameters of the true LBMMed holes, and estimates based on the parameters of the predicted LBMMed holes (Noor et al., 2021a)

The short circuit/arc count has a bad impact on μ EDM machining operation which is undesirable in the machining process. The short circuit is caused by physical contact at the machining zone between the tool and debris or the tool and the workpiece. If the μ EDM machining time is extended, there is a greater possibility that both short circuit/arc count and vertical tool wear will increase. Figure 3.8 demonstrates the strong correlation between machining instability (short circuit/arc) count and vertical tool wear and machining time, with correlation coefficients of more than 0.9. Figure 4.22 and Figure 4.23 shows the short circuit/arc count and tool wear rate during the μ EDM finishing operation. Figure 4.22(a) illustrates that the machining instability (short circuit/arc) happening rate is fairly stable within the range of 5 nos/min for the entire range of incident power. This is probably because the LBMM process removes a significant amount of material, which eases up the second-stage of μ EDM operation. A high rate of short circuit/arc occurred when the low power laser was used in the LBMM process, but this rate drastically decreased when the laser power was raised for scanning speeds of 500 mm/s and above (Figure 4.22(b)–(d)). The dual-stage model's output reveals that the average trend (Figure 4.22a–d) is comparable to the experimental findings. Due to the unpredictability of the short circuit/arc detection, however, it is possible to observe some discrepancies in the experimental results.

During μ EDM operation, the rate of tool wear resembles the trend of short circuit/arc occurrence rate depicted in Figure 4.23 (a–d). In the event that a faster scanning speed (greater than 500 mm/s) and a lower incident laser power (6.4W) are utilized in the LBMM process, the electrode experienced a tool wear rate of less than one micrometer per minute ($1\mu\text{m}/\text{min}$) in the process of μ EDM finishing operation. However, the tool wear rate can be reduced by nearly 50% throughout the μ EDM action if the LBMM process is carried

out at high power (15.5W) with any scanning speed. The decrease in the tool wear rate during the secondary process, namely μ EDM, can be elucidated as follows. When a higher power is applied during the LBMM process, it effectively removes a significant portion of the substantial from the workpiece. Consequently, the μ EDM process requires less time to finely finish the hole, resulting in reduced interaction between the μ EDM plasma and the tool. This diminished dealings between the plasma and the tool contributes to a lower tool wear rate.

Figure 4.24 (a-b) depicts how the number of loops influences the rate of tool wear and the frequency of short circuit/arcing in fine EDM machining (at persistent scanning speed and laser incident power). For LBMMed holes, a higher loop count was used because it removed more material from the ablated zone and eased the μ EDM process by lowering the rate of machining instability (short circuit/arcing) occurrence and tool wear. As a result, both parameters' rates slowly decline.



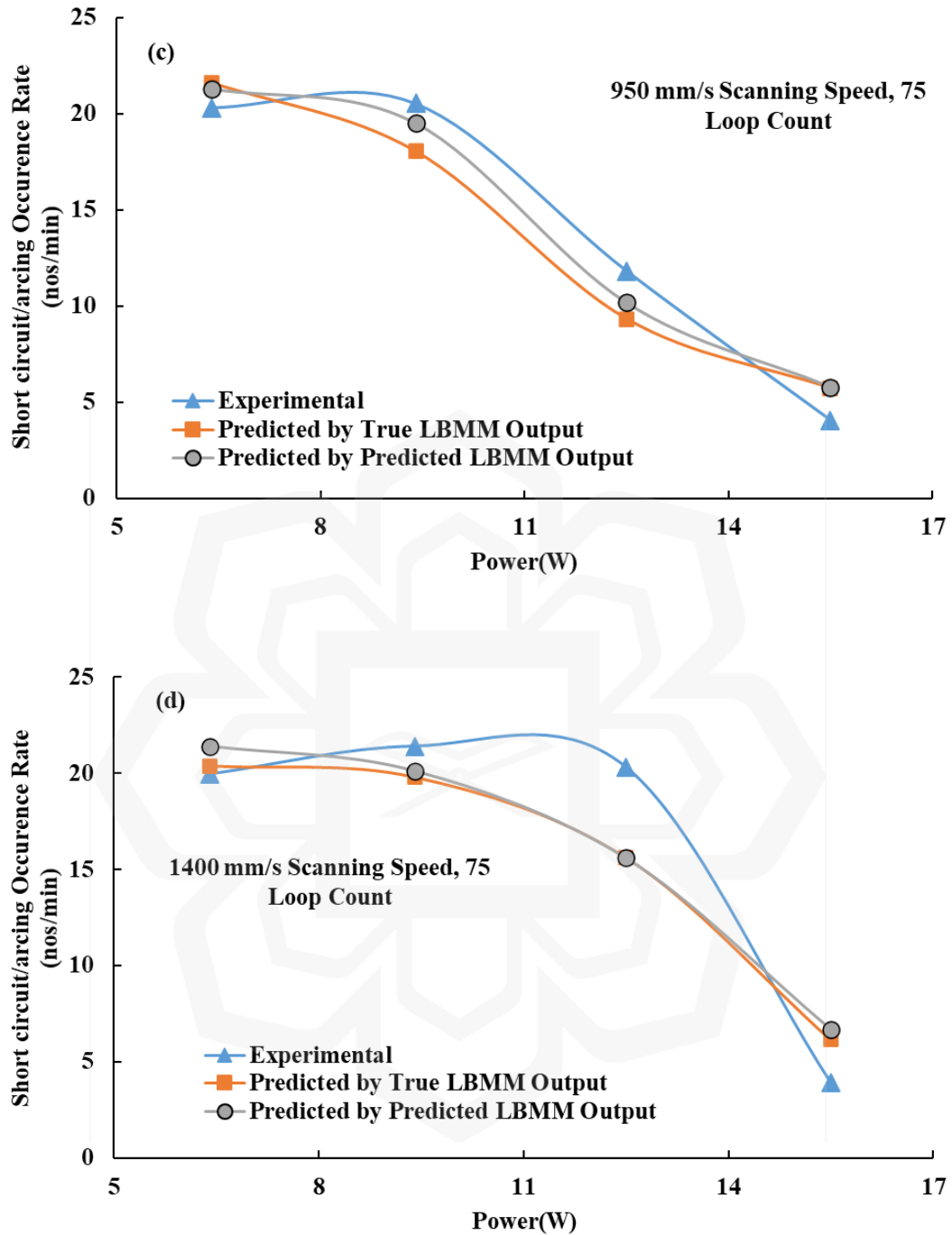
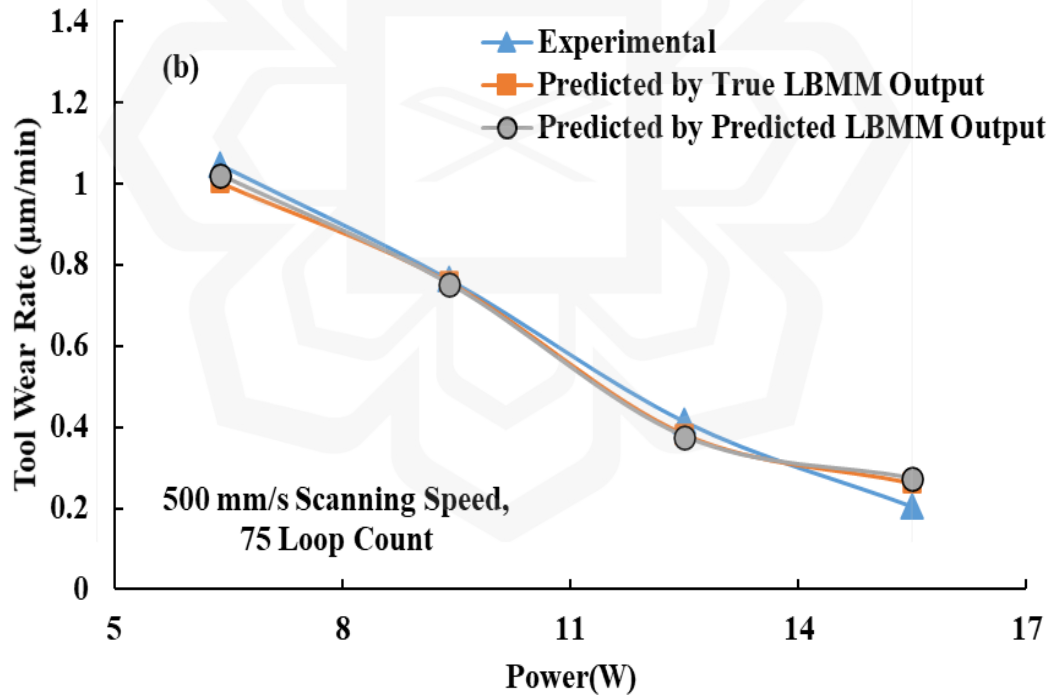
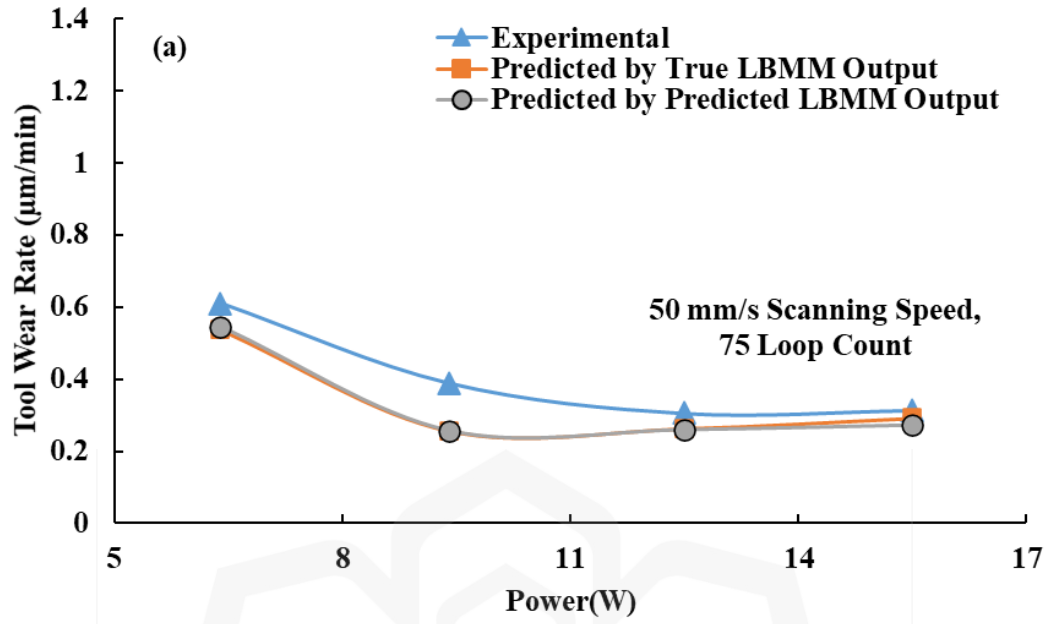


Figure 4.22: Effect of laser power and machining instability/arcing frequency for pre-machined LBMMed holes at various scanning rates with a fixed loop count of 75. The graph shows experimental values, predicted values, and estimates based on the parameters of the true LBMMed holes: (a) 50 mm/s, (b) 500 mm/s, (c) 950 mm/s, and (d) 1400 mm/s (Noor et al., 2021a)



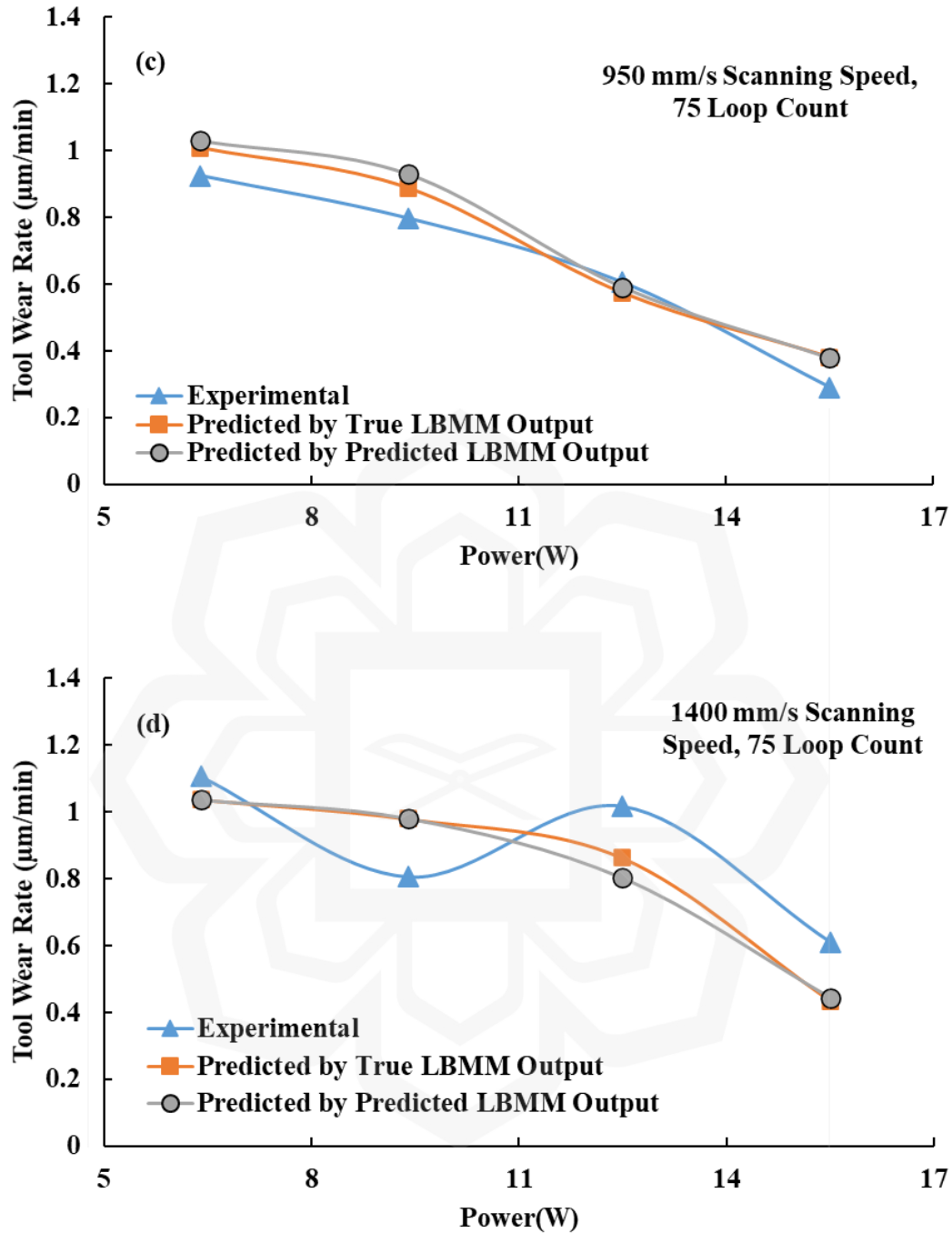


Figure 4.23: HoWatt laser-power affects the rate of tool wear for pre machined holes produced by LBMM. The data on the graph are experimental values, predicted values based on the parameters of the true LBMMed holes, and estimates based on the parameters of the predicted LBMMed holes. The pre-machined holes were produced at different scanning speeds, constant loop count of 75 including (a) 50 mm/s, (b) 500 mm/s, (c) 950 mm/s, and (d) 1400 mm/s (Noor et al., 2021a)

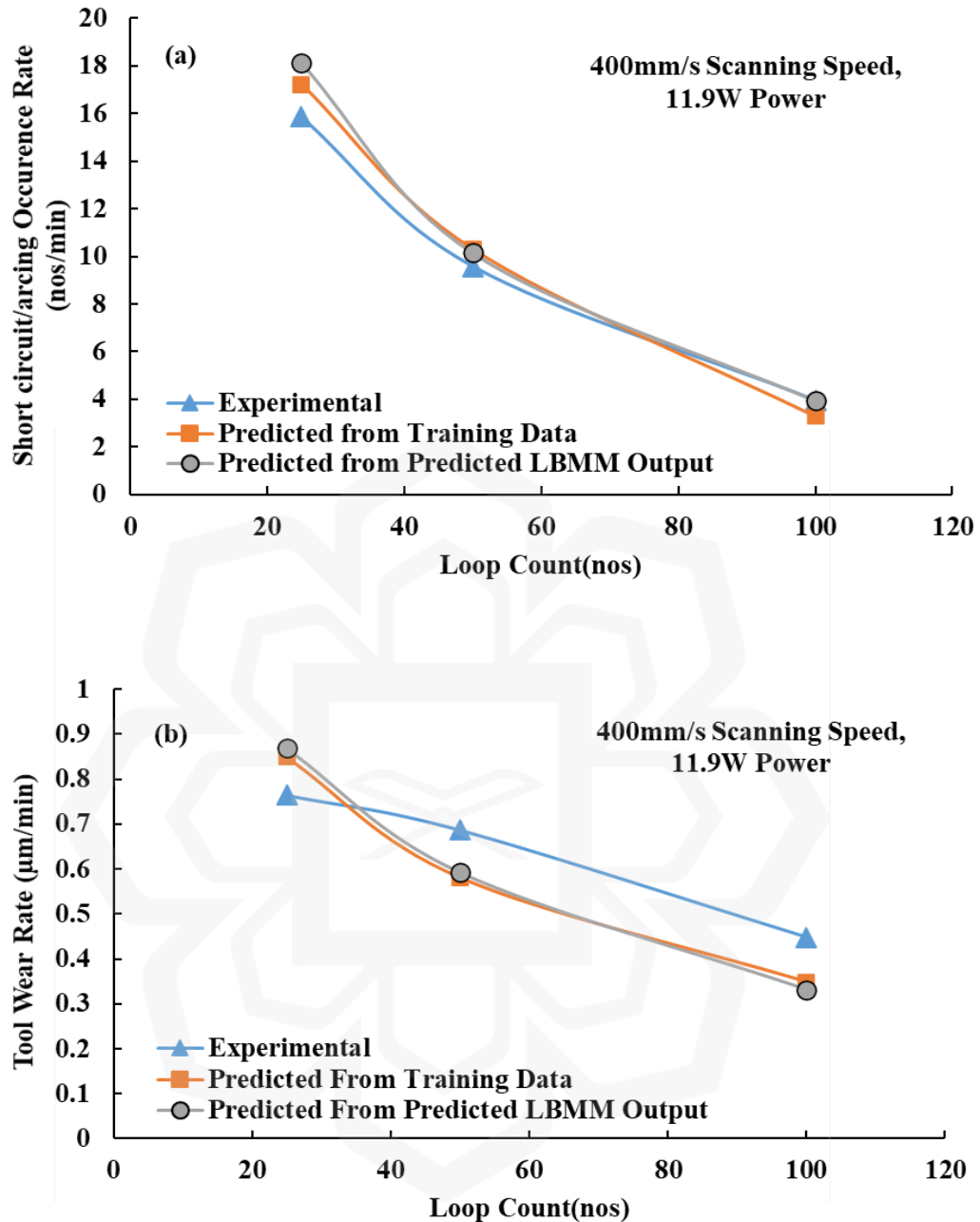


Figure 4.24: How loop count affect machining instability (short circuit/arcing) rate and rate of tool wear for LBMMed pilot holes. The data on the graph comes from experiments, predictions based on the parameters of real LBMMed holes, and estimates based on predictions of the parameters of LBMMed holes. The graphs show how the (a) rate of machining instability (short circuits/arcing) and (b) rate of tool wear change for pre-machined holes scanned at 400mm/s with a 10.66Watt laser-power & 10 KHz pulse repetition rate (Noor et al., 2021a)

4.4 MODELLING OF THE LBMM- μ EDM DRILLING PROCESS CHANGING THE μ EDM PARAMETERS.

The methodology flowchart describes that there is three modelling approach that has been tried in this research (Figure 1.3). In the second modelling, an effort has been made to model the LBMM- μ EDM micro drilling process where the μ EDM parameters were varied alongside the LBMM parameters, unlike the first modelling approach as described in the earlier section 4.3. This section describes the overall modelling performance of the LBMM- μ EDM based micro drilling as both the LBMM and μ EDM parameters were varied.

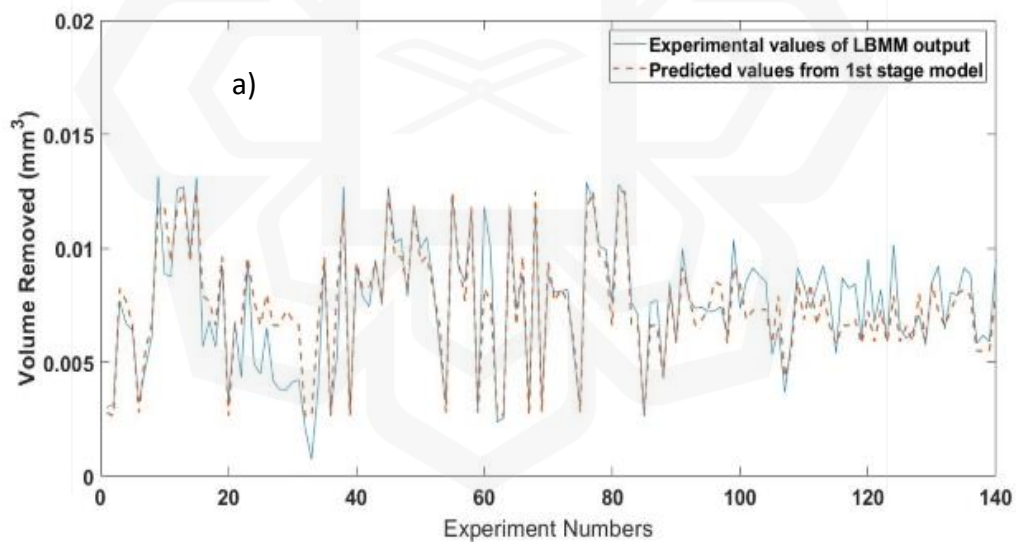
4.4.1 Modelling Performance

The overall modelling architecture is described in Figure 3.10. Each stage of the ANN model's performance in modelling has been evaluated. Predicted outcomes were compared with experimental outcomes via a scatter plot. Since the overall accuracy of the model depends on the accurateness of the first-stage of prediction, this section evaluates the presentation of both the stages of the archetypal individually and the gross performance.

4.4.2 Study of the first-stage model performance

In the first-stage of the model, the most suitable network architecture was identified using a method described in the earlier section to predict the output parameters from the LBMM input parameters (i.e., laser power, scanning speed, and pulse repetition rate). Figure 4.25 compares all three relevant output variables namely volume removed, HAZ, and recast layer—between their definite experimental values and the results predicted by the first-stage model. It is to note that in our earlier modelling technique we used entry and exit area of the LBMMed holes as the output, however this time we used the removed volume as the output parameters for the LBMMed holes. The reason was it helped to converge the model with a better efficiency. Figure 4.25 (a-c) indicates that for the case of the volume removed,

the model prediction fits the experimental results the best. Individual RMSE values for the training dataset's volume removed, HAZ, and recast layer were 0.0917, 0.1291, and 0.1337, respectively, while they were 0.1105, 0.097, and 0.0914 for the test set. Additionally, Figure 4.26 confirms that the volume removed exhibits higher predictability (91%) than the other variables. By examining the Table 3.7, it is possible to determine why the variable LBMMed holes' volume removed is more predictable than other variables. As can be seen from Table 3.7, the volume removed of the LBMMed holes has a higher correlation with the majority of the LBMM inputs than the other parameters of the LBMMed holes. However, there was no noticeable correlation between any of the LBMM's output parameters and the pulse repetition rate.



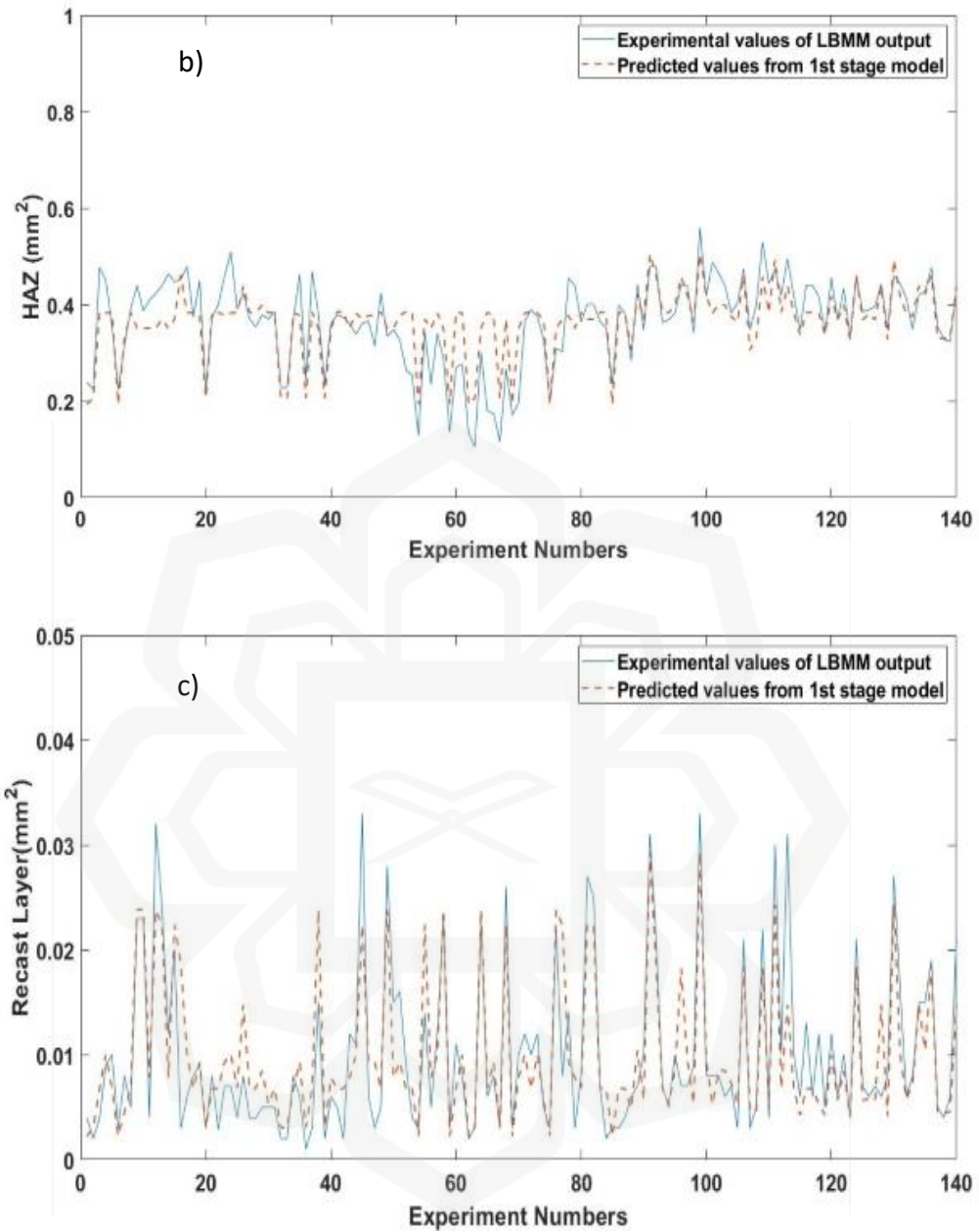


Figure 4.25: Experimental and dual-stage ANN model comparison for the first-stage model, (a) volume removed, (b) HAZ, and (c) recast layer.

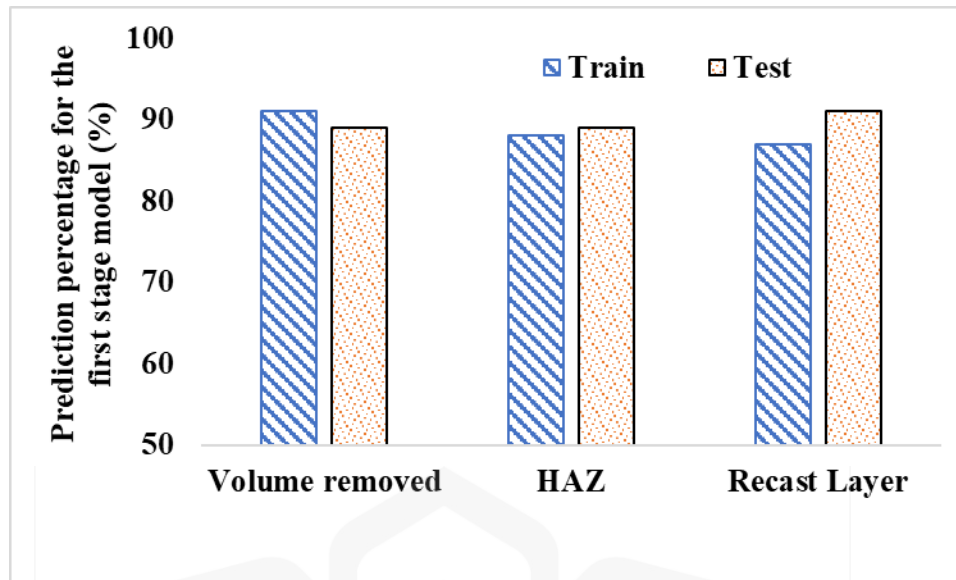


Figure 4.26: Prediction accuracy of the first-stage model's four variables, including the volume removed, the HAZ, and the Recast layer

4.4.3 Study of the second-stage model performance

The second-stage of the model acts as a bridge to explain how the characteristics of the LBMMed pilot holes' output parameters (removed volume, HAZ, and recast layer) as well as the various μ EDM input parameters affect the output parameters of the μ EDM method, which allows for the prediction of the final outcome of the LBMM- μ EDM-based sequential micromachining process.

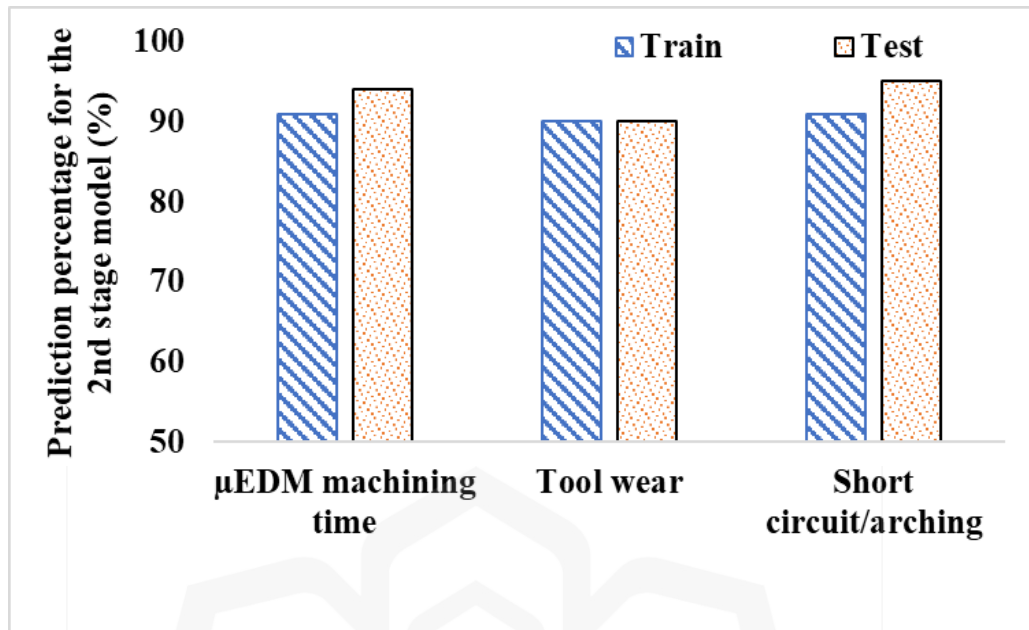
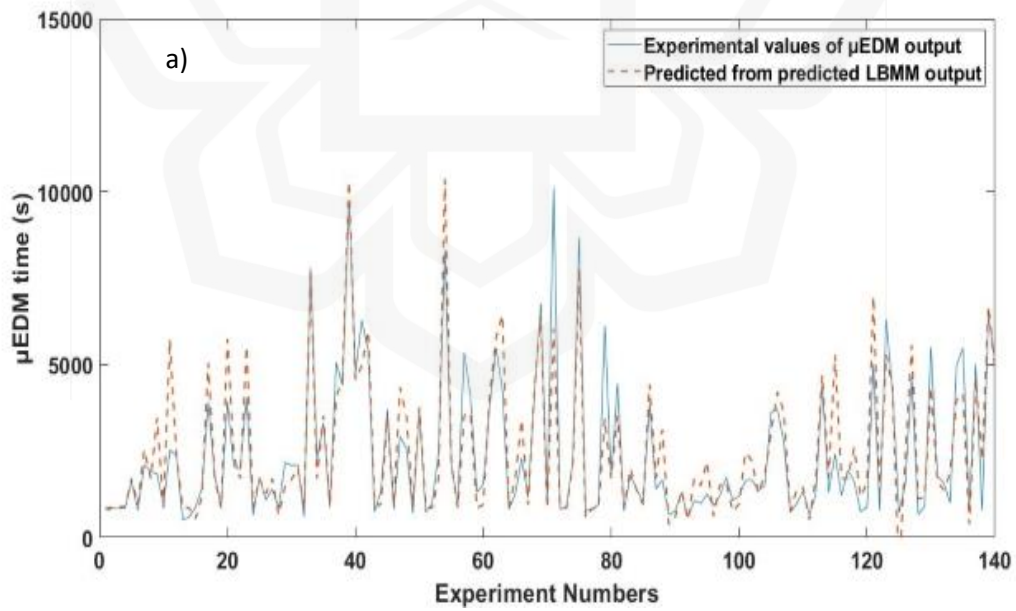


Figure 4.27: μ EDM machining time, machining instability (short circuit/arc) count, and tool wear prediction accuracy from the second-stage model.



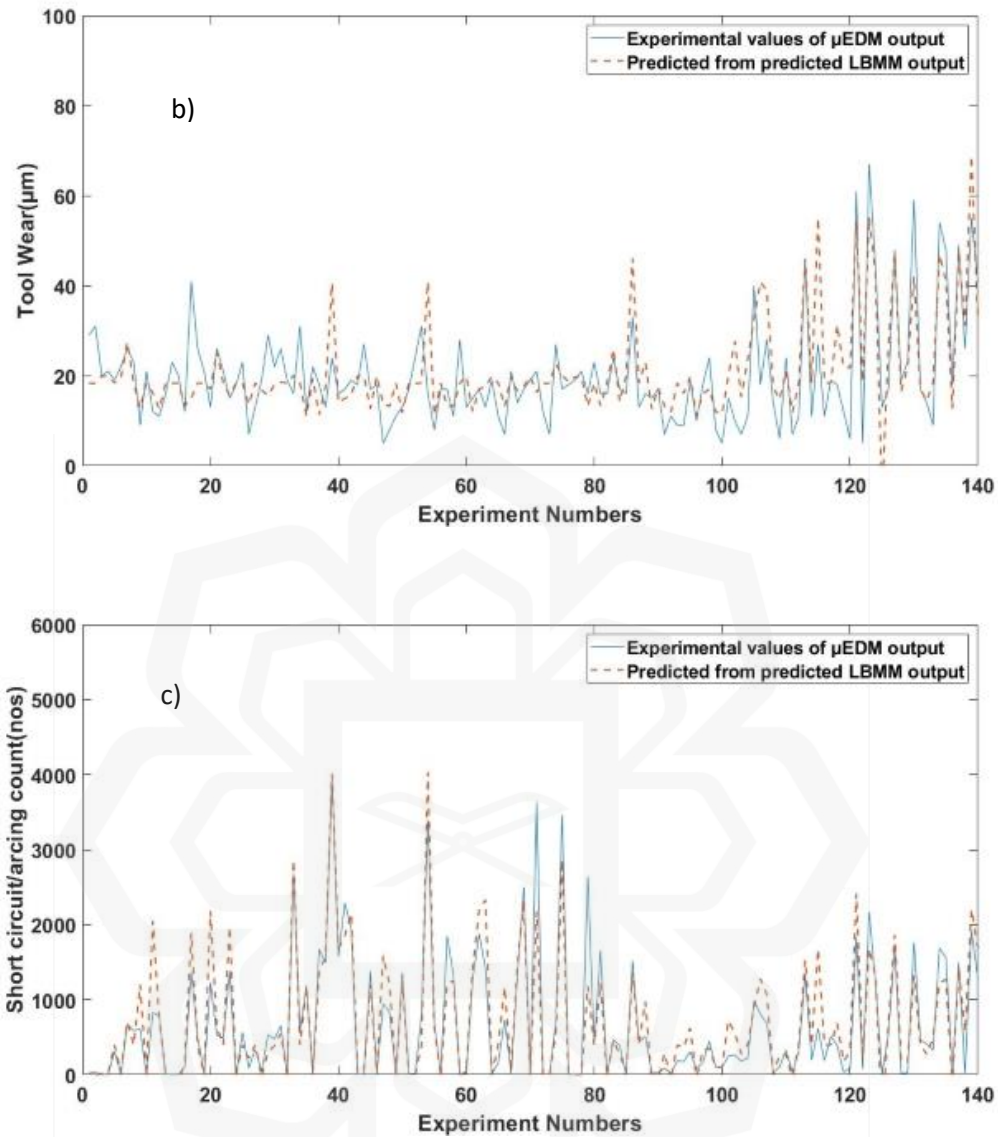


Figure 4.28: Experimental and dual-stage ANN model comparison for second-stage a) μ EDM machining time, b) short circuit/arcing count, and c) tool wear.

The model was trained using the experimental values of the LBMM output parameters (i.e., volume removed, HAZ, and recast layer) and the input parameters of the μ EDM process. Individual RMSE values for EDM machining time, tool wear, and short circuit/arcing count were 0.944, 0.106, and 0.0929 for the training dataset, and 0.0632, 0.1083, and 0.0541 for

the test set, respectively. Figure 4.27 displays the subsequent prediction accurateness for each of the variables. Figure 4.27 illustrates that all of the variables' predictability lies within an analogous range (90% to 94%). Figure 4.28 (a-c) associates the definite ideals of various variables with their projected values for the second-stage model, further demonstrating that all of the variables are predictably within a similar range.

4.4.4 Study of the overall performance of the dual-stage ANN model

In order to test the holistic performance of the proposed model the LBMM inputs were cast-off to forecast the first-stage's outputs. These inputs included power, scanning speed, and pulse repetition rate (volume removed, HAZ, and recast layer). Then these predicted outputs alongside the μ EDM input parameters were fed into the trained model to ultimately predict the secondary process's performance parameters. These parameters are μ EDM machining time, machining instability (short circuit/arc) count, and tool wear. The RMSE for each of the variables was then calculated, and it was discovered to be 0.09, 0.1271, and 0.08 for the μ EDM machining time, tool wear, and machining instability (short circuit/arc) count respectively. In the end, the estimated values from the model for the μ EDM machining time, tool wear, and the number of short circuit counts/arcing were compared with the actual experimental findings. The corresponding prediction accuracy is depicted in Figure 4.29, and it falls somewhere in the range of 88–92%. Figure 4.30 is an additional comparison of the overall network performance that was derived by computing the lumped accuracy as specified by equation 4.4. (Between the first-stage, second-stage, and holistic performance).

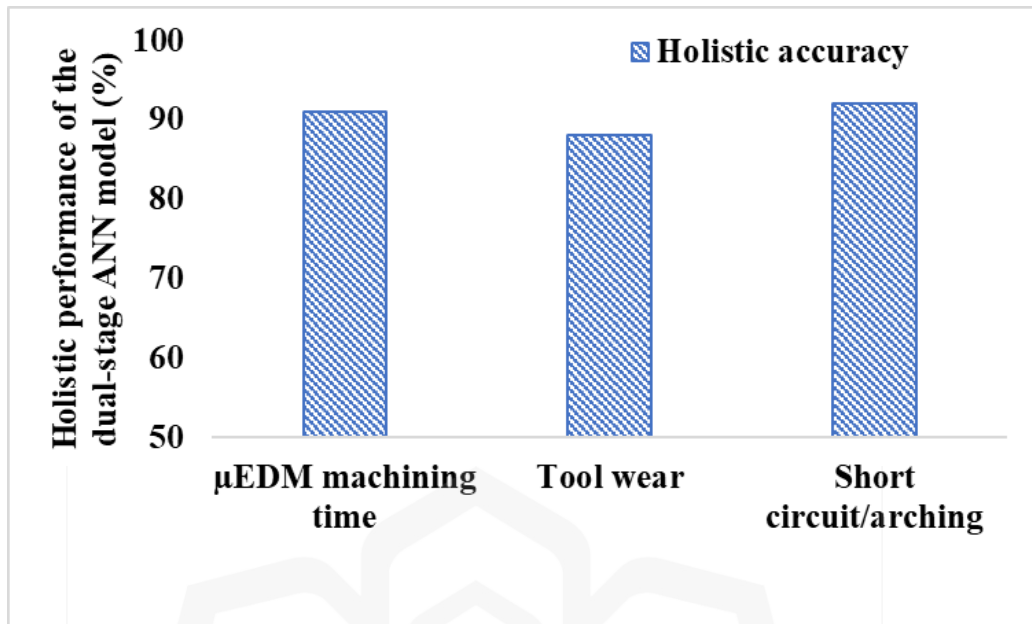


Figure 4.29: The dual-stage ANN model's holistic performance for μ EDM machining time, short circuit/arc count, and tool wear.

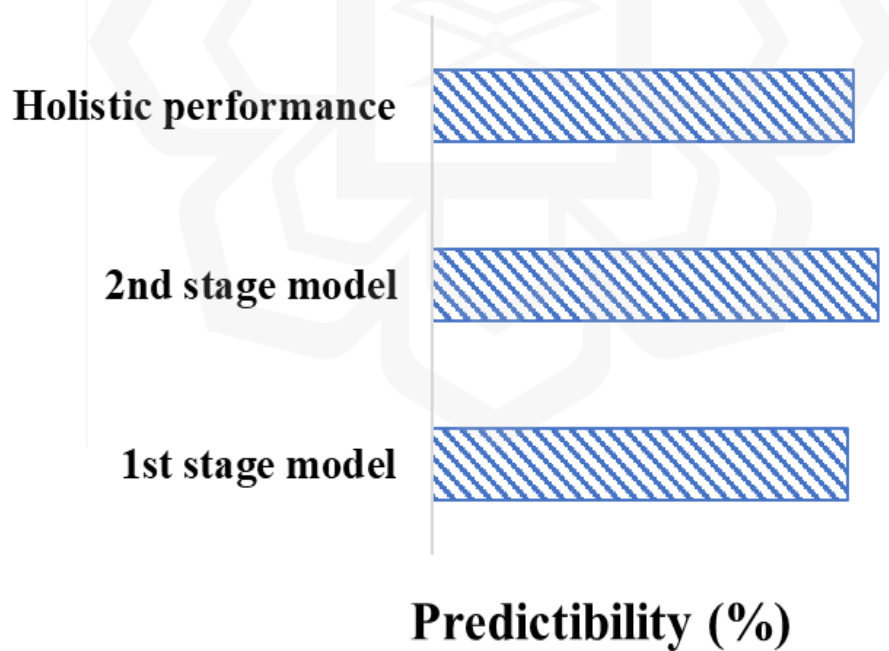


Figure 4.30: Evaluation of the first-stage model, the second-stage model, and the overall efficiency.

4.4.5 Parametric Study

LBMM- μ EDM-based consecutive process output parameters vary with input parameters. The study of sequential micromachining from a parametric point of view helped us to understand how different things are connected. This section described the LBMM input parameters and μ EDM input parameters affect the μ EDM output performance, such as the μ EDM machining time, tool wear, and short circuit count/arching.

4.4.5.1 Machining time for μ EDM

The production rate is largely determined by the LBMM- μ EDM process's machining time. Figure 4.31 exhibits the collective effect of laser scanning speed, incident power, μ EDM discharge energy (μ EDMs capacitance and voltage were converted to discharge energy), and EDM speed/feed rate used to machine the pilot holes on micro EDM's final finishing time. It is noted that Figure 4.31 has been plotted using experimental data and predicted data from a trained dual-stage model. Also, it is to note that the range of discharge energy considered four levels, and the insignificant frequency effect was averaged to draw Figure 4.31.

It is clear from Figure 4.31 that pilot holes machined with the same LBMM parameters require higher time to be fine-finished by the μ EDM process if lower discharge energy is used which is a phenomenon well established by the previous researchers (Noor et al., 2021). It can be further explained from Figure 4.31 (a) & (b) that in general, a significantly higher EDM speed ($\sim 3x$) requires more machining time to conduct the final finishing operation by μ EDM. At a higher EDM speed, debris, and bubbles are accumulated between the gap area and become difficult to be removed. This results in abnormal discharges and short circuits, which ultimately cause frequent electrode pullbacks (Fu et al., 2016). Hence,

the μ EDM machining time for 10 $\mu\text{m}/\text{sec}$ EDM speed becomes higher compared to lower EDM speed (3 $\mu\text{m}/\text{sec}$).

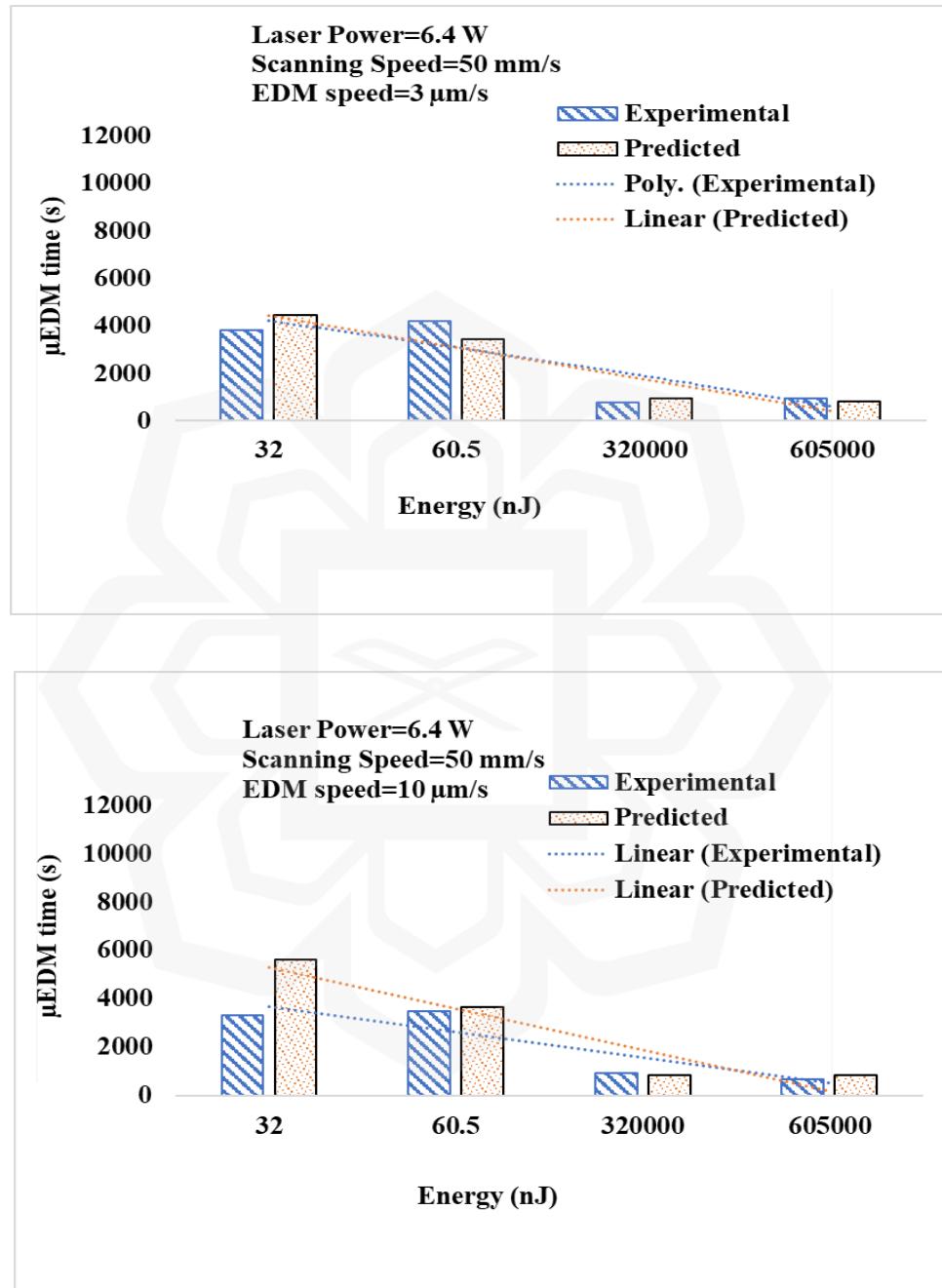
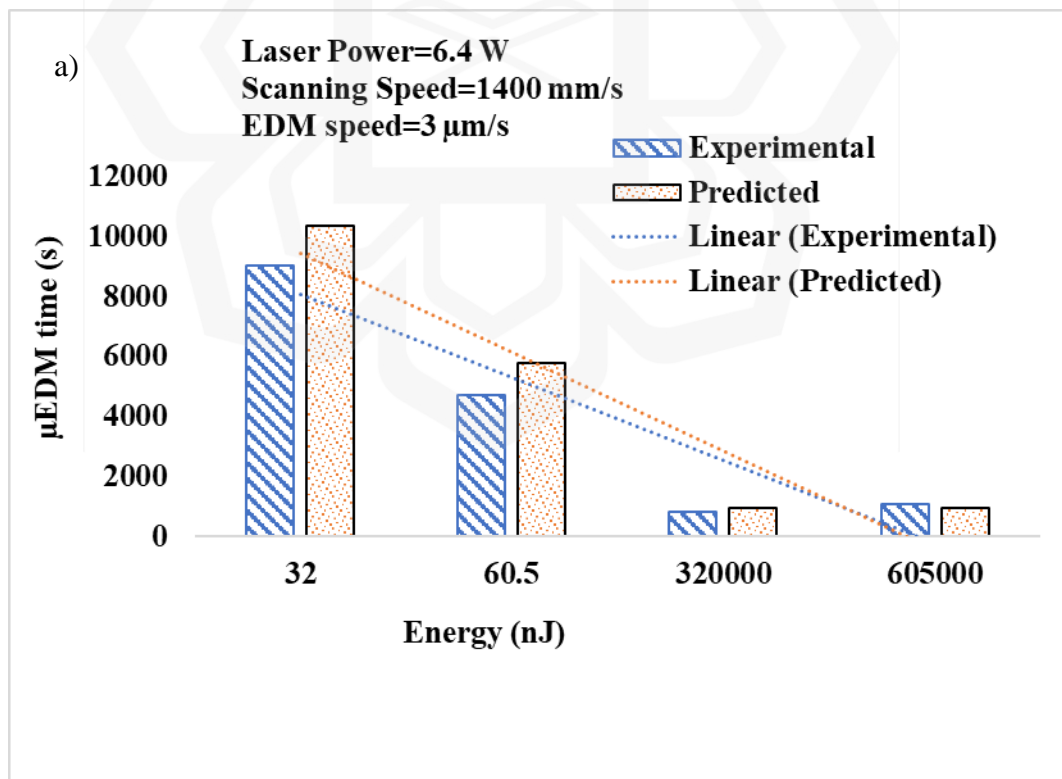


Figure 4.31: μ EDM machining time with LBBMed pre-machined holes at laser power 6.4 W and scanning speed 50 mm per second. The graph shows experimental, predicted, and estimated values from μ EDMed holes' parameters. The holes were machined at (a) 3 μm EDM speed (b) 10 μm EDM speed.

Figure 4.32 (a-b) shows how the laser power used for the pilot hole machining affects the secondary processing time. In both graphs (Figure 4.32) all the parameters were kept the same except for the incident laser power for the pilot hole machining. As a higher laser power removes a high volume from the pilot hole therefore the μ EDM finishing time becomes shorter which can be seen from the comparison between Figure 4.32 (a) and Figure 4.32 (b). Another interesting observation is this phenomenon is dominant at the lowest discharge energy and diminishes with higher μ EDM energy as observed in Figure 4.32. This indicates if a significantly high EDM energy is used to carry out the finishing operation of the LBMMed holes the primary process parameters do not have an effect on the finishing time by the secondary process. However, this will come with a price as higher EDM energy will deteriorate the hole quality.



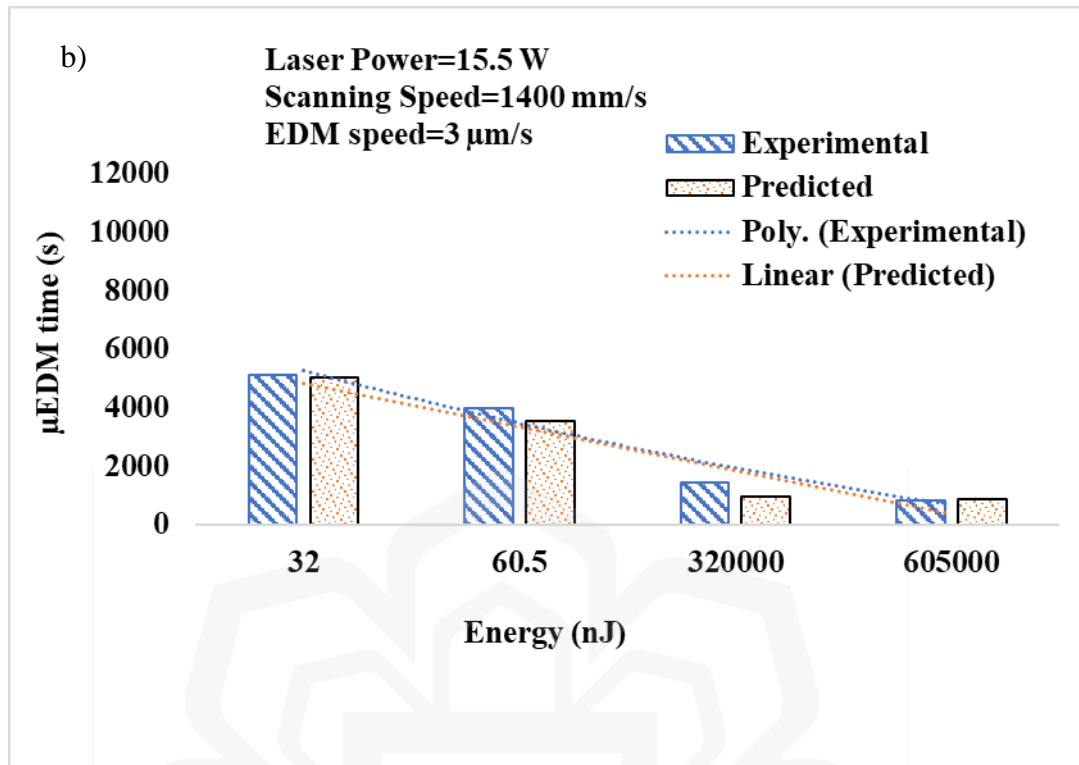


Figure 4.32: Energy used for LBBMed pre-machined holes at scanning speed 1400 mm per second and EDM speed 3 $\mu\text{m/sec}$ affects μEDM machining time. The graph shows experimental, predicted, and estimated values from μEDM holes' parameters. Pre-machined LBMM holes at (a) 6.4 Watt laser-power and (b) 15.5 Watt laser-power.

Figure 4.33 shows that higher scanning speed significantly affects the μEDM machining time to fine-finish the LBMMed holes. (Negarestani & Li, 2012) provided a laser machining energy density equation that shows incident energy density decreases with scanning speed. This would reduce workpiece material removal. Figure 4.33 (a) & (b) shows that higher scanning speed machined LBMM holes require more μEDM machining time due to shorter laser beam-material thermal interaction.

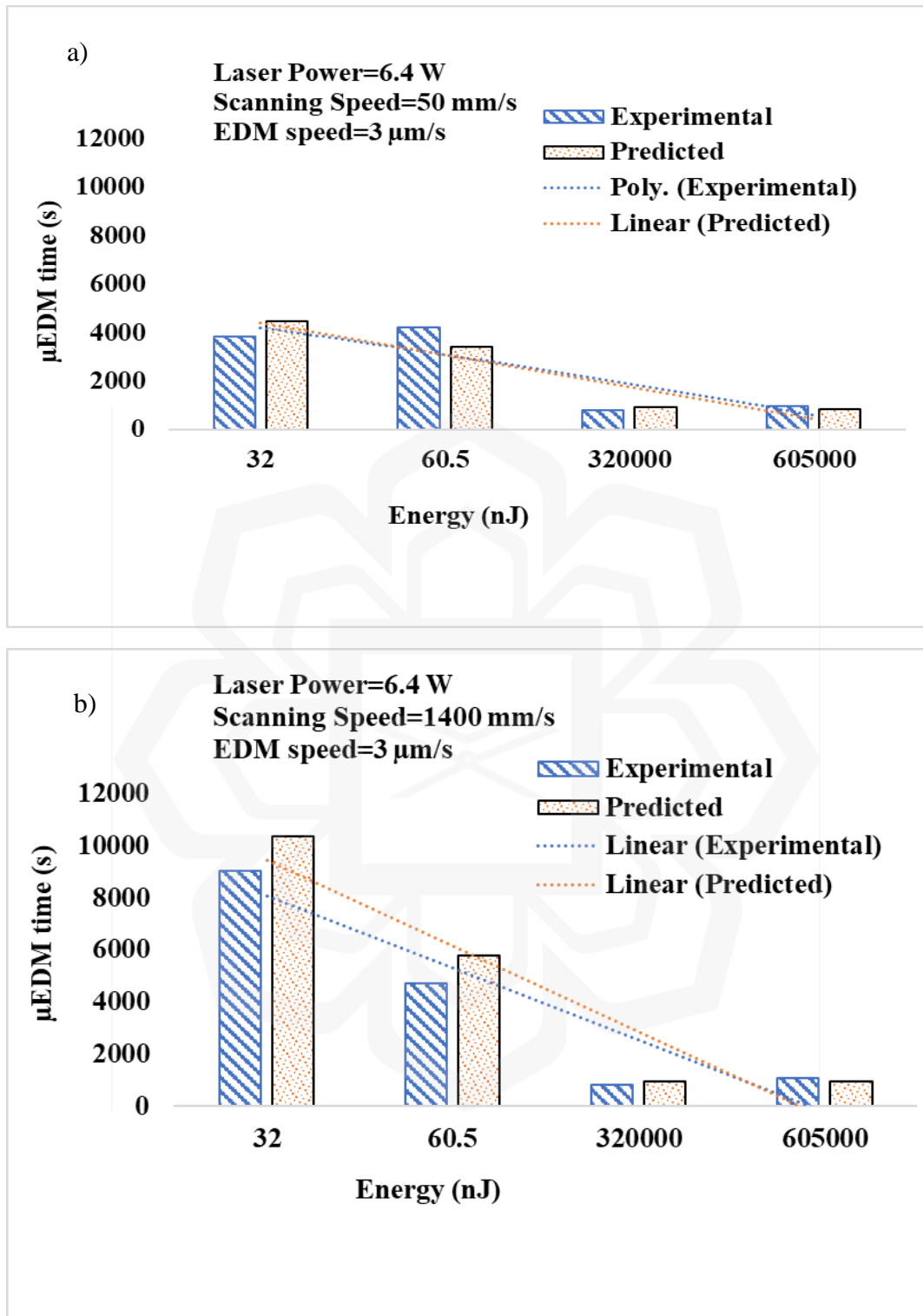


Figure 4.33: μEDM machining time for LBBMed pre-machined holes at laser power 6.4 W and EDM speed 3 μm/sec. The graph shows experimental, predicted, and estimated values from μEDMed holes' parameters. Pre-machined LBMM holes at (a) 50 mm per second scanning speed (b) 1400 mm per second scanning speed.

4.4.5.2 Short circuit/arcing count

The μ EDM finishing process has a built-in short circuit/arcing that is detrimental because it hinders the creation of a good spark. Arcing happens when discharge takes place before the interval voltage reaches the open-circuit voltage. Arcing is frequently observed by a short circuit, and both are thought to be hazardous to μ EDM. Similarly, during an μ EDM operation, the electrode undergoes electrothermal erosion, which inevitably leads to short-circuiting/arcing and tool wear (considered vertical for the purpose of this research). The μ EDM machining time is increased, and the probability of both short circuit/arcing occurrence and vertical tool wear increases (Rashid et al., 2021b).

Figure 4.34 demonstrates that higher EDM energy reduces the number of short circuit occurrences as in higher EDM energy large craters are formed and chances of short circuit incidents become low. Moreover, comparing Figure 4.34 (a and b) it can be said that higher EDM speed may cause a higher number of short circuits, particularly at the low discharge energy setting.

On the other hand, Figure 4.35 illustrated the significant effect of laser power on μ EDM short circuit/arcing count. , Figure 4.35 (a) & (b) were plotted according to Figure 4.32 and observed that short circuit/arcing occurred at a high rate (during the secondary finishing operation) when the laser power was low (6.4 W) during the LBMM process, but dropped dramatically when the laser power was raised (15.5 W).The logical explanation for reducing the short circuit count can be explained as follows. When the loWatt laser-power was used to machine the pilot holes it could not remove enough material from the workpiece surface, as a result, the μ EDM operation was forced to remove those materials

which resulted in higher EDM tool and workpiece contact time and caused more short circuits. Again, the effect is predominant in the low EDM discharge energy setting.

Figure 4.36 shows that at LBMMed holes machined at lower scanning speeds, such as 50 mm/s (Figure 4.36 (a)), the short circuit/arcing occurrence during the secondary EDM process was relatively low as compared to the LBMMed holes machined at a higher laser scanning speed of 1400 mm/s (Figure 4.36 (b)). Huang et al. (2022) also reported the same that the faster laser scanning speed formed light depth on the workpiece with lower power. A huge number of short circuits/arching occurred in the μ EDM machining to remove more material from the outlayer of the LBMM machined holes. Hence, the high volume of material that was detached by the LBMM process with a low scanning speed makes it easier for the second-stage μ EDM operation to take place.

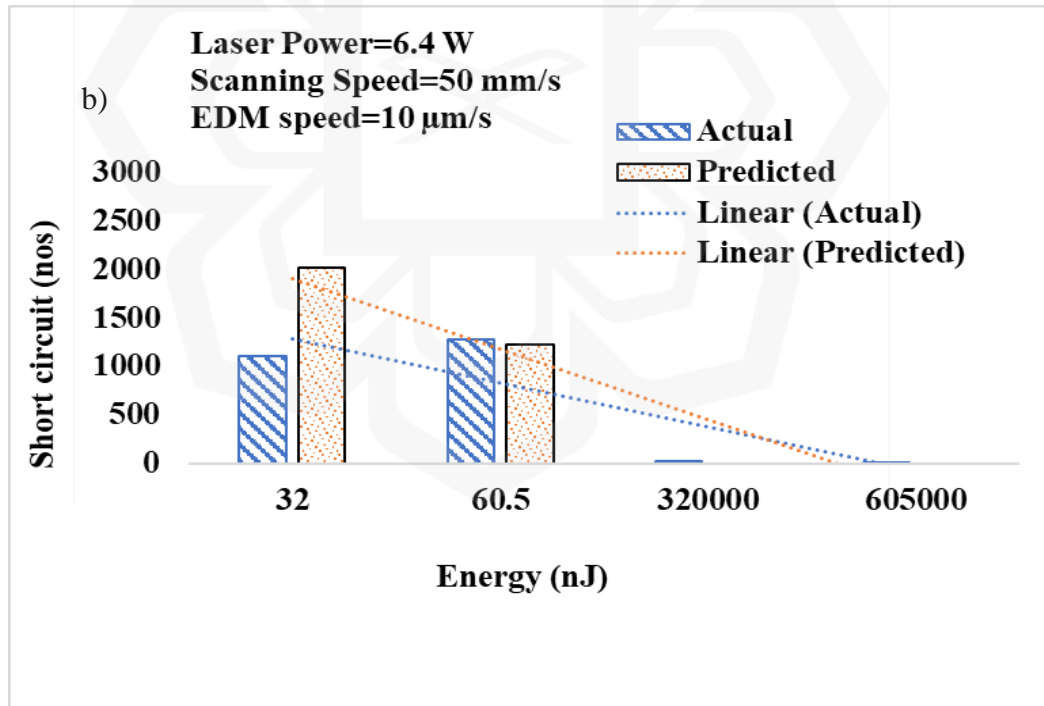
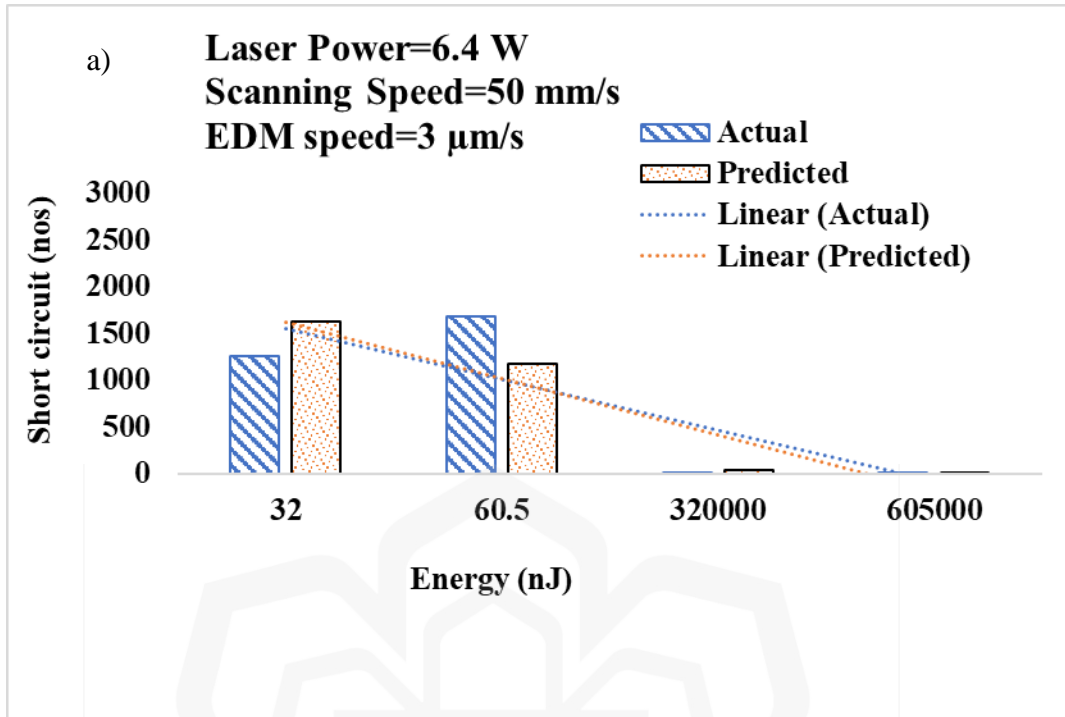


Figure 4.34: μEDM Short circuit count with LBBMed pre-machined holes at laser power 6.4 W and scanning speed 50 mm per second. The graph shows experimental, predicted, and estimated values from μEDM holes' parameters. The holes were machined at (a) 3 μm EDM speed (b) 10 μm EDM speed.

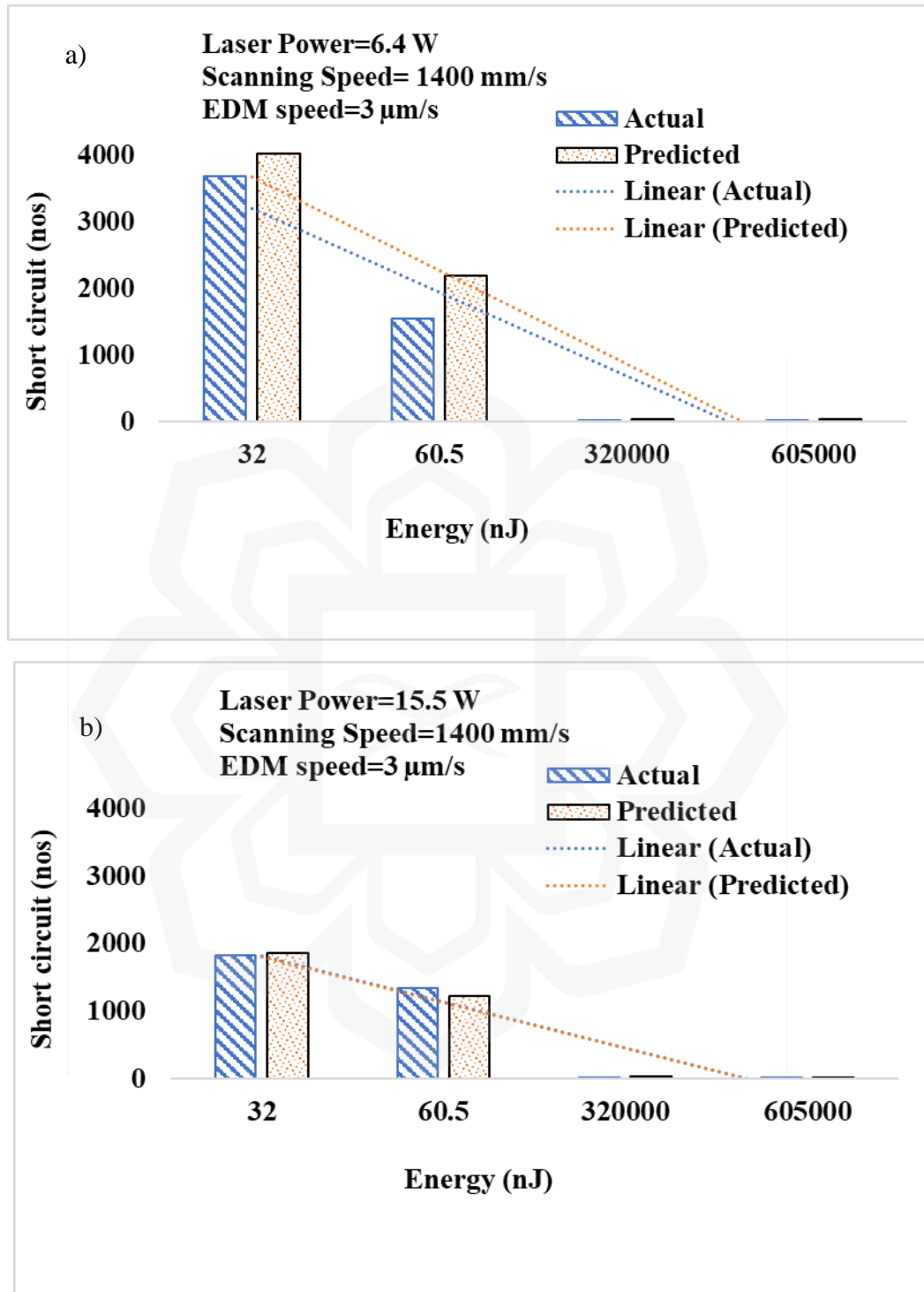


Figure 4.35: Variation of μEDM short circuit with energy used for LBBMed pre-machined holes at scanning speed 1400 mm per second and machining EDM speed 3 $\mu\text{m/sec}$. The graph shows experimental, predicted, and estimated values from μEDM holes' parameters. Pre-machined LBMM holes (a) 6.4 Watt laser-power (b) 15.5 Watt laser-power.

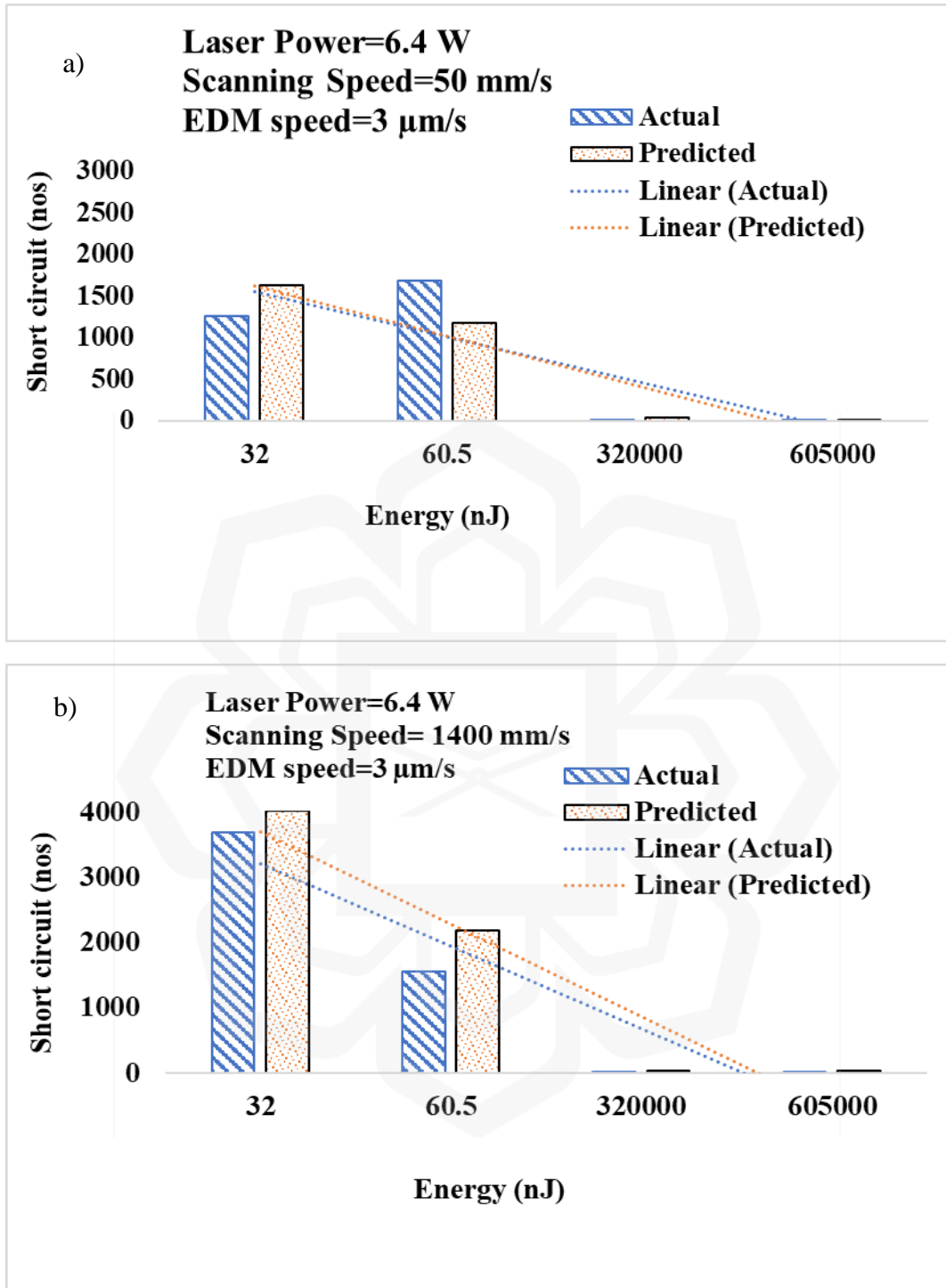


Figure 4.36: μ EDM Short circuit for LBBMed pre-machined holes at laser power 6.4 W and EDM speed 3 μ m/sec. The graph shows experimental, predicted, and estimated values from μ EDMed holes' parameters. Pre-machined LBMM holes at (a) 50 mm per second scanning speed (b) 1400 mm per second scanning speed.

4.4.5.3 Study on tool wear for μ EDM

The tool wear rate during the μ EDM exhibits a pattern resembling the short circuit/arcing occurrence rate mentioned in section 4.4.5.2. Figure 4.37 exhibits that the higher discharge energy causes higher tool wear as reported by other researchers (Ozgedik & Cogun, 2006). Also, higher EDM speed during the secondary finishing operation shows a slight increase in the tool wear keeping other parameters for LBMM and EDM constant. Though the variation might fall within the experimental and computational uncertainty. Further, it was observed that at higher EDM speed the result of the discharge energy on the tool wear gets significantly less prominent (Figure 4.37(b)). Not much noticeable relationship was observed for the outcome of laser power on the electrode/tool wear during the μ EDM finishing process as shown in Figure 4.38 (a-b). However, the effect of the laser scanning speed for the pilot hole machining has a significant effect on the tool wear during the secondary finishing process as can be seen from Figure 4.39 (a-b). The reason why laser power does not have much consequence on the tool wear of the secondary EDM and scanning speed has could be due to the fact that the lower scanning speed affects (by lowering) the μ EDM time more aggressively than the high laser power as can be seen from Figure 4.32 and 4.33.

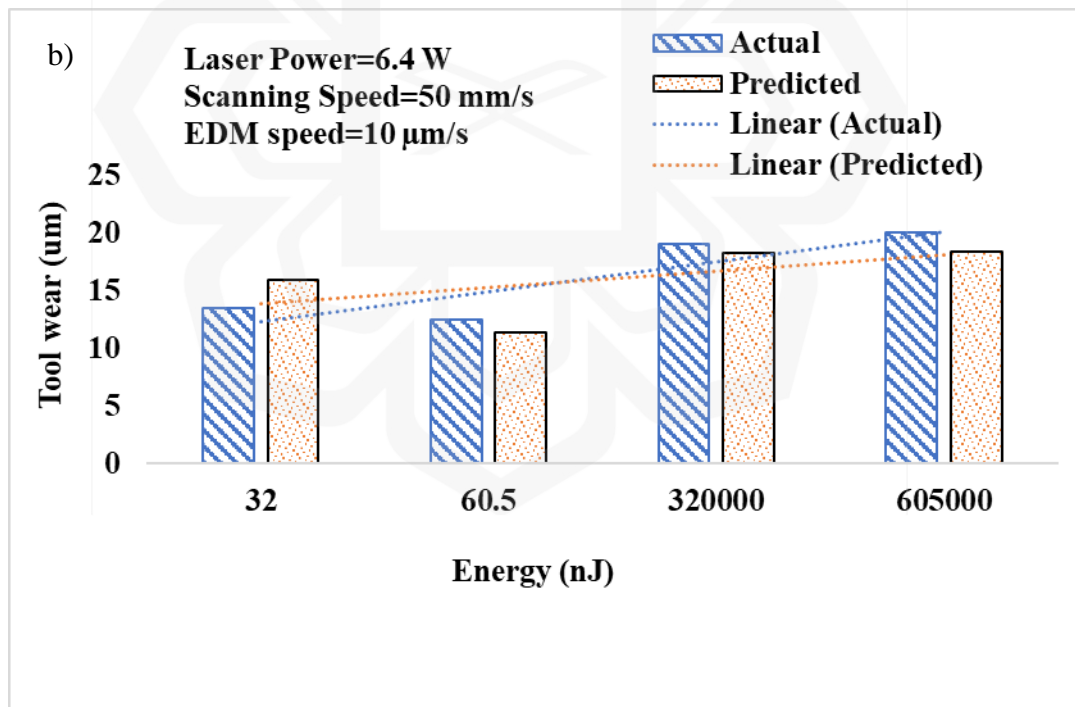
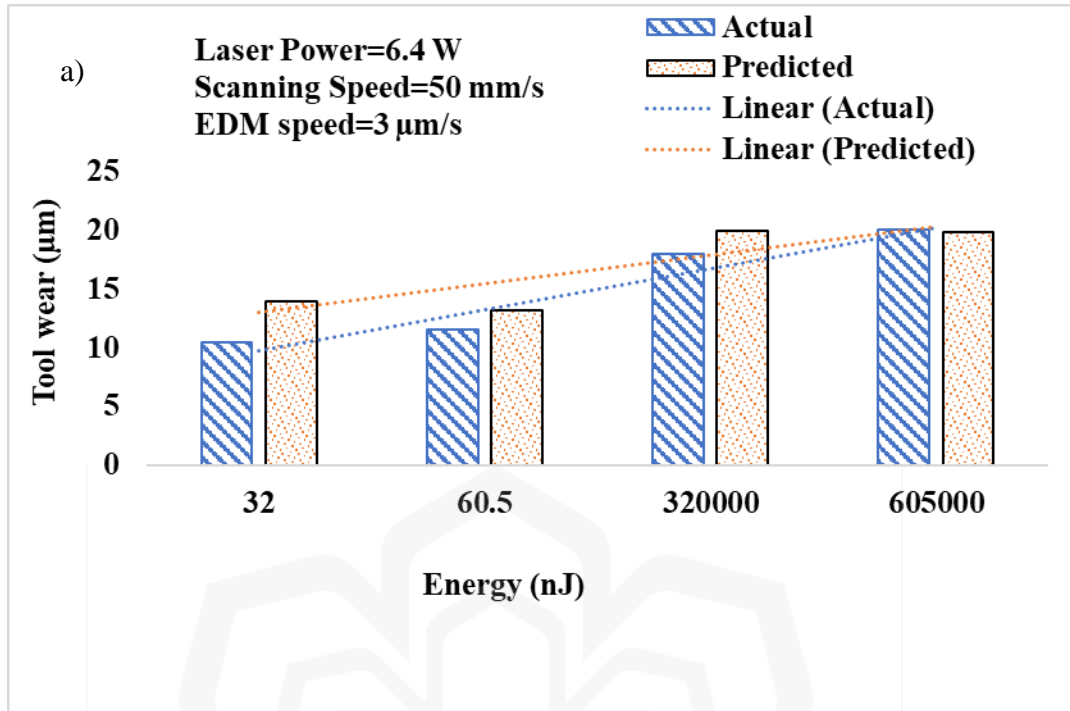


Figure 4.37: Variation of μ EDM Tool wear with Energy for pre-machined LBMMed holes machined with 6.4 Watt laser-power and 50 mm/s scanning speed. Experimental values predicted values from the actual μ EDMed holes' parameters and estimates from predicted EDMed holes' parameters comprise the graph's data. The holes were machined at EDM speeds of (a) 3 μ m and (b) 10 μ m.

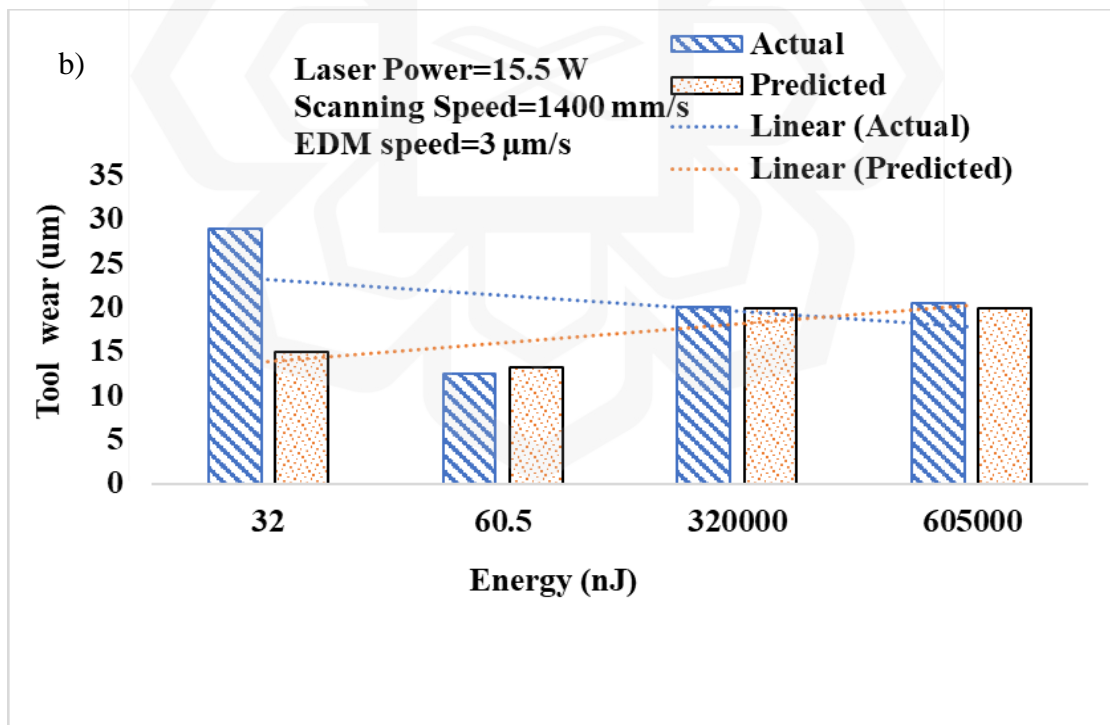
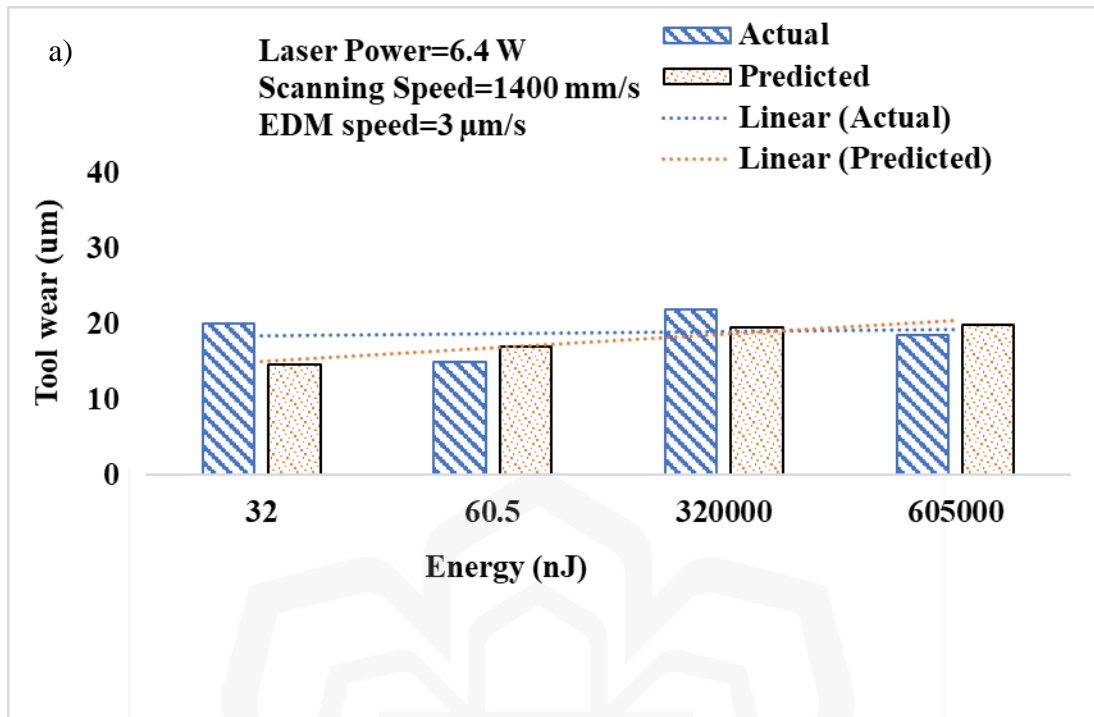


Figure 4.38: Variation of μEDM short circuit with energy used for LBBMed pre-machined holes at scanning speed 1400 mm per second and machining EDM speed 3 $\mu\text{m/sec}$. The graph shows experimental, predicted, and estimated values from μEDM Med holes' parameters. Pre-machined LBMM holes at (a) 6.4 Watt laser-power (b) 15.5 Watt laser-power.

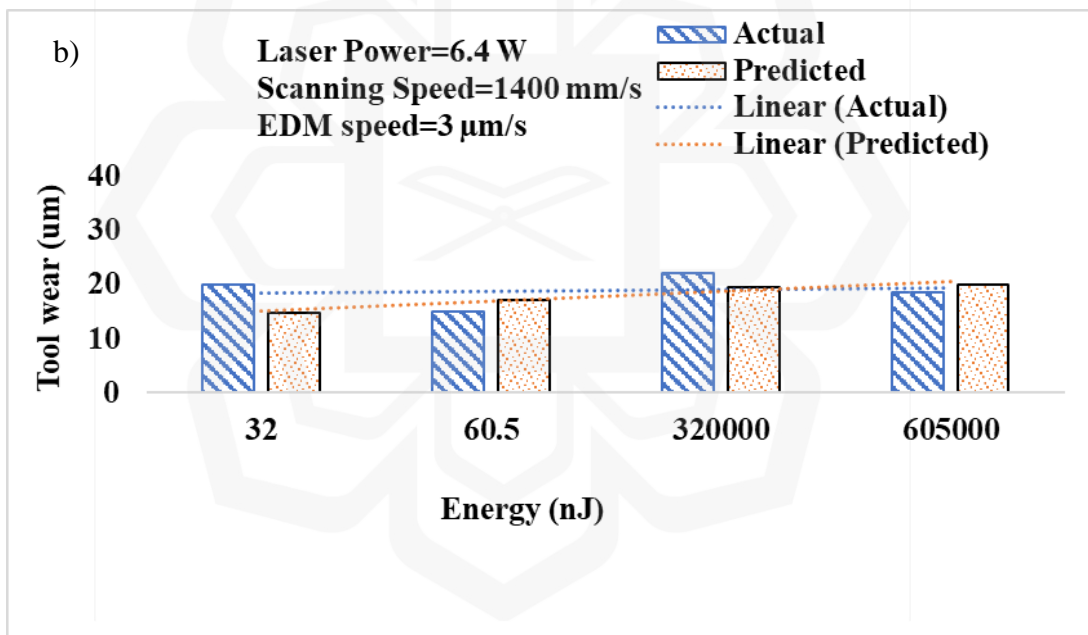
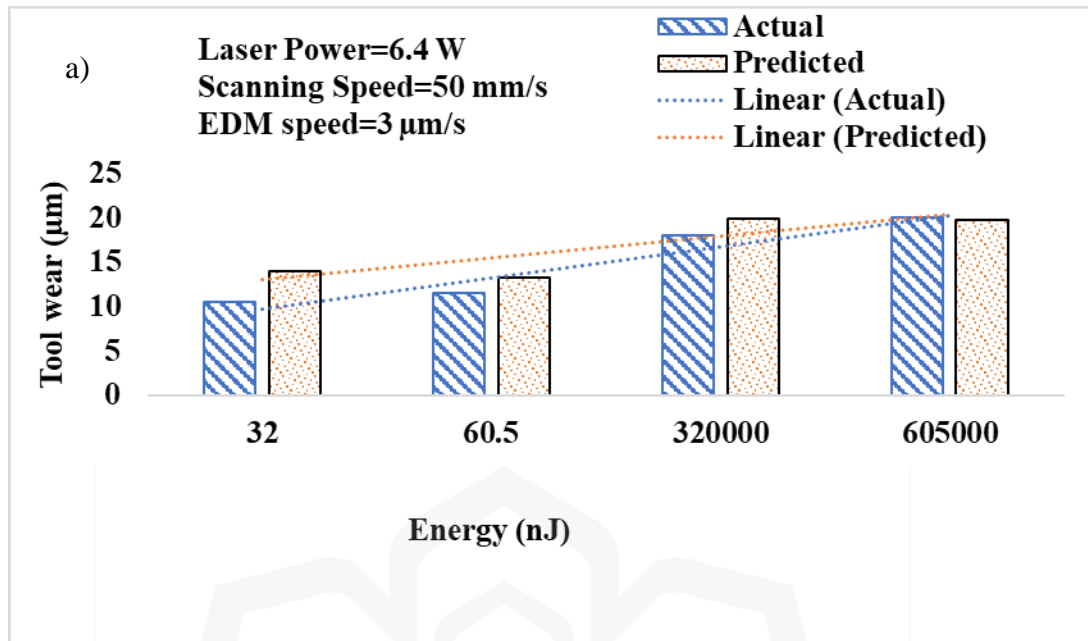


Figure 4.39: μ EDM tool wear for LBBMed pre-machined holes at laser power 6.4 W and EDM speed 3 $\mu\text{m}/\text{sec}$. The graph shows experimental, predicted, and estimated values from μ EDMed holes' parameters. Pre-machined LBMM holes at (a) 50 mm per second scanning speed (b) 1400 mm per second scanning speed.

4.5 MODELLING OF LBMM- μ EDM-BASED HYBRID MICRO-MILLING

This study presents the analysis of mathematical modeling and optimization of the processing parameters (input factors) for Stainless steel (SUS 304) using the LBMM- μ EDM-based micro milling technique. Models are developed considering the LBMM input factors (Scanning speed, power, pulse repetition rate, and loop) using the 3-level Box Behnken Design (BBD) in order to determine the output responses of hybrid micro EDM machining time, Tool wear, and short circuit.

4.5.1 MODEL DEVELOPMENT FOR RESPONSES

The LBMM independent variables utilized for investigation in this study are Scanning speed, power, pulse repetition rate, and loop count. The LBMM- μ EDM-based hybrid micro milling was conducted on stainless steel workpiece (0.5 mm thickness) using the tungsten electrode (0.5 mm) in micro EDM machining. The study examined the output responses of μ EDM milling time, tool wear, and short circuit. Table 4.1 and 4.2 shows numerous input and output parameters used for the modeling method both are related to the LBMM and the μ EDM processes.

Table 4.1 LBMM input parameters in Box Behnken design

Run	A: Scanning speed (mm per second)	B: Power (W)	C: Pulse repetition rate (KHz)	D: Loop (nos)
1	2000	15.5	15	10
2	2000	12.015	10	10
3	2000	15.5	10	15
4	1500	12.015	10	15
5	2000	12.015	5	5
6	2000	12.015	15	5
7	1500	12.015	10	5
8	2500	15.5	10	10
9	2500	8.53	10	10
10	2000	8.53	15	10
11	1500	8.53	10	10
12	2500	12.015	10	5
13	1500	15.5	10	10
14	2000	15.5	10	5
15	2000	12.015	5	15
16	2000	15.5	5	10
17	1500	12.015	15	10
18	2000	8.53	10	15
19	2000	8.53	5	10
20	2500	12.015	5	10
21	2500	12.015	15	10
22	1500	12.015	5	10
23	2000	12.015	15	15
24	2500	12.015	10	15
25	2000	8.53	10	5

Table 4.2 Box Behnken design responses for the LBMM- μ EDM milling.

	Factor 1	Factor 2	Factor 3	Factor 4	Response 1	Response 2	Response 3
Run	A: SS	B: Power	C: Freq	D: Loop	Time	Tool wear	Short circuit
	mm/s	W	KHz	nos	min	μ m	nos
1	2000	15.5	15	10	30.96	29	47
2	2000	12.015	10	10	41.6	31	57
3	2000	15.5	10	15	34.56	26	77
4	1500	12.015	10	15	38.03	19	61
5	2000	12.015	5	5	38.93	26	77
6	2000	12.015	15	5	44.86	28	70
7	1500	12.015	10	5	41.38	29	78
8	2500	15.5	10	10	38.85	26	90
9	2500	8.53	10	10	47.02	27	68
10	2000	8.53	15	10	48.23	33	109
11	1500	8.53	10	10	45.28	31	87
12	2500	12.015	10	5	46.83	31	106
13	1500	15.5	10	10	38.36	31	74
14	2000	15.5	10	5	36.36	29	104
15	2000	12.015	5	15	38.61	23	59
16	2000	15.5	5	10	34.03	23	44
17	1500	12.015	15	10	42.9	33	79
18	2000	8.53	10	15	43.36	24	52
19	2000	8.53	5	10	52.5	41	107
20	2500	12.015	5	10	44.15	31	96
21	2500	12.015	15	10	48.71	36	85
22	1500	12.015	5	10	44.93	28	77
23	2000	12.015	15	15	36.85	26	54
24	2500	12.015	10	15	37.08	24	61
25	2000	8.53	10	5	48.68	39	97

4.5.2 RESPONSE PERFORMANCE OF OUTPUT MODELS

After recording all of the experimental data into the design expert software, the model development is examined using the design expert version 13.0 software. The software analyzes each response using the fit summary, model assortment, analysis of variance (ANOVA), model diagnostics, and the model graph for 3-D plots. If a model contains a lot of meaningless terms, model reduction is advised in order to strengthen the model.

4.5.2.1 Model for μ EDM milling time.

The model development for μ EDM milling time follows the below steps in accordance with the Box Behnken design procedure (Design expert version 13.0).

4.5.2.1.1 Fit Summary Statistics

The fit summary employs regression analysis to govern the causal connection between the individual variables and the chosen response. It is possible for this relationship to be linear, quadratic, or cubic. Fit summary Table 4.3 shows the μ EDM milling time fit summary suggested linear model with significant terms. The highest-order linear is chosen for the μ EDM machining time in order to take care of all available model terms. Therefore, the linear model with an F-value of 13.24 at $P \leq 0.0001$ was approved.

Table 4.3 Fit summary for μ EDM milling time.

Source	Sum of Squares	df	Mean Square	F-value	p-value	
Mean vs Total	43518.13	1	43518.13			
Linear vs Mean	510.88	4	127.72	13.24	< 0.0001	Suggested
2FI vs Linear	39.73	6	6.62	0.6052	0.7224	
Quadratic vs 2FI	53.19	4	13.30	1.33	0.3243	
Cubic vs Quadratic	81.86	8	10.23	1.13	0.5509	Aliased
Residual	18.14	2	9.07			
Total	44221.93	25	1768.88			

4.5.2.1.2 μ EDM Milling Time Model Selection and Analysis of Variance

The probability (Prob>F) column for each model term in the significant models for machining time is checked to see if it falls below the 0.05 significance level, which indicates the model term is significant. Any model term that is greater than this worth denotes inconsequential terms and can be ignored from the overall model equation. Analysis of variance (ANOVA) tests was conducted to determine whether the proposed model fits the data, and the results are shown in Table 4.4. According to Table 4.5, the most significant terms were observed to be laser power and a number of the loop for modeling the secondary μ EDM time.

Table 4.4 Table Analysis of variance for μ EDM milling time.

Source	Sum of Squares	df	Mean Square	F-value	p-value	
Model	510.88	4	127.72	13.24	< 0.0001	significant
A-SS	11.52	1	11.52	1.19	0.2874	
B-Power	431.40	1	431.40	44.72	< 0.0001	
C-Freq	0.0341	1	0.0341	0.0035	0.9532	
D-Loop	67.93	1	67.93	7.04	0.0152	
Residual	192.92	20	9.65			
Cor Total	703.80	24				

4.5.2.1.3 Developed Model for the μ EDM milling time.

Equations 4.6 and 4.7 are models developed for μ EDM milling time and are represented in terms of coded and actual factors. Equation 4.6, which uses coded factors, predicts by comparing factor coefficients. Equation 4.7's factor equation is an analytical model used to reproduce this experiment's results.

$$\text{Time} = 41.722 + 0.98001 * A - 5.995 * B - 0.0533 * C - 2.379 * D \quad (4.6)$$

$$\text{Time} = +52.08902 + 0.001960 * \text{SS} - 0.171310 * \text{Power} - 0.010667 * \text{Freq} - 0.475833 * \text{Loop} \quad (4.7)$$

4.5.2.1.4 Adequacy of the Developed μ EDM milling time.

Validation of the developed model adequacy is performed through statistical features in order to complement the ANOVA. To verify the accuracy of the models, summary statistics on variability, lack-of-fit, R^2 adjusted and predicted R^2 , adequate precision, and residual behavior are used. However, residual analysis is sufficient to determine the suitability of the model.

R squared is a statistic that evaluates how well a model can account for outliers from the mean. The coefficient of determination (R-squared) is not always a reliable measure of model validity because it can rise when irrelevant terms are added to the model. Adj R squared is a statistic that evaluates how well a model can account for outliers from the mean. The adjusted R-squared will drop if adding more terms to the model does not make it better. The model's predicted R-squared measures the amount of new data variation that can be ascribed to it. The metric used to assess accuracy is the signal-to-noise ratio. The average prediction error is assessed in this analysis with respect to the predicted value range at the design points.

For the model to be effective, the adjusted R-squared must be higher than 0.7 and the variation between the adjusted R-squared and predicted R-squared must not be greater than 0.2. It is preferable to have a sufficient precision ratio of at least 4, which denotes sufficient model discrimination (Design Expert-13, 2023). The different values for the μ EDM milling time as produced from the design are shown in Table 4.5.

Table 4.5 Summary Statistic for μ EDM milling time.

Std. Dev.	3.11	R²	0.7259
Mean	41.72	Adjusted R²	0.6711
C.V. %	7.44	Predicted R²	0.5645
		Adeq Precision	12.0595

The difference is less than 0.2 because the Adjusted R² of 0.6711 and the Predicted R² of 0.5645 are reasonably in agreement. Adeq Precision measures the signal-to-noise ratio. The ideal ratio is at least 4. Here, the signal is strong enough based on the Adeq Precision ratio of 12.060. It can be used to design the model in a certain space.

Examining model errors or residuals usually verifies model adequacy. Errors or residuals are the discrepancies between actual statements and regression model fitted values., i.e.

$$\varepsilon_a = y_a - \hat{y}_a (a = 1,2,3,\dots,n) \quad (4.8)$$

According to (Astakhov, 2012), there are several terms that residues should have for a archetypal to be suitable. These requirements are:

1. Residues must be ordinarily scattered.
2. The discrepancy ought to be the same.
3. It should have zero means, and
4. Randomized experiments

To verify whether residuals are generally allocated, the normal plot of the residuals graph of Figure 4.40 is plotted for the μ EDM milling time.

The residual of the data obtained from the equation should be normally scattered, formless (erratically distributed), with steady variance, and zero means, according to (Mullen & Hultquist, 2017). The use of studentized residual is recommended for model adequacy tests since it takes into consideration the existence of a large residual and also large data sets that might have a high effect on the least squares fit (Pike & McNally, 1997). Such analysis may also employ standardized residuals. The residuals' normal plot in Figure 4.40 shows that they are roughly distributed randomly and followed a straight-line pattern. As a result, the μ EDM milling time meets the requirement for normality.

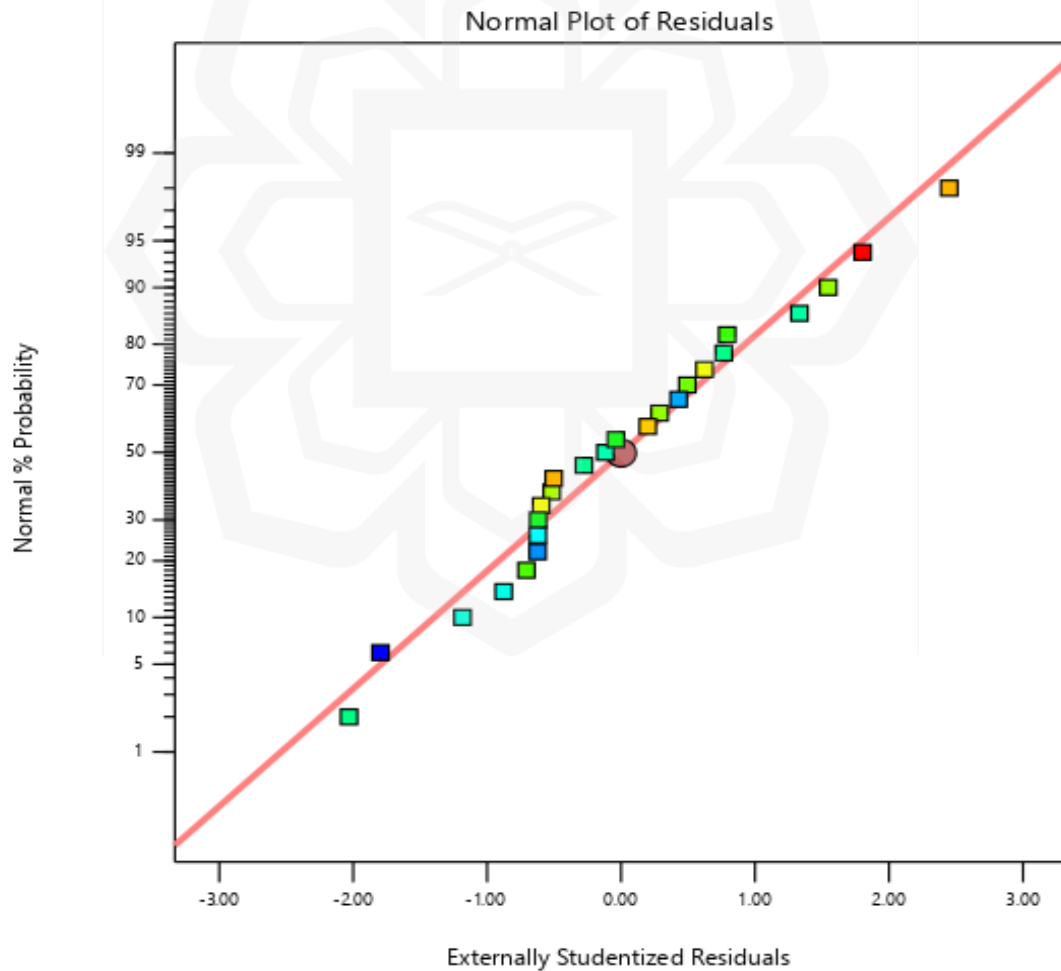


Figure 4.40: Normal probability of residuals for μ EDM milling time.

According to (Montgomery, 2009), the normal probability plot indicates whether the residuals are distributed normally, in which case a straight line will connect the points. Figure 4.40 demonstrates that the plots have a positive value and follow a straight-line pattern. This demonstrates that the residuals are distributed normally.

It was pointed out that there are both positive and negative residuals, that a plot of residuals vs. predicted values will show if the residual has the same variation or not, and for a remaining plot to be perfect and adequate, the residuals should be plotted against the predicted values. The center of the plot of residuals against what was expected must be around zero. The residual plots show that the positive and negative values are spread out randomly, and there is no clear pattern. Figure 4.41 and 4.42 show that the residual plot for constant variance checks for this experiment is acceptable, having the same variance as the original data (constant range of residuals across the graph). Figure 4.41 and 4.42 shows that the residual plot for constant variance checks for this experiment is acceptable, having the same variance as the original data (constant range of residuals across the graph).

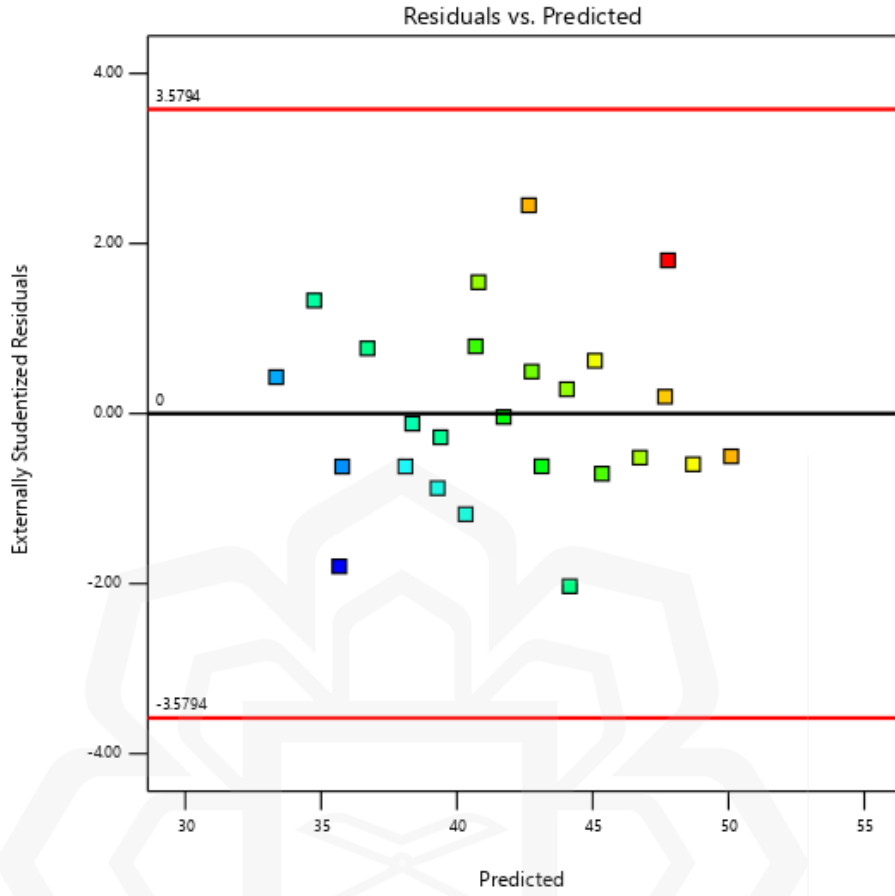


Figure 4.41: Plot of residuals versus predicted values for μ EDM milling time.

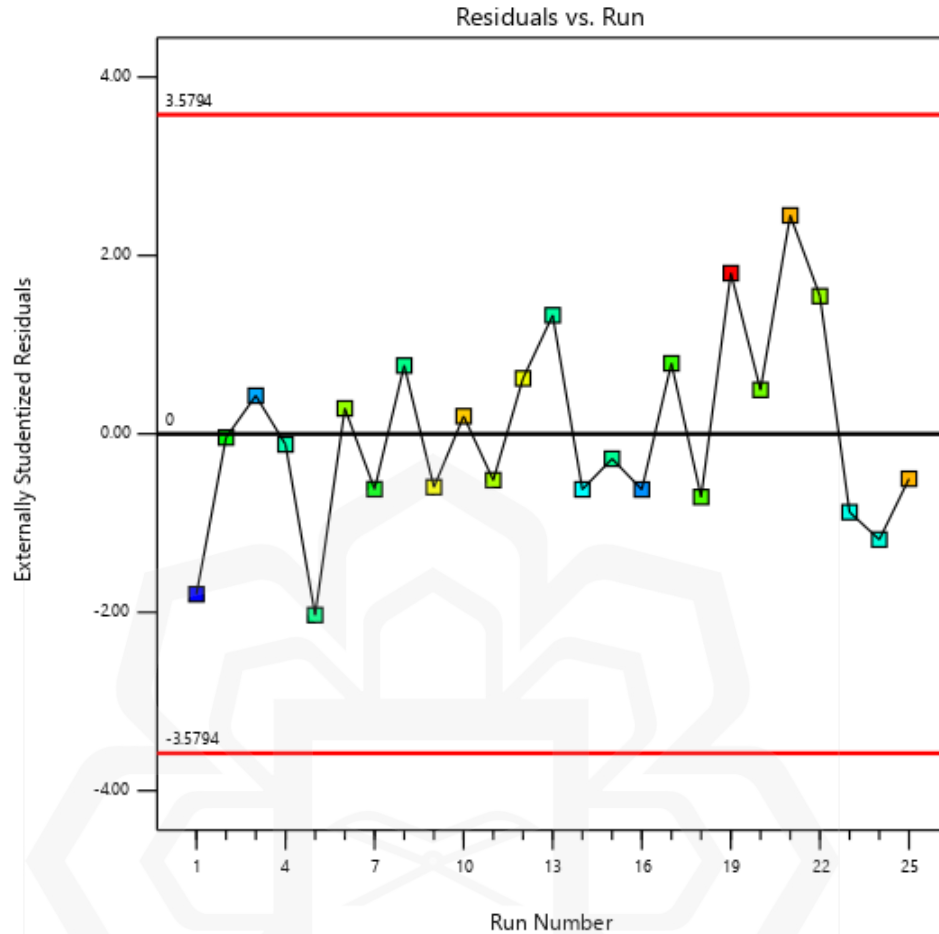


Figure 4.42: Plot of residuals against run order for μ EDM milling time.

4.5.2.1.5 3-Dimensional Surface plots for μ EDM milling time.

Figure 4.43 & 4.44 display the 3-D response surface plots produced by the model for μ EDM milling time. The plots display the μ EDM milling time trend along with changes to the important variables.

Figure 4.43 shows a 3-D surface plot that both scanning speed and laser power influence the μ EDM milling time response value. It is examined that an increase in scanning speed (ss) factors (A) increase the μ EDM milling time slightly. It is also found that laser power increases and the μ EDM milling time is decreasing, which is quite significant as compared

to the scanning speed effect. The power of the incident laser was sufficient to eradicate the high-level material that was present in the majority of the initial LBMMed channel. Higher power created a larger LBMMed milled channel because heat flowed across the material cross-section. As a result, the μ EDM milling process becomes faster. Figure 4.44 illustrated that the loop also has an effect on μ EDM milling time. Actually, a higher loop count in the LBMMed milling process helps to eliminate additional material from the ablated zone, which enhances the μ EDM milling method. Frequency/pulse repetition rate has no effect on the μ EDM milling process to increase or decrease machining time.

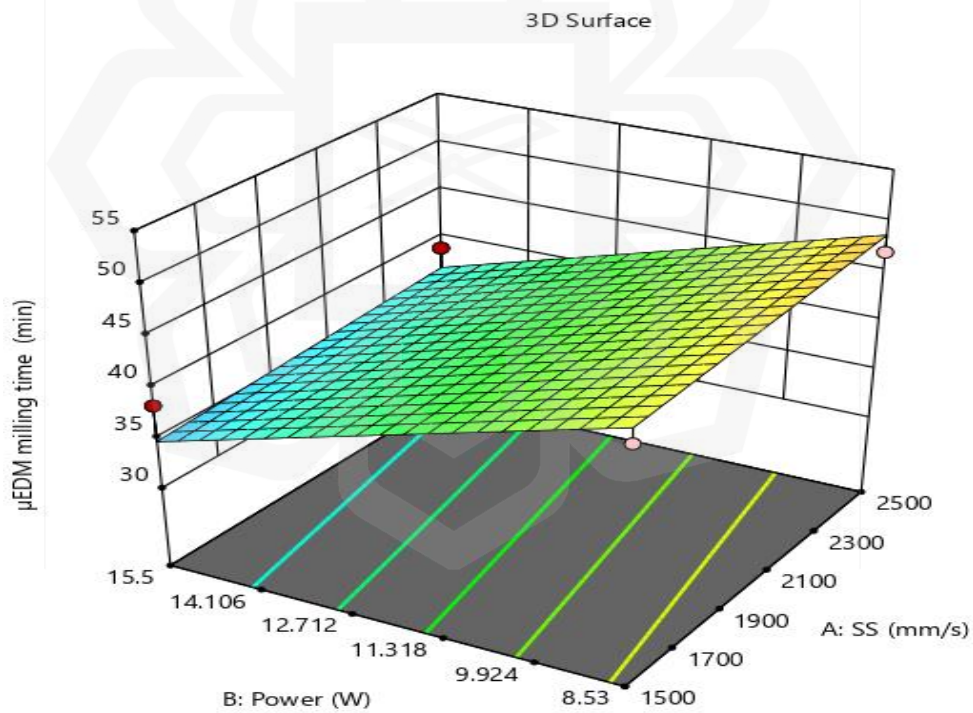


Figure 4.43: 3-D response surface plot for the μ EDM milling time (Power and Scanning speed effect)

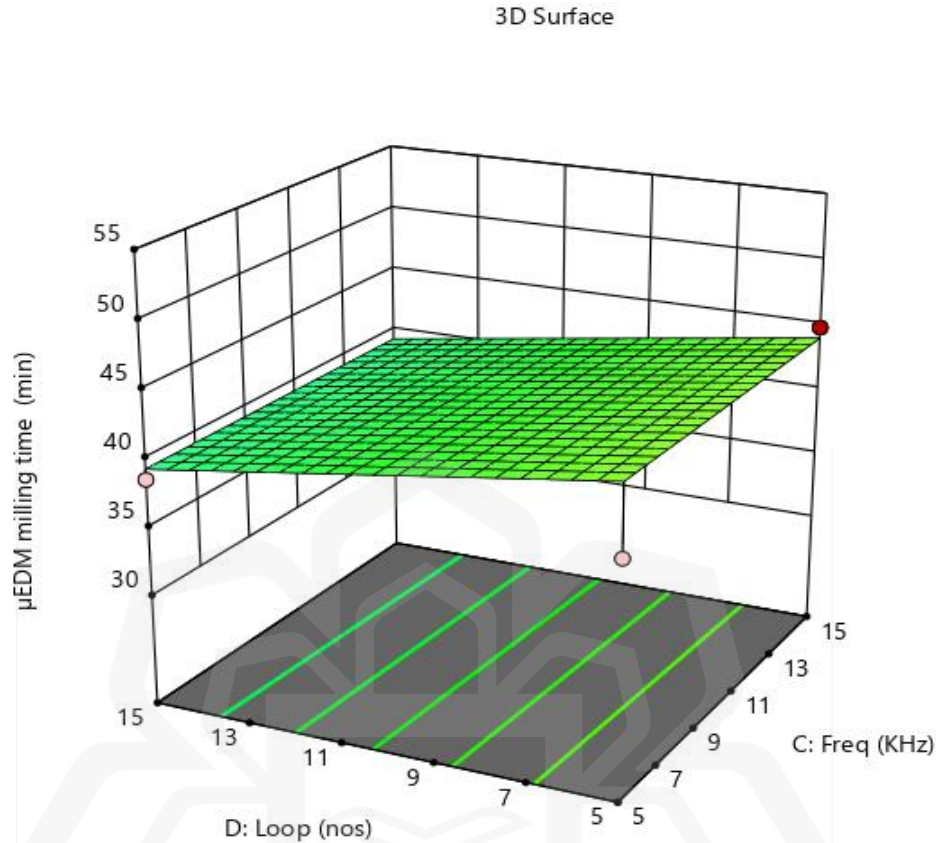


Figure 4.44: 3-D response surface plot for the μ EDM milling time (Loop and frequency effect)

4.5.2.1.6 Study of the model robustness (μ EDM milling time)

In order to estimate the robustness of the model prediction, experiments were conducted to generate more data that were not used at all for the modeling purpose. Figure 4.45 was used to show the level of fitting between the experimental and predicted μ EDM time for the whole dataset. It was observed that 90% of the data for the μ EDM milling time was

predicted within 85% of prediction accuracy which ascertains the model robustness for the μ EDM milling time.

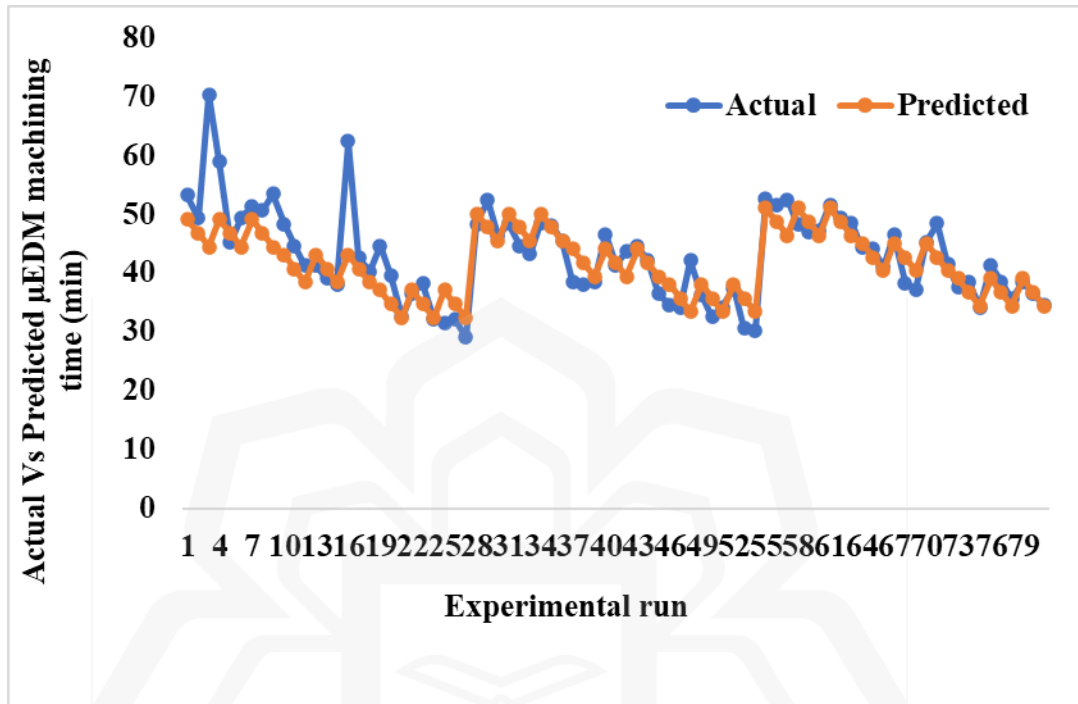


Figure 4.45 Model competency (Actual Vs Predicted) for the μ EDM milling time.

4.5.2.2 Model for Tool wear

The analysis of variance, model adequacy test, model graphs for surface plots, and model prediction competency behaviors for tool wear (μm) in LBMM- μ EDM milling are presented in the following sections.

4.5.2.2.1 Fit Summary Statistics

Fit summary Table 4.6 shows the μ EDM milling tool wear fit summary suggested linear model with significant terms. The highest-order linear is chosen for the μ EDM milling tool

wear in order to take care of all available model terms. As a result, the linear model that has an F-value of 3.01 and a P-value that is less than 0.0427 is accepted.

Table 4.6 Fit summary for μ EDM tool wear

Source	Sum of Squares	df	Mean Square	F-value	p-value	
Mean vs Total	20967.04	1	20967.04			
Linear vs Mean	228.83	4	57.21	3.01	0.0427	Suggested
2FI vs Linear	87.75	6	14.63	0.7003	0.6542	
Quadratic vs 2FI	100.96	4	25.24	1.32	0.3279	
Cubic vs Quadratic	141.67	8	17.71	0.7119	0.7000	Aliased
Residual	49.75	2	24.88			
Total	21576.00	25	863.04			

4.5.2.2.2 μ EDM Tool Wear Model Selection and Analysis of Variance

Analysis of variance (ANOVA) tests are displayed in Table 4.7. According to the analysis of variance (ANOVA) for μ EDM milling tool wear, the model incorporating all terms is significant.

Table 4.7 Analysis of variance for μ EDM milling tool wear

Source	Sum of Squares	df	Mean Square	F-value	p-value	
Model	228.83	4	57.21	3.01	0.0427	significant
A-SS	1.33	1	1.33	0.0702	0.7938	
B-Power	80.08	1	80.08	4.21	0.0534	
C-Freq	14.08	1	14.08	0.7410	0.3995	
D-Loop	133.33	1	133.33	7.02	0.0154	
Residual	380.13	20	19.01			
Cor Total	608.96	24				

4.5.2.2.3 Developed Model for the μ EDM milling tool wear.

Equations 4.9 and 4.10 are models developed for micro μ EDM milling tool wear and are represented in terms of coded and actual factors. By determining the relative impact of the factors, typically by relating the factor coefficients, the equation in terms of coded aspects

(Equation 4.9) is exploited to make projections. A projecting model is used to reestablish the experiment's results, and it is the factor equation presented in Equation 4.10.

$$\text{Tool wear} = +28.96 + 0.3333*A - 2.5*B + 1.08* C - 3.33 *D \quad (4.9)$$

$$\text{Tool wear} = +41.03305 + 0.000667*SS - 0.741272*Power + 0.216667*Freq - 0.6667*Loop \quad (4.10)$$

4.5.2.2.4 Adequacy of the Developed μ EDM milling tool wear

Table 4.8 shows that the improved model term for μ EDM milling tool wear has an R^2 of 0.3758, and the Adjusted R^2 of 0.2509 and Predicted R^2 of 0.0116 are close, so the difference is less than 0.2. The adjusted R^2 for the model is significant which demonstrates the limitation of the model. However, Adeq Precision ratio of 6.0694 indicates a strong signal.

Table 4.8 Summary Statistic for μ EDM milling tool wear.

Std. Dev.	4.36	R²	0.3758
Mean	28.96	Adjusted R²	0.2509
C.V. %	15.05	Predicted R²	0.0116
		Adeq Precision	6.0694

The residuals' normal plot in Figure 4.46 shows that they are distributed randomly and followed a straight-line pattern. As a result, the μ EDM milling tool wear meets the requirement for normality.

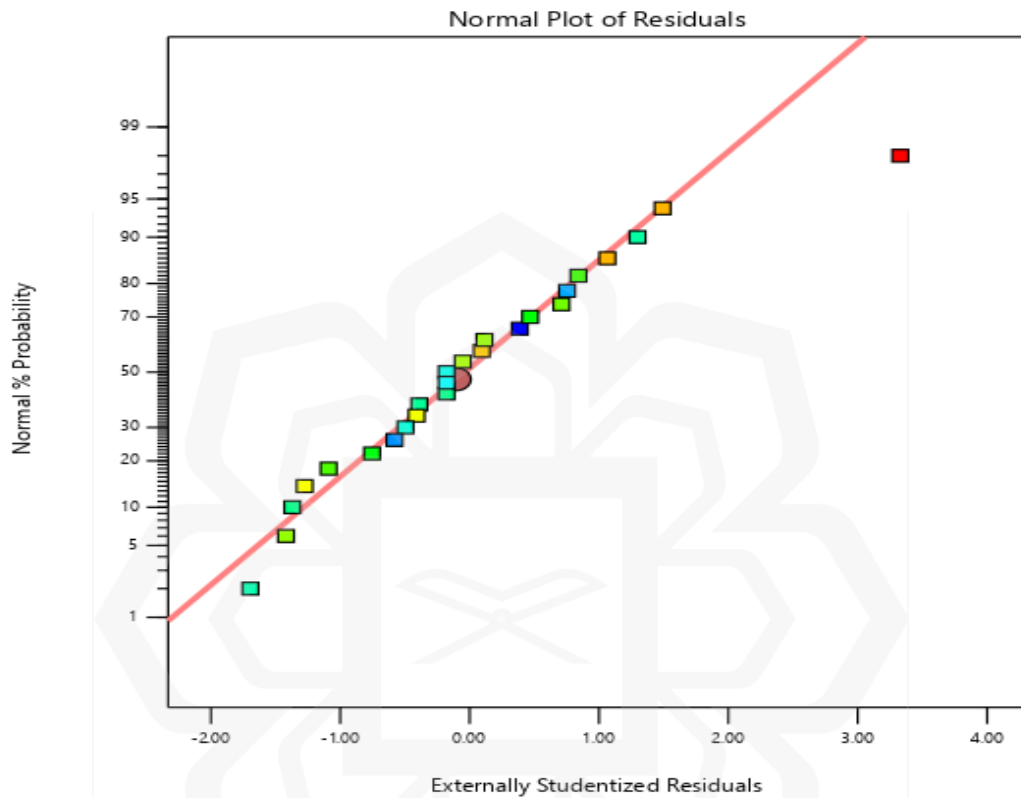


Figure 4.46: Normal probability of residuals for μ EDM milling tool wear.

Residual plot versus predicted values of μ EDM milling tool wear shown in Figure 4.47 signify that the data did not take any unusual structures or patterns for the experimental conditions. The fitted values are randomly scattered, thus indicating that the variances of the initial observations are continuous for all standards. Hence, the constant variance hypothesis is also satisfied for the μ EDM milling tool wear models.

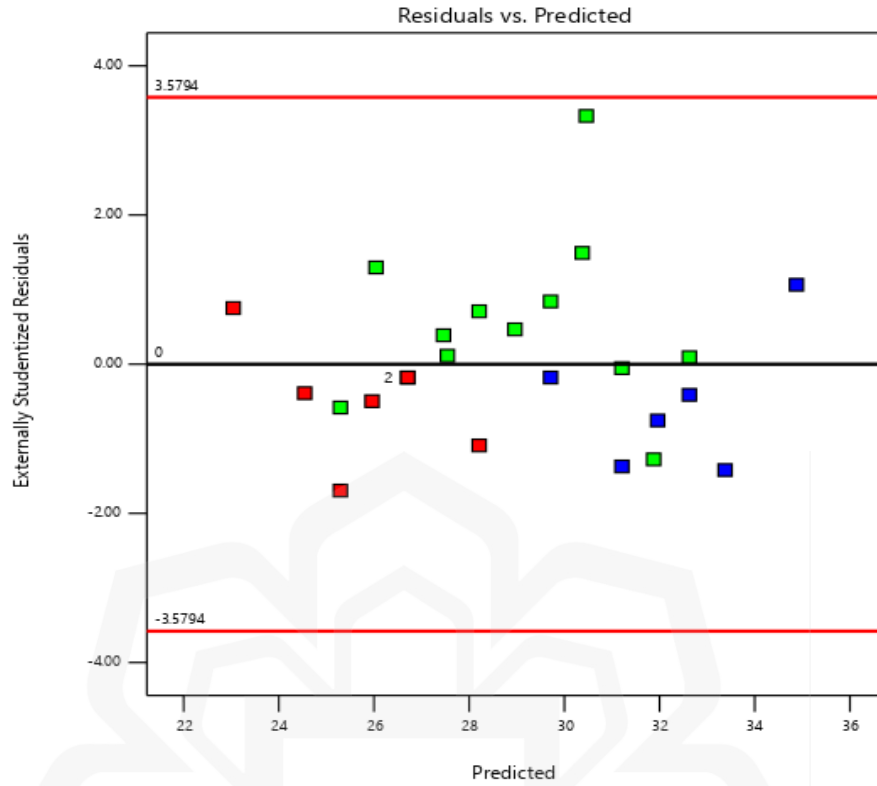


Figure 4.47: Plot of residuals against predicted values for μ EDM milling tool wear.

Figure 4.48 shows the μ EDM milling tool wear residual plot against run order. The plot showed no data relationship to either end. The model can predict μ EDM milling tool wear because the errors are independent.

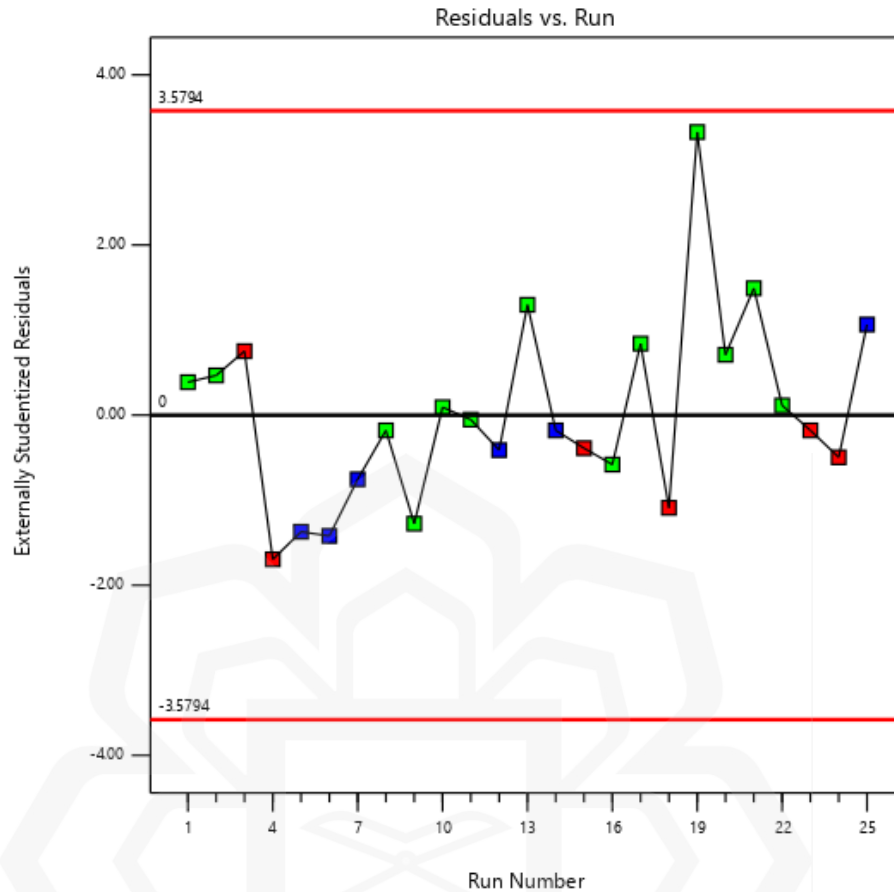


Figure 4.48: Plot of residuals against run order for μ EDM milling tool wear.

4.5.2.2.5 3-Dimensional Surface plots for μ EDM milling tool wear.

Figure 4.49 & 50 display the 3-D response surface plots produced by the model for μ EDM milling tool wear. The plots give the μ EDM milling tool wear curve with simultaneous variations in the substantial factors.

It is observed in Figure 4.49 & 50 that laser power and loops have a significant impact on the μ EDM milling tool wear. The increasing trend of power decreases the μ EDM milling tool wear because the high laser power removes the workpiece material to a large extent and in the μ EDM milling condition less time is required to complete the milling process. Due to this reason, tool wear during μ EDM milling is decreased. Similarly, the loop number

is increased means the more ablated zone is created in the LBMM milled channel which require shorter time to end up the μ EDM milling process. It also reduces the tool wear rate in the μ EDM milling.

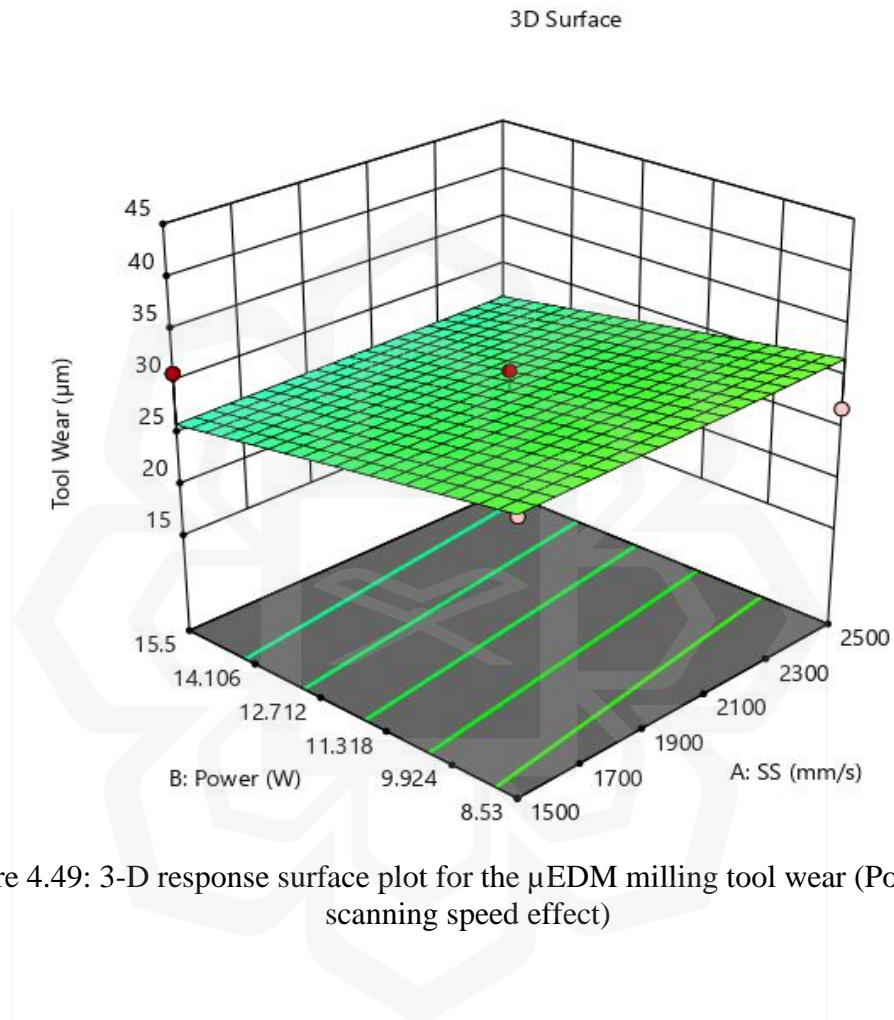


Figure 4.49: 3-D response surface plot for the μ EDM milling tool wear (Power and scanning speed effect)

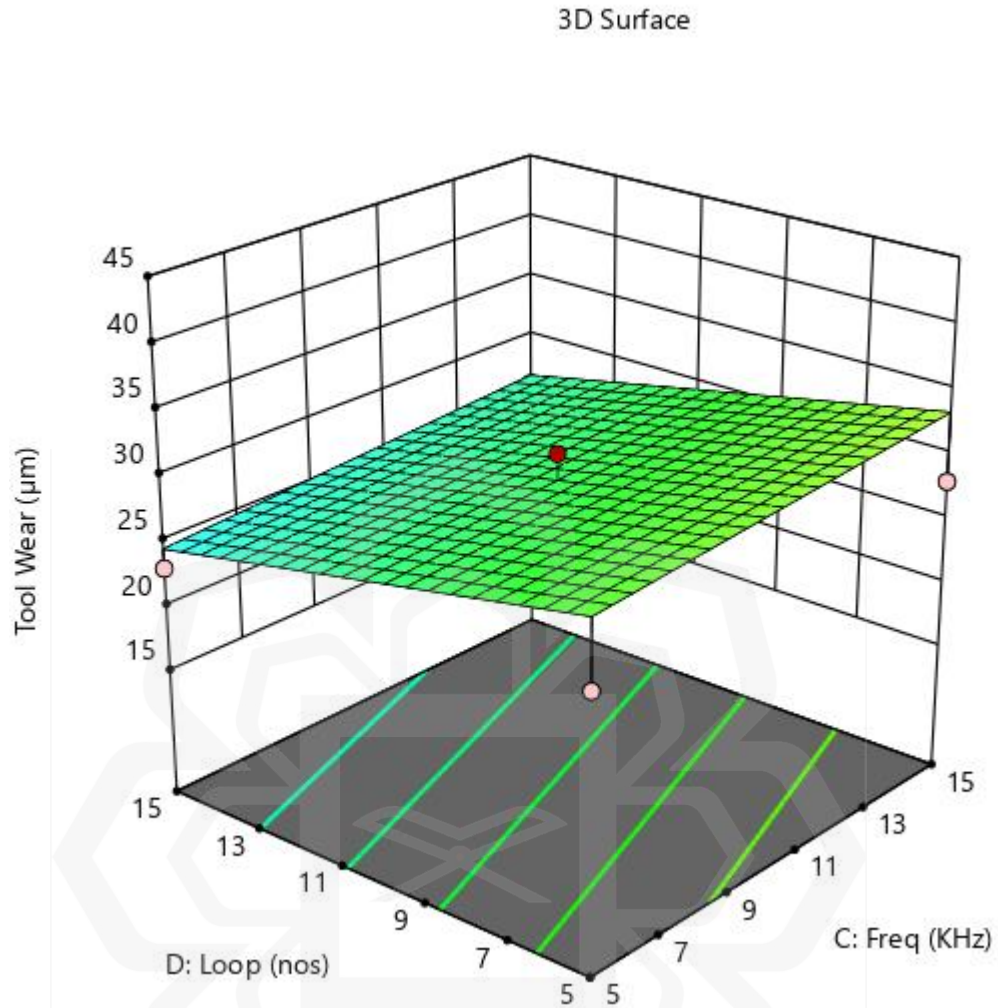


Figure 4.50: 3-D response surface plot for the μ EDM milling tool wear (loop and frequency effect)

4.5.2.2.6 Study of the model robustness (tool wear)

Similar to μ EDM milling time study Figure 4.51 was used to show the level of fitting between the experimental and predicted tool wear for the whole dataset. It was observed that 86% of the data for the tool wear was predicted within 80% of prediction accuracy which ascertains the model robustness however not as good as for the μ EDM milling time.

was found that more than 85% of data can be explained by the predicted data.

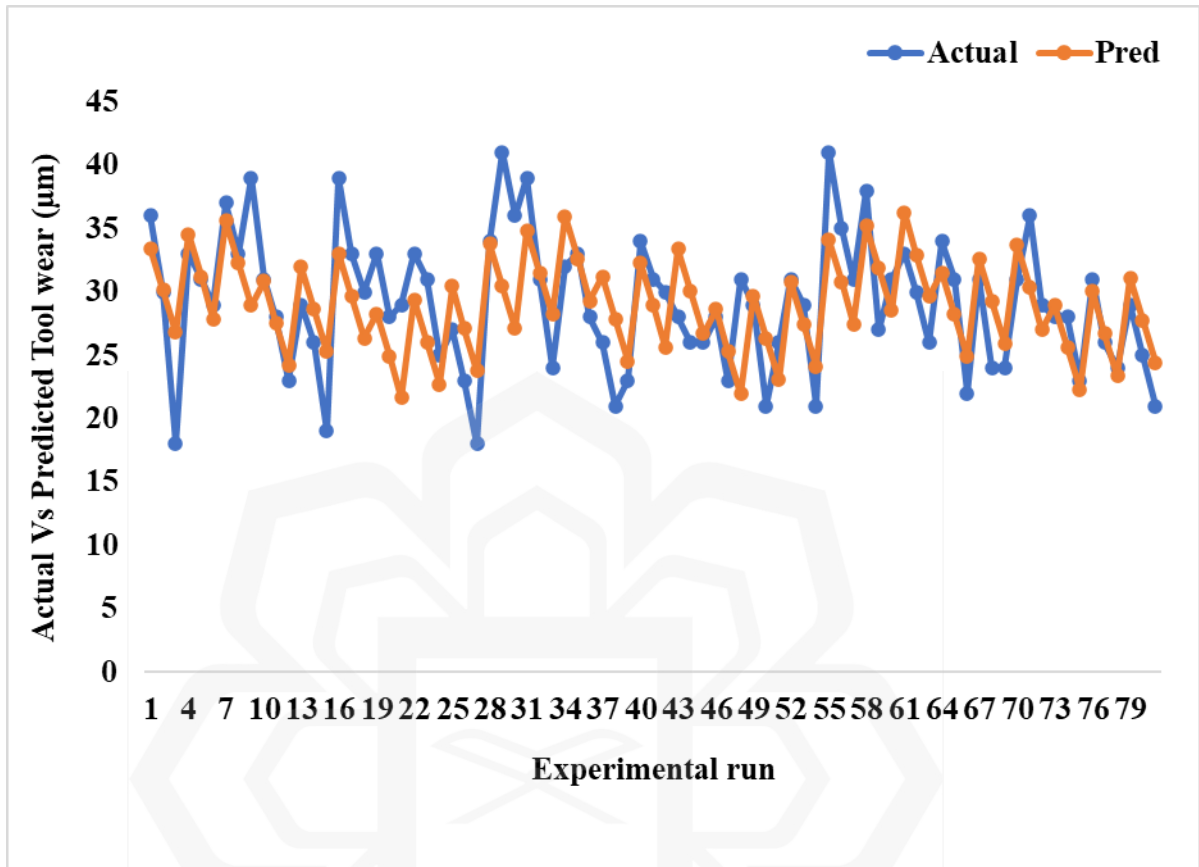


Figure 4.51: Actual Versus predicted data plot for μ EDM milling tool wear.

4.5.2.3 Model for Short circuit

In order to develop the model for μ EDM milling short circuits the procedure in section 4.5.2.2 is utilized. The analysis of variance, model adequacy test, model graphs for surface plots, and model prediction competency are presented for the μ EDM milling short circuit model confirmation.

4.5.2.3.1 Fit Summary Statistics

The fit summary table (Table 4.9) shows the μ EDM milling short circuit fit summary suggested linear model with significant terms. However, the p-value is not to a lesser extent than 0.05 which indicates the model fit is poor.

Table 4.9 Fit summary for μ EDM milling short circuit.

Source	Sum of Squares	df	Mean Square	F-value	p-value	
Mean vs Total	1.468E+05	1	1.468E+05			
Linear vs Mean	3169.67	4	792.42	2.67	0.0622	Suggested
2FI vs Linear	626.75	6	104.46	0.2753	0.9393	
Quadratic vs 2FI	843.18	4	210.79	0.4718	0.7558	
Cubic vs Quadratic	3975.83	8	496.98	2.02	0.3731	Aliased
Residual	492.33	2	246.17			
Total	1.560E+05	25	6238.00			

4.5.2.3.2 μ EDM Short Circuit Model Selection and Analysis of Variance

ANOVA tests are displayed in Table 4.10 Analysis of variance for μ EDM milling short circuit.. According to the ANOVA for μ EDM milling short circuit, the model is significant by incorporating all the terms.

Table 4.10 Analysis of variance for μ EDM milling short circuit.

Source	Sum of Squares	df	Mean Square	F-value	p-value	
Model	3148.33	3	1049.44	3.70	0.0279	significant
A-SS	208.33	1	208.33	0.7341	0.4012	
B-Power	588.00	1	588.00	2.07	0.1648	
D-Loop	2352.00	1	2352.00	8.29	0.0090	
Residual	5959.43	21	283.78			
Cor Total	9107.76	24				

4.5.2.3.3 Developed Model for the μ EDM milling short circuit.

The prediction of the model equation for μ EDM milling short circuit profile is represented in equations 4.11 and 4.12. The models are developed considering the significant terms from the improved analysis of variance in Table ANOVA. Equation 4.11 identifies the relative influence of each sort out parameter on μ EDM milling short circuit based on the coefficient of each parameter. It is observed from the calculation that the most impacting approach parameter in the order of significance is Loop, Power, and scanning speed. Equation 4.12 is a diagnostic model equation used to rebuild the results of the experiment.

$$\text{Short circuit} = +76.64 + 4.17*A - 7.00*B - 14.00*D \quad (4.11)$$

$$\text{Short circuit} = +112.10676 + 0.008333*SS - 2.00861*Power - 2.80* Loop \quad (4.12)$$

4.5.2.3.4 Adequacy of the Developed μ EDM milling short circuit

Table 4.11 Summary of model statistics for μ EDM milling short circuit. shows that the improved model term for μ EDM milling short circuit has an R^2 of 0.345, Adjusted R^2 of 0.2522 and Predicted R^2 0.0882 are close, so the difference is less than 0.2. The adjusted R^2

for the model is significant which demonstrates the limitation of the model. However, Adeq Precision ratio of 6.233 indicates a strong signal.

Table 4.11 Summary of model statistics for μ EDM milling short circuit.

Std. Dev.	16.85	R²	0.3457
Mean	76.64	Adjusted R²	0.2522
C.V. %	21.98	Predicted R²	0.0882
		Adeq Precision	6.2330

Figure 4.52 displays the common plots of the residuals, showing that the data residuals largely adhere to linear patterns.

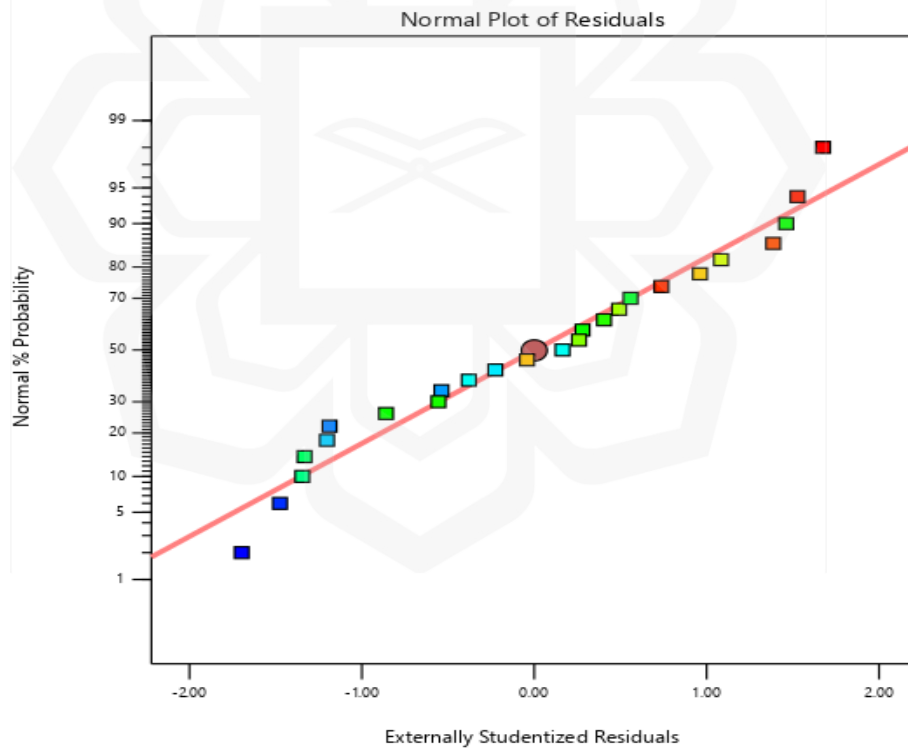


Figure 4.52: Normal probability of residuals for μ EDM milling short circuit

Residual plot versus predicted values of μ EDM milling short circuit shown in Figure 4.53 signifies that the data did not take any unusual structures or patterns for the experimental conditions. The fitted values are randomly scattered, thus indicating that the variances of the earliest observations are continuous for all values. Hence, the constant variance hypothesis is also fulfilled for the μ EDM milling short circuit models.

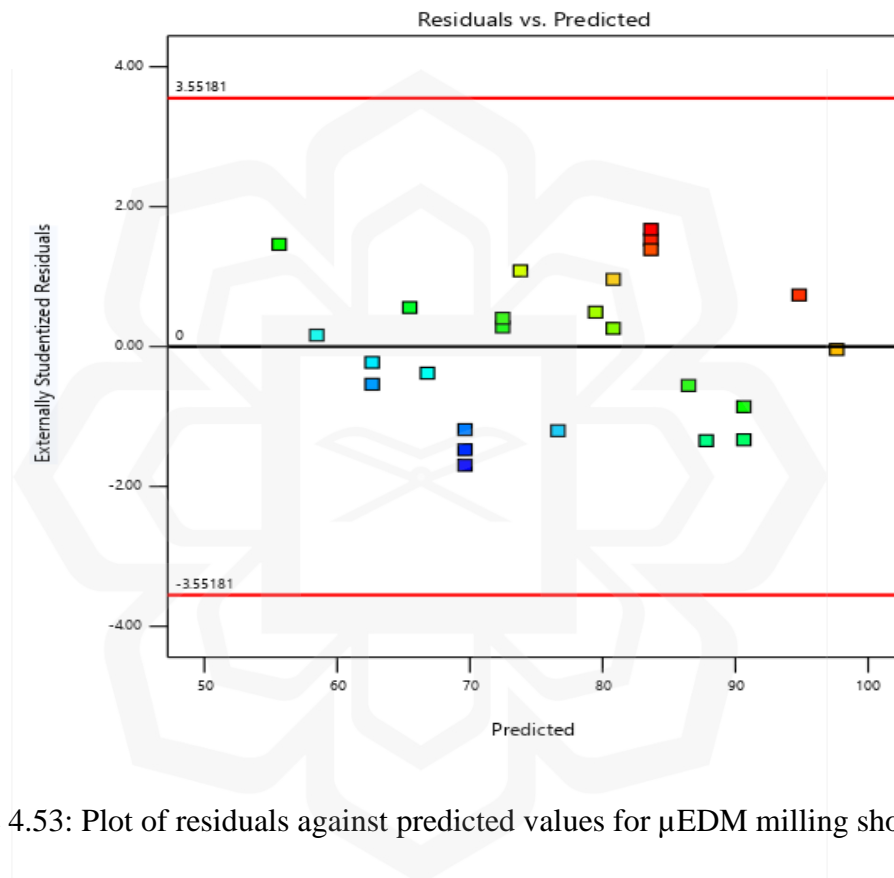


Figure 4.53: Plot of residuals against predicted values for μ EDM milling short circuit.

Figure 4.54 shows μ EDM milling short circuit residual plot against run order. The plot showed no data relationship to either end. The model can predict μ EDM milling short circuits because the errors are independent.

created in the LBMM milled channel which requires a shorter time to end up the μ EDM milling process. It also reduces the short circuit in the μ EDM milling.

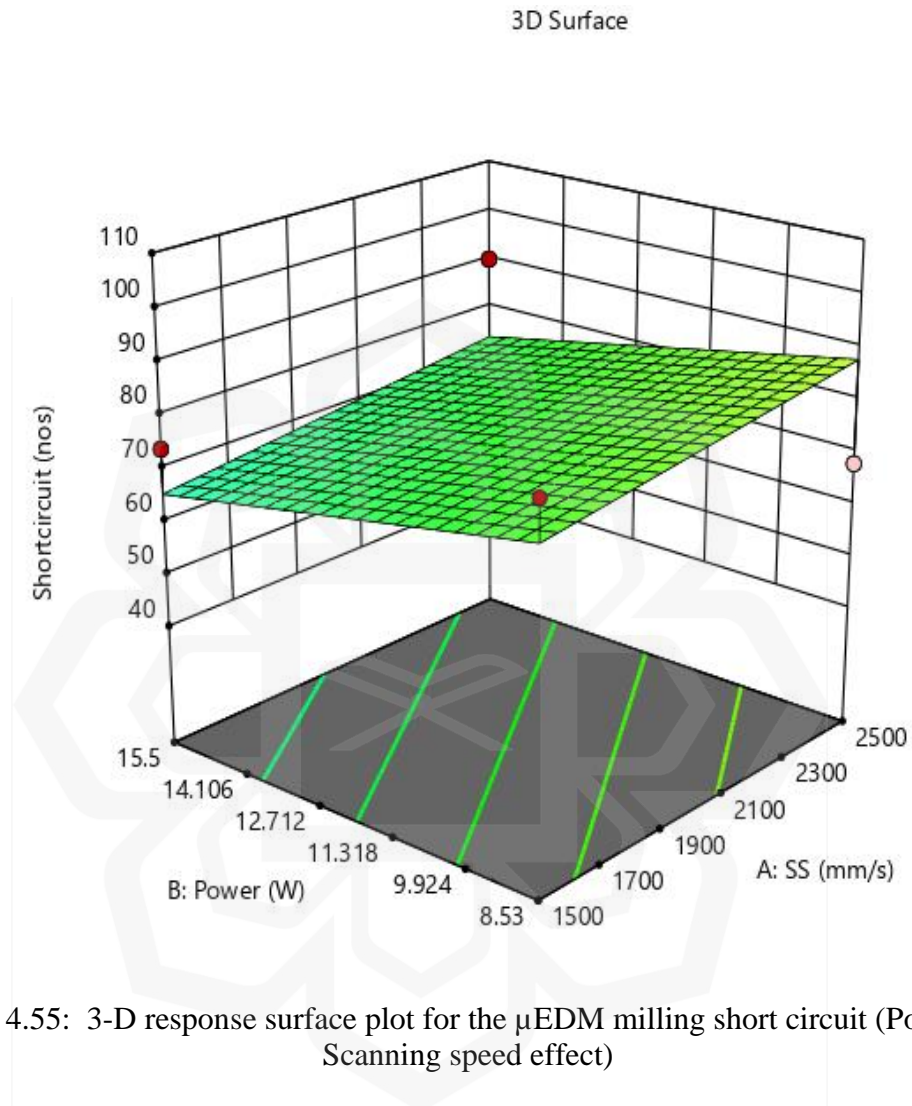


Figure 4.55: 3-D response surface plot for the μ EDM milling short circuit (Power and Scanning speed effect)

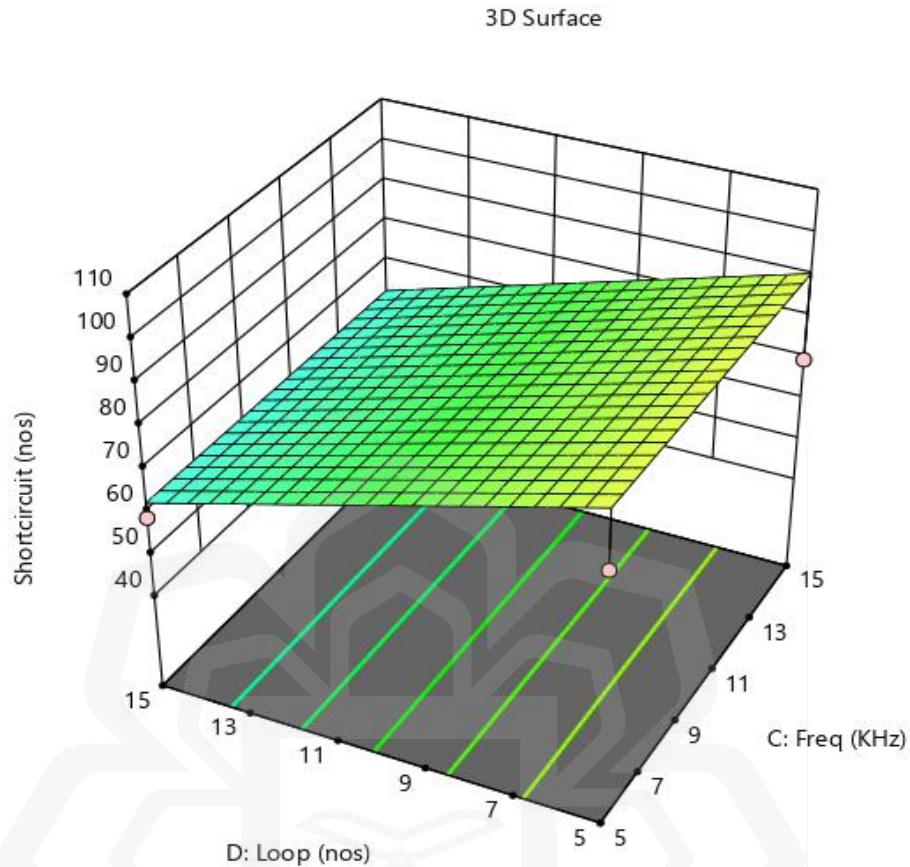


Figure 4.56: 3-D response surface plot for the μ EDM milling short circuit (frequency and loop effect)

4.5.2.3.6 Study of the model robustness (short circuit/arching count)

Similar to μ EDM milling time study Figure 4.57 was used to show the level of fitting between the experimental and predicted tool wear for the whole dataset. It was observed that 70% of the data for the short circuit was predicted within 85% of prediction accuracy which ascertains the model robustness however not as good as for the μ EDM milling time.

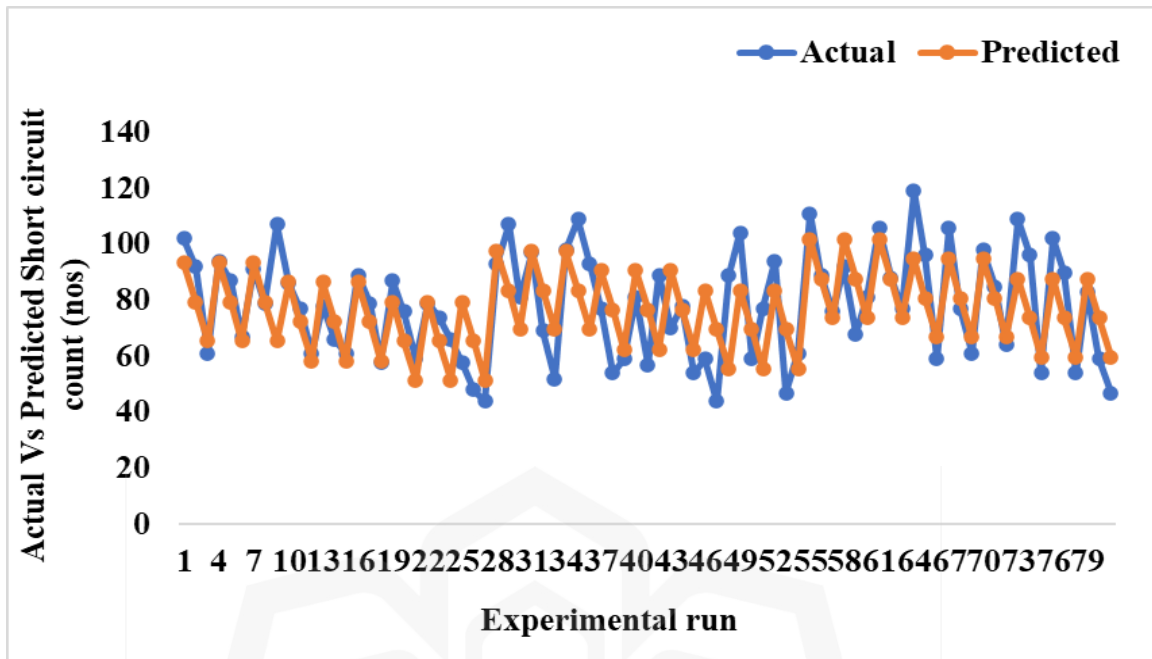


Figure 4.57: Scattered plots of predicted against the actual values for μ EDM milling short circuit.

4.5.3 Summary

In this study, we examined at how different laser parameters affected different performance metrics for the sequential micromachining process based on LBMM- μ EDM. We found that LBMM input parameters significantly affect the output performance of μ EDM machining. From the initial phase of the investigational study, comparing to pure EDM, it was found that the LBMM- μ EDM method could reduce the manufacture time for forming micro-holes by a factor of $\sim 2.65x$ while keeping the same level of machined hole quality in terms of being free of recast layers, circularity, etc. It was found that the machining time for the μ EDM process can be reduced by up to 250% by using a high laser power and a slow scanning speed to create the pilot holes as opposed to a loWatt laser-power and a fast-scanning speed. The dual stage ANN modeling of the LBMM- μ EDM drilling with a constant μ EDM parameter was examined in the second phase of the experimental study. It

was found that μ EDM machining time, machining instability (short circuit/arc) count, and tool wear, overall estimation accuracy were $\sim 87\%$, $\sim 89\%$, and $\sim 90\%$ respectively. The third step of the experimental study was conducted to develop a dual-stage ANN modeling of the LBMM- μ EDM drilling with variable EDM Parameters. The model's overall estimation accuracy for μ EDM machining time, tool wear, and machining instability (short circuit/arc) count was achieved at 0.050 (95%), 0.040 (96%), and 0.110 (89%) respectively. The model also predicted that if the time-consuming scanning speed of 50 mm/s is used for 6.5 Watt laser-power during LBMM pilot hole machining, 320000 nJ discharge energy, and 3 μ m/sec feed rate, μ EDM completing time can be affirmed within 936 sec (15.6 min). In the final phase of this study, 3-D hybrid micromachining (milling) was tested using Response Surface Methodology (RSM) to identify the significant factors influencing this sequential hybrid micromachining. It was found that laser milling input parameters affect significantly the output responses of μ EDM machining time, tool wear, and machining instability (short circuit/arc). The developed model was fairly robust as at least 70% of the experimental data (including unused data for modelling) are predictable within an accuracy of at least 80% for all the three parameters. Table 4.12 shows the summary of the main results based on my research objectives.

Table 4.12 Summary of the main results based on my research objectives.

No.	Objectives	Summary of Results
01.	To experimentally investigate the Laser- μ -EDM based hybrid micromachining (micro drilling and micro milling) process on stainless steel (SUS 304) in terms of various performance indicators such as Machining	It was found that the LBMM- μ EDM method could reduce the fabrication time for creating micro-holes by a factor of $\sim 2.65x$ while keeping the same level of machined hole quality in terms of being free of recast layers, circularity, etc

	time, Tool wear, Machining instability/short circuit count.	
02.	To develop a mathematical model for hybrid micro drilling describing the relationship between the primary processes' (LBMM) input parameters and secondary process's (μEDM) output parameters.	The dual stage ANN modeling of the LBMM-μEDM drilling with a constant μEDM parameter was examined. It was found that μEDM machining time, machining instability (short circuit/arc) count, and tool wear, overall estimation accuracy were ~87%, ~89%, and ~90 % respectively. Secondly, a dual-stage ANN modeling of the LBMM- μEDM drilling with variable EDM Parameters was examined & it was found that The model's overall estimation accuracy for μEDM machining time, tool wear, and machining instability (short circuit/arc) count was achieved at 0.050 (95%), 0.040 (96%), and 0.110 (89%) respectively
03.	To develop a mathematical model for hybrid micro milling describing the relationship between the primary processes (LBMM) input parameters and the secondary processes (μEDM) output parameters.	3-D hybrid micromachining (milling) was tested using Response Surface Methodology (RSM). It was found that RSM based developed model was fairly robust as at least 70% of the experimental data (including unused data for modelling) are predictable within an accuracy of at least 80% for all the three parameters.

CHAPTER FIVE

CONCLUSION AND RECOMMENDATION

5.1 CONCLUSION

This study proposes three different phases of sequential hybrid micromachining. The first phase of this research investigated LBMM- μ EDM based hybrid micromachining & ANN modeling without changing the μ EDM parameters, LBMM- μ EDM based hybrid micromachining and ANN modeling with changing both LBMM & μ EDM parameters (2nd phase), and Finally LBMM- μ EDM based milling without changing the μ EDM parameters based on RSM modeling. In this research all the findings can be summarized as follows:

An investigation into the avenues in which various laser parameters influence the various performance indicators of an LBMM-EDM based sequential micromachining process has been carried out. It was discovered that the LBMM-EDM process could cut the time for creating micro-holes by a factor of approximately 2.65 times while maintaining the same level of machined hole quality with regard to the absence of recast layers, circularity, and other factors. When it comes to machining time, it was found that using a high laser power and a slow scanning speed to create the pilot holes (as opposed to using a low watt laser-power and a fast-scanning speed) can reduce the amount of time needed for machining when utilizing the EDM process by up to 250%. This was observed when comparing the two methods of creating the pilot holes. Additionally, it was noted that the size of the LBMMed holes machined by different LBMM parameters had a significant impact on tool wear and the incidence of short circuits during the μ EDM process. If loWatt laser-power and high scanning speed were used for the LBMMed holes, then high tool wear

rate and short circuit rate ($\sim 1\text{mm}/\text{min}$ and $\sim 20\text{nos}/\text{min}$, respectively) were observed during the EDM operation. Lastly, if the planned diameter for the LBMM process was cut in half, the residual spatter zone that came from the LBMM process could be completely eliminated by the μEDM process. Because of this, the machining time, tool wear, and short circuit frequency of the LBMM- μEDM process were all reduced, but overall, they were still much better than those of the pure μEDM process. The second part of this investigation focused on the training and assessment of a dual-stage artificial neural network (ANN) model for LBMM- μEDM based sequential micro-drilling. Altering the settings of the LBMM input while maintaining the parameters of the EDM input allowed for an accurate estimation of not only the amount of time required to finish using the μEDM method but also the amount of tool wear and the number of arcing and short circuits that occurred throughout the finishing process. In light of the findings, it was determined that the model's overall estimation accuracy for μEDM machining time, short circuit/arcing count, and tool wear was, respectively, 87%, 89%, and 90%. The trained model has a tendency to generalize the trend rather than converging locally, which suggests that it is not overfitting the data, based on the parametric analysis. Next the dual stage sequential model was further extended to incorporate the variation of both the LBMM parameters and μEDM parameters. Root Mean Square Errors (RMSEs) were calculated for every data set for each output parameter (i.e., μEDM time, short circuit/arcing count, and tool wear) to assess the model's accuracy. Average RMSE was calculated to be 0.050 (95% accuracy), 0.040 (96% accuracy), and 0.110 (89% accuracy) for the previously mentioned parameters.

In the third phase of sequential hybrid micromachining, the laser input parameter and EDM input parameter are modified in order to evaluate the output performance of final

products. In the first step of the dual-stage model, several LBMM process outputs were predicted using varying laser input parameters. Using the LBMM predicted outputs (volume removed, recast layer, and heat affected zone) and EDM input parameters. In the final stage of modeling it was found that the Root Mean Square Errors (RMSEs) were generated for each data set for each output parameter (i.e., EDM time, short circuit/arcing count, and tool wear) to assess the model's accuracy. The average RMSE was calculated to be 0.050 (95% accuracy), 0.040 (96% accuracy), and 0.110 (89% accuracy) for the aforementioned data.

In the final phase of this study, 3-D hybrid micromachining (milling) was tested using Response Surface Methodology (RSM) to identify the significant factors influencing this sequential hybrid micromachining. It was found that laser milling input parameters affect significantly the output responses of μ EDM machining time, tool wear, and short circuit. The developed model was fairly robust with a prediction accuracy of 90%, 85% for at least 70% of the dataset.

5.2 RECOMMENDATIONS

The following recommendations can be considered to extend the research to the next stage.

1. A machine tool can be developed to accommodate both processes. It will help to reduce the setup error and the chances of damaging the workpiece during the transfer process from the LBMM setup to the mEDM machine. Also, the new machine will be free from time loss due to the transfer of the sample from one machine to the other.

2. The developed models can be integrated into a single software to accommodate all the variations of the machining. Also, the proposed software can be integrated with the retraining facility with a new dataset.
3. Finally, this research did not cover the optimization of the LBMM- μ EDM-based micromachining which can be considered in the future.



REFERENCES

- Afiq Rashid, M., Rahman, M., & Senthil Kumar, A. (2016). A study on compound micromachining using laser and Electric Discharge Machining (EDM). *Advances in Materials and Processing Technologies*, 2(2), 258–265.
- Aggarwal, C. C. (2018). Neural networks and deep learning. *Springer*, 10(978), 3.
- Ahmad Athif Mohd Faudzi, Yaser Sabzehmeidani, K. S. (2020). Application of Micro-Electro-Mechanical Systems (MEMS) as Sensors: A Review. *Journal of Robotics and Mechatronics*, 32(2), 281–288.
- Al-Ahmari, A. M. A., Rasheed, M. S., Mohammed, M. K., & Saleh, T. (2016). A Hybrid Machining Process Combining Micro-EDM and Laser Beam Machining of Nickel-Titanium-Based Shape Memory Alloy. *Materials and Manufacturing Processes*, 31(4), 447–455.
- Alajmi, M. S., & Almeshal, A. M. (2020). Prediction and optimization of surface roughness in a turning process using the ANFIS-QPSO method. *Materials*, 13(13), 1–23.
- Arnaiz-González, Á., Fernández-Valdivielso, A., Bustillo, A., & López de Lacalle, L. N. (2016). Using artificial neural networks for the prediction of dimensional error on inclined surfaces manufactured by ball-end milling. *International Journal of Advanced Manufacturing Technology*, 83(5–8), 847–859.
- Arrizubieta, J. I., Klocke, F., Gräfe, S., Arntz, K., & Lamikiz, A. (2015). Thermal Simulation of Laser-assisted Turning. *Procedia Engineering*, 132, 639–646.
- Aspinwall, D. K., Dewes, R. C., Burrows, J. M., & Paul, M. A. (2001). Hybrid high speed machining (HSM): System design and experimental results for grinding / HSM and EDM / HSM. *CIRP Annals - Manufacturing Technology*, 50(1), 145–148.
- Astakhov, V. P. (2012). Design of experiment methods in manufacturing: Basics and practical applications. *Statistical and Computational Techniques in Manufacturing*, 9783642258, 1–54.
- Bennamoun, L. V. J. H. L. F. B. W. B. M. (2022). Hands-On Bayesian Neural Networks—A Tutorial for Deep Learning Users. *IEEE Computational Intelligence Magazine*, 17(2), 29–48.
- Beruvides, G., Quiza, R., del Toro, R., Castaño, F., & Haber, R. E. (2014). Correlation of the hole's quality with the force signals in a micro drilling process of a sintered

- tungsten-copper alloy. *International Journal of Precision Engineering and Manufacturing*, 15(9), 1801–1808.
- Bian, Q., Chen, S., Kim, B. T., Leventis, N., Lu, H., Chang, Z., & Lei, S. (2011). Micromachining of polyurea aerogel using femtosecond laser pulses. *Journal of Non-Crystalline Solids*, 357(1), 186–193.
- Bissacco, G., Valentincic, J., Hansen, H. N., & Wiwe, B. D. (2010). Towards the effective tool wear control in micro-EDM milling. *International Journal of Advanced Manufacturing Technology*, 47(1–4), 3–9.
- Biswas, R., Kuar, A. S., Sarkar, S., & Mitra, S. (2010). A parametric study of pulsed Nd:YAG laser micro-drilling of gamma-titanium aluminide. *Optics and Laser Technology*, 42(1), 23–31.
- Borse, S. C., & Kadam, M. S. (2018). Experimental Study in Micromilling of Inconel 718 by Fiber Laser Machining. *Procedia Manufacturing*, 20, 213–218.
- Brown, M. S., & Arnold, C. B. (2010). *Laser Precision Microfabrication*. 135, 91–120.
- Burden, F., & Winkler, D. (2008). Bayesian regularization of neural networks. *Methods in Molecular Biology*, 458, 25–44.
- Calfee, R., & Piontkowski, D. (2016). Design and analysis of experiments. In *Handbook of Reading Research*.
- Casalino, G., Losacco, A. M., Arnesano, A., Facchini, F., Pierangeli, M., & Bonserio, C. (2017). Statistical Analysis and Modelling of an Yb: KGW Femtosecond Laser Micro-Drilling Process. *Procedia CIRP*, 62, 275–280.
- Chavoshi, S. Z., & Luo, X. (2015). Hybrid micro-machining processes: A review. *Precision Engineering*, 41, 1–23.
- Chern, G. L., Wu, Y. J. E., & Liu, S. F. (2006). Development of a micro-punching machine and study on the influence of vibration machining in micro-EDM. *Journal of Materials Processing Technology*, 180(1–3), 102–109.
- Debnath, S., Kunar, S., Anasane, S. S., & Bhattacharyya, B. (2017). *Non-traditional Micromachining Processes: Opportunities and Challenges*.
- Demir, A. G., Previtali, B., & Bestetti, M. (2010). Removal of spatter by chemical etching after microdrilling with high productivity fiber laser. *Physics Procedia*, 5(PART 1), 317–326.

- Dhara, S. K., Kuar, A. S., & Mitra, S. (2008). An artificial neural network approach on parametric optimization of laser micro-machining of die-steel. *International Journal of Advanced Manufacturing Technology*, 39(1–2), 39–46.
- Dhupal, D., Doloi, B., & Bhattacharyya, B. (2008). Parametric analysis and optimization of Nd:YAG laser micro-grooving of aluminum titanate (Al₂TiO₅) ceramics. *International Journal of Advanced Manufacturing Technology*, 36(9–10), 883–893.
- Ding, H., Shen, N., & Shin, Y. C. (2012). Journal of Materials Processing Technology Thermal and mechanical modeling analysis of laser-assisted micro-milling of difficult-to-machine alloys. *Journal of Materials Processing Tech.*, 212(3), 601–613.
- Dubey, A. K., & Yadava, V. (2008a). Experimental study of Nd:YAG laser beam machining-An overview. *Journal of Materials Processing Technology*, 195(1–3), 15–26.
- Dubey, A. K., & Yadava, V. (2008b). Laser beam machining-A review. *International Journal of Machine Tools and Manufacture*, 48(6), 609–628.
- D'Urso, G., Maccarini, G., Quarto, M., Ravasio, C., & Caldara, M. (2016). Micro-electro discharge machining drilling of stainless steel with copper electrode: The influence of process parameters and electrode size. *Advances in Mechanical Engineering*, 8(12), 1–16.
- El-Khoury, M., Voisiat, B., Kunze, T., & Lasagni, A. F. (2020). Prediction of optimum process parameters fabricated by direct laser interference patterning based on central composite design. *Materials*, 13(18).
- Faisal, N., Zindani, D., Kumar, K., & Bhowmik, S. (2019). *Laser Micromachining of Engineering Materials—A Review*. Springer International Publishing.
- Feng, S., Huang, C., Wang, J., & Jia, Z. (2019). *Materials Science in Semiconductor Processing Surface quality evaluation of single crystal 4H-SiC wafer machined by hybrid laser-waterjet: Comparing with laser machining*. 93(September 2018), 238–251.
- Ferreira, S. L. C., Bruns, R. E., Ferreira, H. S., Matos, G. D., David, J. M., Brandão, G. C., da Silva, E. G. P., Portugal, L. A., dos Reis, P. S., Souza, A. S., & dos Santos, W. N. L. (2007). Box-Behnken design: An alternative for the optimization of analytical methods. *Analytica Chimica Acta*, 597(2), 179–186.
- Förster, D. J., Jäggi, B., Michalowski, A., & Neuenschwander, B. (2021). Review on experimental and theoretical investigations of ultra-short pulsed laser ablation of metals with burst pulses. *Materials*, 14(12).

- Fu, Y., Miyamoto, T., Natsu, W., Zhao, W., & Yu, Z. (2016). Study on Influence of Electrode Material on Hole Drilling in Micro-EDM. *Procedia CIRP*, 42(Isem Xviii), 516–520.
- Gautam, G. D., & Pandey, A. K. (2018). Pulsed Nd:YAG laser beam drilling: A review. *Optics and Laser Technology*, 100, 183–215.
- Gower, M. C. (2000). Industrial applications of pulsed laser micromachining. *Conference on Lasers and Electro-Optics Europe - Technical Digest*, 7(2), 247.
- Gujrathi, A., Dongre, S., & Nandan, H. (2021). A Review of Laser Micromachining. *Article in International Journal of Engineering Science Advanced Computing and Bio-Technology*, August.
- Hamad, A. H. (2016). Effects of Different Laser Pulse Regimes (Nanosecond, Picosecond and Femtosecond) on the Ablation of Materials for Production of Nanoparticles in Liquid Solution. *High Energy and Short Pulse Lasers*.
- Harfield, A. (2012). *Empirical Modelling for constructionist learning in a Thai secondary school mathematics class*. December, 13–14.
- Hasan, M., Zhao, J., & Jiang, Z. (2017). A review of modern advancements in micro drilling techniques. *Journal of Manufacturing Processes*, 29, 343–375.
- Hendow, S. T., & Shakir, S. A. (2010). Structuring materials with nanosecond laser pulses. *Optics Express*, 18(10), 10188.
- Ho, W. H., Tsai, J. T., Lin, B. T., & Chou, J. H. (2009). Adaptive network-based fuzzy inference system for prediction of surface roughness in end milling process using hybrid Taguchi-genetic learning algorithm. *Expert Systems with Applications*, 36(2 PART 2), 3216–3222.
- Hocheng, H., Tsai, H. Y., Jadhav, U. U., Wang, K. Y., & Lin, T. C. (2014). Laser Surface Patterning. In *Comprehensive Materials Processing* (Vol. 9). Elsevier.
- Hossain, A., Hossain, A., Nukman, Y., Hassan, M. A., Harizam, M. Z., Sifullah, A. M., & Parandoush, P. (2016). A Fuzzy Logic-Based Prediction Model for Kerf Width in Laser Beam Machining. *Materials and Manufacturing Processes*, 31(5), 679–684.
- Huang, Y., Han, R., Zhang, H., & Zhao, C. (2022). The effect of laser power and scanning speed on forming structure in selective laser melting process. *Materials Research Express*, 9(5).
- Jabbareh, M. A., & Asadi, H. (2013). Numerical Simulation of Heat Affected Zone Microstructure During Laser Surface Melting. *Journal of Advanced Materials and Processing*, 1(3), 27–34.

- Karaboga, D., & Kaya, E. (2019). Adaptive network based fuzzy inference system (ANFIS) training approaches: a comprehensive survey. *Artificial Intelligence Review*, 52(4), 2263–2293.
- Kibria Bhattacharyya J Paulo Davim Editors, G. B. (2017). *Materials Forming, Machining and Tribology Non-traditional Micromachining Processes Fundamentals and Applications*.
- Kim, S., Kim, B. H., Chung, D. K., Shin, H. S., & Chu, C. N. (2010). Hybrid micromachining using a nanosecond pulsed laser and micro EDM. *Journal of Micromechanics and Microengineering*, 20(1).
- Koç, M., & Özel, T. (2011). Fundamentals of Micro-Manufacturing. *Micro-Manufacturing: Design and Manufacturing of Micro-Products*, May 2021, 1–23.
- Kumar, Er. A. (2022). Laser Beam Machining: Definition, Construction, Working Principle, Advantages, Application Title. *The Mechanical Engineering.Com*, 1(1), 1–10.
- Kumar, N., Mandal, N., & Das, A. K. (2020). Micro-machining through electrochemical discharge processes: a review. *Materials and Manufacturing Processes*, 35(4), 363–404.
- Kumar, R., Chohan, J. S., Goyal, R., & Chauhan, P. (2020). Impact of process parameters of resistance spot welding on mechanical properties and micro hardness of stainless steel 304 weldments. *International Journal of Structural Integrity*, 12(3), 366–377.
- Lauwers, B., Klocke, F., Klink, A., Tekkaya, A. E., Neugebauer, R., & McIntosh, D. (2014). Hybrid processes in manufacturing. *CIRP Annals - Manufacturing Technology*, 63(2), 561–583.
- Li, L., Diver, C., Atkinson, J., Giedl-Wagner, R., & Helml, H. J. (2006). Sequential laser and EDM micro-drilling for next generation fuel injection nozzle manufacture. *CIRP Annals - Manufacturing Technology*, 55(1), 179–182.
- Li, X., & Guan, Y. (2020). Theoretical fundamentals of short pulse laser-metal interaction: A review. *Nanotechnology and Precision Engineering*, 3(3), 105–125.
- Li, Y., Hou, W., Xu, J., & Yu, H. (2016). An investigation on drilling micro holes in different processes using micro-EDM. *2016 IEEE International Conference on Mechatronics and Automation, IEEE ICMA 2016*, 1283–1288.
- Liu, K., Lauwers, B., & Reynaerts, D. (2010). Process capabilities of Micro-EDM and its applications. *International Journal of Advanced Manufacturing Technology*, 47(1–4), 11–19.

- M Azadi Moghaddam, F. K. (2020). Modeling and optimization of the electrical discharge machining process based on a combined artificial neural network and particle swarm optimization algorithm. *Scientia Iranica*, 27(3), 1206–1217.
- Mahardika, M., Tsujimoto, T., & Mitsui, K. (2008). A new approach on the determination of ease of machining by EDM processes. *International Journal of Machine Tools and Manufacture*, 48(7–8), 746–760.
- Mahendran, S., Devarajan, R., Nagarajan, T., & Majdi, A. (2010). *A Review of Micro-EDM. II*.
- Maity, K. P., & Choubey, M. (2019). A review on vibration assisted EDM, micro-EDM and WEDM. *Surface Review and Letters*, 26(5).
- Masuzawa, T., Fujino, M., Kobayashi, K., Suzuki, T., & Kinoshita, N. (1985). Wire Electro-Discharge Grinding for Micro-Machining. *CIRP Annals - Manufacturing Technology*, 34(1), 431–434.
- Masuzawa, T., Klocke, F., Hochschule Aachen, T., J-P Kruth, G., Universiteit Leuven, K., McGeough, B. J., & Allen, D. (1997). *Keynote Papers method Keynote Papers injection EDM etching molding turning electro-coining milling forming electro-punching forming grinding LBM I BM Presented at the Scientific Technical Committee Paper Discussion Sessions Three-Dimensional Micromachinin*.
- Miller, P. R., Aggarwal, R., Doraiswamy, A., Lin, Y. J., Lee, Y. S., & Narayan, R. J. (2009). Laser micromachining for biomedical applications. *Jom*, 61(9), 35–40.
- Mishra, S., & Yadava, V. (2015). Laser Beam MicroMachining (LBMM) - A review. *Optics and Lasers in Engineering*, 73, 89–122.
- Mohd Adnan, M. R. H., Sarkheyli, A., Mohd Zain, A., & Haron, H. (2015). Fuzzy logic for modeling machining process: a review. *Artificial Intelligence Review*, 43(3), 345–379.
- Montgomery, D. (2009). *Design_Mont_Part1.Pdf* (p. 299).
- Moradi, M., & KaramiMoghadam, M. (2019). High power diode laser surface hardening of AISI 4130; statistical modelling and optimization. *Optics and Laser Technology*, 111(September 2018), 554–570.
- Mullen, K., & Hultquist, R. A. (2017). Introduction to Statistics. *Biometrics*, 26(3), 590.
- N, S., Hiremath, S. S., & J, S. (2014). Prediction of Material Removal Rate using Regression Analysis and Artificial Neural Network of ECDM Process. *International Journal of Recent Advances in Mechanical Engineering*, 3(2), 69–81.

- Nadda, R., & Nirala, C. K. (2020). Thermal modeling of single discharge in prospect of tool wear compensation in μ EDM. *International Journal of Advanced Manufacturing Technology*, 107(11–12), 4573–4595.
- Negarestani, R., & Li, L. (2012a). Laser machining of fibre-reinforced polymeric composite materials. In *Machining Technology for Composite Materials* (pp. 288–308). Elsevier.
- Negarestani, R., & Li, L. (2012b). Laser machining of fibre-reinforced polymeric composite materials. In *Machining Technology for Composite Materials* (pp. 288–308). Elsevier.
- Noor, W. I., Saleh, T., Rashid, M. A. N., Mohd Ibrahim, A., & Ali, M. S. M. (2021a). Dual-stage artificial neural network (ANN) model for sequential LBMM- μ EDM-based micro-drilling. *International Journal of Advanced Manufacturing Technology*, 117(11–12), 3343–3365.
- Noor, W. I., Saleh, T., Rashid, M. A. N., Mohd Ibrahim, A., & Ali, M. S. M. (2021b). Dual-stage artificial neural network (ANN) model for sequential LBMM- μ EDM-based micro-drilling. *The International Journal of Advanced Manufacturing Technology* 2021 117:11, 117(11), 3343–3365.
- Norman, S. (2010). Pulsed Fiber Lasers for Precision Marking, Engraving and Micromachining. *EPMT Conference*, 1–29.
- Ozgedik, A., & Cogun, C. (2006). An experimental investigation of tool wear in electric discharge machining. *International Journal of Advanced Manufacturing Technology*, 27(5–6), 488–500.
- P. M, A., & D, C. (2020). Prediction and analysis of process failures by ANN classification during wire-EDM of Inconel 718. *Advances in Manufacturing*, 8(4), 519–536.
- Pandey, A. K., & Dubey, A. K. (2012). Taguchi based fuzzy logic optimization of multiple quality characteristics in laser cutting of Duralumin sheet. *Optics and Lasers in Engineering*, 50(3), 328–335.
- Pandey, A. K., & Dubey, A. K. (2013). Fuzzy expert system for prediction of kerf qualities in pulsed laser cutting of titanium alloy sheet. *Machining Science and Technology*, 17(4), 545–574.
- Parandoush, P., & Hossain, A. (2014). A review of modeling and simulation of laser beam machining. *International Journal of Machine Tools and Manufacture*, 85, 135–145.
- Paul, L., Babu, J., & Paulo Davim, J. (2020). *Non-conventional Micro-machining Processes*.

- Pike, E. R., & McNally, B. (1997). Theory and design of photon correlation and light-scattering experiments. In *Applied Optics* (Vol. 36, Issue 30).
- Pradhan, M. K. (2010). Modeling and Simulation of Thermal Stress in Electrical Discharge Machining Process. *4th International Conference on Advances in Mechanical Engineering, S.V.N.I.T, Surat, India*, 360–364.
- Pradhan, S., Dash, P. B., Kumari, K., & Dhupal, D. (2021). Study of micro machining characteristics by Nd-YAG Laser on NiTiNol shape memory alloy. *Advances in Materials and Processing Technologies*, 00(00), 1–15.
- Prakash, S., & Kumar, S. (2015). Fabrication of microchannels: A review. *Proceedings of the Institution of Mechanical Engineers, Part B: Journal of Engineering Manufacture*, 229(8), 1273–1288.
- Raj, D., Reddy, B. V. R., Maity, S. R., & Pandey, K. M. (2019). Laser beam micromachining of metals: A review. *Materials Today: Proceedings*, 18, 98–103.
- Rajesh, P., Nagaraju, U., Gowd, G. H., & Vardhan, T. V. (2017). Experimental and parametric studies of Nd:YAG laser drilling on austenitic stainless steel. *International Journal of Advanced Manufacturing Technology*, 93(1–4), 65–71.
- Rajurkar, K. P., Levy, G., Malshe, A., Sundaram, M. M., McGeough, J., Hu, X., Resnick, R., & DeSilva, A. (2006). Micro and nano machining by electro-physical and chemical processes. *CIRP Annals - Manufacturing Technology*, 55(2), 643–666.
- Rajurkar, K. P., Sundaram, M. M., & Malshe, A. P. (2013). Review of electrochemical and electrodischarge machining. *Procedia CIRP*, 6, 13–26.
- Rao, S., Brevern, P., El-Tayeb, N. S. M., & Vengкатesh, V. C. (2009). GUI Based Mamdani Fuzzy Inference System Modeling To Predict Surface Roughness in Laser Machining. *International Journal of Electrical & Computer Sciences IJECS-IJENS*, 9(9), 37–43.
- Rashid, M. A. N., Saleh, T., Noor, W. I., & Ali, M. S. M. (2021a). Effect of laser parameters on sequential laser beam micromachining and micro electro-discharge machining. *The International Journal of Advanced Manufacturing Technology*.
- Rashid, M. A. N., Saleh, T., Noor, W. I., & Ali, M. S. M. (2021b). Effect of laser parameters on sequential laser beam micromachining and micro electro-discharge machining. *International Journal of Advanced Manufacturing Technology*, 114(3–4), 709–723.
- Richa Agrawal, C. (Peggy) W. (2016). Laser Beam Machining Title. *Springer Netherlands*, 2(978), 1–15.

- Richard, J., & Giandomenico, N. (2018). Electrode Profile Prediction and Wear Compensation in EDM-milling and Micro-EDM-Milling. *Procedia CIRP*, 68(April), 819–824.
- R.P. Patel, D. M. P. (2014). Grey relational analysis based optimization of laser cutting process parameters for aluminum alloy—a review. *Int. J. Eng. Res. Technol*, 3(3), ISSN: 2278-0181.
- Russbueltd, P., Mans, T., Hoffmann, D., & Schippel, S. (2016). High-average power ultrafast YB: Innoslab-amplifier. In *Springer Series in Optical Sciences* (Vol. 195).
- Schaeffer, R. D., & Kardos, G. (2008, May). *Post-Laser Processing Cleaning Techniques / Industrial Laser Solutions*.
- Schmid, B., Schindelin, J., Cardona, A., Longair, M., & Heisenberg, M. (2010). A high-level 3D visualization API for Java and ImageJ. *BMC Bioinformatics*, 11.
- Schneider, C. A., Rasband, W. S., & Eliceiri, K. W. (2012). NIH Image to ImageJ: 25 years of image analysis. *Nature Methods*, 9(7), 671–675.
- Sen, A., Doloi, B., & Bhattacharyya, B. (2014). *EXPERIMENTAL STUDIES ON FIBRE LASER MICRO-MACHINING OF Ti-6Al-4V*. *Aimtdr*, 1–7.
- Shalahim, N. S. M., Mon, T. T., Ismail, M. F., Rashid, M. F. F., & Rejab, M. R. M. (2010). Finite element simulation of laser-micromachining. *Proceedings of the International MultiConference of Engineers and Computer Scientists 2010, IMECS 2010, III*, 2221–2223.
- Shao, B., & Rajurkar, K. P. (2015). Modelling of the crater formation in micro-EDM. *Procedia CIRP*, 33, 376–381.
- Sharma, A., & Yadava, V. (2018). Experimental analysis of Nd-YAG laser cutting of sheet materials – A review. *Optics and Laser Technology*, 98, 264–280.
- Shivakoti, I., Kibria, G., Pradhan, P. M., Pradhan, B. B., & Sharma, A. (2019). ANFIS based prediction and parametric analysis during turning operation of stainless steel 202. *Materials and Manufacturing Processes*, 34(1), 112–121.
- Shrivastava, P. K., & Dubey, A. K. (2014). Electrical discharge machining-based hybrid machining processes: A review. *Proceedings of the Institution of Mechanical Engineers, Part B: Journal of Engineering Manufacture*, 228(6), 799–825.
- Singh, A. K., Patowari, P. K., & Deshpande, N. V. (2017). Effect of tool wear on microrods fabrication using reverse μ EDM. *Materials and Manufacturing Processes*, 32(3), 286–293.

- Suganthi, X. H., Natarajan, U., Sathiyamurthy, S., & Chidambaram, K. (2013). Prediction of quality responses in micro-EDM process using an adaptive neuro-fuzzy inference system (ANFIS) model. *International Journal of Advanced Manufacturing Technology*, 68(1–4), 339–347.
- Sun, A., Chang, Y., & Liu, H. (2018). Metal micro-hole formation without recast layer by laser machining and electrochemical machining. *Optik*, 171, 694–705.
- Wang, H., Li, Y., Chen, X., Jia, Y., Chi, G., Wang, Y., & Wang, Z. (2021). Micro-milling/micro-EDM combined processing technology for complex microarray cavity fabrication. *International Journal of Advanced Manufacturing Technology*, 113(3–4), 1057–1071.
- Williams, E. (2014). *Experimental and Theoretical Investigations of Nanosecond Fibre Laser Micromachining*.
- Wilson, P., & Mantooth, H. A. (2013). Chapter 11—Statistical and stochastic modeling.No Title. *Model-Based Engineering for Complex Electronic Systems*. Newnes, Oxford, 369–400.
- Yeo, S. H., Aligiri, E., Tan, P. C., & Zarepour, H. (2009). A new pulse discriminating system for Micro-EDM. *Materials and Manufacturing Processes*, 24(12), 1297–1305.
- Zeng, Z., Wang, Y., Wang, Z., Shan, D., & He, X. (2012). A study of micro-EDM and micro-ECM combined milling for 3D metallic micro-structures. *Precision Engineering*, 36(3), 500–509.
- Zhang, K., Lv, G., Guo, S., Chen, D., Liu, Y., & Feng, W. (2020). Evaluation of subsurface defects in metallic structures using laser ultrasonic technique and genetic algorithm-back propagation neural network. *NDT and E International*, 116(July), 102339.
- Zhang, L., Tong, H., & Li, Y. (2015). Precision machining of micro tool electrodes in micro EDM for drilling array micro holes. *Precision Engineering*, 39, 100–106.
- Zhu, Z., Dhokia, V. G., Nassehi, A., & Newman, S. T. (2013). A review of hybrid manufacturing processes - State of the art and future perspectives. *International Journal of Computer Integrated Manufacturing*, 26(7), 596–615.

PUBLICATIONS

1. **Rashid, M. A. N.**, Saleh, T., Noor, W. I., & Ali, M. S. M. (2021). Effect of laser parameters on sequential laser beam micromachining and micro electro-discharge machining. *The International Journal of Advanced Manufacturing Technology*, 114(3), 709-723. <https://doi.org/10.1007/s00170-021-06908-8> (ISI: Q1)
2. Noor, W. I., Saleh, T., **Rashid, M. A. N.**, Mohd Ibrahim, A., & Ali, M. S. M. (2021). Dual-stage artificial neural network (ANN) model for sequential LBMM- μ EDM-based micro-drilling. *The International Journal of Advanced Manufacturing Technology*, 117(11), 3343-3365. <https://doi.org/10.1007/s00170-021-07910-w> (ISI: Q1)
3. Noor, W., Saleh, T., **Rashid, M. A. N.**, & Ibrahim, A. M. (2022, June). Effect of process parameters on the laser micro drilling performance of stainless steel, aluminium and copper. In *IOP Conference Series: Materials Science and Engineering* (Vol. 1244, No. 1, p. 012020). IOP Publishing. <https://doi:10.1088/1757-899X/1244/1/012020>.
4. **RASHID, M. A. N.**, Saleh, T., Hamid, S. A., & RASHID, M. M. (2023, October). Analysis And Modelling of Laser-Micro Edm-Based Hybrid Micro Milling On Stainless Steel (Sus304) Using Box Behnken Design. In *IIUM Engineering Congress Proceedings* (Vol. 1, No. 1, pp. 14-18). <https://doi.org/10.31436/iiumecp.v1i1.2996>

APPENDIX A: DATASET FIRST-STAGE EXPERIMENT USED IN SECTION 4.2 AND 4.3

Table A.1: Dataset created from the experiments conducted during the hybrid LBMM- μ EDM micro drilling with constant EDM parameters.

Hole No.	LBMM input parameters			LBMM target parameters/ μ EDM input parameters					μ EDM target parameters		
	Loop Count (nos)	Scanning Speed (mm/s)	Power (W)	Pulse Repetition Rate (kHz)	Entry Area (mm ²)	Exit Area (mm ²)	HAZ Area (mm ²)	Recast Area (mm ²)	μ EDM Machining Time (mins)	Short Circuit/Arcing Count (nos)	Tool Wear (μ m)
1	75	50	6.4	5	0.073	0.036	0.303	0.023	18.93	87	14
2	75	50	6.4	10	0.074	0.035	0.218	0.018	18.17	49	11
3	75	50	6.4	15	0.074	0.034	0.219	0.022	18.92	41	7
4	75	50	6.4	20	0.072	0.036	0.479	0.017	17.83	47	13
5	75	50	9.4	5	0.076	0.045	0.589	0.027	15.97	46	7
6	75	50	9.4	10	0.078	0.045	0.623	0.045	17.07	39	8
7	75	50	9.4	15	0.078	0.044	0.66	0.04	15.62	43	4
8	75	50	9.4	20	0.078	0.044	0.605	0.045	17.7	75	7
9	75	50	12.5	5	0.08	0.049	0.571	0.028	17.03	39	8
10	75	50	12.5	10	0.077	0.049	0.54	0.029	14.62	41	3
11	75	50	12.5	15	0.079	0.05	0.486	0.03	16.83	43	4

12	75	50	12.5	20	0.08	0.049	0.54 5	0.038	16.15	44	5
13	75	50	15.5	5	0.08 6	0.052	0.50 1	0.035	14.45	32	4
14	75	50	15.5	10	0.08 5	0.053	0.43 1	0.036	14.7	37	3
15	75	50	15.5	15	0.08 4	0.053	0.47 6	0.026	15.03	33	5
16	75	50	15.5	20	0.08 5	0.053	0.48 9	0.028	15.88	46	7
17	75	500	6.4	5	0.06 8	0	0.21 7	0.011	49.25	100 7	52
18	75	500	6.4	10	0.06 3	0	0.24 8	0.01	34.53	457	47
19	75	500	6.4	15	0.05 7	0	0.26 1	0.017	49.52	977	48
20	75	500	6.4	20	0.05 9	6.13E -05	0.24 7	0.014	64.87	132 7	52
21	75	500	9.4	5	0.06 5	0.000 405	0.51 7	0.026	32.95	401	33
22	75	500	9.4	10	0.06 4	0.001 65	0.44 2	0.028	25.52	177	13
23	75	500	9.4	15	0.06 7	0.001 22	0.52 5	0.016	54.5	106 1	37
24	75	500	9.4	20	0.07	1.69E -05	0.47 7	0.016	48.23	979	42
25	75	500	12.5	5	0.07 2	0.014	0.72 5	0.025	23.28	147	15
26	75	500	12.5	10	0.06 1	0.017 8330 1	0.65	0.037	22.97	141	6
27	75	500	12.5	15	0.06 3	0.021	0.61 7	0.036	19.97	105	7
28	75	500	12.5	20	0.06 7	0.02	0.66 4	0.03	19.93	79	8
29	75	500	15.5	5	0.06 9	0.042	0.69 1	0.03	16.32	33	4
30	75	500	15.5	10	0.07	0.04	0.73 6	0.025	17.48	78	5
31	75	500	15.5	15	0.06 8	0.041	0.74 1	0.014	16.95	50	2
32	75	500	15.5	20	0.07 8	0.042	0.65 8	0.044	17.78	64	3
33	75	950	6.4	5	0.06	0	0.24 6	0.014	55.07	122 3	55

34	75	950	6.4	10	0.06 1	0	0.25 2	0.015	57.92	123 5	53
35	75	950	6.4	15	0.06 4	0	0.21 6	0.016	46.07	902	49
36	75	950	6.4	20	0.05 7	0	0.25 4	0.015	54.25	987	39
37	75	950	9.4	5	0.06 7	0.001 01	0.37 4	0.019	40.15	875	24
38	75	950	9.4	10	0.06 4	0.000 734	0.39 8	0.021	48.07	966	41
39	75	950	9.4	15	0.06 7	0.000 902	0.36 9	0.023	51.17	102 0	44
40	75	950	9.4	20	0.06 6	0.000 471	0.39	0.02	53.57	109 1	47
41	75	950	12.5	5	0.06 3	0.003 49	0.55 7	0.024	28.17	506	21
42	75	950	12.5	10	0.07	0.005 4900 2	0.53 8	0.028	27.93	410	12
43	75	950	12.5	15	0.06 7	0.004 4626	0.53 1	0.026	24.93	187	14
44	75	950	12.5	20	0.06 4	0.005 5469 02	0.52 1	0.022	24.8	178	17
45	75	950	15.5	5	0.07 3	0.013 9098 2	0.66 4	0.048	17.77	107	10
46	75	950	15.5	10	0.07 1	0.014 6628 4	0.67 6	0.036	17.52	64	3
47	75	950	15.5	15	0.07 6	0.019	0.67	0.053	17.92	51	3
48	75	950	15.5	20	0.07 4	0.015 1835	0.62 1	0.045	18.9	69	5
49	75	1400	6.4	5	0.06 7	0	0.23 9	0.013	50.33	986	39
50	75	1400	6.4	10	0.06 4	0	0.19 3	0.012	56.57	110 7	44
51	75	1400	6.4	15	0.06 2	0	0.22 6	0.012	54.67	122 6	88
52	75	1400	6.4	20	0.06 5	0	0.20 9	0.014	47.43	867	60
53	75	1400	9.4	5	0.06 8	0	0.38 3	0.016	47.23	106 4	31
54	75	1400	9.4	10	0.06 8	0	0.30 5	0.014	36.1	781	28

55	75	1400	9.4	15	0.064	0	0.357	0.014	38.67	787	27
56	75	1400	9.4	20	0.061	0	0.357	0.013	46.7	988	51
57	75	1400	12.5	5	0.069	0.00259842	0.502	0.013	40.37	823	38
58	75	1400	12.5	10	0.07	0.00205	0.466	0.017	38.28	771	33
59	75	1400	12.5	15	0.067	0.00379302	0.485	0.014	32.08	635	31
60	75	1400	12.5	20	0.067	0.00103	0.435	0.018	37.68	793	49
61	75	1400	15.5	5	0.068	0.00942211	0.629	0.023	22	97	8
62	75	1400	15.5	10	0.075	0.013	0.627	0.038	16.32	57	10
63	75	1400	15.5	15	0.07	0.01044373	0.594	0.032	16.6	61	11
64	75	1400	15.5	20	0.067	0.010813	0.685	0.03	16.12	67	13
65	25	1400	6.4	10	0.06	0	0.227	0.016	55.05	1155	68
66	50	1400	6.4	10	0.063	0	0.208	0.017	57.85	1104	74
67	75	1400	6.4	10	0.068	0	0.236	0.016	47.43	1012	69
68	75	1400	6.4	10	0.068	0	0.263	0.015	63.48	1276	81
69	100	1400	6.4	10	0.064	0	0.265	0.016	62.52	1488	86
70	25	50	15.5	10	0.087	0.047	0.392	0.046	18.95	89	7
71	50	50	15.5	10	0.082	0.051	0.463	0.045	16.67	37	2
72	75	50	15.5	10	0.089	0.053	0.408	0.045	17.83	43	4
73	75	50	15.5	10	0.081	0.053	0.467	0.041	17.78	77	5
74	100	50	15.5	10	0.081	0.053	0.408	0.042	19.17	83	5
75	25	400	10.7	10	0.066	0.00021015	0.355	0.019	39.45	689	31

76	25	400	11.3	10	0.067	0.00027	0.375	0.021	40.25	736	38
77	25	400	11.9	10	0.068	0.00040441	0.405	0.025	36.6	580	28
78	25	600	10.7	10	0.063	0	0.317	0.021	40.45	671	33
79	25	600	11.9	10	0.062	6.22E-05	0.357	0.022	39.83	721	36
80	25	600	13.1	10	0.064	0.00025506	0.422	0.021	45.15	782	33
81	25	700	12.5	10	0.063	0	0.369	0.025	52.18	897	49
82	25	700	13.1	10	0.064	0	0.386	0.022	49.08	816	42
83	25	700	13.7	10	0.064	0	0.427	0.022	59.17	1172	59
84	25	900	10.7	10	0.06	2.40E-05	0.343	0.019	60.33	1241	54
85	25	900	11.3	10	0.06	0	0.326	0.02	43.02	758	35
86	25	900	11.9	10	0.061	8.80E-05	0.349	0.02	49.35	981	41
87	25	1400	13.1	10	0.062	0.000471	0.401	0.019	48.85	966	43
88	25	1400	14.3	10	0.064	0.00079012	0.426	0.022	45.05	807	44
89	25	1400	14.9	10	0.065	0.0010562	0.469	0.023	43.38	765	39
90	50	400	10.7	10	0.061	0.00073279	0.434	0.019	37.65	691	28
91	50	400	11.3	10	0.067	0.00197965	0.448	0.029	33.97	511	25
92	50	400	11.9	10	0.06	0.004206834	0.523	0.019	26.2	251	18
93	50	600	10.7	10	0.064	0.00050653	0.391	0.023	62.02	1156	52
94	50	600	11.9	10	0.064	0.000686951	0.398	0.024	26.07	211	17

95	50	600	13.1	10	0.063	0.001507734	0.504	0.021	25.22	188	13
96	50	700	12.5	10	0.063	0.001151301	0.487	0.025	38.77	587	27
97	50	700	13.1	10	0.065	0.00184682	0.462	0.018	26.02	222	16
98	50	700	13.7	10	0.068	0.001691439	0.514	0.026	27.73	230	14
99	50	900	10.7	10	0.063	0.000268868	0.366	0.018	44.97	788	39
100	50	900	11.3	10	0.064	0.000273766	0.356	0.022	52.18	941	53
101	50	900	11.9	10	0.063	0.00046654	0.394	0.021	51.28	1022	47
102	50	1400	13.1	10	0.062	0.001237941	0.437	0.022	44.8	831	37
103	50	1400	14.3	10	0.065	0.00206935	0.499	0.021	34.53	593	29
104	50	1400	14.9	10	0.066	0.00278	0.518	0.02	23.88	223	16
105	100	400	10.7	10	0.059	0.01907776	0.711	0.016	24.4	167	14
106	100	400	11.3	10	0.059	0.021	0.465	0.022	14.47	59	4
107	100	400	11.9	10	0.068	0.03	0.455	0.022	15.63	62	7
108	100	600	10.7	10	0.059	0.0081604	0.557	0.022	17.97	119	5
109	100	600	11.9	10	0.057	0.0110431	0.545	0.018	16.33	105	6
110	100	600	13.1	10	0.059	0.0194692	0.617	0.015	18.27	87	5
111	100	700	12.5	10	0.058	0.011267956	0.551	0.024	28.62	337	21
112	100	700	13.1	10	0.065	0.0143772	0.611	0.024	16.9	59	5

						7					
113	100	700	13.7	10	0.064	0.019186627	0.657	0.032	33.75	491	23
114	100	900	10.7	10	0.064	0.000954463	0.47	0.022	24.75	233	18
115	100	900	11.3	10	0.063	0.00162465	0.492	0.019	37.42	624	24
116	100	900	11.9	10	0.062	0.002178024	0.544	0.022	27.12	267	15
117	100	1400	13.1	10	0.063	0.00265903	0.542	0.023	31.07	527	16
118	100	1400	14.3	10	0.064	0.00416066	0.582	0.023	25.53	257	14
119	100	1400	14.9	10	0.066	0.00790337	0.639	0.026	24.13	184	15

APPENDIX B: DATASET SECOND-STAGE EXPERIMENT USED IN SECTION 4.4

Table A.2: Dataset created from the experiments conducted during the hybrid LBMM- μ EDM Drilling with Variable EDM Parameter

Hole No.	LBMM-uEDM input parameters						LBMM output parameters			μ EDM target parameters		
	Loop Count (nos)	Scanning Speed (mm/s)	Power (W)	Pulse Repetition Rate (kHz)	Discharge Energy (nJ)	EDM speed (μ m/sec)	Volume removed (mm^3)	HAZ Area (mm^2)	Recast Area (mm^2)	μ EDM Machining Time (mins)	Short Circuit/ Arcing Count (nos)	Tool Wear (μ m)
1	75	1400	6.4	20	605000	10	0.003006533	0.239	0.004	776.5	23	29
2	75	1400	6.4	5	320000	10	0.003157095	0.224	0.002	838.5	34	31
3	75	1400	15.5	20	605000	3	0.00767702	0.477	0.004	831.5	2	20
4	75	1400	15.5	5	605000	3	0.006686593	0.45	0.009	849.5	3	21
5	75	725	11	12.5	4512.5	6.5	0.006399907	0.356	0.01	1602.87	311	19
6	75	1400	6.4	20	320000	3	0.003247099	0.224	0.003	791.5	3	22
7	75	725	8.7	12.5	4512.5	6.5	0.004732751	0.316	0.008	2110.87	667	26
8	75	725	11	12.5	4512.5	6.5	0.006122056	0.392	0.005	1901.87	589	23
9	75	50	15.5	5	60.5	3	0.032001759	0.44	0.023	1837.81	611	9
10	75	50	15.5	5	320000	10	0.024395855	0.387	0.023	931.81	3	21
11	75	50	6.4	5	32	10	0.024407595	0.409	0.004	2521.81	827	12
12	75	50	15.5	5	60.5	10	0.031157148	0.423	0.032	2375.81	781	11

13	75	50	15.5	20	605000	10	0.031373 323	0.439	0.024	516.81	6	16
14	75	50	6.4	5	605000	10	0.026088 964	0.464	0.012	583.81	3	23
15	75	50	15.5	20	605000	3	0.031966 157	0.447	0.02	877.81	3	20
16	75	725	13.23	12.5	4512.5	6.5	0.005695 416	0.452	0.003	1427.87	107	12
17	75	1400	15.5	5	32	3	0.006812 039	0.479	0.006	3914.5	1376	41
18	75	725	11	12.5	4512.5	6.5	0.005659 09	0.374	0.008	1814.87	504	26
19	75	50	6.4	20	320000	10	0.025186 688	0.449	0.009	903.81	16	21
20	75	1400	6.4	5	60.5	3	0.003240 284	0.221	0.003	3941.5	1231	13
21	75	725	11	12.5	3828.1 25	6.5	0.006777 124	0.372	0.008	2056.87	533	26
22	75	725	11	12.5	4512.5	6.5	0.004325 694	0.4	0.002872 7	1972.87	491	21
23	75	50	6.4	20	32	10	0.025576 016	0.459	0.007	4061.81	1384	15
24	75	1400	15.5	5	605000	10	0.004914 559	0.509	0.007	642.5	1	18
25	75	725	11	12.5	4512.5	6.5	0.004494 093	0.391	0.004	1733.87	563	23
26	75	387.5	11	12.5	4512.5	6.5	0.016778 292	0.424	0.008	1084.45	87	7
27	75	725	11	12.5	4512.5	6.5	0.004187 553	0.37	0.004	1400.87	341	13
28	75	725	11	12.5	45125	6.5	0.003801 182	0.354	0.004	861.87	47	19
29	75	725	11	8.75	4512.5	6.5	0.003784 449	0.379	0.005	2168.87	534	29
30	75	725	11	16.25	4512.5	6.5	0.004125 375	0.37	0.005	2086.87	476	22

31	75	725	11	12.5	4512.5	8.25	0.004224 455	0.386	0.005	2100.87	653	26
32	75	1400	6.4	5	605000	10	0.002107 243	0.228	0.002	599.5	2	19
33	75	1400	6.4	5	32	10	0.000727 828	0.228	0.002	7810.5	2684	16
34	75	725	11	12.5	4512.5	6.5	0.003805 643	0.37	0.008	2251.87	587	31
35	75	50	6.4	20	60.5	10	0.025703 501	0.463	0.006	3312.81	1187	12
36	75	1400	6.4	5	320000	3	0.002788 91	0.244	0.001	870.5	7	22
37	75	1400	15.5	20	60.5	10	0.005320 032	0.468	0.003	5055.5	1673	18
38	75	50	15.5	5	32	10	0.031283 274	0.38	0.015	4404.81	1491	13
39	75	1400	6.4	5	32	3	0.002701 387	0.236	0.002	9748.5	3981	24
40	75	50	6.4	5	32	3	0.025190 555	0.361	0.006	4756.81	1577	16
41	75	1400	15.5	20	32	3	0.007884 011	0.379	0.005	6281.5	2289	17
42	75	1400	15.5	20	32	10	0.007426 965	0.374	0.002	5418.5	1959	19
43	75	50	6.4	5	320000	3	0.025460 416	0.36	0.012	738.81	5	18
44	75	1400	15.5	5	320000	3	0.007520 275	0.338	0.011	1326.5	9	27
45	75	50	15.5	20	60.5	3	0.031189 779	0.361	0.033	3710.81	1380	17
46	75	50	6.4	20	320000	3	0.026850 199	0.366	0.006	818.81	4	18
47	75	50	6.4	20	32	3	0.027100 968	0.314	0.003	2912.81	945	5
48	75	1400	15.5	20	60.5	3	0.007894 187	0.424	0.005	2573.5	841	8

49	75	50	15.5	5	605000	10	0.029988 91	0.334	0.028	692.81	5	11
50	75	50	6.4	5	60.5	10	0.026193 798	0.348	0.015	3638.81	1362	13
51	75	50	6.4	20	605000	10	0.027092 35	0.327	0.016	734.81	10	17
52	75	1400	15.5	20	320000	10	0.008525 444	0.264	0.009	975.5	17	24
53	75	725	11	12.5	4512.5	6.5	0.005744 009	0.254	0.004	2435.87	786	31
54	75	1400	6.4	20	32	3	0.003133 525	0.128	0.003	8315.5	3398	16
55	75	50	15.5	20	60.5	10	0.030493 527	0.343	0.014	2135.81	688	8
56	75	50	6.4	5	320000	10	0.024920 917	0.235	0.005	961.81	13	17
57	75	1400	15.5	5	60.5	3	0.008537 747	0.34	0.012	5350.5	1851	17
58	75	50	15.5	5	32	3	0.029956 058	0.289	0.023	4096.81	1327	11
59	75	1400	6.4	20	320000	10	0.002912 424	0.136	0.003	1310.5	12	28
60	75	1400	15.5	20	320000	3	0.009571 608	0.27	0.011	1534.5	13	13
61	75	1400	15.5	5	60.5	10	0.009955 243	0.277	0.008	3783.5	1279	15
62	75	1400	6.4	20	60.5	3	0.002381 445	0.133	0.002	5472.5	1876	17
63	75	1400	6.4	5	60.5	10	0.002555 999	0.105	0.003	4265.5	1421	13
64	75	50	15.5	5	320000	3	0.029890 106	0.301	0.023	814.81	11	19
65	75	725	11	12.5	4512.5	6.5	0.007276 511	0.18	0.006	1251.87	156	11

66	75	50	6.4	20	60.5	3	0.024541 304	0.174	0.008	2288.81	731	7
67	75	1400	6.4	5	605000	3	0.003044 012	0.116	0.003	1153.5	17	21
68	75	50	15.5	20	32	10	0.029535 677	0.266	0.026	4158.81	1326	14
					60.5	10	0.003246 534	0.171	0.003	6768.5	2498	17
69	75	1400	6.4	20	605000	3	0.024267 759	0.196	0.01	980.81	11	19
70	75	50	6.4	5	32	10	0.008061 082	0.366	0.012	10119.5	3631	21
71	75	1400	15.5	5	605000	10	0.008094 203	0.389	0.01	806.5	5	12
72	75	1400	15.5	20	320000	10	0.008192 221	0.375	0.012	885.5	9	7
73	75	1400	15.5	5	4512.5	6.5	0.005393 862	0.328	0.005	2192.63	688	27
74	75	1062.5	11	12.5	32	10	0.003009 605	0.197	0.003	8683.5	3459	17
75	75	1400	6.4	20	605000	3	0.031625 801	0.309	0.022	764.81	3	18
76	75	50	15.5	5	320000	3	0.030477 131	0.303	0.008	821.81	3	19
77	75	50	15.5	20	605000	3	0.026317 711	0.455	0.014	953.81	6	21
78	75	50	6.4	20	60.5	3	0.026342 443	0.44	0.003	6113.81	2641	16
79	75	50	6.4	5	4512.5	6.5	0.007611 589	0.364	0.008	1765.87	411	23
80	75	725	11	12.5	32	3	0.031587 114	0.401	0.027	4453.81	1658	16
81	75	50	15.5	20	320000	10	0.030776 444	0.401	0.025	766.81	3	16

82	75	50	15.5	20	4512.5	4.75	0.007621 099	0.365	0.007	1796.87	469	24
83	75	725	11	12.5	5253.1 25	6.5	0.007091 388	0.352	0.002	1389.87	387	17
84	75	725	11	12.5	605000	3	0.002614 485	0.235	0.003	1019.5	2	16
85	75	1400	6.4	20	451.25	6.5	0.007624 468	0.399	0.003	3852.87	1516	33
86	75	725	11	12.5	4512.5	6.5	0.007708 557	0.382	0.004	1400.87	439	13
87	75	725	11	12.5	4512.5	8.25	0.004305 037	0.285	0.006	1667.63	511	16
88	75	1062.5	8.7	12.5	45125	6.5	0.008466 447	0.442	0.007	646.87	26	15
89	75	725	13.2	16.25	45125	4.75	0.005836 636	0.347	0.01	760.63	25	17
90	75	1062.5	11	12.5	4512.5	4.75	0.026047 87	0.479	0.031	1296.45	87	7
91	75	387.5	13.2	12.5	52531. 25	6.5	0.007770 149	0.479	0.021	591.87	19	11
92	75	725	13.2	12.5	4512.5	6.5	0.007359 969	0.363	0.007	1062.87	185	9
93	75	725	11	12.5	5253.1 25	8.25	0.007411 598	0.369	0.005	980.87	176	9
94	75	725	11	16.25	3828.1 25	8.25	0.007209 127	0.382	0.01	1260.87	306	19
95	75	725	11	8.75	5253.1 25	6.5	0.018785 684	0.441	0.007	911.45	81	10
96	75	387.5	11	8.75	3828.1 25	6.5	0.019489 454	0.439	0.007	1202.45	161	18
97	75	387.5	11	16.25	5253.1 25	6.5	0.006186 077	0.342	0.009	1736.63	448	24
98	75	1062.5	11	16.25	4512.5	8.25	0.026503 302	0.559	0.033	1073.45	97	8
99	75	387.5	13.2	12.5	5253.1 25	6.5	0.019558 828	0.418	0.008	1197.45	102	5

100	75	387.5	11	16.25	3828.1 25	8.25	0.008570 618	0.488	0.008	1647.87	251	15
101	75	725	11	16.25	3828.1 25	4.75	0.009137 857	0.465	0.008	1665.87	261	10
102	75	725	11	8.75	5253.1 25	8.25	0.008793 497	0.439	0.006	1358.87	182	7
103	75	725	11	8.75	4512.5	4.75	0.008536 005	0.383	0.007	1497.45	219	11
104	75	387.5	8.7	12.5	3828.1 25	6.5	0.005346 869	0.403	0.003	3617.63	988	40
105	75	1062.5	11	16.25	525.31 25	6.5	0.008938 238	0.474	0.021	3709.87	801	18
106	75	725	13.2	12.5	4512.5	4.75	0.003676 122	0.348	0.003	2757.63	689	28
107	75	1062.5	8.7	12.5	5253.1 25	6.5	0.005916 394	0.398	0.005	733.87	27	14
108	75	725	8.7	12.5	3828.1 25	6.5	0.022874 903	0.53	0.022	972.45	111	6
109	75	387.5	11	8.75	5253.1 25	4.75	0.008361 408	0.444	0.004	1349.87	327	24
110	75	725	11	16.25	4512.5	6.5	0.010302 736	0.473	0.03	655.87	31	7
111	75	725	13.2	8.75	4512.5	6.5	0.008315 61	0.419	0.01	1241.87	311	11
112	75	725	11	12.5	451.25	8.25	0.022885 096	0.495	0.031	4417.45	1338	46
113	75	387.5	11	12.5	4512.5	6.5	0.007853 675	0.418	0.01	1309.87	197	11
114	75	725	11	12.5	451.25	6.5	0.005387 531	0.348	0.006	2411.87	616	27
115	75	725	8.7	16.25	4512.5	6.5	0.008689 374	0.44	0.013	1210.87	187	11
116	75	725	11	12.5	4512.5	6.5	0.008249 746	0.44	0.006	1937.87	513	19

117	75	725	11	12.5	3828.1 25	4.75	0.008424 768	0.417	0.012	1631.87	387	18
118	75	725	11	16.25	45125	6.5	0.006030 265	0.342	0.005	746.87	37	12
119	75	725	8.7	16.25	4512.5	4.75	0.009523 174	0.456	0.012	865.63	81	6
120	75	1062.5	13.2	12.5	451.25	4.75	0.006739 78	0.368	0.006	5026.63	1838	61
121	75	1062.5	11	12.5	5253.1 25	4.75	0.008166 229	0.433	0.01	776.87	76	5
122	75	725	11	8.75	451.25	6.5	0.005904 369	0.333	0.004	6294.87	2166	67
123	75	725	8.7	8.75	382.81 25	6.5	0.010157 53	0.461	0.021	4215.87	1218	44
124	75	725	13.2	12.5	45125	8.25	0.006453 581	0.385	0.007	716.63	12	13
125	75	1062.5	11	12.5	3828.1 25	6.5	0.006039 508	0.389	0.006	1553.63	537	17
126	75	1062.5	11	8.75	451.25	8.25	0.006353 226	0.396	0.007	4645.63	1697	48
127	75	1062.5	11	12.5	45125	4.75	0.008773 956	0.443	0.006	666.45	20	19
128	75	387.5	11	12.5	45125	6.5	0.005750 128	0.349	0.008	892.87	24	23
129	75	725	8.7	8.75	451.25	6.5	0.008497 277	0.46	0.027	5500.87	1761	59
130	75	725	13.2	8.75	4512.5	8.25	0.009211 673	0.444	0.016	1768.63	468	17
131	75	1062.5	13.2	12.5	5253.1 25	6.5	0.006461 41	0.413	0.006	1578.63	411	14
132	75	1062.5	11	8.75	4512.5	8.25	0.008067 021	0.349	0.008	1005.45	328	9
133	75	387.5	8.7	12.5	45125	8.25	0.011703 391	0.42	0.015	4961.45	1689	54
134	75	387.5	11	12.5	451.25	6.5	0.009120 124	0.428	0.015	5483.87	1561	48
135	75	725	13.2	16.25	38281. 25	6.5	0.008866 852	0.477	0.019	821.87	19	18
136	75	725	13.2	12.5	525.31 25	6.5	0.005825 2	0.355	0.005	5022.87	1497	49
137	75	725	8.7	12.5	38281. 25	6.5	0.006175 429	0.328	0.004	777.87	21	26
138	75	725	8.7	12.5	382.81 25	6.5	0.005904 856	0.323	0.006	6387.87	19017	55

139	75	725	8.7	12.5	451.25	4.75	0.009477 535	0.431	0.021	5156.45	1288	41
140	75	387.5	11	12.5	605000	10	0.003006 533	0.239	0.004	776.5	23	29

APPENDIX C: DATASET 3RD STAGE EXPERIMENT USED IN SECTION 4.5

Table A.3: Dataset created from the experiments conducted during the hybrid LBMM- μ EDM micromachining (milling) with constant EDM Parameters

No.	LBMM input parameters				μ EDM output parameters (Actual)		
	Loop (nos)	Scanning speed (mm/s)	Power Percentage (%)	Pulse repetition rate	μ EDM Time (min)	Tool wear (μ m)	Short circuits (nos)
1	5	1500	20	5	53.2	36	102
2	10	1500	20	5	49.25	30	92
3	15	1500	20	5	70.28	18	61
4	5	1500	20	10	59.02	33	94
5	10	1500	20	10	45.17	31	87
6	15	1500	20	10	49.26	29	67
7	5	1500	20	15	51.35	37	91
8	10	1500	20	15	50.56	33	79
9	15	1500	20	15	53.48	39	107
10	5	1500	55	5	48.31	31	86

11	10	1500	55	5	44.56	28	77
12	15	1500	55	5	41.21	23	61
13	5	1500	55	10	41.23	29	78
14	10	1500	55	10	39.08	26	66
15	15	1500	55	10	38.08	19	61
16	5	1500	55	15	62.37	39	89
17	10	1500	55	15	42.54	33	79
18	15	1500	55	15	40.31	30	58
19	5	1500	90	5	44.56	33	87
20	10	1500	90	5	39.56	28	76
21	15	1500	90	5	32.48	29	59
22	5	1500	90	10	36.51	33	79
23	10	1500	90	10	38.22	31	74
24	15	1500	90	10	32.08	25	66
25	5	1500	90	15	31.59	27	58
26	10	1500	90	15	32.16	23	48
27	15	1500	90	15	29.07	18	44
28	5	2000	20	5	48.31	34	93
29	10	2000	20	5	52.3	41	107
30	15	2000	20	5	46.29	36	81
31	5	2000	20	10	48.41	39	97
32	10	2000	20	10	44.59	31	69
33	15	2000	20	10	43.22	24	52

34	5	2000	20	15	48.44	32	98
35	10	2000	20	15	48.14	33	109
36	15	2000	20	15	45.37	28	93
37	5	2000	55	5	38.56	26	77
38	10	2000	55	5	38.08	21	54
39	15	2000	55	5	38.37	23	59
40	5	2000	55	10	46.57	34	81
41	10	2000	55	10	41.36	31	57
42	15	2000	55	10	43.59	30	89
43	5	2000	55	15	44.52	28	70
44	10	2000	55	15	42.06	26	78
45	15	2000	55	15	36.51	26	54
46	5	2000	90	5	34.5	28	59
47	10	2000	90	5	34.02	23	44
48	15	2000	90	5	42.11	31	89
49	5	2000	90	10	36.22	29	104
50	10	2000	90	10	32.55	21	59
51	15	2000	90	10	34.21	26	77
52	5	2000	90	15	37.41	31	94
53	10	2000	90	15	30.58	29	47
54	15	2000	90	15	30.22	21	61
55	5	2500	20	5	52.57	41	111
56	10	2500	20	5	51.54	35	89

57	15	2500	20	5	52.48	31	76
58	5	2500	20	10	48.21	38	92
59	10	2500	20	10	47.03	27	68
60	15	2500	20	10	47.19	31	81
61	5	2500	20	15	51.59	33	106
62	10	2500	20	15	49.3	30	88
63	15	2500	20	15	48.51	26	77
64	5	2500	55	5	44.31	34	119
65	10	2500	55	5	44.09	31	96
66	15	2500	55	5	41.01	22	59
67	5	2500	55	10	46.5	31	106
68	10	2500	55	10	38.32	24	77
69	15	2500	55	10	37.05	24	61
70	5	2500	55	15	45.11	31	98
71	10	2500	55	15	48.43	36	85
72	15	2500	55	15	41.49	29	64
73	5	2500	90	5	37.49	28	109
74	10	2500	90	5	38.39	28	96
75	15	2500	90	5	34.11	23	54
76	5	2500	90	10	41.2	31	102
77	10	2500	90	10	38.51	26	90
78	15	2500	90	10	35.55	24	54
79	5	2500	90	15	38.49	29	83

80	10	2500	90	15	36.44	25	59
81	15	2500	90	15	34.56	21	47

